Neurochemical and Neuropharmacological Studies on a Range of Novel Psychoactive Substances

by

Barbara Loi

Dissertation

Submitted to the University of Hertfordshire in partial fulfilment of the requirements of the degree of

Doctor of Philosophy

Psychopharmacology, Drug Misuse and Novel Psychoactive Substances Research Unit

Hertfordshire, UK

School of Life and Medical Sciences

University of Hertfordshire

Date: November 2017

Table of contents

Table of contents 2
List of figures 6
List of tables 10
Aknowledgements 11
List of abbreviations 12
Abstract 14
Aims, objectives and hypotheses of the overall PhD project 17
Chapter 1: Novel Psychoactive Substances (NPS) 20
1.1) NPS - general overview 20
1.2) Epidemiology of NPS drugs 21
1.3) NPS classification 24
Chapter 2: Index compounds in the present PhD project 30
2.1) Synthetic cannabinoids 30
2.1.1) Classification of synthetic cannabinoids 30
2.1.2) Third generation synthetic cannabinoids 31
2.1.3) 'Spice' drugs 35
2.1.4) Epidemiology of synthetic cannabinoids 36
2.1.5) Social issues represented by synthetic cannabinoids and their effects 37
2.1.6) Pharmacology of synthetic cannabinoids, focus on their effects on the reward circuit 38
2.1.7) Synthetic cannabinoids and pharmacodynamics 43
2.2 Pipradrol-derivatives 44
2.2.1) Pharmacological studies on 2-DPMP and D2PM 45
2.2.2) Social issues represented by 2-DPMP and D2PM and their effects 46
2.3) 5-(2-Aminopropyl)indole (5-IT) 47
2.3.1) Social issues represented by 5-IT and its effects 47
2.3.2) Pharmacological studies on 5-IT 48
2.4) Aminorex derivatives: focus on 4,4'-DMAR 49
2.4.1) Pharmacological studies on 4,4'-DMAR 50
2.4.2) Social issues represented by 4,4'-DMAR and its effects 51
2.5) Dieting aid compound 2,4-DNP 51
2.5.1) Social issues represented by 2,4-DNP and its effects 53
2.5.2) Pharmacological studies on 2,4-DNP: focus on preclinical studies 54
Chapter 3: In vitro quantitative autoradiography studies 54
3.1) In vitro quantitative autoradiography overview 54

3.2) Competition binding assay 55
3.3) Autoradiography procedure 56
3.4) Synthetic cannabinoids and autoradiography studies 58
3.4.1) SCs and CB_1 receptor autoradiography studies: materials and methods 60
3.4.2) SCs and CB_1 receptor autoradiography studies: results 62
3.4.3) SCs and NMDA receptor autoradiography studies: materials and methods 69
3.4.4) SCs and NMDAR autoradiography studies: results 70
3.4.5) CB_1R and NMDAR autoradiography studies with SCs: discussion 75
3.5 Synthetic stimulants and DAT autoradiography studies 77
3.5.1) Synthetic stimulants and DAT autoradiography studies: materials and methods 78
3.5.2) Synthetic stimulants and DAT autoradiography studies: results 80
3.5.3) Synthetic stimulants and DAT autoradiography studies: discussion 84
Chapter 4: In vitro fast scan cyclic voltammetry studies 85
4.1) In vitro fast scan cyclic voltammetry overview 85
4.2) Fast scan cyclic voltammetry principles 87
4.3) BB-22 and FSCV studies: aims 89
4.4) BB-22 FSCV studies: materials and method 90
4.5) BB-22 FSCV studies: results 93
4.6) BB-22 and FSCV studies: discussion 94
Chapter 5: Microdialysis studies 96
5.1) Microdialysis overview 96
5.2) Synthetic cannabinoids and microdialysis studies 101
5.2.1) Synthetic cannabinoid microdialysis studies: materials and methods 103
5.2.2) Results for experiment 1: Effect of BB-22 administration on DA transmission in the NAc shell, core and in the mPFCx 106
5.2.3) Results for experiment 2: Role mediated by CB_1 receptors on the increase of DA release in the NAc shell DA induced by BB-22 109
5.2.4) Results for experiment 3: Effect of 5F-PB-22, 5F-AKB-48, and STS-135 administration on DA transmission in the NAc shell 109
5.2.5) Synthetic cannabinoids and microdialysis studies: discussion 112
5.3) 2,4-Dinitrophenol (2,4-DNP) and microdialysis studies 113
5.3.1) 2,4-DNP microdialysis studies: materials and methods 114
5.3.2) 2,4-DNP microdialysis studies: results 116
5.3.3) 2,4-DNP microdialysis studies: discussion 118
5.4) 2-DPMP and D2PM microdialysis studies 119
5.4.1) 2-DPMP and D2PM microdialysis studies: materials and methods 120
5.4.2) 2-DPMP microdialysis experiment: results 122

5.4.3) D2PM microdialysis experiment: results 124
5.4.4) 2-DPMP and D2PM microdialysis experiments: discussion 126
Chapter 6: Molecular modelling studies 128
6.1) Molecular modelling overview 128
6.2) Homology modelling overview 132
6.3) Molecular Docking overview 139
6.4) SCs and in silico CB_1 receptor studies, aim and goals 148
6.5) CB_1 receptor homology modelling studies: methods 149
6.6) CB_1 receptor homology modelling studies: results and discussion 150
6.7) Quality estimation of the CB_1 receptor homology model 152
6.8) Homology model refinement and preparation for docking process 160
6.9) Ligand building and preparation for docking process 161
6.10) Docking of referent compounds against the homology model of the rodent CB_1 receptor, approach validation: methods 161
6.11) Docking of representative CB_1R agonists and antagonists against the CB_1 receptor (Rattus Norvegicus) homology model: results and discussion 162
6.12) Vina binding energies against experimental K_i values for representative CB_1 receptor agonists and antagonists 165
6.13) Conclusions of the docking approach validation 166
6.14) Docking of a range of novel synthetic cannabinoids against the CB_1 receptor (Rattus Norvegicus) homology model: methods 171
6.15) Docking of the novel synthetic cannabinoids against the CB_1 receptor (Rattus Norvegicus) homology model: results 171
6.16) Vina binding energies against experimental K_i values for each third generation SC under study 172
6.17) Docking of representative CB_1R agonists and antagonists against the crystal structure of the human CB_1 receptor: approach validation 176
6.18) Docking of representative CB_1R agonists and antagonists against the crystal structure of the human CB_1 receptor: results and discussion 177
6.19) Vina and Autodock 4.0 binding affinities against experimental K_i values for representative CB_1 receptor agonists and antagonists 180
6.20) Conclusions of the docking approach validation 181
6.21) Docking of a range of novel synthetic cannabinoids against the crystal structure of the human CB_1 receptor: methods 190
6.22) Docking of a range of novel synthetic cannabinoids with the crystal structure of the human CB_1 receptor: results and discussion 190
6.23) Vina and Autodock 4.0 binding affinities against experimental K_i values for each novel SC under study 192
6.24) Comparison among docking outcomes obtained using the CB_1 receptor homology model (Rattus Norvegicus) and the crystal structure of the human CB_1 receptor 197

6.25) Vina and Autodock binding energies against experimental K_i values: comparison between outcomes obtained with the CB_1R homology model and the crystal structure 205

6.26) SCs and CB_1 receptor docking studies: Conclusions 206

7.1) Web-based study on 4,4′-Dimethylaminorex misuse: aim 208

7.2) Web-based study on 4,4′-Dimethylaminorex misuse: methods 209

7.3) Web-based study on 4,4′-Dimethylaminorex misuse: results 209

7.4) Web-based study on 4,4′-Dimethylaminorex misuse: discussion 212

Chapter 8: Overall discussion of the PhD project 214

8.1) Conclusions 220

8.2) Summary of the methodologies employed and analysis of the findings obtained for each drug assessed 220

8.3) Future studies 222

References 224

Published work included in this thesis 257

Poster presentations 258

List of figures

Figure 1: Chemical structures of JWH-018 and BB-22 31

Figure 2: Chemical structures of JWH-018 and 5F-PB-22 32

Figure 3: Chemical structures of JWH-018 and 5F-AKB-48 33

Figure 4: Chemical structures of JWH-018 and STS-135 34

Figure 5: Cannabinoid signal in the brain..... 42

Figure 6: Chemical structure of 2-DPMP 44

Figure 7: Chemical structure of D2PM..... 45

Figure 8: Chemical structure of 5-IT 47

Figure 9: Chemical structure of 4,4'-DMAR..... 49

Figure 10: Chemical structure of 2,4-DNP 51

Figure 11: Statistical results (2-way ANOVA) on the left, and graphical representation on the right of the binding data of [^{3}H]CP-55,940 in presence of increasing concentrations of BB-22, 5F-PB-22, 5F-AKB-48, STS-135 in both Cortex and CPu..... 64

Figure 12: Effect of increasing concentrations of BB-22 on [^{3}H]CP-55,940 autoradiographic binding. Representative computer-enhanced images of brain slices (on the left) and graphical representation of pooled data (on the right) showing the binding of [^{3}H]CP-55,940 to CB_1R in presence of increasing concentration of BB-22 in both Cortex and CPu.. 65

Figure 13: Effect of increasing concentrations of 5F-PB-22 on [^{3}H]CP-55,940 autoradiographic binding. Representative computer-enhanced images of brain slices (on the left) and graphical representation of pooled data (on the right) showing the binding of [^{3}H]CP-55,940 to CB_1R in presence of increasing concentration of 5F-PB-22 in both Cortex and CPu.. 66

Figure 14: Effect of increasing concentrations of 5F-AKB-48 on [^{3}H]CP-55,940 autoradiographic binding. Representative computer-enhanced images of brain slices (on the left) and graphical representation of pooled data (on the right) showing the binding of [^{3}H]CP-55,940 to CB_1R in presence of increasing concentration of 5F-AKB-48 in both Cortex and CPu..... 67

Figure 15: Effect of increasing concentrations of STS-135 on [^{3}H]CP-55,940 autoradiographic binding. Representative computer-enhanced images of brain slices (on the left) and graphical representation of pooled data (on the right) showing the binding of [^{3}H]CP-55,940 to CB_1R in presence of increasing concentration of STS-135 in both Cortex and CPu..... 68

Figure 16: Effect of increasing concentrations of BB-22 on [^{3}H]MK-801autoradiographic binding. Representative computer-enhanced images of brain slices (on the left) and graphical representation of pooled data (on the right) showing the binding of [^{3}H]MK-801 to NMDAR in presence of increasing concentration of BB-22 in both Cortex and CPu 71

Figure 17: Effect of increasing concentrations of 5F-PB-22 on [^{3}H]MK-801autoradiographic binding. Representative computer-enhanced images of brain slices (on the left) and graphical representation of pooled data (on the right) showing the binding of [^{3}H]MK-801 to NMDAR in presence of increasing concentration of 5F-PB-22 in both Cortex and CPu 72

Figure 18: Effect of increasing concentrations of 5F-AKB-48 on [^{3}H]MK-801autoradiographic binding. Representative computer-enhanced images of brain slices (on the left) and graphical representation of pooled data (on the right) showing the binding of [^{3}H]MK-801 to NMDAR in presence of increasing concentration of 5F-AKB-48 in both Cortex and CPu..... 73

Figure 19: Effect of increasing concentrations of STS-135 on [^{3}H]MK-801autoradiographic binding. Representative computer-enhanced images of brain slices (on the left) and graphical representation of pooled data (on the right) showing the binding of [^{3}H]MK-801 to NMDAR in presence of increasing concentration of STS-135 in both Cortex and CPu..... 74

Figure 20: Statistical results of the binding data of [^{125}I]RTI-121 to DAT in presence of increasing concentrations of 5-IT and 2-DPMP in CPu and NAc shell (1-way and tree way-ANOVAs)..... 81

Figure 21: Effect of increasing concentrations of 5-IT on [^{125}I]RTI-121 autoradiographic binding. Representative computer-enhanced images of brain slices (on the left) and graphical representation of pooled data (on the right) showing the binding of [^{125}I]RTI-121 to DAT in presence of increasing concentration of 5-IT in both NAc shell and CPu..... 82

Figure 22: Effect of increasing concentrations of 2-DPMP on [^{125}I]RTI-121 autoradiographic binding. Representative computer-enhanced images of brain slices (on the left) and graphical representation of pooled data (on the right) showing the binding of [^{125}I]RTI-121 to DAT in presence of increasing concentration of 2-DPMP in both NAc shell and CPu 83

Figure 23: Fast Scan Cyclic Voltammetry set up (generator, potentiostat, amplifier, computer, sample and hold circuit) 89

Figure 24: BB-22 FSCV studies. Dopamine Peak height (Ph) data after BB-22 administration 94

Figure 25: Picture of the microdialysis probe..... 97

Figure 26: Picture of the stereotaxic apparatus..... 98

Figure 27: Picture of the microdialysis set-up 100

Figure 28: *In vivo* effect of BB-22 administration on DA transmission in the NAc shell, NAc core, and mPFC 108

Figure 29: Blockade of BB-22 effect on increase of DA transmission in the NAc shell mediated by AM-251..... .109

Figure 30: In vivo effect of 5F-PB-22, 5F-AKB-48, STS-135 administration on DA transmission in the NAc shell 111

Figure 31: *In vivo* effect of 2,4-DNP (20 mg/kg i.p.) administration on DA transmission in the NAc shell and CPu 117

Figure 32: Effect of 2,4-DNP (20 mg/kg i.p.) administration on body temperature..... 118

Figure 33: *In vivo* effect of 2-DPMP administration on DA transmission in the NAc shell 123

Figure 34: *In vivo* effect of 2-DPMP administration on DA transmission in the CPu..... 124

Figure 35: *In vivo* effect of D2PM administration on DA transmission in the NAc shell..... 125

Figure 36: *In vivo* effect of D2PM administration on DA transmission in the CPu 126

Figure 37: Target-template alignment: CB_1 receptor sequence (Rattus Norvegicus)-5TGZ1.A sequence 151

Figure 38: Top left: Three-dimensional structure of the CB_1 receptor homology model (Rattus Norvegicus); Top right: global quality plot; bottom left: comparison plot; bottom right: local quality plot 152

Figure 39: Ramachandran plot, generated by Rampage server, of the CB_1 receptor homology model (Rattus Norvegicus). 153

Figure 40: Ramachandran plot of the CB_1 receptor homology model (Rattus Norvegicus) generated by Procheck software..... 155

Figure 41: Main chain parameters of the CB_1 receptor homology model (Rattus Norvegicus) generated by Procheck..... 156

Figure 42: Overall side chain properties of the CB_1 receptor homology model (Rattus Norvegicus) generated by Procheck 157

Figure 43: Residue by residue properties of the CB_1 receptor homology model (Rattus Norvegicus) generated by Procheck**.** 159

Figure 44: Residues of the CB_1 receptor homology model (Rattus Norvegicus) with planarity deviations according to Procheck..... 160

Figure 45: Ligand protein interaction diagrams of JWH-018, WIN-55,212-2, Anandamide, 2-AG, CP-55,940, Δ9-THC complexed with the CB_1R (Rattus Norvegicus) homology model. The complexes shown are the most favourable poses obtained using the molecular docking software Vina. 167

Figure 46: Lists of interactions observed between JWH-018, WIN-55,212-2, 2-AG, Anandamide, CP-55,940, Δ9-THC and the CB_1R (Rattus Norvegicus) homology model and obtained using the molecular docking software Vina. 168

Figure 47: Ligand protein interaction diagrams of AM-251, AM-6358, Otenabant, rimonabant, taranabant complexed with the CB_1R (Rattus Norvegicus) homology model. The complexes shown are the most favourable poses obtained using the molecular docking software Vina**.** 169

Figure 48: Lists of interactions observed between AM-251, AM-6358, otenabant, rimonabant, taranabant and the CB_1 receptor (Rattus Norvegicus) homology model obtained using the molecular docking software Vina 170

Figure 49: Ligand protein interaction diagrams of BB-22, 5F-PB-22, 5F-AKB-48, STS-135 complexed with the CB_1R (Rattus Norvegicus) homology model. The complexes shown are the most favourable poses obtained using the molecular docking software Vina 174

Figure 50: Lists of interactions observed between BB-22, 5F-PB-22, 5F-AKB-48, STS-135 and the CB_1R (Rattus Norvegicus) homology model obtained using the molecular docking software Vina. 175

Figure 51: Ligand protein interaction diagrams of JWH-018, WIN-55,212-2, Anandamide, 2-AG, CP-55,940, Δ9-THC complexed with the CB_1R crystal structure. The complexes shown are the most favourable poses obtained using the molecular docking software Vina 182

Figure 52: Lists of interactions observed between JWH-018, WIN-55,212-2, 2-AG, Anandamide, CP-55,940, Δ9-THC and the CB_1R crystal structure and obtained using the molecular docking software Vina..... 183

Figure 53: Ligand protein interaction diagrams of JWH-018, WIN-55,212-2, 2-AG, Anandamide, CP-55,940, Δ9-THC complexed with the CB_1R crystal structure. The complexes shown are the most favourable poses obtained using the molecular docking software Autodock 4.0. 184

Figure 54: Lists of interactions observed between JWH-018, WIN-55,212-2, 2-AG, Anandamide, CP-55,940, Δ9-THC and the CB_1R crystal structure and obtained using the molecular docking software Autodock 4.0..... 185

Figure 55: Ligand protein interaction diagrams of AM-251, AM-6358, otenabant, rimonabant, taranabant complexed with the CB_1R crystal structure. The complexes shown are the most favourable poses obtained using the molecular docking software Vina 186

Figure 56: Lists of interactions observed between AM-251, AM-6358, otenabant, rimonabant, taranabant and the CB1 receptor crystal structure obtained using the molecular docking software Vina. 187

Figure 57: Ligand protein interaction diagrams of AM-251, AM-6358, Otenabant, rimonabant, taranabant complexed with the CB_1R crystal structure. The complexes shown are the most favourable poses obtained using the molecular docking software Autodock 4.0 188

Figure 58: Lists of interactions observed between AM-251, AM-6358, otenabant, rimonabant, taranabant and the CB1 receptor crystal structure obtained using the molecular docking software Autodock 4.0..... 189

Figure 59: Ligand protein interaction diagrams of BB-22, 5F-PB-22, 5F-AKB-48, STS-135 complexed with the CB_1R crystal structure. The complexes shown are the most favourable poses obtained using the molecular docking software Vina 193

Figure 60: Lists of interactions observed between BB-22, 5F-PB-22, 5F-AKB-48, STS-135 and the CB_1R crystal structure obtained using the molecular docking software Vina 194

Figure 61: Ligand protein interaction diagrams of BB-22, 5F-PB-22, 5F-AKB-48, STS-135 complexed with the CB_1R crystal structure. The complexes shown are the most favourable poses obtained using the molecular docking software Autodock 4.0. 195

Figure 62: Lists of interactions observed between BB-22, 5F-PB-22, 5F-AKB-48, STS-135 and the CB_1R crystal structure obtained using the molecular docking software Autodock 4.0 196

List of tables

Table 1: Statistical results of the binding data of [^{3}H]CP-55,940 in presence of increasing concentrations of BB-22, 5F-PB-22, 5F-AKB-48, STS-135 in both Cortex and CPu 63

Table 2: Key interacting residues crucial for CB_1 ligand binding recognition according to experimental mutation studies 132

Table 3: Vina binding energies related to the best binding poses of representative CB_1R agonists and antagonists at the CB_1R homology model (Rattus Norvegicus) against experimental K_i values 166

Table 4: Vina binding energies related to the best binding poses of BB-22, 5F-PB-22, 5F-AKB-48, STS-135 at the CB_1R homology model (Rattus Norvegicus) against experimental K_i values.....173

Table 5: Vina and Autodock 4.0 binding energies related to the best binding poses of representative CB_1R agonists and antagonists at the CB_1R crystal structure, against experimental Ki values..... 181

Table 6: Vina and Autodock 4.0 binding energies related to the best binding poses of BB-22, 5F-PB-22, 5F-AKB-48, STS-135 at the CB_1R crystal structure, vs experimental Ki values. 192

Aknowledgements

Foremost, I am deeply thankful to my supervisors Professor Fabrizio Schifano, Professor Mire Zloh, Mr John Corkery, Professor Colin Davidson who have guided, supported, and assisted me through this learning experience and through the process of researching and writing this dissertation.

A special thanks to Professor Gaetano Di Chiara, Professor Jolanta Opacka-Juffry and Doctor De Luca, who were involved in this research project and who provided me with premises, facilities, expertise and constant guidance and support during this PhD project.

I gratefully acknowledge the PhD studentship support from the University of Hertfordshire. This project was supported in part by grants of the European Commission (Drug Prevention and Information Programme 2014–2016; contract JUST/2013/DPIP/AG/4823; EU-MADNESS project). Further financial support was provided by the EU Commission-targeted call on cross border law enforcement cooperation in the field of drug trafficking—DG Justice/DG Migrations and Home Affairs (JUST/2013/ISEC/DRUGS/AG/6429) Project EPS/NPS (Enhancing Police Skills concerning Novel Psychoactive Substances; NPS). Professor Schifano is a full member of the U.K. Advisory Council on the Misuse of Drugs (ACMD) and a member of its NPS Committee; EMA Advisory board member. Mr Corkery is a co-opted member of the ACMD's Technical and NPS Committees and its Drug-Related Deaths Working Group. The members of this project have no other relevant affiliations or financial involvement with any organization or entity with a financial interest in or financial conflict with the subject matter or materials discussed in the manuscript apart from those disclosed.

Finally, last but by no least, I would like to thank my husband, my parents, and my sisters for supporting me spiritually and emotionally throughout my years of study and through the process of researching and writing this dissertation. This accomplishment would not have been possible without them.

List of abbreviations

5-HT: Serotonin

ADHD: Attention deficit hyperactivity disorder

Aminoalkylindoles: AAIs

ARG: Autoradiography

CB_1R: Cannabinoid receptor type 1

CPu: Caudate Putamen

DA: Dopamine

DAT: Dopamine transporter

ECL2: Extracellular Loop 2

EDM: Electronic Dance Music

E_{max}: Maximal Efficacy

EMCDDA: European Monitoring Centre for Drugs and Drug Addiction

ESPAD: European School Survey Project on Alcohol and Other Drugs

FSCV: Fast Scan Cyclic Voltammetry

GC-EI-MS: Gas Chromatography Mass Spectrometry with Electron Ionisation

GDS: Global Drug Survey

GPCR: G-protein-Coupled Receptors

HEK: Human Embryonic Kidney

HPLC: High-Performance Liquid Chromatography

IC_{50}: Half minimal inhibitory concentration

IPSCs: Inhibitory Postsynaptic Currents

MAO_A: Monoamine Oxidase, type A

MAO_B: Monoamine Oxidase, type B

MPFCx: Medial Prefrontal Cortex

NAc: Nucleus Accumbens

NDRI: Norepinephrine-Dopamine Reuptake Inhibitors

NE: Norepinephrine

NET: Norepinephrine transporter

NMDAR: N-methyl-D-aspartate receptor

NMR: Nuclear Magnetic Resonance

NPIS: National Poison Information Service

NPS: Novel psychoactive Substances

OFDT: Observatoire Français des Drogues et des Toxicomanies (French Observatory of Drugs and Drug Addiction)

PDB: Protein Data Bank

RMS: Root Mean Squared

ROAs: Routes of administration

ROIs: Regions of interest

SCs: Synthetic Cannabinoids

SERT: Serotonin transporter

TAAR: Trace Amine Associated Receptors

UNODC: United Nations Office on Drugs and Crime

$VMAT_2$: Vesicular Monoamine Transporter type 2

VP: Ventral globus pallidum

VTA: Ventral Tegmental Area

Abstract

Introduction: Over recent decades, there has been an increase in the availability and use of Novel Psychoactive Substances (NPS) all over the world. They include several classes of chemicals that mimic the effects of illicit drugs and have been purposefully introduced into the market to circumvent or undermine the purpose of legal regulation. Currently, there is information lacking on the pharmacology of these substances; however, the increasing number of cases and outbreaks of intoxications/deaths is becoming a cause for deepening concern. Multi-disciplinary research in the fields of biology, chemistry, clinical medicine and web analysis is needed to develop responses against this tidal wave.

Aim: The overall aim of this project is to gain insights into pharmacological, neurochemical and molecular properties of selected NPS to provide a reliable background needed for detection, assessment, and management of NPS-related harms. A range of approaches and methodologies was employed and a spectrum of different fields of knowledge has been engaged to gain some understanding into the complex multi-faceted phenomenon of NPS.

Methods: Different substances have been selected as targets for the present project according to the clinical pattern of toxicity raised by their worldwide use and the lack of scientific knowledge available about them. The methods employed were: *in vitro* quantitative autoradiography (to evaluate the binding properties of the novel SCs BB-22, 5F-PB-22, 5F-AKB-48 and STS-135 at the cannabinoid receptor type 1 and N-methyl-D-aspartate receptor; and the binding properties of the synthetic stimulants 5-IT and 2-DPMP at the dopamine transporter in rat brain slices); *in vitro* Fast Scan Cyclic Voltammetry (to assess the effects of BB-22 on evoked dopamine efflux and dopamine re-uptake half-life in nucleus accumbens brain slices); *in vivo* microdialysis (to monitor dopamine release in terminal areas of the reward system after acute administration of the synthetic cannabinoids BB-22, 5F-PB-22, 5F-AKB-48 and STS-135; the dieting aid compound 2,4-DNP; the synthetic stimulants 2-DPMP and D2PM in freely moving animals); *in silico* molecular docking (to investigate the intermolecular interactions of the SCs BB-22, 5F-PB-22, 5F-AKB-48 and STS-135, and other referent compounds, with a homology model of the rodent cannabinoid receptor type 1 (CB_1R) and the crystal structure of the human CB_1R); and a web-based analysis approach (to analyse the information provided by a range of fora communities on 4,4'-DMAR use, additionally critical reviewing the available evidence-based literature on this topic).

Results: Our *in vitro* quantitative autoradiography studies, confirmed that the index compounds BB-22, 5F-PB-22, 5F-AKB-48 and STS-135, behave as highly potent CB_1R ligands able to compete with the radioligand [^{3}H]CP-55,940 in cortical and striatal brain slices. On the other hand, all synthetic cannabinoids tested were unable to compete with the radioligand [^{3}H]MK-801 in the same cerebral areas, rejecting the hypothesis of their potential binding to the N-methyl-D-aspartate receptor (NMDAR) at all concentrations investigated. Consistent with previous *in vitro* studies, 5-IT and 2-DPMP behaved as highly potent dopamine transporter (DAT) ligands able to compete with the radioligand [^{125} I]RTI-121 in a concentration-dependent way in the Caudate Putamen (CPu) and Nucleus Accumbens (NAc) brain slices. Notably, 2-DPMP was able to displace the radioligand in both cerebral regions, starting from lower concentrations compared to 5-IT.

In vitro Fast Scan Cyclic Voltammetry findings demonstrated that local application of the synthetic cannabinoid BB-22 in brain slices, was unable to change evoked dopamine efflux and dopamine reuptake time-constant in the NAc shell at any doses tested. The results obtained would suggest the relative contributions of complex neuronal circuits, either within or outside the NAc, whose modulation would interfere with the interactions between BB-22 and dopaminergic neurons and represent critical pathways accounting for some of the rewarding properties of BB-22 exposure.

In vivo microdialysis outcomes suggested that all SCs tested could increase dopamine release in the NAc shell at specific doses, while no changes in dopamine output were observed in other areas of the reward system, namely NAc core and medial prefrontal cortex (mPFCx) after BB-22 administration. These outcomes provided a circumstantial pre-clinical evidence for a greater putative abuse liability of SCs compared to the natural compound found in cannabis (Δ9-THC). Furthermore, the acute treatment with 2,4-DNP did not cause any change in dopamine release in the NAc shell and CPu rejecting the hypothesis of psychoactivity of this substance at the dose tested. On the other hand, the synthetic stimulant 2-DPMP elicited a comparable increase of dopamine (DA) release in the NAc shell and CPu at the higher doses tested, while D2PM caused a selective increase of DA release in the NAc shell, providing a circumstantial preclinical evidence for a putative abuse liability of this compound at the highest dose assessed.

The *in silico* molecular docking studies demonstrated that the SCs BB-22, 5F-PB-22, 5F-AKB-48 and STS-135 interact with CB_1 receptor residues that, according to previous mutation and computational studies, are considered crucial for synthetic cannabinoid binding recognition.

Additionally, they share some interacting residues with other aminoalkylindole derivatives (e.g. WIN-55,212-2).

The web-based analysis focused on 4,4'-DMAR, suggested that fora members co-operate in exchanging an extensive body of knowledge about this drug, and the recurring topics of discussion include: routes of administration and dosages; desired and undesired effects; comparison and association with other drugs and medications; overall impression; provision of harm reduction advice. This approach has been useful to better understand some of the clinical and psychopharmacological issues pertaining to 4,4'-DMAR.

Conclusions: Overall, these studies provided new pharmacological, neurochemical and molecular knowledge on a range of Novel Psychoactive Substances essential for identifying potential therapeutical approaches against their use/abuse. The novelty of this project lies in the adoption of a multi-disciplinary approach involving a range of methodologies from different areas of expertise (neurobiology, pharmacology, chemistry, netnography) all integrated to clarify some aspects of the index NPS, which were not yet available in the current literature. Additional studies are needed to better explain short and long-term effects of the index NPS, their abuse potential, and their interactions with other drugs of abuse.

Aims, objectives and hypotheses of the overall PhD project

Over the past decades, the unprecedented use/abuse of NPS has led to many toxicity events, hospital emergency admissions, and fatalities over the world. Although some progress has been made by the international community to address the NPS phenomenon, the exponential increase of the NPS market still represents a policy challenge and further efforts are necessary to tackle the wide escalation of NPS use. For these reasons, accurate evaluation of the pharmacological effects of these drugs, along with careful analysis of the biological mechanisms underlying their clinical effects, may contribute to improve the quality of public health on a global level.

In view of the above, the present PhD project adopted a multi-disciplinary approach that best addresses the complexities of NPS use/abuse, aiming to understand how compounds belonging to different chemical groups, interact with biological systems. Different areas of expertise, including biology, *in silico* molecular modelling, and netnography have been involved. Biological studies have been carried out by performing *in vitro* (using animal tissues) and *in vivo* (using live animals) research to predict what effect(s) the drugs under study might have in specific cerebral areas. *In silico* molecular modelling studies were performed to investigate the complex intermolecular interactions between a range of NPS and their targets; while the netnography approach was engaged to assess some of the psychopharmacological issues inherent to NPS use.

The index substances in the present PhD project included the synthetic cannabinoids BB-22, 5F-PB-22, 5F-AKB-48 and STS-135; the synthetic stimulants 2-DPMP, D2PM, 5-IT, 4,4'-DMAR; and the dieting aid compound 2,4-DNP. These chemicals were all selected for a range of reasons, including: evidence of health and social harms associated to their use (e.g. great number of Emergency Department admissions, toxicity events and fatalities); continued illegal use despite their prohibition; lack of pharmacological and neurochemical data currently available; limited prevention strategies and therapeutic approaches presently planned against their use/abuse; limited awareness of their associated health risks; misperception of their safety, lacking information available on their potential interactions with other drugs in the context of polydrug intake; urge to better draft a risk profile for these drugs; necessity to disseminate the most current NPS-related information to health professionals and the general public.

Although the second largest group monitored by the EMCDDA at the time of our study was the synthetic cathinone class, our analysis focused on synthetic stimulants belonging to other different pharmacological classes (e.g. pipradrol derivatives, tryptamines).

The rationale behind this choice was related to the wider neuropharmacological gap of knowledge found for these compounds in the preclinical and clinical literature available, compared to synthetic cathinones. The effects of several cathinones was already reported in *in vitro* brain slice studies (Opacka-Juffry et al., 2014) as well as *in vivo* (Pehek et al 1991; Suyama et al., 2016), providing important preclinical knowledge on the neurobiological effects of these compounds. However, no neurochemical studies were conducted before ours in freely moving animals and in brain slices using the index compounds in our study, highlighting the necessity to further investigate their activity in the brain.

Along the same lines, 2,4-DNP was chosen to be evaluated for the potential activity on the central nervous system the first time in our studies, in order to find a neuropharmacological explanation behind the current alarming use/abuse responsible for several cases of multiple body system failures all over the world.

Multiple hypotheses were generated based on the type of analysis performed. In detail:

- a potential binding of BB-22, 5F-PB-22, 5F-AKB-48 and STS-135 to the cannabinoid receptor, type 1 (CB_1R) and N-methyl-D-aspartate receptor (NMDAR) and a likely binding of 5-IT and 2-DPMP to the dopamine transporter (DAT) were hypothesised and assessed using the *in vitro* autoradiography studies;
- a local change in evoked dopamine (DA) release in the nucleus accumbens (NAc) shell after BB-22 application was hypothesised and assessed with *in vitro* Fast Scan Cyclic Voltammetry (FSCV) studies;
- a psychoactive effect mediated by DA release increase in specific cerebral areas of the reward system for BB-22, 5F-PB-22, 5F-AKB-48 and STS-135, 2-DPMP and D2PM and 2,4-DNP, was hypothesised and assessed using *in vivo* microdialysis;
- specific ligand interactions between BB-22, 5F-PB-22, 5F-AKB-48 and STS-135 and the CB_1 receptor homology model and crystal structure consistent with those observed for other aminoalkylindole (AAI) derivates, were hypothesised and investigated, using the molecular docking approach;

- some of the clinical and psychopharmacological information pertaining to 4,4'-DMAR and retrieved from specific online fora, were hypothesised to be consistent with those available in the current literature, and were investigated using a critical approach.

All the data obtained using different approaches, were critically discussed in the light of the available published literature. To identify peer-reviewed papers and online reports commenting on selected compounds, a comprehensive search on the Embase, Scopus; Google Scholar and Pubmed/Medline databases, was undertaken. Among the chemicals under study, particular attention was given to SCs primarily responsible for drug-related emergencies involving NPS (UNODC, 2016).

Overall, the present project aimed to gain new knowledge on selected compounds that could be used as valuable background to develop valid management strategies and clinical treatment approaches against their use/abuse.

Chapter 1: Novel Psychoactive Substances (NPS)

1.1) NPS - general overview

Over the past years, significant advances in the modern society contributed to widely change the international drug market in terms of substance supply; availability; use and prevalence; promoting the incessant emergence and diffusion of NPS, and giving rise to a worldwide public health threat that is difficult to contain (Reuter et al., 2017).

The speed and complexity of the NPS phenomenon has led to a wide range of challenges in prevention management, policy responses and clinical intervention, highlighting the necessity for continuous reviewing and further development of alternative options to cope with this highly dynamic threat (Baumann et al., 2016).

According to the alarming pace of the NPS phenomenon diffusion, different regional patterns on NPS emergence have been reported across the world and mostly in Europe, Asia, Africa, Americas and Oceania (UNODC, 2016). The European scene has been characterised by a growing number of NPS released into the market. By the end of 2016, the EMCDDA had been notified more than 620 NPS, with 423 substances being notified in the last five years and 66 compounds being detected for the first time in Europe. Synthetic cannabinoids (SCs) continue to be the largest group of novel substances monitored by the EMCDDA, followed by synthetic cathinones. According to the EMCDDA report, the number of NPS that emerged for the first time in 2016 (66), was lower compared to that recorded in 2015 (75). The cause of this decrease was likely related to the adoption of stricter control measures and law enforcement operations especially targeted to the Chinese laboratories and web-marketing platforms responsible for spreading a large number of NPS over different countries (EMCDDA, 2017).

NPS synthesis is based on the production of molecules being chemically/pharmacologically similar to existing illicit drugs and sometimes more harmful than their parental compounds in terms of toxicity, adverse reactions, dependence, long-term effects, fatalities and psychiatric consequences (Schifano et al., 2016). The increasing availability of NPS led to broader public health and social harms and often ended up with outbreaks of mass poisonings recorded by Emergency Departments (ED) and fatalities across the world (EMCDDA, 2016).

The wide diffusion of NPS is mostly related to the global nature of the Web that is frequently used as a platform for the open sale of NPS (Soussan et al., 2016) and represents the most

popular source of information about NPS use (Nelson et al., 2014) with web social communities being extensively used as discussion areas on this topic (Orsolini et al., 2015).

The open sale of NPS products is characterised by deceptive advertising that promotes these preparations with attractive and curious names and depicts them as "*legal*", "*natural*" and "*safe*", but "*not intended for human consumption*" or "*not tested for hazards or toxicity*", as a stratagem to avoid legal restrictions (Musselman et al., 2014).

Furthermore, the lack of safety data information reported on the packaging; the extremely changeable and unpredictable composition characterising these products; the abuse/misuse of unsafe preparations and their consumption along with other drugs, may all account for significantly growing emergency admissions all over the world (Miliano et al., 2016).

The principal reasons that drive NPS use include curiosity; novelty attraction; accessible price and availability; undetectability through standard screening tests; legality; perceived high quality and safety. Other incentives overlap with those for using traditional drugs like stimulants (e.g. sought-after self-confidence, cognitive enhancement, disinhibition) or hallucinogens (e.g. spiritual and intellectual self-exploration, pursued detachment from reality and altered perceptions) (Soussan et al., 2016; EMCDDA, 2015).

1.2) Epidemiology of NPS drugs

Epidemiological studies on NPS are limited and mostly reflect published epidemiological data on different populations and/or substances. Evidences from surveys showed that NPS use is mainly confined to generally young male users with previous drug history and sometimes knowledgeable about drugs in general. The wide range of chemicals commonly marketed entails several motivations for using them. External reasons include price, easy availability, and legal status; while more personal reasons include curiosity, pro-social sought-after effects, self-exploration and pleasure (Soussan et al., 2016).

Recently, an online survey focused on drug use history and reasons for use, was performed on a large sample of 619 drug users with experiences with both traditional drugs and NPS (Soussan et al., 2016). According to this survey, most of the participants (85%) had used several NPS on the last five years, and some users (30%) tried nine or more different NPS mainly belonging to different drug groups, highlighting the novel sensation seeking attitude that characterised these users. Globally, 177 different NPS belonging to different pharmacological classes (e.g.

hallucinogens, stimulants, dissociatives, synthetic cannabinoids) had been used and most participants were young males. Some 40% of the NPS described in this study were obtained through friends or dealers rather than online, and this occurred especially for banned drugs. The most common motivations for using NPS in general were pleasure and enjoyment, with most of the participants planning on using NPS again. The reasons and attitudes clearly changed and sometimes overlapped based on each drug group. Specifically, use of SCs was mainly motivated by affordable price, availability, non-detectability in screening tests; use of hallucinogens and dissociatives was related to inner exploration and spiritual attainment; use of opioids was primarily connected with addiction; while the reasons for using stimulants were mainly linked to mental/physical enhancement and pro-social sought-after effects (Soussan et al., 2016).

In 2015, the European School Survey Project on Alcohol and Other Drugs (ESPAD) performed an international survey to monitor substance use among 15-16-year-old students from 35 European countries, including 23 EU Member States and Norway. According to this survey, lifetime use of NPS was reported by 4 % of students, with a higher prevalence among boys and highest rates in Estonia and Poland. These substances seemed to be more commonly used than other traditional drugs (e.g. amphetamine, ecstasy, cocaine or LSD) (ESPAD, 2015).

More recently, a comprehensive EU-wide survey on NPS use was conducted among young people aged 15 to 24 years randomly selected across the 27 EU Member States (the Flash Eurobarometer). According to this survey, lifetime use of NPS was reported by 8% of participants, mainly males, with higher prevalence rates in France and Ireland (Flash Eurobarometer, 2016).

Another international online survey was conducted to investigate the reasons for using NPS and the level of awareness about potential health risks associated with their use. People from 17 countries, mainly from Europe, participated to the survey, and most responses came from university students. According to this survey, 65% of the respondents were knowledgeable about NPS, and among them, the majority was male, employed, with a bisexual or homosexual orientation. Additionally, awareness of NPS was greater in those in employment but it was unaffected by level of education. Overall, some 14% of participants were NPS users, with nearly half of them having limited perception of the potential health risks associated with NPS use (Deligianni et al., 2017).

Another survey-based study was performed to provide some data about NPS misuse. A questionnaire was administered to both, a sample of healthy subjects and a sample of psychiatric patients. Socio-economic characteristics and substance use with a special focus on the use of some NPS (e.g. spice, bath salts, methamphetamine, phenethylamines, methoxetamine, etc.) were investigated. The samples of healthy participants and psychiatric patients were mainly composed of females with an average age of about 22 years and high school education. Most of them were living with their parents and some of them were students. This survey showed a higher prevalence of NPS consumption in the psychiatric group compared to the healthy one, with a relevant use of SCs and cathinone derivatives (Martinotti et al., 2014).

An additional survey on the extent of NPS use was conducted in a high-risk population composed by attendees of electronic dance music (EDM) parties at nightclubs and festivals in New York City in 2015. The prevalence of self-reported use of NPS was assessed on a sample of 682 adults (age 18–25). According to this survey, some 35% of participants reported lifetime use of NPS with a greater prevalence of use of synthetic cannabinoids, followed by phenethylamines, other psychedelics, tryptamines, and dissociatives. Overall, risk factors for NPS use included higher frequency of nightclub/festival attendance; use of Ecstasy, LSD, and ketamine; and bisexual orientation (Palamar et al., 2016).

Another online survey was conducted in France in 2014, in the context of the I-TREND3 project, aiming to gain insights into the profiles, reasons and practices of NPS users. The respondents were mainly previous conventional drug users (cannabis, stimulants, hallucinogens). The mean age of participants was 28, with women in a minority and some users aged over 30 and over 50, suggesting that NPS phenomenon is not just confined to younger generations. NPS users were predominantly urban, with fairly high level of education. Their professional situation was highly dependent on their age, with those aged under 25 years being mainly college or university students, and those over 25 years being primarily employed and mostly having their own accommodation. For the majority of respondents, last use of NPS occurred in the company of friends and it took place at the user's or friends' home. NPS were mainly used to modify perception, to get stoned; to bond with others, to socialise; to give more energy; to reduce anxiety levels; for simply curiosity; to stimulate intellectual activity. Most widely consumed NPS classes at last use included: phenethylamines, cathinones,

arylcyclohexylamines, cannabinoids, tryptamines. Direct online purchases of NPS appeared to be more frequent among older users compared to younger respondents (OFDT, 2014).

Further epidemiological studies are needed to better outline a socio-demographic profile of the NPS users and to develop prevention and harm reduction strategies geared toward a specific target population.

1.3) NPS classification

Considering the wide number of NPS, classifying them represents the starting point from which all the other insights may be developed. The parameters used for NPS classification may be chemical, or alternatively, pharmacological/clinical. Chemical classification includes: synthetic cathinones, phenethylamines, tryptamines, piperazines, pipradrol derivatives, arylcyclohexylamines, aminoindanes, aminoalkylindoles; while the pharmacological/clinical classification comprises cannabis-like compounds, hallucinogens, stimulants, entactogens (Schifano et al., 2015; Miliano et al., 2016).

Synthetic cathinones

The chemical structure of synthetic cathinones is related to the natural stimulant compound cathinone found in the leaves of the 'khat plant' (Catha edulis) (Kalix et al., 1990). Differences from amphetamines are due to the additional presence of a ketone oxygen group at the ß-position which confers higher polarity with consequent decrease in the central nervous system penetration (Simmler et al., 2013; Nelson et al., 2014). This property may drive users to increase drug dosages with consequent more profound adverse peripheral effects. Commonly marketed over the internet as 'bath salts', 'plant food', 'insecticides', their popularity was likely driven by a scarce availability of good quality amphetamine, cocaine or MDMA, combined with more restrictive legal regulations. Snorting, ingestion, injection are the most typical routes of administration (ROAs) used, while tablets, capsules and liquids are the most common available formulations. Synthetic cathinones are the second widest group of NPS monitored by the EMCDDA. Globally, 118 compounds were detected, with 14 of them being notified for the first time in 2016 (EMCDDA, 2017). The potency levels at the serotonin, dopamine and noradrenaline transporters (SER, DAT, NET, respectively) can change considerably among different compounds but all typically exhibit sympathomimetic effects. Specifically, some cathinones are aspecific monoamine transporter inhibitors with some of them being also serotonin releasers acting at the SERT (e.g. butylone, ethylone, mephedrone, methylone)

and/or dopamine releaser acting at the DAT (methcathinone and flephedrone), while some others being highly potent and selective DAT and NET inhibitors without releasing properties (e.g. pyrovalerone and MDPV). Additionally, some of them (e.g. mephedrone) exhibit interactions with serotoninergic receptors $5HT_{2A}$ and/or α_{-2} adrenergic receptors, leading to an increased risk of experiencing a serotonergic syndrome or a catecholaminergic toxicity (López-Arnau et al., 2012). Cathinone-related effects include increased alertness, agitation, aggression, euphoria, excited delirium, hallucinations, tachycardia, hypertension, hyperthermia and mood disturbances. Many fatalities (hundreds in the UK alone) have been linked to some cathinones such as mephedrone, methylone and butylone. Tolerance, dependence and withdrawal symptoms related to synthetic cathinones were reported as well (EMCDDA, 2015).

Phenethylamine/MDMA-like drugs

This class includes molecules like 2C- and 3C-series drugs (2C-B, 2C-I, 2C-E, 3C-bromo-Dragonfly), 4-MTA, MPA, 6-APB, and NBOMe series drugs. These chemicals typically show high affinity for the serotonin receptors 5-$HT2_{A/C}$ sometimes coupled with monoamine reuptake inhibition. They are usually marketed and consumed as MDMA substitutes, and may elicit a range of entactogenic, stimulant and hallucinogenic effects (increased empathy and confidence, openness, feeling of friendliness, emotional closeness to others, euphoria, energy, alertness, disinhibition, perceptual alterations, hallucinations). The consumption of these drugs has become a cause for concern as a result of a range of serotonergic and sympathomimetic toxicity effects developed after their use (e.g. tachycardia, hypertension, hyperthermia, vomiting, diarrhoea, convulsions, sweatiness, acute renal failure). Among these drugs, 3C-bromo-Dragonfly ("B-Fly") has been considered an extremely potent stimulant with long-lasting hallucinogenic effects (up to 3 days of psychoactive effects) associated with confusion and anxiety (Schifano et al., 2015). NBOMe drugs show LSD-like effects, and include the 25X-NBOMe series of hallucinogens. They interact with several receptors and exhibit a significant higher affinity for 5-HT_{2A} receptors. The most commonly reported psychedelic effects include: mood lift, greatly heightened awareness, changes in visual, auditory, tactile, olfactory, gustatory, and kinaesthetic perceptions. Symptoms of acute toxicity include tachycardia, hypertension, agitation, aggression, seizures, liver and kidney failure. 25C-NBOMe ("N-bomb", "Pandora") is one of the most harmful among the NBOMe compounds. It is a partial agonist of 5-HT_{2A} receptors and it is typically consumed orally or sublingually. It produces stimulation, hallucinations, and unpredictable violent episodes (Schifano et al., 2015). Overall,

several cases of toxicity events and fatalities have been linked to Phenethylamines/MDMA like drugs (Miliano et al., 2016; Schifano et al., 2015 and 2016).

Tryptamines

Tryptamine derivatives include several compounds chemically related to the endogenous compounds serotonin (5-HT) and melatonin (N-acetyl-5-methoxytryptamine) naturally produced by the human/animal body. Many tryptamines are naturally found in certain fungi (psilocin and psilocybin), plants (DMT and 5-MeO-DMT) and as constituents of venoms from some amphibians (bufotenin, 5-hydroxy-indolethylamines) (Schultes et al., 1979; Cimino et al., 1978). Additionally, other tryptamines have been synthesised and researched as medications for migraine (Brandes et al., 2007; Schifano et al., 2016). Synthetic tryptamines appeared in the drug scenario in the 1990s and dominated the market until they were listed as narcotics in 2007 (Schifano et al., 2016). Nevertheless, several novel tryptamines continue to be sold as designer drugs over the Internet, including: 5-MeO-DALT, AMT, 5-MeO-AMT and 5-IT (EMCDDA, 2015). While natural tryptamines are sold as products containing dried mushrooms ('magic mushrooms'), synthetic tryptamines are typically found as components of capsules, powders, tablets, or liquids. Sniffing, swallowing, smoking or injections are the most typical ROAs used, while brand names for tryptamines include 'Foxy-Methoxy', 'alpha-O', 'alpha', 'changa' (www.bluelight.com).

The primary clinical symptoms produced by tryptamines are visual hallucinations and psychedelic effects resulting from agonistic activity at the level of $5HT_{1A}$, $5HT_{2A}$, and $5HT_{2C}$ receptors with lower affinity for $5HT_{2A}$ receptors compared to phenethylamines. Other targets involved in tryptamine activity are serotonin transporters, vesicular monoamine transporters type 2 (VMAT2) and trace amine-associated receptors (TAAR) (Fantegrossi et al., 2008; Su et al., 2009; Ray, 2010). Other clinical symptoms are euphoria, pro-social effects, alterations in sensory perceptions and depersonalization; while side-effects include common sympathomimetic effects (e.g. agitation, aggression, anxiety, tachycardia, hypertension) and serotoninergic toxicity (high body temperature, tremor, sweating, dilated pupils, diarrhoea, seizures) (Dargan and Wood, 2013; Schifano et al., 2016). Additionally, hallucinogen persisting perception disorder (HPPD) with recurrent presence of sensory disturbances, may be sometimes observed, causing a serious concern related to the emergence of psychiatric symptoms/syndromes following tryptamine exposure (Orsolini et al., 2017). Among tryptamines, AMT caused the highest number of fatalities in the UK with an overall amount of

7 fatalities between 2012 and 2013 (Schifano et al., 2016). 5-IT, a positional AMT isomer, appeared in the illicit market since 2012 and it exhibits both hallucinogenic and stimulant effects (Sanders et al., 2008). Recently, the tryptamine class has spread to another subclass of tryptamines called 'ergolines' which are derivatives of LSD (Tittarelli et al., 2015; ACMD 2014[a]). They produce effects similar to LSD as a result of their activity at the level of $5HT_{2A}$ receptors with subtle different potencies on cortical neurons. Some novel LSD derivatives include: LSZ (lysergic acid 2,4-dimethylazetidide), ETH-LAD (6-ethyl-6-nor-lysergic) and AL-LAD (6-allyl-6-nor-lysergic acid diethylamide). Clinical effects are similar to those produced by LSD and include: headache, nausea, hyperthermia, perceptual disturbances, distortions of body image, synaesthesia. Although the psychedelics' pharmacological mechanism of action has been widely debated over the years, the most commonly accepted theory involves the stimulation of serotonin $5HT_{2A}$ receptors on cortical neurons. The hyperactivation of these receptors, following psychedelic exposure, may affect cognitive and sensory information by disrupting the functioning of the cortico-striato-thalamo-cortical pathways, causing occurrence of aberrant feelings and altered perceptions (Rolland et al., 2014).

Piperazines

Piperazines belong to a wide class of chemical compounds that contain a core piperazine functional group. They are synthetic substances without natural counterparts, initially intended to be used as antihelminthic drugs but later researched as antidepressants (Nelson et al., 2014). Benzylpiperazines and phenylpiperazines are the main subclasses of piperazines used with recreational purposes. Among them the most common piperazines encountered are 1-benzylpiperazine (BZP), 1-methyl-4-benzylpiperazine,1-(3-trifluoromethylphenyl)piperazine (TFMPP), 1-(2-methoxy-phenyl)piperazine, 1-(3-chlorophenyl)piperazine (Iversen et al., 2014; Nelson et al., 2014). They have become popular on the online market to mimic Ecstasy effects as MDMA became forbidden. They may be found as constituents of capsules, pills, tablets, powders or liquids, under different brand names like: 'Rapture,' 'Herbal ecstasy', 'Legal X' (Iversen et al., 2014). They may also be present in preparations containing mixtures of piperazines (BZP/TFMPP) along with other drugs and especially stimulants (Nelson et al., 2014). Benzylpiperazines are monoamine releasing agents acting at the level of DAT, SERT, NET. In contrast, phenylpiperazines (e.g. TFMPP) act as serotonin releasers at the SERT and interact with serotonin receptors (likely responsible for their hallucinogenic effects), but have little effects on dopamine or norepinephrine pathways (Nelson et al., 2014). Among

piperazines, the onset, peak time, and duration of symptoms change considerably (Iversen et al., 2014). Overall, the most common reported side-effects are: anxiety, agitation, aggression, tremors, confusion, insomnia, appetite loss, nausea, psychosis, hallucinations, serotoninergic syndrome; while desired effects include MDMA-like effects (e.g. euphoria, disinhibition, pro-social effects, enhanced empathy and sociability) (Arbo et al., 2012; Schifano et al., 2015). Several BZP-related fatalities have been described with piperazines being found in post-mortem samples as causative agents or contributory factors (Nelson et al., 2014).

Pipradrol-derivatives

Pipradrol derivatives are synthetic stimulants that are typically sold as replacements for MDMA. Recreational use of pipradrol-derivatives was first detected in 2007 with a quick increase in popularity the year after. They are usually sold in powder form highly soluble in liquids and act as norepinephrine-dopamine reuptake inhibitors (NDRI), with some of them showing an additional releasing activity at these transporters (Simmler et al., 2014). Typical desired effects include: euphoria, sociability, increased energy, alertness and awareness; while untoward effects are: hypertension, tachycardia, sweating, tremors, insomnia, aggression, psychosis (Corkery et al., 2012).

Arylcyclohexylamines

The arylcyclohexylamine chemical class includes phencyclidine analogues **(**e.g. methoxetamine, ketamine, 3-MeO-PCP, 3-MeO-PCE and 3-MeO-PCPr) that have emerged as legal alternatives to phencyclidine (PCP). Common routes of administration include: oral, sublingual or nasal administration and when administered, produce hallucinogenic and highly dose-sensitive dissociative effects. These chemicals, similarly to PCP, act as NMDA receptor antagonists and SERT inhibitors. Positive effects include: perceptions enhancement, stimulation and dissociative effects; while side-effects consist of mania, delusions, psychosis and sensory suppressions (Roth et al., 2013).

Aminoindanes

The class of aminoindanes is represented by molecules that are based on the 2-aminoindane nucleus. According to the UNODC, the most commonly aminoindanes reported were 5-iodo-2-aminoindane (5-IAI), 5,6-methylenedioxy-2-aminoindane (MDAI) and 2-aminoindane (2-AI). Commonly sold over the Internet with brand names such as ‘Blurberrys’, ‘Champagne’ ‘gold’, ‘Groove-e’, ‘Pink’, are typically found as powder, capsules, tablets and may be ingested

or snorted (Schifano et al., 2016). Since 2010, aminoindanes became increasingly popular over the Internet as legal alternatives to MDMA and sought for their hallucinogenic, entactogenic and stimulant properties (Sainsbury et al., 2011; Coppola et al., 2013). Common sought-after effects are: hallucinations, euphoria, increased energy, increased libido and empathy; while untoward effects include nausea, vomiting, hypertension, hyperthermia, sweatiness, tremors, psychosis (Schifano et al., 2016). Some cases of fatalities consistent with a serotonin syndrome have occurred over the years with aminoindanes being identified at post-mortem. Specifically, in the UK, 3 fatalities related to MDAI alone or in combination with other drugs of abuse were reported (Corkery et al., 2013; Schifano et al., 2016). Recently, the pharmacological activity of 5-IAI and MDAI was studied using *in vitro* release assays in human embryonic kidney 293 cells (HEK 293) that highly express DAT, NET and SERT. According to this study, 5-IAI and MDAI, similarly to MDMA, were more potent SERT and NET inhibitors vs DAT inhibitors and both showed monoaminergic releasing activity at SERT. On the other hand, MDAI showed additional norepinephrine releasing properties while 5-IAI mediated additional dopamine releasing properties (Simmler et al., 2014). *In vitro* release assays in brain synaptosomes showed slightly different results with both MDAI and 5-IAI being more potent SERT and DAT vs. NET inhibitors (Johnson et al., 1991; Simmler et al., 2014). Differently from MDAI and MDMA, 5-IAI interacts with 5-HT_{2A} receptors, leading to hallucinogenic effects (Nichols et al., 2004). Drug discrimination studies in rats demonstrated that both 5-IAI and MDAI substituted for MDMA although they seem less neurotoxic (Nichols et al., 1991; Simmler et al., 2014). The comparable subjective effects of MDAI and MDMA are furthermore supported by users' reports (Corkery et al., 2013). Among aminoindanes, 2-AI exhibits a profile like BZP as it is a selective NET inhibitor with additional norepinephrine- and dopamine-releasing properties. Based on this profile it is a mild psychostimulant compared to MDMA.

Aminoalkylindoles

The fast-changing class of aminoalkylindoles (AAIs) comprises hundreds of CB_1/CB_2 agonists, often referred to as synthetic cannabinoids as they mimic the pharmacological actions of Δ9-tetrahydrocannabinol (Δ9-THC), the key psychoactive ingredient found in cannabis. The lead compound of this AAI class is the synthetic cannabinoid JWH-018 originally synthesized in 1995 in the laboratory of Clemson University (USA) for research purposes and subsequently marketed all over the world along with other synthetic cannabinoids (e.g. dybenzopirans, cycloesyphenols) as a psychoactive component of recreational smoking herbal products commonly known as 'Spice', 'Fire, 'Smoke', 'Yucatan', 'Skunk'. When compared to the

partial CB_1 agonist Δ9-THC, JWH-018 shows a full CB_1 agonistic activity with fourfold affinity (3.4 ± 0.6 nM) (De Luca et al., 2015). Euphoria, well-being, increased creativity, sense of relaxation, emotional alterations, sedation are the most common positive effects reported, while hallucinations, psychomotor agitation, aggressiveness, intense paranoia and psychotic episodes, are the typical side-effects linked to the aminoalkylindoles (Fattore and Fratta, 2011).

Chapter 2: Index compounds in the present PhD project

2.1) Synthetic cannabinoids

The history of synthetic cannabinoids (SCs) started in the 1960s when Raphael Mechoulam and his colleague Yehiel Gaoni, firstly identified and synthesized delta-9-tetrahydrocannabinol (Δ9-THC), the principal psychoactive compound in cannabis. Their discovery opened the door to the synthesis of a range of novel SCs chemically/pharmacologically related to Δ9-THC and potentially useful to provide new insights into the activities of the endogenous cannabinoid system. HU-210, widely known as the lead compound of the dibenzopyran group, was the first SC designed in Mechoulam's lab with the purpose of probing the endogenous cannabinoid system. Along this path, between 1970 and 1980 the cyclohexylphenol CP-55,940 was synthesized in Pfizer's laboratory and designed to target cannabinoid receptors. In the 1990s, the new chemical group of aminoalkylindoles was designed in John W. Huffman's laboratory, with WIN-55,212-2 and JWH-018 investigated as potential pharmacotherapies (Castaneto et al., 2014). Aware of the powerful psychoactive activities produced by these designer drugs, clandestine laboratories started synthesising a range of SCs illegally, kicking off the illicit trading of these drugs over the internet, smart shops, head shops, gas/petrol stations. In a few years, they became quickly popular as powerful/abusable psychoactive components of Spice drugs and for their undetectability in standard cannabinoid screening tests (EMCDDA, 2014).

2.1.1) Classification of synthetic cannabinoids

Starting in 2009, legal restrictions aimed at some SCs, promoted the synthesis of three subsequent generations of analogue replacements, purposefully added to herbal mixtures to emphasize the sought-after desired effects of Spice preparations (ACMD, 2009, 2012, 2014[b]; Pintori et al., 2017).

The first generation of SCs comprises compounds considered harmful according to the first round of control (enacted in 2009) under the Misuse of Drugs Act 1971 and includes: alkyl, alkenyl, cycloalkylmethyl, cycloalkylethyl derivatives of naphthoylindoles (e.g. JWH-018,

JWH-073, WIN-55,212-2); naphthylmethylindoles (e.g. JWH-075, JWH-084); naphthoylpyrroles (e.g. JWH-145, 146); naphthylmethylindenes (e.g. JWH-176); phenylacetylindoles (e.g. JWH-167, 203); cyclohexylphenols (CP-47,497); and dibenzopyrans (HU-210) (ACMD, 2009).

Over a couple of years, the second generation of synthetic cannabinoids appeared on the market and embraced all chemicals outside the scope of the 2009 control (ACMD, 2012), including compounds with haloalkyl side chains (e.g. AM-694, MAM-2201); with (N-methylpiperidin-2-yl)methyl side chains (e.g. cannabipiperidiethanone, AM-2233, AM-1220); Benzoylindoles (e.g. AM-679, 1-pentyl-3-(4-methoxybenzoyl)indole, pentyl-3-(2-methoxybenzoyl)indole); Adamantoylindoles (e.g. AM-1248, AB-001); 3-(2,2,3,3-Tetramethylcyclopropylcarbonyl)indoles (e.g. UR-144).

Since the SC market continued growing exponentially, in 2014 the ACMD proposed a revised generic control covering a wide number of third generation SC compounds chemically related to JWH-018, and showing specific modifications on its substructures (indole ring, pentyl substituent, methanone and naphthyl ring). Some controlled modifications include: substitution of the indole ring with indazole, imidazole, benzimidazole; replacement of the pentyl substituent with alkyl, benzyl, cycloalkylethyl; replacement of the methanone group with a carboxylate, ethanone, methylene bridge, carboxamide; replacement of the 1-naphthyl ring with adamantyl, benzoyl, cycloalkyl, quinolinyl, piperazinyl (ACMD, 2014[b]).

2.1.2) Third generation synthetic cannabinoids

BB-22

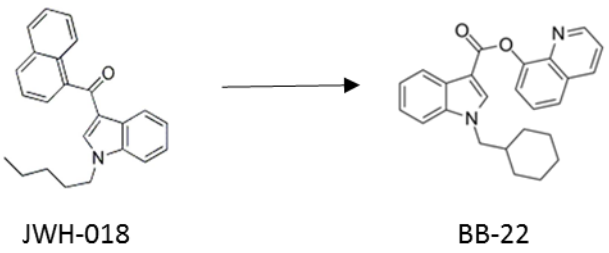

Figure 1: Chemical structures of JWH-018 and BB-22

BB-22 or 1-(cyclohexylmethyl)-1H-indole-3-carboxylic acid 8-quinolinyl ester) (see Figure 1) is a synthetic cannabinoid marketed online as a recreational drug whose popularity quickly

increased due to its powerful psychoactive effects that have been described as stronger compared to the parental compound JWH-018. The recreational use of BB-22 was first reported in Japan in 2013 (Uchiyama et al., 2013) and in a couple of years began spreading in the worldwide NPS market. Analytical investigations identified BB-22 in recreational herbal preparations commonly smoked by users seeking cannabis-like effects. Typical street names are "QUCHIC" or "VERTEX" and a range of emergency admissions in the UK has been recently reported (Abouchedid et al., 2017; De Luca et al., 2016).

Compared to JWH-018, BB-22 preserves the indole structure, shows replacement of the pentyl substituent with a cyclohexylmethyl group, substitution of the 1-naphthyl ring with a quinolinyl group and replacement of the methanone group with a carboxylate.

The extremely high CB_1 affinity, potency, dose-response efficacy of BB-22 may potentially concur for more severe psychoses (paranoia, hallucinations) and side-effects (agitation, tachycardia, anxiety, hypertension) compared to JWH-018, giving rise to even more worrying clinical concerns. Since 14th December 2016, BB-22 is a Class B drug under the Misuse of Drugs Act 1971. This makes it an offence to import, export, supply, possess, produce this drug without Home Office authorization (ACMD, 2016).

5F-PB-22

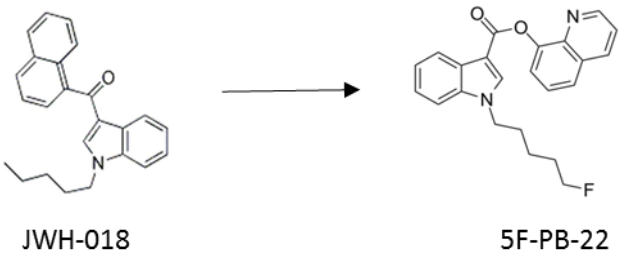

Figure 2: Chemical structures of JWH-018 and 5F-PB-22

5F-PB-22 or Quinolin-8-yl 1-pentyfluoro-1H-indole-3-8-carboxylate (see Figure 2) is a synthetic cannabimimetic showing slight chemical differences compared to BB-22. It is marketed as an herbal incense product and it is typically found as a component of herbal preparations alone or along with other analogues. Psychoactive effects (mood lift, increased energy and sociability) have been described as powerful and comparable to those produced by BB-22 (De Luca et al., 2016); while several toxicity events (Fujita et al., 2016) and deaths (Behonick et al., 2014) have been reported after its consumption alone or in combination with

other substances. Typical street names are ‘QUPIC’, ‘atomic bomb’, ‘black mamba’ (Pintori et al., 2017). Compared to JWH-018, 5F-PB-22 preserves the indole group, shows a fluorination on the pentyl tail, substitution of the 1-naphthyl ring with a quinolinyl secondary structure (similarly to BB-22), and replacement of the methanone group with a carboxylate (ester bond).

The ester bond featured by 5F-PB-22 (and BB-22 as well) may undergo *in vivo* hydrolysis reaction mediated by carboxylesterase enzymes, causing an accumulation of toxic metabolites that is not observed with compounds featuring a ketone group instead of the ester bond, like JWH-018 (Behonick et al., 2014). The accumulation of toxic metabolites may be one of the mechanisms underlying the extreme harmfulness that characterises quinolinyl carboxylate synthetic cannabinoids.

Since 14th December 2016, 5F-PB-22 is a Class B drug under the Misuse of Drugs Act 1971 (ACMD, 2016).

5F-AKB-48

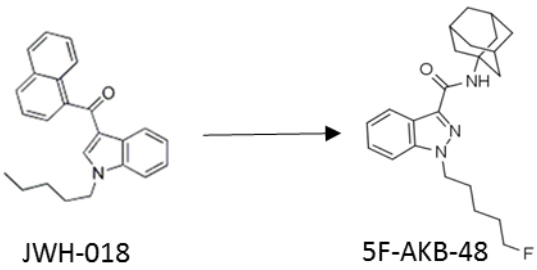

Figure 3: Chemical structures of JWH-018 and 5F-AKB-48

5F-AKB-48 or N-(Adamantan-1-yl)-1-(5-fluoropentyl)-1H-indazole-3-carboxamide (see Figure 3) is an indazole-based synthetic cannabinoid commonly contained in herbs often mixed with tobacco and smoked using bongs, joints and pipes. Common street names are: ‘5F-APINACA’, ‘Sweet Leaf C-Liquid’, ‘Aladin Legend 3rd Edition’, ‘Super snake green’, ‘Voodoo’, ‘Voodoo Gold’. The main routes of administration reported are smoking, oral, followed by inhalation and sniffing (World Health Organization, 2016).

Compared to JWH-018, 5F-AKB-48 shows a fluorination on the pentyl tail, substitution of the indole core with an indazole group, replacement of the 1-naphthyl ring with an adamantyl structure and substitution of the methanone group with a carboxamide.

Structurally, it is identical to AKB-48 except for a fluorination on the terminal carbon of the pentyl side chain. The presence of the indazole structure may promote 5-$HT2_A$ receptor dysfunction and cause hallucinations, psychosis and serotonin syndrome. Furthermore, the fluorination of the pentyl side chain may facilitate diffusion through the blood-brain barrier enabling rapid absorption of the compound (Schifano et al., 2015), and increase CB_1 receptor activity in the range of 2 to 5-fold higher compared to corresponding defluorinated analogues (Banister et al., 2015).

Overall, users describe 5F-AKB-48 as a very short-acting cannabinoid with a quick high, and rapid developing dependence. A range of side-effects has been reported such as tachycardia, agitation, panic attacks, nausea, vomiting, hallucinations, hypertension, psychosis, seizures; while withdrawal symptoms include chest pains, tachycardia, insomnia, paranoia. Since 14th December 2016, 5F-AKB-48 is a Class B drug under the Misuse of Drugs Act 1971 (ACMD, 2016).

STS-135

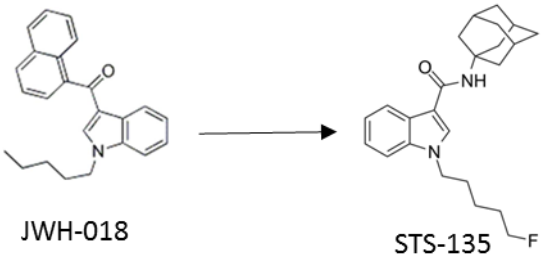

Figure 4: Chemical structures of JWH-018 and STS-135

STS-135 or (N-(adamantan-1-yl)-1-(5-fluoropentyl)-1H-indole-3-carboxamide (see Figure 4) is a psychoactive substance that originated in Thailand, typically found in herbal incense products and dried herbal preparations suitable for smoking. Liquid injectable formulations are also available along with dry powder formulations suitable for oral administration. Its common street name is '5F-APICA'.

Compared to JWH-018, STS-135 shows a fluorination on the pentyl tail, replacement of the 1-naphthyl ring with an adamantyl structure and substitution of the methanone group with a carboxamide. Structurally, it is identical to 5F-AKB-48 except for the presence of the indole group instead of the indazole ring.

The adamantyl-cannabinoids like STS-135, along with 5F-AKB-48, have been the most popular SCs marketed in the UK. However, they are still undetectable through conventional toxicology screening tests (Mcllroy et al., 2016).

STS-135 is rapidly metabolized with only 25% initial compound remaining after three hours of incubation with human hepatocytes. By high resolution mass spectrometry, about thirty-nine potentially active or toxic metabolites of STS-135 resulting from processes of monohydroxylation, dihydroxylation, trihydroxylation, with or without glucuronidation were isolated (Gandhi et al., 2015).

Compared to cannabis, the abuse of STS-135 has been associated with more serious side-effects and toxicity events in general. Reported cognitive effects include anxiety, paranoia, emotionality enhancement, psychosis, dream suppression; while physical effects comprise cardiovascular disturbances (myocardial infarction) typically observed with compounds with adamantyl moieties (Mcllroy et al., 2016).

According to its recognised potential to cause life-threatening conditions, since 14th December 2016, STS-135 has been classified as a Class B drug under the Misuse of Drugs Act 1971 (ACMD, 2016).

2.1.3) 'Spice' drugs

'Spice' drugs are herbal preparations that contain synthetically-derived compounds (synthetic cannabinoids) targeting CB_1 receptors. They were initially traded as legal alternatives to marijuana in Europe in the early 2000s, and they became quickly very popular. The term 'Spice', originally used as a brand name, is nowadays used as a generic term for SC preparations (Castaneto et al., 2014).

These products are suitable for smoking through traditional cigarette papers, cannabis pipes or electronic cigarettes; alternatively, they can be inhaled or consumed as infusions (Pintori et al., 2017). Brand names are quite curious and attractive (e.g. 'K2', 'Black mamba', 'Black magic smoke', 'Herbal Incense', 'Blue Berry Yum-Yum', 'Ace of Spades', 'Atomic bomb') aiming to capture the imagination and attention of millions of people of every age, race and gender (Corazza et al., 2014; Support Spice Addiction, 2017).

Their widespread distribution can be attributed to ingenious marketing strategies which typically adopt multi-coloured packaging and misleading labels intended to depict Spice drugs

as ‘safe’ herbal mixtures which are ‘not intended for human consumption’. Despite law enforcement and other regulatory efforts to curb their accessibility, commercial Spice products remain available on the web, fuelling illegal business activities and giving users the deceive idea that these drugs are ‘harmless’ and ‘natural’. Overall, the main reasons that drive SC use are their intense psychoactive effects; novelty attraction; accessible price and availability; lack of detectability in drug screening tests; legality and misperceived safety (Pintori et al., 2017).

Analysing the pharmacological analogies between SCs and Δ9-tetrahydrocannabinol (Δ9-THC), has been a subject of huge relevance in the scientific field. In this regard, in a variety of *in vitro* and *in vivo* assays, SCs have been described as showing higher binding affinity, potency and efficacy at CB_1 receptors compared to the partial agonist Δ9-THC (De Luca et al., 2016). Furthermore, metabolites of SCs may preserve higher CB_1 affinity compared to Δ9-THC explaining the increased mortality and toxicity events linked to SC use/abuse, compared to marijuana (Tai et al., 2014).

2.1.4) Epidemiology of synthetic cannabinoids

Over the past years, several epidemiological studies have been conducted on SC use, and especially three worldwide surveys have turned out to be of key importance to picture the SC user profile (Vandrey et al., 2012; Winstock and Barratt, 2013; Winstock et al., 2015; Castaneto et al., 2014).

The first one was carried out between 2011-2012 and included members from 13 different countries and 42 US states, mainly engaged from online web fora focusing on SCs. Only first-hand SC users from 18 years onwards, and English-speaking, were considered (168 out 391 individuals in total). Most of them turned out to be White men, with at least a high school education. The average age of first SC use was 26 years. The concomitant intake of alcohol or cannabis along with SCs, was frequently reported. Smoking followed by oral, rectal and vaporizing were the most typical routes of administration described, while the main reasons driving SC use were curiosity, sought-after desired effects, and positive drug test avoidance. About 15% of them experienced dependence and withdrawal effects (e.g. anxiety, irritability, depression) as a result of SC abuse (Vandrey et al., 2012; Castaneto et al., 2014).

The second worldwide survey was the ‘Global Drug Survey’ (GDS, 2012) that was conducted between November and December 2011 and it was widely advertised over the Internet and especially through social networking media (e.g. Facebook and Twitter). Overall, this survey

collected data from different countries including US, UK, Australia, Canada, Finland, Hungary, Ireland, Mexico, New Zealand, Japan, Poland and South Africa. Most respondents were White, males, with an average age of 26 years old.

Overall 14,966 participants responded, and 6.5% of them described themselves as recent SC users (last 12-month use). Among recent users, most of them were White, males, heterosexual, with an average age of 25 years, currently employed and typically living with their parents. The main countries of origin were US followed by UK. Among those who reported a recent use of SCs, the majority described a weekly frequency of use. Almost all recent SC users were previous natural cannabis users with the majority of them reporting to prefer cannabis over SCs because of the latter's untoward effects. On the other hand, the remaining ones, preferred using SCs for other reasons, such as cheapness, easy availability, recreational effects, undetectability in standard toxicological screening tests (Winstock and Barratt, 2013).

At the time of this survey just a very small number of participants was reported asking for emergency medical treatment following the use of SCs; however, two years after Winstock et co-authors found that, according to the data obtained from another online worldwide survey (with 22,289 respondents), the risk of asking for emergency medical treatment was 30 times lower for natural cannabis users compared to SC users (Winstock et al., 2015).

Additionally, more recent figures from the latest Global Drug Survey (GDS, 2017) demonstrated that the risk of seeking emergency medical treatment was higher in men compared to women with men over the age of 25 years old being most at risk. Notably, episodes of three or more withdrawal symptoms were recorded in people who have used SCs on at least 50 days in the last year. A total of 1240 last year SC users participated in this survey, and most of them obtained SCs from friends rather than online (GDS, 2017).

2.1.5) Social issues represented by synthetic cannabinoids and their effects

To date, several different SCs have been found widely differing in chemical structure, potency, and pharmacodynamics. The SC-based preparations themselves are herbal blends onto which potent SCs are sprayed (Fattore and Fratta, 2011). The acute adverse symptoms reported after use of SC products are tachycardia, agitation, anxiety, psychosis, vomiting and seizures (Castellanos and Thornton, 2012; Hoyte et al., 2012).

Recent studies demonstrated the higher health risks caused by SCs compared to cannabis according to their distinct pharmacodynamics which may contribute to the observed toxicity.

Additionally, the interactive effects resulting from multi-compound formulations and their active metabolites, highpoint the intrinsic threat related to the use of these substances (Schifano et al., 2015). Ready-to-use drug formulations generally contain a couple of grams of herbal material such as '*Leonotis leonurus'*, commonly known as 'wild dagga', and '*Pedicularis densiflora'* typically advertised as 'Indian warrior' (Zuba et al., 2011). The herbal-based substrate gives the users the false feeling they are consuming a 'safe' and 'natural' product, without realising the powerful and dangerous effects of SCs laced with the plant material (Seely et al., 2012). To synthetise these preparations, SCs are first dissolved in ethanol or acetone and then mixed with plant material. Once the solvent evaporates, variable concentrations of these toxic drugs result laced with herbal material suitable for smoking (Fattore and Fratta, 2011). Compared to marijuana, SCs are extremely cheap, widely available, and particularly attractive for young users who want to experience cannabis-like effects, but are concerned of legal/social repercussions (Vandrey et al., 2012). Overall, Spice use is a serious public health threat, especially since several clinical reports demonstrated it can cause acute cardiovascular and central nervous system toxicity (Gunderson et al., 2012).

The public health concern caused by these drugs gave rise to several regulations in most European countries and in the U.S. where the most popular SCs were classified into the Schedule 1 drugs under the Controlled Substances Act of the Drug Enforcement Administration (Fantegrossi et al., 2014). Although the research around SCs is quite challenging, it is also continuously evolving, and several testing laboratories started relying on analytical applications to assess SCs in human samples (Lovett et al., 2013). Considering the wide popularity of SC abuse around the world, a preclinical characterisation of these compounds is needed; additionally, a full understanding of their pharmacological, pharmacodynamical and toxicological properties is necessary. Particularly, these findings will support public health and administrative activities willing to draft a health impact profile for these drugs (Seely et al., 2012).

2.1.6) Pharmacology of synthetic cannabinoids, focus on their effects on the reward circuit

Most SCs identified in herbal blends have higher binding affinity at the CB_1 receptor compared to Δ9-tetrahydrocannabinol (Δ9-THC), and greater affinity at the CB_1 compared to the CB_2 receptor. The CB_1 receptor is the major subtype found in the brain, but it also occurs in the peripheral nervous system, and in organs such as the heart, lung, liver, in the vascular endothelium and reproductive system (Castaneto et al., 2014; Howlett et al., 2002). On the

other hand, CB_2 receptors are mainly expressed in the immune system, while their expression in the central nervous system is minimal and significantly lower than CB_1 receptors (Onaivi et al., 2008; Castaneto et al., 2014).

The CB_1 receptors may be activated by endogenous (anandamide and 2-arachidonoylglycerol) and exogenous cannabinoids (e.g. Δ9-THC, and SCs). Physiologically, the endocannabinoids play important roles in the regulation of synaptic brain functions as they may act as 'retrograde messengers' in various brains regions (e.g. NAc and ventral tegmental area) by activating CB_1 receptors located in the presynaptic terminals and promoting a cascade of events such as: changes in calcium influx and potassium efflux, presynaptic hyperpolarisation, and reduction in neurotransmitter release (Alger, 2002; Wilson, 2002; Howlett et al., 2010) (see Figure 5, panel A). On the other hand, exogenous SCs directly interact with CB_1 receptors enabling similar mechanisms (see Figure 5, panel A) (Ameri, 1999).

It is likely that positive effects promoted by SCs (e.g. pleasure, euphoria, increased energy and sociability, relaxation, talkativeness) are mediated by activation of CB_1 receptors located in the brain reward circuit (Gardner, 2002).

This central neuronal circuit originates from a structure of the mesencephalon (ventral tegmental area) containing dopaminergic neurons, whose terminals interact with GABAergic medium spiny neurons located in the ventral striatum or NAc (area of the limbic forebrain) and glutamatergic neurons located in the frontal cortex. The ventral tegmental area (VTA) also contains GABAergic neurons which project to the NAc and the prefrontal cortex or locally target DA neurons through axon collaterals. Furthermore, the VTA receives glutamatergic projections from the amygdala, medial prefrontal cortex, pedunculopontine nucleus, and the subthalamic nucleus, while NAc sends axonal projections to the ventral globus pallidum (VP). Overall, the VTA, NAc, and VP are interconnected through reciprocal axonal projections whose functional integrity is crucial to observe drug-related reward behaviour in self-administration studies (Lupica et al., 2004).

It is possible that SCs, similarly to Δ9-THC, act upon the central drug reward circuit increasing DA release in the target regions of the VTA DA neurons (Di Chiara and Imperato, 1988). To study the activity of SCs on the reward system, researchers usually refer to Δ9-THC as an element of comparison.

Previous preclinical microdialysis studies in freely moving rats demonstrated the ability of Δ9-THC to increase DA release in the NAc after intravenous administration. This increase was reversed through three different methods: eliminating the calcium from the dialysate; blocking sodium channels with administration of tetrodotoxin; antagonising opioid receptors with systemic administration of naloxone (Chen et al., 1990). A subsequent study demonstrated that the synthetic cannabinoid WIN-55,212-2, similarly to Δ9-THC, enhances DA function in the NAc and this effect was reversed antagonising either CB_1 receptors with systemic administration in the VTA of SR141716A, or opioid receptors with the infusion in the VTA of the antagonist naloxone. Overall, these data demonstrated that, similarly to other abused drugs, SCs can increase DA release in the NAc through mechanisms critically dependent on action potentials and calcium activity, but also demonstrated that opioid and cannabinoid systems interact somehow in the reward circuit (Lupica et al., 2004). In particular, it is likely that cannabinoids may promote the opioidergic inhibition of GABA release onto DA neurons, suggesting a CB_1-mediated disinhibitory mechanism (see Figure 5, panel B) (Lupica et al., 2004).

Additional electrophysiological studies (single unit recordings) in rodents (Gessa et al., 1998) and in brain slices containing VTA (Cheer et al., 2000), demonstrated that Δ9-THC and synthetic cannabinoids such as WIN-55,212-2, HU-210, and CP-55,940 may cause an increase of the DA neuron-firing rate and DA neuron burst activity in the VTA with consequent enhancement of terminal release of DA in the NAc (see Figure 5, panel B). These effects were reversed either with the CB_1 receptor antagonist SR141716A (confirming an involvement of CB_1 receptors) or with the $GABA_A$ receptor antagonist bicuculline, suggesting a disinhibitory mechanism mediated by CB_1 receptors similar to that observed for opioid receptors (Gessa et al., 1998, Cheer et al., 2000).

This hypothesis was furthermore supported by the ability of WIN-55,212-2 to decrease electrically evoked inhibitory postsynaptic currents (IPSCs $GABA_A$ -mediated) in brain slices containing the VTA, suggesting an activation of CB_1 receptors present on GABAergic neuron terminals of the VTA, which was antagonised by the CB_1 antagonist SR141716A (Szabo et al., 2002; Lupica et al., 2004).

Overall, SCs are thought to modulate the activity of GABAergic projections originating in the NAc and targeting $GABA_B$ receptors located on VTA DA neurons, and the activity of

GABAergic neurons within the VTA that target $GABA_A$ receptors on VTA DA neurons (see Figure 5, panels B and C) (Lupica et al., 2004).

Both the observed presynaptic inhibition of neurotransmitter release (Hoffman and Lupica, 2000) and the high concentration of CB_1 receptors in GABAergic terminals of the central nervous system helped to characterise the effects of synthetic cannabinoids at the level of the reward circuit (Freund et al., 2003).

Furthermore, part of the rewarding actions of the SCs are mediated by actions occurring within the NAc, where these drugs are thought to reduce GABA release from intrinsic interneurons onto medium spiny neurons, producing a disinhibition of this GABAergic output to the VTA and other brain structures. Additionally, SCs can inhibit excitatory input from the prefrontal cortex onto GABA neurons by activation of CB_1 receptors in the glutamatergic terminals thereby decreasing the inhibition of DA neurons in the VTA (see Figure 5, panel B) (Robbe et al., 2001).

Overall, these observations highlighted the relative contributions of complex neuronal circuits, either within or outside the VTA (e.g. intrinsic and extrinsic GABAergic, glutamatergic, opioidergic pathways), whose modulation interferes with the interactions between cannabinoids and DA neurons and represent critical pathways accounting for some of the rewarding properties of cannabinoid exposure (Lupica et al., 2004).

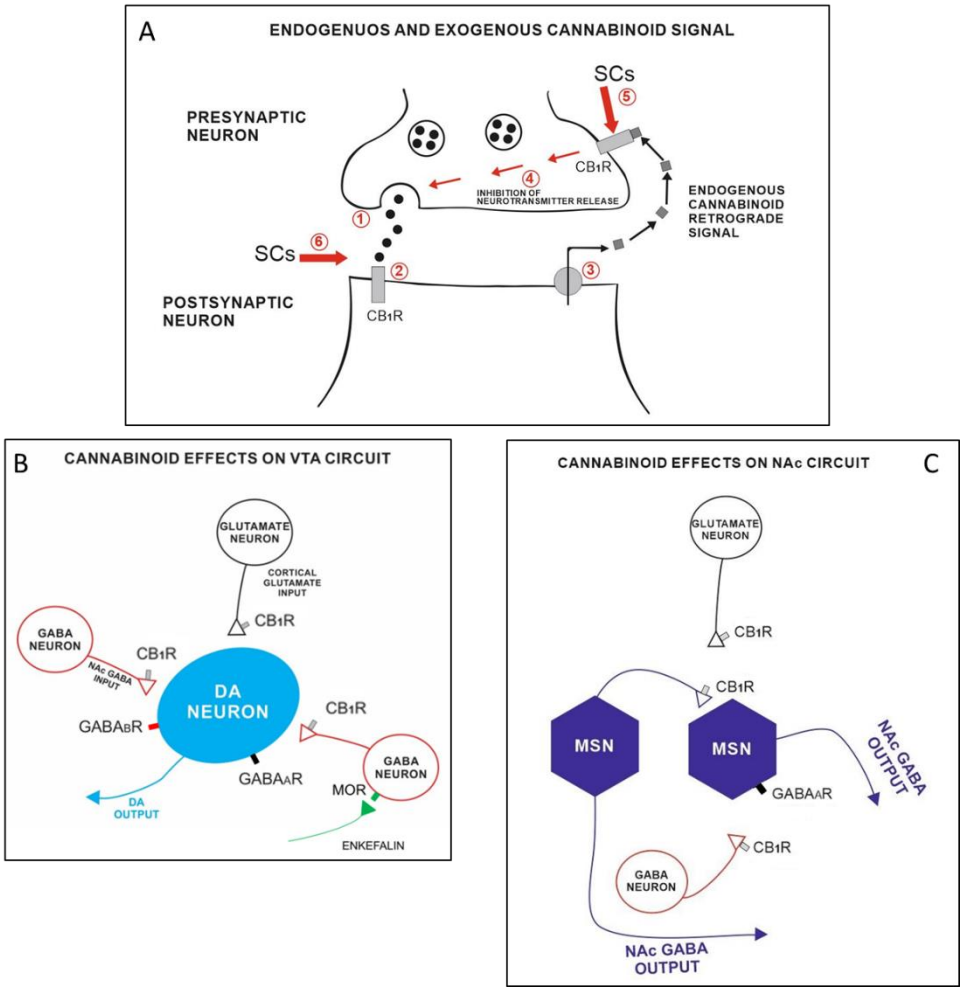

Figure 5: Cannabinoid signal in the brain. Panel A: The mechanism of action of cannabinoids and the multi-step retrograde signalling pathway. 1) neurotransmitter is released from vescicles within the presynaptic neuron; 2) the postsynaptic CB_1R is activated and endocannabinoids are synthesised and released; 3) the endogenous CB_1R ligand diffuses back and activates the presynaptic CB_1R; 4) activation of the presynaptic CB_1R results in inhibition of neurotransmitter release; 5 and 6) SCs directly activate CB_1 receptors and enhance the function of the cannabinoid system (this picture was adapted from Ware et al., 2008). Panel B: Simplified schematic demonstrating cannabinoid actions in the VTA. Panel C: Simplified schematic demonstrating cannabinoid actions in the NAc (These pictures were adapted from Lupica et al., 2004).

2.1.7) Synthetic cannabinoids and pharmacodynamics

According to recent pharmacodynamical studies, the majority of SCs detected in herbal products possess higher affinity, efficacy and lower K_i values compared to the natural partial CB_1 agonist Δ9-THC (Castaneto et al., 2014; De Luca et al., 2015).

The pharmacodynamic properties of some Spice components have been recently fully investigated in rat cortical membranes using the radio-labelled competition binding assay (De Luca et al., 2016). The cortical brain area has been selected as target cerebral region as it exhibits a high expression of CB_1 receptors and a negligible presence of CB_2 receptors (Pertwee, 2005).

According to these studies, JWH-018 fully inhibited the specific binding of [^{3}H]CP-55,940 with a K_i of 3.4 ± 0.6 nM. On the other hand, the K_i values of BB-22 (0.11 ± 0.03 nM), 5F-PB-22 (0.13 ± 0.01 nM), 5F-AKB-48 (0.87 ± 0.14 nM) and STS-135 (1.93 ± 0.18 nM) were significantly lower compared to the first-generation SC JWH-018. According to these results, the rank order of CB_1 receptor affinity was as follows: JWH-018< STS-135<5F-AKB-48< BB-22=5F-PB-22 (De Luca et al., 2016).

Additionally, all molecules showed high potency at the level of CB_1 receptors, with BB-22 and 5F-PB-22 showing EC_{50} values (2.9 ± 0.6 and 3.7 ± 0.6 nM) significantly lower than JWH-018 (20.2 ± 1.3 nM), while no differences were observed compared to STS-135 (32.3 ± 2.9 nM) and 5F-AKB-48 (31.0 ± 7.5 nM). As regards to the efficacy (E_{max}), BB-22, 5F-PB-22 and 5F-AKB-48 exhibited higher efficacy (217 ± 4; 203 ± 2; 190 ± 11% over basal) compared to JWH-018 (163 ± 3% over basal) and STS-135 (168 ± 9% over basal) (De Luca et al., 2016). Overall, all SCs tested stimulated in a concentration-dependent and saturable way [^{35}S]GTPγS binding, with BB-22 and 5F-PB-22 producing a greater stimulation compared to WIN-55,212-2 (De Luca et al., 2016). This effect was reversed by the CB_1 receptor antagonist/inverse agonist AM-251, suggesting the involvement of the activation of G-proteins paired with CB_1 receptors.

In another study [^{35}S]GTPγS binding assay was repeated in CB_1 knockout mice, using the same SCs and no activation of G protein was observed. These findings confirmed the involvement of the CB_1 receptor in G protein stimulation (De Luca et al., 2016).

2.2 Pipradrol-derivatives

Desoxypipradol (2-DPMP)

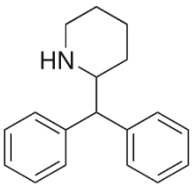

Figure 6: Chemical structure of 2-DPMP

Desoxypipradrol, also known as 2-diphenylmethylpiperidine (2-DPMP) (see Figure 6), is chemically related to methylphenidate and pipradrol and shares with them a similar pharmacology. It is a highly lipophilic molecule with longer duration of action when compared to most psychostimulants of the same class. The absence of polar functional groups, usually targeted by metabolic enzymes, accounts for its long elimination half-life and persistent activity after use. Initially developed by the pharmaceutical company CIBA for research in the application of narcolepsy and ADHD (Attention deficit hyperactivity disorder) (Tripod et al., 1954), it was quickly replaced with the short acting compound methylphenidate and researched for alternative applications, such as promotion of recovery from anaesthesia, but without success (Bellucci, 1955).

Starting from 2008, the popularity of 2-DPMP and its availability for purchase dramatically increased in the UK. Originally marketed under the brand name of 'Ivory Wave', 'Whack', 'Lunar Wave' as a white crystal powder with a purity of up to 99.9%, quickly spread over the internet, head shops, smart shops, causing several accidents and emergency admissions. The most typical used routes of administration were: oral, insufflation, injection, rectal with dosages ranging from 1-10 mg depending on the route used (Corkery et al., 2012). Toxic symptomatology was characterised by long-lasting agitation (lasting up to five days) sometimes requiring physical restraint, hallucination, paranoia, psychosis, muscle spasms. Numerous emergency room toxicology reports led to the decision to classify Desoxypipradrol as a Class B drug in the UK under the Misuse of Drugs Act, 1971 on 13 June 2012 (Home Office, 2012).

Diphenylprolinol (D2PM)

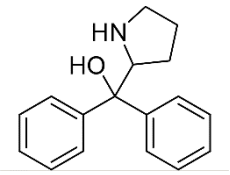

Figure 7: Chemical structure of D2PM

Diphenylprolinol also known as D2PM or diphenyl-2-pyrrolidin-2-yl-methanol (see Figure 7), is a pyrrolidine analogue of pipradrol, sold primarily over the Internet and found in Ecstasy tablets as replacement for MDMA. Recreational use of D2PM started in March 2007, but only developed slowly, achieving a peak in spring 2011 with several Emergency Department admissions recorded. It was typically marketed as 'head candy' and described as an odourless crystalline powder easily soluble in liquids and with high purity levels (e.g. ≥98%). The most typical used route of administration was rectal followed by snorting and oral (Corkery et al., 2012). Following several reports of acute toxicity and fatalities related to its use, Diphenylprolinol was classified as a Class B drug in the UK under the Misuse of Drugs Act, 1971 on 13 June 2012 (Home Office, 2012).

2.2.1) Pharmacological studies on 2-DPMP and D2PM

From a pharmacological point of view, 2-DPMP and D2PM may act as potent DAT and NET inhibitors with a weak activity at the level of SERT. The activity at the NET, DAT, SERT was evaluated in human embryonic kidney 293 cells (HEK 293) that highly and stably express these transporters. Initially the cells were incubated with increasing concentrations of either 2-DPMP or D2PM (10^{-10}-10^{-3}M) for 10 minutes, then DA, NE, 5-HT tritiated were added to the buffer in order to promote uptake transport of labelled monoamines for another ten minutes. The uptake was then blocked by separating the cells from the buffer through rapid centrifugation. Afterwards, the tubes were frozen, the cell pellet was isolated from the essay buffer layers, and scintillation fluid was added in order to count the radioactivity in a beta-counter. Specific uptake was assessed by subtracting the non-specific uptake (determined in the presence of nisoxetine for NET cells, mazindol for DAT cells, fluoxetine for SERT cells) from the total counts. The IC_{50} values were then calculated and the DAT/SERT ratios were established to predict the psychoactive properties of these substances. Higher activity at the DAT may indicate a higher abuse potential, while greater potency at SERT may predict MDMA-like effects with lower abuse potential. Overall, according to this study, the pipradrol derivatives 2-

DPMP and D2PM, were more potent DAT and NET vs. SERT inhibitors. IC_{50} values for 2-DPMP were as follows: 0.04 µM for DAT, 0.14 µM for NET and >10 for SERT, while IC_{50} values for D2PM were 0.86 µM for DAT, 0.41 µM for NET and 38 µM for SERT (Simmler et al., 2014).

In another study, the effects of 2-DPMP and D2PM (100 mM) on transporter-mediated NE, 5-HT, and DA release were assessed in HEK 293 cells. Briefly the cells were preloaded with NE, DA, 5-HT tritiated and release was evaluated by adding release buffer containing either 2-DPMP or D2PM (100 mM). After 15 minutes for serotonin and dopamine cells, and 45 minutes for norepinephrine cells, an adequate amount of radioactivity was released and a comparison with controls was made. The negative control conditions were assessed using nisoxetine (NET cells), mazindol (DAT cells) and citalopram (SERT cells). The release was stopped by removing the buffer and washing the cells twice with fresh buffer. The radioactivity was then quantified and the compounds showing greater monoamine release compared to the respective transporter inhibitors, were considered monoamine releasers. Overall, according to this study, the pipradrol derivatives 2-DPMP and D2PM were not substrate releasers at the level of monoaminergic transporters (Simmler et al., 2014).

Furthermore, another *in vitro* study demonstrated the ability of 2-DPMP to stimulate evoked dopamine efflux in NAc brain slices to a greater extent compared to cocaine. Briefly, rat brain slices from the NAc core were exposed to cocaine or 2-DPMP for 60 minutes, and then DA release was evoked and recorded using Fast Scan Cyclic voltammetry (FSCV). According to this study 2-DPMP (1, 3 or 10 µM) increased evoked DA efflux and slowed DA reuptake to a greater extent compared to cocaine at the same doses. Specifically, the increase of evoked DA efflux was two-fold higher, while the inhibition of DA reuptake was 3-fold higher compared to cocaine.

These data suggested that 2-DPMP stimulated evoked DA efflux without releasing activities in a more potent way than cocaine, and this mechanism accounts for its psychotogenic effects (Davidson and Ramsey, 2012).

2.2.2) Social issues represented by 2-DPMP and D2PM and their effects

According to some user fora reports, the effects of 2-DPMP start within one hour and may last up to 48 hours (ACMD, 2010), while desired psychoactive effects of D2PM begin after 15 minutes and may last up to 10 hours. The sought-after effects of the pipradrol-derivatives are

similar to those of other stimulants and include euphoria, stimulation, increased energy, alertness, arousal, disinhibition; while untoward effects are anxiety, agitation, aggression, paranoia, psychosis, delusions, tachycardia, sweating, hypertension, hyperthermia, headache, chest pain, tremors (Corkery et al., 2012). In 2010, the biological samples of 19 patients who presented to an Edinburgh ED with untoward psychiatric effects after using 'Ivory Wave', tested positive for 2-DPMP (James et al., 2011; Corkery et al., 2012). Recently Wood et al. (2012) reported a case series of five individuals, aged between 21 and 33 years old, showing long-lasting psychiatric symptoms, agitation, anxiety, aggression and insomnia lasting up to 24-96 h after ingestion. All urine samples were tested positive for D2PM (Wood et al., 2012; Corkery et al., 2012). Another study reported a case of a male patient, with no risk factors for ischemic heart disease, complaining of chest pain following the ingestion of two units of 'Head Candy'. Blood and urine analyses detected the presence of D2PM and glaucine (Lidder et al., 2008; Wood et al., 2008). Additionally, in August 2010, three cases of fatalities were linked in the UK to 2-DPMP use (Corkery et al., 2012).

2.3) 5-(2-Aminopropyl)indole (5-IT)

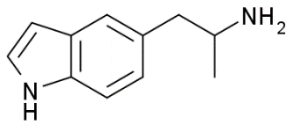

Figure 8: Chemical structure of 5-IT

2.3.1) Social issues represented by 5-IT and its effects

5-(2-Aminopropyl)indole (5-API or 5-IT) (see Figure 8) is a tryptamine derivative considered particularly harmful because of its side-effects. It is a positional isomer of alpha-methyltryptamine (AMT) and a substituted phenethylamine with stimulant and hallucinogenic properties.

In 2012, an overall number of 21 fatalities (15 in Sweden, 2 in Hungary and 4 in the UK) occurred with 5-IT being found in biological samples alone or in combination with other drugs of abuse (e.g. 5-APB, MDMA) or medications (Seetohul and Pounder, 2013; EMCDDA, 2014). Additionally, numerous toxicity events consistent with sympathomimetic toxidromes have been linked to 5-IT (EMCDDA, 2014). Originally developed for research purposes, it has

been recently diverted to the illicit market as a 'MDMA' replacement and improperly advertised as 'benzofury' or 'ecstasy' (Seetohul and Pounder, 2013). Overall, 5-IT detection was reported in several countries including United Kingdom, Denmark, Finland, Germany, Hungary, the Netherlands, Sweden and Norway (EMCDDA, 2014). Powders, tablets and capsules were the most described physical forms for 5-IT; while ingestion, insufflation were the most typical ROAs used, although injection occurred as well. Side-effects linked to 5-IT include tachycardia, hyperthermia, hypertension, agitation, anxiety, disorientation (Herraiz and Brandt, 2014).

2.3.2) Pharmacological studies on 5-IT

A recent study confirmed that the clinical effects of 5-IT partly result from selective and reversible inhibition of monoamine oxidase, type A (MAO_A), enzymes which ultimately may contribute to increase the levels of monoamine in the synaptic cleft and account for serotoninergic/catecholaminergic effects. The effect of 5-IT on human MAO_A and MAO_B isozymes was assessed by monitoring the conversion of the kynuramine substrate in 4-hydroxyquinoline using high-performance liquid chromatography (HPLC). According to this study, 5-IT was able to fully inhibit MAO_A with high potency (IC_{50}=1.6 μM and K_i=0.25μM) while MAO_B inhibition was not detected (Herraiz and Brandt, 2014). A more recent study demonstrated the additional role played by 5-IT in potentiating serotonergic/monoaminergic effects, by coupling MAO_A inhibition with monoamine releasing activity. The monoamine releasing properties of 5-IT were monitored using *in vitro* release assays in brain synaptosomes prepared from rat striatum for DAT, and obtained from the entire rat brain except striatum and cerebellum, for SERT and NET (Marusich et al., 2016). For release assay procedures synaptosomes were pre-loaded with the labelled DAT/NET substrate ($[^3H]MPP^+$), and with $[^3H]$serotonin for SERT. Reserpine was added in the buffer to block vesicular uptake of labelled substrates and unlabelled inhibitors were added to block uptake by competing transporters. Release assays were promoted incubating pre-loaded synaptosomes with the test drug for 30 minutes for DAT and NET studies or for 5 minutes for SERT studies. Then release was stopped using vacuum filtration and radioactivity was measured by liquid scintillation counting (Marusich et al., 2016). According to this study 5-IT mediated full efficacy releasing activity with 8-fold selectivity for DAT (EC_{50} 12.9 ± 1.5 nM) and NET (EC_{50} 13.3 ± 1.8) compared to its activity at SERT (EC_{50} 104.8 ± 18.2 nM) and higher selectivity for DAT (13-fold) and NET (7-fold) compared to MDMA. Overall, this compound seems to act similar to MDMA, mephedrone, methylone and BZP, while behaving differently to other cathinones like

MDPV and pyrovalerone, which are pure monoaminergic transporter inhibitors without releasing properties. As previously observed with other drugs of abuse, the high selectivity for DAT/NET versus SERT accounts for the high abuse potential of 5-IT in humans and animals (Banks et al., 2014; Negus and Miller, 2014).

2.4) Aminorex derivatives: focus on 4,4'-DMAR

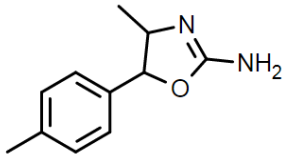

Figure 9: Chemical structure of 4,4'-DMAR

This class includes a range of molecules chemically related to the parent compound aminorex that retain the primary amine function and show some modifications of the phenyl ring. 4-methylaminorex (2-Amino-4-methyl-5-phenyl-2-oxazoline) and aminorex (2-amino-5-phenyl-oxazoline) were both first synthesized by McNeil Laboratories in the 1960s and introduced as prescription drugs for weight loss in Europe in 1965 (Poos et al, 1963; Carson et al., 1965). Because of serious adverse effects and fatal complications reported (Follath et al., 1971; Gurtner et al., 1985), aminorex and 4-MAR were classified under schedule 1 of the Misuse of Drugs Act 1971. From a pharmacological point of view, aminorex derivatives are monoamine-releasing agents that display high potency at all three monoamine transporters (DAT, SERT, NET), producing typical stimulant effects (e.g. increased energy, euphoria, sociability) and monoaminergic toxicity (hypertension, hyperthermia, tremors, sweatiness, cardiovascular disturbances). Recently the novel aminorex derivative 4,4'-DMAR (4-methyl-5-(4-methylphenyl)-4,5-dihydrooxazol-2-amine) (see Figure 9) has emerged in the illicit drug market as a popular drug of abuse, gaining the attention of people looking for some MDMA legal alternatives. 4,4'-DMAR is an oxazoline derivative which can be found as (±)-cis or (±) trans isomer, with the former one being involved in many deaths (Brandt et al., 2014).

Since 2012, the popularity of this drug quickly spread from the Netherlands to other countries including United Kingdom, Denmark, Finland, Romania, Poland, Sweden with a preferential availability in the Hungarian drug market (EMCDDA and Europol, 2014). Powders with curious and attractive multi-coloured packaging, or tablets in all sorts of shapes, sizes and

colours were the most typical formulations found for 4,4'-DMAR. Sometimes, mislabelling such as 'ecstasy' or 'amphetamine' was adopted in the packaging to highlight the similarity of 4,4'-DMAR preparations to traditional drug products in terms of psychoactive effects. Typical alternative brand names used for these preparations were 'Speckled Cherry' or 'Speckled Cross', and the presence of 4,4'-DMAR alone or mixed with other stimulants (e.g. synthetic cathinones, benzofurans) was analytically confirmed (EMCDDA and Europol, 2014). According to some fora reports, the most widely used routes of administration were nasal insufflation and ingestion, followed by inhalation and injection, while commonly reported desired effects included: euphoria, disinhibition increased energy and confidence (ACMD, 2014[c]; EMCDDA and Europol, 2014; Loi et al., 2017).

As a result of serious adverse effects and fatalities reported, this drug was classified under schedule 1 of the Misuse of Drugs Act 1971 (ACMD, 2014[c]) and then it was internationally controlled under schedule 2 of the Convention on Psychotropic Substances of 1971 (UNODC, 2016).

2.4.1) Pharmacological studies on 4,4'-DMAR

Recently, the pharmacological activity of 4,4'-DMAR was studied using *in vitro* release assays in brain synaptosomes. For release assay procedures synaptosomes were pre-loaded with the labelled DAT/NET substrate ([^{3}H]MPP+), and with [^{3}H]serotonin for SERT in Krebs-phosphate buffer for one hour (steady state). Reserpine was added into the buffer to block vesicular uptake of labelled substrates and unlabelled inhibitors were added to inhibit uptake by competing transporters. Release assays were promoted incubating pre-loaded synaptosomes with the test drug. Then release was stopped using vacuum filtration and radioactivity was measured by liquid scintillation counting. According to this study, (±)cis-4,4′-DMAR acted as a monoamine-releasing agent at the level of DAT, SERT, NET and showed greater potency at the SERT and similar potency at the DAT and NET compared to aminorex and d-amphetamine (Brandt et al., 2014). In another recent study the monoamine-releasing activity of both isomers (±)cis-4,4'-DMAR and (±)trans-4,4'-DMAR was compared to that of MDMA in rat brain synaptosomes using the same procedure. According to this study, both racemates exhibited a greater potency at the DAT and NET compared to MDMA, while (±)cis-4,4'-DMAR acted as a fully effective releasing agent at the SERT and (±)trans-4,4'-DMAR acted as a pure serotonin transporter inhibitor without releasing properties (McLaughlin et al., 2015).

2.4.2) Social issues represented by 4,4'-DMAR and its effects

Since October 2013, several fatalities have occurred with 4,4'-DMAR being found alone or along with other recreational drugs (e.g. cocaine, amphetamines, cannabis) and/or prescribed medications (benzodiazepines, antidepressants, second-generation antipsychotics, opioids) at post-mortem (ACMD, 2014[c]). Specifically, 47 deaths have been recorded up to date, with 38 of them being reported in the UK, 1 in Poland and 8 in Hungary (ACMD, 2014[c]; EMCDDA and Europol, 2014). Notably, the decrease in fatalities observed in 2015 likely occurred because of its legal restriction and as a result of a decreasing number of people using it because of its adverse effects (Corkery, 2016; Loi et al., 2017).

Non-fatal toxicity events were characterised by agitation, confusion hyperthermia, muscular spasm, seizures, cardiac and respiratory arrest, convulsions, unconsciousness, aggression and paranoia. The 4,4′-DMAR activity on catecholamine transporters may account for these side-effects that may be exacerbated if the molecule is concomitantly used with compounds acting on similar targets, increasing the risks of serotoninergic syndrome or catecholaminergic toxidrome (McLaughlin et al., 2015; Loi et al., 2017).

2.5) Dieting aid compound 2,4-DNP

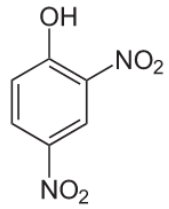

Figure 10: Chemical structure of 2,4-DNP

2,4-DNP (see Figure 10) is an organic compound extensively used as a dieting aid from 1933 to 1938 according to its ability to increase basal metabolic rate; accelerate gluconeogenesis and glycolysis and promote fat mobilization (Tainter et al., 1933 and 1934). During the 1930s, it was advertised as a safe medication and it was commercialised without prescription (Tainter et al.,1933 and 1934); as a result, between 1933 and 1935 about 100,000 patients (mostly women) took 2,4-DNP. Capsules containing about 100 mg of 2,4-DNP were generally ingested 1-3 times per day, depending on the desired total dose (Tainter et al., 1933 and 1934). This compound was particularly attractive because, apparently, it was able to promote fat and carbohydrates breakdown, without causing proteolysis (Cutting et al., 1933). The diffusion

occurred despite the concerns raised by the Council on Pharmacy and Chemistry related to the potential toxicity of this compound (Council on Pharmacy and Chemistry, 1935). Because of several episodes of toxicity and fatalities, this drug was banned in 1938 by the Food and Drug Administration (FDA) in the U.S. (Parascandola et al., 1974; Kurt et al., 1986). Additionally, in 2003 the UK Food Standard Agency declared DNP as 'not for human consumption' (Food Standard Agency, 2003); and in 2015 INTERPOL issued a global alert for potential lethal illicit diet drugs, including 2,4-DNP (INTERPOL, 2015).

Despite legal restrictions, 2,4-DNP continues to be illegally marketed through the internet as a supplement for weight reduction, gaining popularity among bodybuilders, athletes and young males and females (Lee et al., 2014). Usually sold in the form of a yellow and crystalline powder, tablets or pills, is typically ingested by users (Cutting et. al, 1933).

2,4-DNP is highly toxic because it is rapidly absorbed by all routes of administration: swallowing, inhalation, skin and eye contact. Dermal exposure has been described as the most common route of unintentional exposure (Grundlingh et al., 2011) resulting from 2,4-DNP use in the manufacturing of dyes, fungicides, photographic developers and insecticides (Parascandola et al., 1974). By contrast, the oral route is currently the most common route of conscious exposure. According to previous studies, 2,4-DNP's half-life ranges from 3 hours (Korde et al., 2005) to 5–14 days (Hsiao et al., 2005).

The toxicity of 2,4-DNP is related to its ability to affect cellular energy production by increasing the proton conductance of the mitochondria with conversion of the energy released as heat and resulting thermogenesis (Harper et al., 2001; Ray et al., 2008). Increase of metabolic rate; glycolysis; lipolysis; fat store reduction; extensive production of pyruvic acid and lactic acid, are also observed after 2,4-DNP exposure (Agency for Toxic Substances and Disease Registry, 1995; Grundlingh et al., 2011). Additionally, the risk of toxicity increases after concomitant use of 2,4-DNP with other anorectic compounds (amphetamines) able to uncouple oxidative phosphorylation similarly to 2,4-DNP.

Classic symptoms associated with brief or long-term use of 2,4-DNP include anorexia, nausea, vomiting, headache, dizziness, respiratory distress, muscle rigidity, hyperpyrexia, yellow skin, agranulosis, as well as generalized weakness and weight loss (Tewari et al., 2009).

2.5.1) Social issues represented by 2,4-DNP and its effects

2,4-DNP and emergency admissions

Over the last years, the National Poison Information Service (NPIS) commissioned by Public Health England, has been expressing its concern about the sharply increase in frequency of enquiries related to 2,4-DNP toxicity despite a warning from the Food Standards Agency (FSA) issued in November 2012 (Kamour et al. 2015; Food Standards Agency, 2012). The clinical features reported were severe and the majority of them concerned subacute exposure of 2,4-DNP with a prevalent involvement of male body builders or body sculptors. Toxicity symptoms reported by enquirers to the NPIS were consistent with those reported previously (Agency for Toxic Substances and Disease Registry, 1995; Grundlingh et al., 2011). Clinical reported features included: yellow skin, agitation, confusion, alteration of the conscious level, seizures, metabolic acidosis, liver and renal functions impairment, muscle rigidity and the severity of toxicity was dose-dependent (Colman et al., 2007; Barlett et al., 2010). In another study, two cases of 2,4-DNP misuse in Hong Kong Chinese patients were reported (Lee et al., 2014). Clinical presentations were recognised as consequences of adverse reactions of 2,4-DNP use. The observed symptoms were: skin rash associated to the immunogenic reactions toward the compound, hyperthermia and muscle injury related to 2,4-DNP thermogenic properties.

According to the latest NPIS report, during 2016/17, both the numbers of patients who called asking about systemic 2,4-DNP exposure, and the number of accesses to the TOXBASE entry on 2,4-DNP, sharply decreased compared to 2015/2016 (NPIS, 2017).

2,4-DNP-related fatalities

Fatalities related to 2,4-DNP intake have been reported since the turn of the twentieth century. Perkins et al. (1919) published the largest publication of deaths due to occupational exposure to 2,4-DNP in munition factories in Paris (Perkins et al., 1919). As reported by Grundlingh et al. (2011), during the 1930s, 2,4-DNP-related fatalities were all individuals who had taken it for weight loss. After the 1930s, there was a decline in fatalities which reflected 2,4-DNP prohibition released by the US Food and Drug Administration in 1938. Over the last years, several deaths have been occurred related to 2,4-DNP exposure. Specifically, Grundlingh et al. (2011) claimed that from 2001 to 2010, there have been 12 deaths related to 2,4-DNP use/exposure. These fatalities have been linked to deliberate overdose, accidental toxicity and accidental occupational exposure. Recent studies reported several Emergency Department admissions in the UK and fatalities occurred after 2,4-DNP use. These data included

respectively outcomes of patients reported to the National Poisons Information Service (NPIS) and to the National Programme on Substance Abuse Deaths (NPSAD) (Kamour et al. 2015; Corkery et al., 2014). In detail, during 2016/17, two fatalities related to 2,4-DNP have been recorded by the NPIS service, leading to an increase of the total number of DNP-related deaths reported to the service to 13 since 2008 (NPIS, 2017).

2.5.2) Pharmacological studies on 2,4-DNP: focus on preclinical studies

Preclinical studies on 2,4-DNP toxicity were performed mostly in the 1930s -1940s, when this drug firstly became popular as a dieting aid.

In line with clinical observations, oral administration by gavage (forced administration of a drug typically by means of a tube leading down the throat to the stomach) in rats caused dose-dependent mortality with 100% of fatalities recorded at 100 mg/kg and no cases of fatal intoxication occurred in the dose range of l0-27 mg/kg. The cause of death in these acute studies was generally related to the pyretic effect mediated by 2,4-DNP resulting from an increase in metabolic rate (Spencer et al., 1948).

On the other hand, intraperitoneal administration of 2,4-DNP (16, 20, 25, 31, 39 mg/kg) in rats, promoted a malignant hyperpyrexia as a result of oxidative phosphorylation disruption, with higher doses (e.g. 39 mg/kg, i.p.) causing a significant increase of body temperature (e.g. $\Delta T=6.7 \pm 0.4$) and 100% mortality rate. Conversely, lower doses (e.g. 20 mg/kg, i.p.) lead to a moderate increase of temperature (e.g. $\Delta T=2.3 \pm 0.2$) and respiration rate without fatal complications (Gatz and Jones, 1970).

Additionally, rats exhibit a strong taste aversion to this drug and when exposed to a dietary concentration of 2,4-DNP (≈420 mg/kg/day), they consumed about 50% less food than the control group, and all died within 94 days. Starvation probably contributed to mortality among rats exposed to high levels of dietary 2,4-DNP. A significant reduction of body weight was observed as well (Tainter, 1938).

Chapter 3: *In vitro* quantitative autoradiography studies

3.1) *In vitro* quantitative autoradiography overview

Over the years, the growing availability of radioactively labelled compounds that bind with high affinity and selectivity to neurotransmitter receptors and transporters, has allowed researchers to label and quantitatively assay the proteins that mediate some effects of many

psychotropic drugs in the brain, including NPS. Such studies have indeed resulted in a significant increase in our understanding of the underlying mechanisms of psychoactive drugs through the discovery of their high-affinity binding sites. The amount of information in this rapid-growing field of research continues to increase especially in view of novel ligand/drugs being introduced in the market (Reuter et al., 2017).

After initial studies performed on tissue homogenates, some additional refined methods were developed to establish the anatomical distribution of drug-target interactions in the central nervous system. In this regard, *in vitro* autoradiographic binding-site assay is a radiological technique which may be used in neuroscience as a tool to identify the targets (receptors, transporters) of novel drugs on which little is known in terms of pharmacology and pharmacodynamics in the brain (Davenport, 2005).

Specifically, *in vitro* autoradiography in brain slices, enables the interpretation of the regional distribution of binding sites by employing pharmacological techniques originally developed for binding studies on homogenates (e.g. competition analysis) and providing a high anatomical resolution. Autoradiography has indeed the advantage of preserving tissue architecture, producing a detailed and reliable regional distribution of binding sites (Davenport and Russell, 1996).

An extensive range of radionuclides can be employed in autoradiography, including: ^{3}H, ^{35}S, ^{125}I. The radioligand selected depends on the aim of the study, and should meet the following criteria: high purity; high stability; high specific activity; biological activity; high degree of affinity and selectivity for the target protein (Boulton et al., 1998).

The *in vitro* quantitative autoradiography presents several advantages: small amounts of ligands are required, more than one target protein can be assessed in serial brain slices from the same animal, different protocols can be employed (competition or full saturation studies). On the other hand, the main disadvantage of this technique is that the incubation with the ligand occurs in artificial solution which may not exactly reproduce the *in vivo* physiological conditions (Boulton et al., 1998).

3.2) Competition binding assay

Neuroprotein–ligand interactions play a crucial role in modern pharmacology development and numerous assays (such as competition experiments) can be employed to screen novel chemicals.

The basic assumption in autoradiography is that in the presence of low concentrations of the radioligand most of the binding occurs to specific saturable binding sites (recognition), and only small concentrations bind with low affinity to non-saturable and non-specific binding sites. Specifically, the competition binding assays rely on the availability of increasing concentrations of a non-labelled molecule which compete with a fixed concentration of a radio-labelled ligand (Knoche, 1991) which binds to a specific active site on the target protein. Increasing concentrations of the unlabelled ligand (e.g. drug) cause a proportional decrease of the amount of radioactive ligand bound to the target of interest (specific binding) until the achievement of mass equilibrium.

The specific binding of a radioligand can be quantified by subtraction of the total binding (which includes both specific and non-specific binding) from the non-specific binding (not displaceable binding to lipids, membrane, other proteins). The affinity of the unlabelled ligand for the target protein can be established by calculating the quantity of the unlabelled ligand (drug) required to inhibit 50% of the radioactive ligand binding (IC_{50}).

Differently from competition binding studies, in saturation experiments, the slices are exposed to increasing concentrations of the radioligand in the presence (non-specific binding) or absence (total binding) of an excess of displacer. This study provides a measure of the equilibrium dissociation constant (K_d) and the maximum number of binding sites (B_{max}) (Davenport and Russel, 1996).

3.3) Autoradiography procedure

Dissections and brain preparation

Brain slices for autoradiography studies are obtained from whole brains extracted from rats sacrificed through dislocation. In detail, the brain is extracted as follows: the head is removed, a midline incision is made from the nose to the neck to expose the skull; the neck muscles are trimmed off to expose the base of the neck, the sharp end of a pair of scissors is positioned into the foramen magnum and moved into the inner surface of the skull. A cut is made on both sides extending to the distal edge of the posterior skull surface. The brain is gently lifted using a spatula, the olfactory bulbs and nervous connections are cut, the meninges still connecting the brain to the skull are trimmed away and the whole brain is extracted. Afterwards, brains are rapidly frozen (2 minutes) at −40 °C in a beaker containing dry ice and isopentane and stored at −80 °C.

Brain sectioning

Authenticity of information in autoradiography depends on proper tissue preparation and preservation. Frozen sectioning is performed with a cryostat that allows motorized or manual cutting of thin frozen sections (20 nM) at low temperature (-30 °C). The cryostat is usually an upright freezer powered by electricity, with a wheel mounted outside the chamber for rotating the microtome. Frozen brains are typically mounted on a metal chuck and placed on the microtome. During cutting, the wheel is rotated and the brain advances towards the cutting blade. Cutting of thin sections requires a sharp and cold knife and the development of specific skills.

The thickness of the slices (20 nM) provides optimal absorption of radioactivity and minimizes superimposition of structures. Once the brain is cut to a satisfactory quality, thaw mounting is done by lowering the polysine-coated glass slide to the surface of the knife and by performing a quick touch of the slice section with the polysine surface of the slide without any pressure. Notably, during tissue preparation the temperature of the tissue must not increase in order to minimize tissue disruption. After cutting the slides are stored in a deep freezer (-80º C) until the day of the experiment.

Incubation and washing

On the day of the experiment brain slices are left to thaw out and then are incubated with the radioligand at optimal conditions (proper pH and temperature) to allow the highest degree of specific binding. Increasing concentrations of the drug are then added to compete with the fixed concentration of a radio-labelled ligand. Non-specific binding determination can be measured by adding to the incubation buffer a ligand (antagonist or agonist) with high affinity for the target protein which acts as a 'block'. Various buffers (e.g. Tris-HCl, phosphate) are employed as media in binding assays with a pH usually maintained at 7.4-7.6. The concentration of the radioligand should be kept relatively low to reduce the non-specific component of total binding. Measurement of the ligand bound to tissue requires separation of the bound and free ligand. This can be achieved by multiple washings with the buffer. At the end of the incubation, slides are rinsed in cold distilled water and left to dry overnight.

Apposition and development

The autoradiography (ARG) experiment is followed by apposition of the slides to specific films in X-ray cassettes wrapped in aluminium foil, folded up in black plastic bags and stored in a fridge (4 ºC) to optimize the process of photographic exposure.

During the apposition, the energy emitted from the radioisotope contained in the specimen is absorbed by the emulsion crystals of the film causing the conversion of silver ions into silver atoms. The activation of the film is proportional to the amount of radioactivity contained in the slices. The period of apposition changes according to the specific activity of the radioligand employed. At the end of the apposition period, the films are removed from the cassettes and immersed into a fluid containing reducing agents in alkaline solutions (developing fluid) for one minute. The immersion into the developing fluid enables the conversion of the remaining silver ions into silver atoms with consequent opacification of the emulsion and formation of a negative visual image. Afterwards, the film is immersed in a stopping solution for one minute to block the developing process and then immersed in a fixing solution for three minutes to remove any remaining silver ions and fix the negative visual image (film fixation). At the end of the fixation process the film is washed under running water for 30 minutes and left to dry overnight.

Image capturing and analysis

During image capturing, autoradiographic films are placed over a Northern Light desktop illuminator and scanned electronically by a video camera with constant focal point and lens aperture. The images are then saved and analysed using the image analysis software (MCID^{TM}). The localization of binding sites in autoradiography, relies on the recognition of the anatomical regions and comparison of the labelled regions with anatomical landmarks taken from the stereotaxic atlas of Paxinos and Watson (1998), while the quantification of binding sites is based on the measure of optical densities of radioactive-sensitive films that have been exposed to a radiation source originating from the specimen. The density readings of brain regions on the autoradiograms are typically compared with those of commercial calibration scales (standards) and then converted into molar concentrations per mg of protein. Notably, density readings of non-specific binding must be systematically detracted from the corresponding total binding values to obtain precise quantitative readings for specific binding. Multiple readings should be taken for each region and high standard deviations could provide information on the anatomical heterogeneity within each structure.

3.4) Synthetic cannabinoids and autoradiography studies

Aims

Over the years, the binding properties of several SCs have been assessed in animal tissues using different procedures. One common finding this wide family of drugs shares is the binding to

the CB_1 receptors with affinity, potency, and efficacy properties that vary according to the chemical classes. The first aim of the present study was to investigate the potential binding properties of four different synthetic cannabinoids (BB-22, 5F-BP-22, 5F-AKB-48 and STS-135), all belonging to the third-generation class, to the CB_1 receptors.

The rationale behind the choice of these drugs was related to the growing concern about the serious health implications raised by using these new generation SCs potentially resulting from their peculiar pharmacodynamical profile.

The binding properties of these drugs, have been recently fully investigated on tissue homogenates (rat cortical membranes) using the radio-labelled competition binding assay (De Luca et al., 2016). According to these recent studies, these SCs were described as full agonists at the CB_1 receptors able to inhibit the specific binding of [^{3}H]CP-55,940 with the following K_i values: BB-22 (0.11 ± 0.03 nM), 5F-PB-22 (0.13 ± 0.01 nM), 5F-AKB-48 (0.87 ± 0.14 nM) and STS-135 (1.93 ± 0.18 nM) (De Luca et al., 2016). In view of these initial binding studies performed on tissue homogenates, we decided to employ the ARG procedure which is a more refined method used to establish the anatomical distribution of drug-target interactions in specific areas of coronal brain sections with the advantage of preserving tissue architecture. Consistent with the experiments performed on tissue homogenates, we employed the competition binding assay, by which increasing concentrations of SCs were tested for their ability to compete with a fixed concentration of the radio-labelled ligand [^{3}H]CP-55,940 characterised by high affinity and selectivity for the CB_1 receptor (Dalton et al., 2010). The target regions examined were the Cortex and the CPu which exhibit a high expression of CB_1 receptors (Pertwee, 2005). The concentration range used was in accordance with that employed on tissue homogenate experiments (0.1 nM-10 μM), although in the present studies, only five concentrations were assessed (0.3, 1.0, 3.0, 10, 30 μM). The small number of concentrations used represented a limitation of our study, as a wider number of concentrations tested would have allowed us to calculate reliable concentration-effect curves and IC_{50} values. In view of the above, we limited the elaborations of our data to the statistical analysis and graphical representation of the binding data of [^{3}H]CP-55,940 in the presence of increasing concentrations of the SCs in both Cortex and CPu. The methods used were the same described by Dalton et al. (2010).

The second aim of the present study was to investigate the potential binding properties of the same SCs at the level of glutamate NMDA receptors. The rationale behind this choice was related to the necessity to discover the underlying pharmacological mechanism responsible for

hallucinogenic events experienced by SC users. Hallucinations may indeed result from $NMDA_R$ dysfunction, which has been previously described as a potential and specific hallucinatory mechanism (Rolland et al., 2014). In this regard, the effects of SCs have been sometimes described by users comparable to those experienced with the dissociative anaesthetic phencyclidine (PCP) which exhibits antagonistic effects on NMDA receptors and causes a combination of hallucinations and dissociative symptoms resulting from disruption of the cortico-striato-thalamo-cortical loops, acting directly in the limbic striatum (Richardson et al., 2016).

From a chemical point of view, it was not excluded that SCs could act as NMDA receptor ligands, since other SCs of previous generations (e.g. HU-211) have been described as NMDA receptor antagonists (Belayev et al., 1995). Additionally, SCs similarly to PCP can induce cognitive deficits (likely related to glutamatergic pathway dysfunctions), and psychotic symptoms (potentially linked to a NMDAR hypofunction and considered to be a major neurobiological hypothesis for psychosis) (Rolland et al., 2014). The concentrations tested (0.3, 1, 3, 10, 30 µM) in our study and the target areas investigated (Cortex and CPu) were the same used in the CB_1 autoradiography experiments especially considering the high concentrations of NMDA receptors present in both areas. The methods employed were the same as those described by Lee et al. (2011).

3.4.1) SCs and CB_1 receptor autoradiography studies: materials and methods

Animals

Adult male Wistar rats (body weight: 250 grams) used for our experiments were housed in groups of four per cage. The animal environment was kept under an inverted 12:12 hour light/dark cycle and at a constant temperature of 22 ± 2 °C and humidity of about 60%. Tap water and standard food were available ad libitum in the home cage.

Dissections and brain preparation

Brain slices for autoradiography studies were obtained from six whole brains extracted from rats sacrificed through dislocation. Brains were rapidly frozen (two minutes) at −40 °C in a beaker containing dry ice and isopentane, and stored at −80 °C.

Brain cutting and slides preparation

Frozen brains from six animals were coronally and serially sliced using a cryostat (Bright instruments), into 20 nM sections in a rostro-caudal direction from +3.0 to +1.0 mm versus

bregma, to harvest slices containing the Cortex and the CPu. The slices were collected using glass polysine-coated slides (4 slices per slide) and then stored in a deep freezer (-80 degree Celsius) until the day of the experiment (Dalton et al., 2010). Four different synthetic cannabinoids were tested (BB-22, 5F-PB-22, STS-135, 5F-AKB-48) at six different concentrations: 0 (or total), 0.3, 1, 3, 10, 30 μM on serial brain sections. Overall 21 slides were prepared per drug (84 in total), individually containing 2 pairs of slices (168 pairs in total), each one destined at different concentrations of a drug (2 concentrations per slide) except for 3 slides destined for the binding block.

Chemicals used for autoradiography experiment

The radioligand for CB_1 receptors, [^{3}H]CP-55,940 (specific activity 154.2 Ci/mM) was purchased from Perkin Elmer (UK) while the synthetic cannabinoids were bought from an Internet source (www.researchchemist.co.uk) and chemically identified with nuclear magnetic resonance (NMR). The other chemicals were purchased from Sigma-Aldrich (UK).

Preincubation, incubation, washing

On the day of the experiment the slides were removed from the deep freezer and allowed to thaw for three hours in trays. The sections were then preincubated for one hour at room temperature in 50 mM tris buffer (pH 7.4) containing 5% bovine serum albumin (BSA). The preincubation ensured the removal of endogenous ligands present in the tissue. Different concentrations of the drugs were prepared from initial concentrations (7 mM for BB-22 and 5F-PB-22 and 10 mM for 5F-AKB-48 and STS-135) through serial dilutions with the working ligand (50 mM tris buffer + 1 μM AM360 + 5% Albumin Bovine serum + 5 nM [^{3}H]CP-55,940) for two hours at room temperature. AM-360 1 μM was added into the working ligand buffer to block CB_2 receptors while albumin bovine serum was used because of its ability to increase signal in assays without affecting biochemical reactions.

In detail, during incubation, 18 slides for each drug were incubated with 0.5 ml of working ligand buffer in the absence of antagonist, while non-specific binding (block) was determined by incubating 3 slides per drug with 0.5 mL of buffer in the same way as described above but in the presence of the CB_1 antagonist rimonabant (10 μM) and in the absence of the tested drug. Slides were washed two times for two hours in tris buffer with 1% albumin bovine serum then dipped in cold deionised water and left to dry overnight.

Apposition and film development

The day after the slides were apposed to an x-ray film (Kodak biomax MR film) and left in x-ray cassettes folded up in aluminium foil, wrapped in black plastic bags and stored in a fridge (4 ºC) for ten weeks (Dalton et al., 2010). Afterwards, the films were removed from the cassettes and immersed in a fluid containing reducing agents in alkaline solutions (developing fluid, Kodak). Each film was then immersed for one minute in a stopping solution (diluted solution of acetic acid) and afterwards in a fixing solution (Kodak rapid fixer, purchased from Sigma Aldrich, UK) for three minutes in order to remove any remaining silver ions and fix the negative visual image (film fixation). At the end of the fixation process the film was washed under running water for thirty minutes and left to dry overnight.

Image capturing and analysis

During image capturing, autoradiographic films were placed over a Northern Light desktop illuminator B95 equipped with a Nikon camera (50mm, f2.8 lens), by which the images were scanned electronically and saved for analysis. Image analysis was performed using the image analysis software MCID^{TM} (version 7.0, Imaging Research Inc., Interfocus Ltd, UK). Flat field correction was applied. Measurement of the optical densities was performed on both hemispheres in the frontal Cortex and dorsal striatum (regions of interest or ROIs) of each section. A standard brain atlas was used to identify brain regions for quantification (Paxinos and Watson, 2008). The means of optical density values from both sides of duplicate sections were calculated to assess the specific binding. To ensure consistency during the sampling, the size of the ROIs was kept constant. Changes in the optical densities were calculated as the average percentage of changes in adjacent brain sections against the control value (100%).

CB_1 receptor and statistical analysis of autoradiography data

Autoradiography data on radioligand binding were analysed by using one-way and two-way ANOVAs followed by post-hoc Tukey's tests. Data were presented as mean percentage ± standard error of mean (SEM) against the control value with significance set at $p<0.05$. Binding of [^{3}H]CP-55,940 in presence of increasing concentrations of the drugs in both Cortex and CPu was analysed. Statistica (version 10) was used as the statistical software.

3.4.2) SCs and CB_1 receptor autoradiography studies: results

The displacement of [^{3}H]CP-55,940 was examined in both Cortex and CPu. Figures 12, 13, 14, 15 show autoradiograms of relevant brain sections labelled with this radioligand. According to our findings, there was a marked effect of SCs on the intensity of tritium signal in brain

tissue indicating competition between SCs and [^{3}H]CP-55,940. One-way ANOVA for each drug (see Table 1) revealed a significant effect of SC concentrations in both Cortex and CPu vs controls where no drugs were present (total binding). Post-hoc Tukey's test showed that all drugs at all dosages caused significantly greater displacement of [^{3}H]CP-55,940 compared to the controls. Moreover, the analysis of the binding data for all drugs in Cortex and CPu separately (two-way ANOVA), showed a significant effect of the drug types; drug concentrations; and interaction drug types x concentrations, with BB-22 and 5F-PB-22 showing a similar trend both in Cortex and CPu compared to 5F-AKB-48 and STS-135 (see Figure 11).

	One-way ANOVA	
Drugs	**Cortex**	**CPu**
BB-22	F(5,30)=62.21 p<0.0001	F(5,30)=88.91 p<0.0001
5F-PB-22	F(5,30)=76.03 p<0.0001	F(5,30)=139.9 p<0.0001
5F-AKB-48	F(5,30)=45.39 p<0.0001	F(5,30)=29.51 p<0.0001
STS-135	F(5,30)=27.5 p<0.0001	F(5,30)=34.3 p<0.0001
	Two-way ANOVA	
Drugs	**Cortex**	**CPu**
BB-22, 5F-PB-22, 5F-AKB-48, STS-135	$F_{interaction}$ (15, 120) =4.25 p<0.0001 F_{drug} (3, 120) = 32.51 p<0.0001 F_{conc} (5, 120) = 186.7 p<0.0001	$F_{interaction}$(15, 120) = 6.26 p<0.0001 F_{drug} (3, 120) = 51.44 p<0.0001 F_{conc} (5, 120) = 209 p<0.0001

Table 1: Statistical results of the binding data of [^{3}H]CP-55,940 in presence of increasing concentrations of BB-22, 5F-PB-22, 5F-AKB-48, STS-135 in both Cortex and CPu. One-way and two-way ANOVA analyses (post-hoc Tukey's tests).

.

Drugs		Significance
0.3 µM		
5F-AKB-48 vs. 5F-PB-22	****	p<0.0001
5F-AKB-48 vs. BB-22	****	p<0.0001
5F-PB-22 vs. STS-135	****	p<0.0001
BB-22 vs. STS-135	****	p<0.0001
1µM		
5F-AKB-48 vs. 5F-PB-22	*	p<0.05
5F-AKB-48 vs. BB-22	***	p<0.0005
5F-AKB-48 vs. STS-135	*	p<0.05
5F-PB-22 vs. STS-135	****	p<0.0001
BB-22 vs. STS-135	****	p<0.0001
3µM		
5F-PB-22 vs. STS-135	***	p<0.001
BB-22 vs. STS-135	**	p<0.005
10µM		
5F-AKB-48 vs. 5F-PB-22	*	p<0.05
5F-AKB-48 vs. BB-22	*	p<0.05
5F-PB-22 vs. STS-135	*	p<0.05
30µM		
5F-AKB-48 vs. 5F-PB-22	*	p<0.05

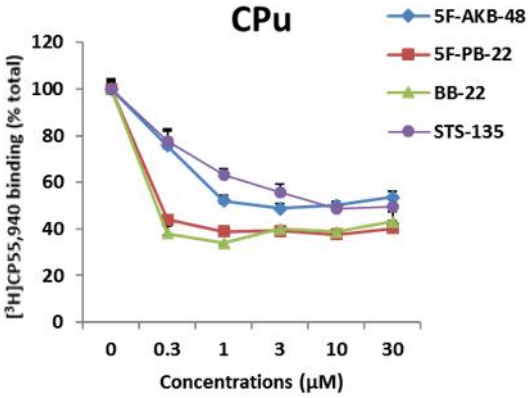

Drugs		Significance
0.3 µM		
5F-AKB-48 vs. BB-22	**	p<0.005
5F-AKB-48 vs. STS-135	***	p<0.001
5F-AKB-48 vs. 5F-PB-22	*	p<0.05
BB-22 vs. STS-135	****	p<0.0001
STS-135 vs. 5F-PB-22	****	p<0.0001
1µM		
5F-AKB-48 vs. STS-135	**	p<0.005
BB-22 vs. STS-135	****	p<0.0001
STS-135 vs. 5F-PB-22	***	p<0.001
3µM		
5F-AKB-48 vs. STS-135	*	p<0.05
BB-22 vs. STS-135	**	p<0.005
STS-135 vs. 5F-PB-22	***	p<0.001
10µM		
5F-AKB-48 vs. BB-22	**	p<0.005
5F-AKB-48 vs. 5F-PB-22	**	p<0.005
30µM		
5F-AKB-48 vs. BB-22	*	p<0.05
5F-AKB-48 vs. 5F-PB-22	**	p<0.005

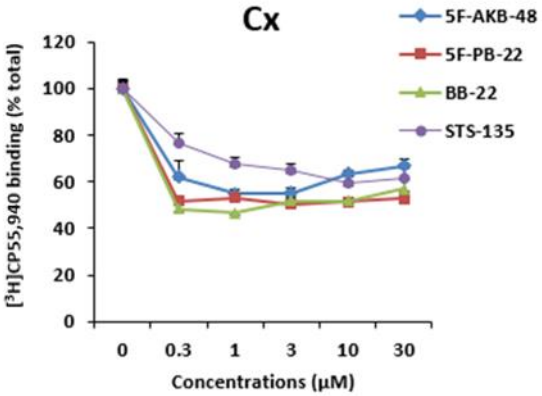

Figure 11: Statistical results (two-way ANOVA) on the left, and graphical representation on the right, of pooled data from six animals, showing the binding data of [^{3}H]CP-55,940 in presence of increasing concentrations of BB-22, 5F-PB-22, 5F-AKB-48, STS-135 in both CPu and Cortex. Data are expressed as mean percentage ± standard error of mean (SEM) against the control value with significance set at $p<0.05$. Two-way ANOVA analysis (****$p<0.0001$, *** $p<0.001$, ** $p<0.005$, *$p<0.05$, post-hoc Tukey's tests).

Effect of increasing concentrations of BB-22 on [^{3}H]CP-55,940 autoradiographic binding

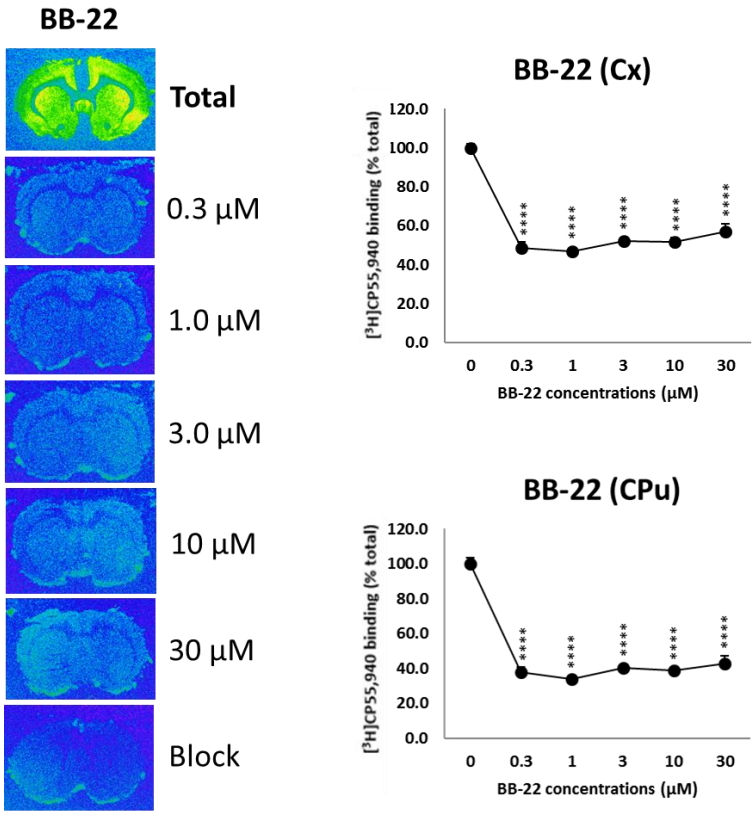

Figure 12: Representative computer-enhanced images of brain slices (on the left) and graphical representation of pooled data from six animals (on the right) showing the binding of [^{3}H]CP-55,940 to CB_1R in presence of increasing concentrations of BB-22 in both Cortex and CPu. Data are expressed as mean percentage ± standard error of mean (SEM) against the control value with significance set at $p<0.05$. One-way ANOVA analysis (****$p<0.0001$, post-hoc Tukey's test).

Effect of increasing concentrations of 5F-PB-22 on [^{3}H]CP-55,940 autoradiographic binding

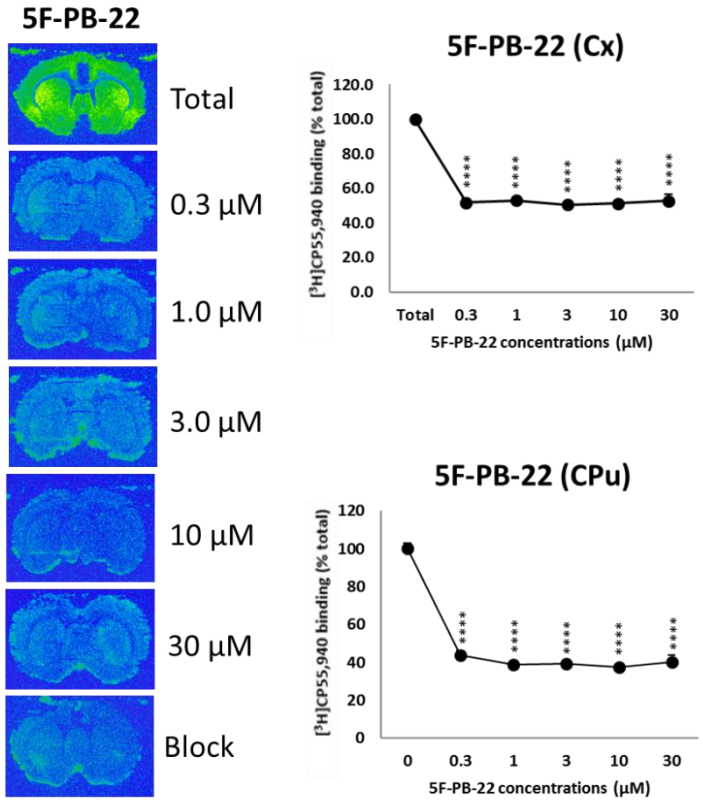

Figure 13: Representative computer-enhanced images of brain slices (on the left) and graphical representation of pooled data from 6 animals (on the right) showing the binding of [^{3}H]CP-55,940 to CB_1R in presence of increasing concentrations of 5F-PB-22 in both Cortex and CPu. Data are expressed as mean percentage ± standard error of mean (SEM) against the control value with significance set at $p<0.05$. One-way ANOVA analysis (****$p<0.0001$, post-hoc Tukey's tests).

Effect of increasing concentrations of 5F-AKB-48 on [^{3}H]CP-55,940 autoradiographic binding

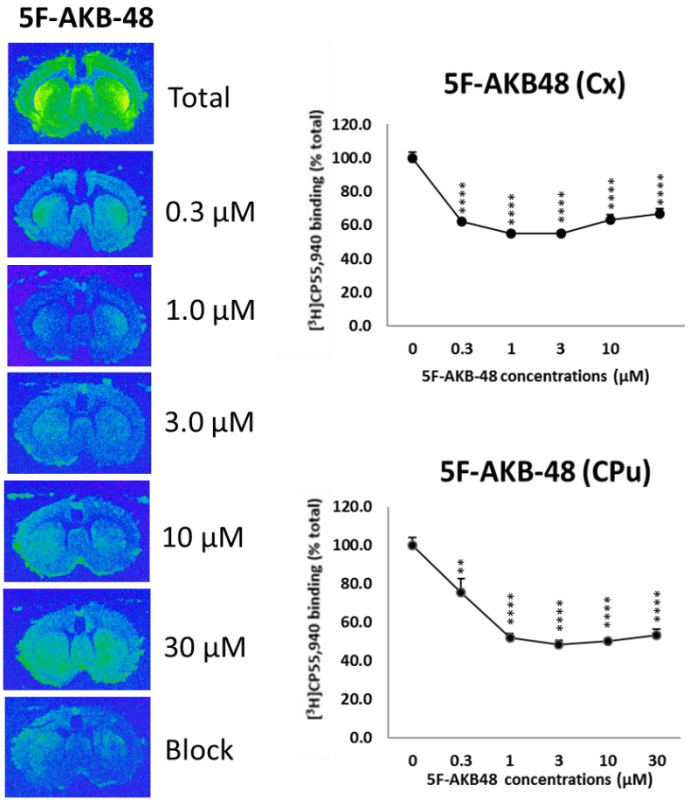

Figure 14: Representative computer-enhanced images of brain slices (on the left) and graphical representation of pooled data from six animals (on the right) showing the binding of [^{3}H]CP-55,940 to CB_1R in presence of increasing concentrations of 5F-AKB-48 in both Cortex and CPu. Data are expressed as mean percentage ± standard error of mean (SEM) against the control value with significance set at $p<0.05$. One-way ANOVA analysis (****$p<0.0001$, **$p<0.01$, post-hoc Tukey's tests).

Effect of increasing concentrations of STS-135 on [^{3}H]CP-55,940 autoradiographic binding

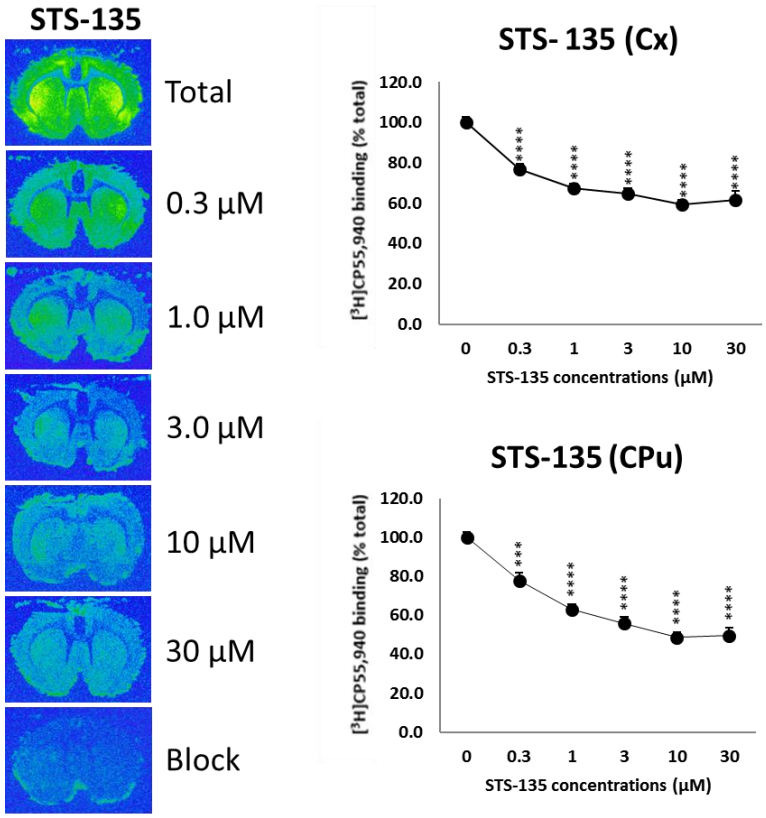

Figure 15: Representative computer-enhanced images of brain slices (on the left) and graphical representation of pooled data from six rats (on the right) showing the binding of [^{3}H]CP-55,940 to CB_1R in presence of increasing concentrations of STS-135 in both Cortex and CPu. Data are expressed as mean percentage ± standard error of mean (SEM) against the control value with significance set at $p<0.05$. One-way ANOVA analysis (****$p<0.0001$, ***$p<0.001$, post-hoc Tukey's tests).

3.4.3) SCs and NMDA receptor autoradiography studies: materials and methods

Brain cutting and slides preparation

Frozen brains from six adult Wistar rats (body weight: 250 grams) were coronally and serially sliced into 20 nM sections in a rostro-caudal direction using a cryostat (Bright instruments). The slices containing the Cortex and the CPu were collected using glass polysine-coated slides (4 slices per slide) and then stored in a deep freezer (-80 °C) until the day of the experiment. Four different synthetic cannabinoids were tested (BB-22, 5F-PB-22, STS-135, 5F-AKB-48) at six different concentrations: 0 (or total), 0.3, 1, 3, 10, 30 μM on serial brain sections. Overall 21 slides were prepared per drug (84 in total), individually containing 2 pairs of slices (168 pairs in total), each one destined at different concentrations of a drug (2 concentrations per slide) except for 3 slides destined for the binding block.

Chemicals used for NMDA autoradiography experiment

The radioligand for NMDA receptors, [^{3}H]MK-801 (specific activity 26.4 Ci/mmol) was purchased from Perkin Elmer (UK). The synthetic cannabinoids were purchased from an Internet source (www.researchchemist.co.uk) and chemically identified with NMR. The other chemicals were purchased from Sigma-Aldrich (UK).

Preincubation and incubation

On the day of the experiment the slides were removed from the deep freezer and allowed to thaw for three hours in trays. The sections were then preincubated for thirty minutes at room temperature in 0.5 ml of TrisGG (Tris 50 mM + 30 μM glutamate + 10 μM glycine). Different concentrations of the drugs were prepared from initial concentrations (7 mM for BB-22 and 5F-PB-22 and 10 mM for 5F-AKB-48 and STS-135) through serial dilution with the working ligand (50 mM Tris + 5 nM [^{3}H]MK-801 + 30 μM glutamate + 10 μM glycine). In detail, during incubation, 18 slides for drug were incubated for two hours in 0.5 ml of working ligand buffer, while non-specific binding (block) was determined by incubating 3 slides per drug with 0.5 mL of buffer in the same way as described above but in the presence of (+) MK-801 (cold) (50μM) and in the absence of the tested drug. Following incubation, the slides were washed twice for thirty minutes in tris buffer at room temperature, then rinsed for ten seconds in cold deionised water. Slides were then air dried overnight (Lee et al., 2011).

Apposition and film development

The day after the slides were apposed to an x-ray film (Kodak biomax MR film), left into x-ray cassettes and stored in a fridge (4 ºC) for ten weeks (Lee et al., 2011). Afterwards, the films were developed, washed under running water for thirty minutes and left to dry overnight.

Image capturing and analysis

The images were captured and analysed. The means of optical density values from both sides of duplicate sections were calculated to assess the specific binding. Measurement of the optical densities was performed on both hemispheres in the frontal Cortex and CPu (regions of interest or ROIs) of each section. Changes in the optical densities were calculated as the average percentage of changes in adjacent brain sections against the control value (100%).

NMDA receptor and statistical analysis of autoradiography data

Autoradiography data on radioligand binding were analysed using one-way ANOVA. Data were presented as mean percentage ± standard error of mean (SEM) against the control value with significance set at $p<0.05$. Binding of [^{3}H]MK-801 in presence of increasing concentrations of the drugs in both Cortex and CPu was analysed. Statistica (version 10) was used as the statistical software.

3.4.4) SCs and NMDAR autoradiography studies: results

The displacement of [^{3}H]MK-801 was examined in both Cortex and CPu. Figures 16, 17, 18, 19, show autoradiograms of relevant brain sections labelled with this radioligand. According to our findings, data analysis revealed no effect of all SCs at all concentrations tested on the intensity of tritium signal in brain tissue indicating the absence of competition between SCs and [^{3}H]MK-801.

Effect of increasing concentrations of BB-22 on [^{3}H]MK-801 autoradiographic binding

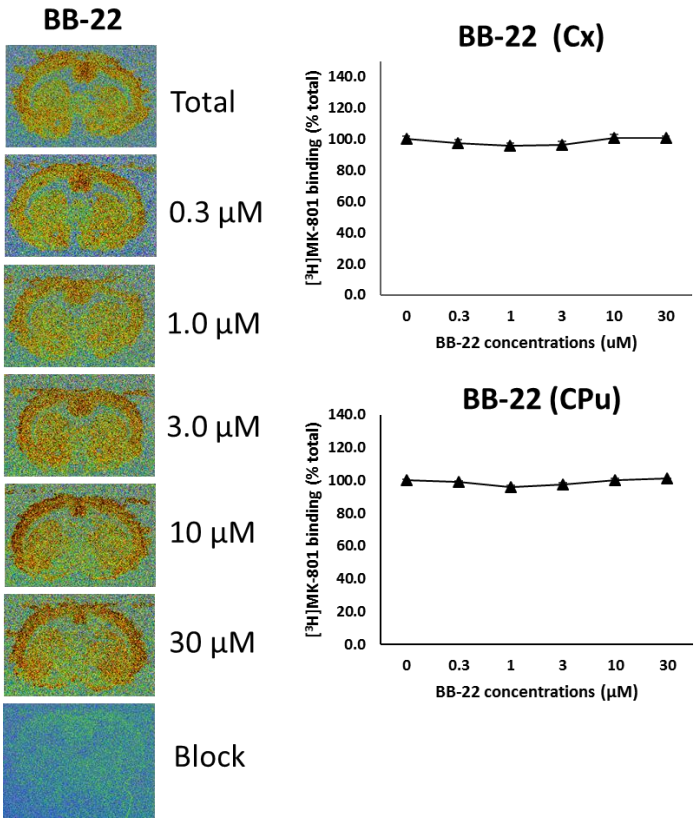

Figure 16: Representative computer-enhanced images of brain slices (on the left) and graphical representation of pooled data from 6 rats (on the right) showing the binding of [^{3}H]MK-801 to NMDAR in presence of increasing concentrations of BB-22 in both Cortex and CPu. Data are expressed as mean percentage ± standard error of mean (SEM) against the control value with significance set at $p<0.05$. One-way ANOVA analysis.

Effect of increasing concentrations of 5F-PB-22 on [^{3}H]MK-801 autoradiographic binding

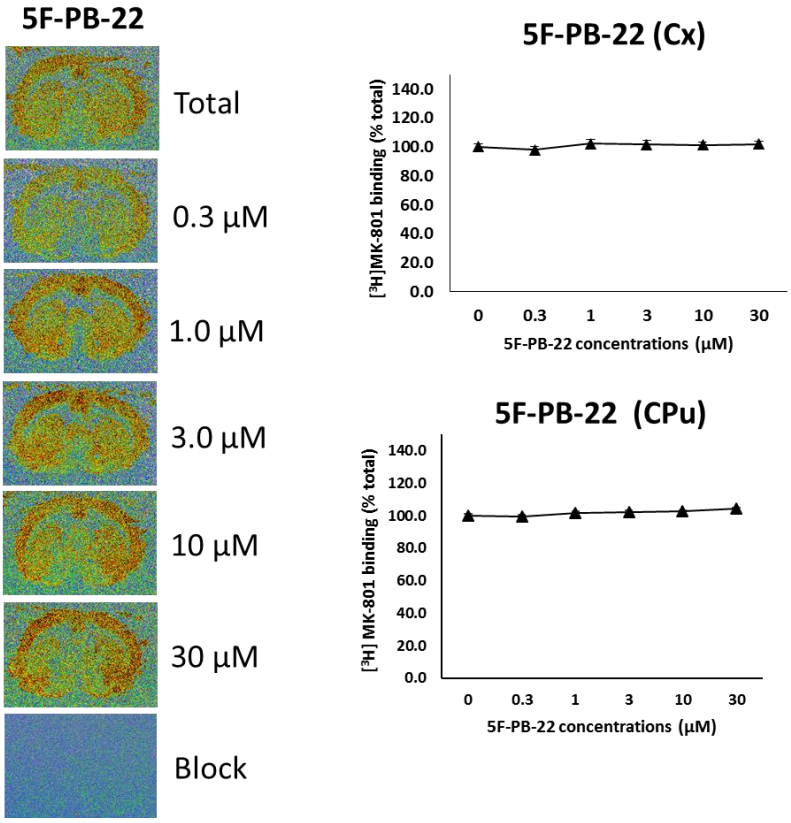

Figure 17: Representative computer-enhanced images of brain slices (on the left) and graphical representation of pooled data from 6 rats (on the right) showing the binding of [^{3}H]MK-801 to NMDAR in presence of increasing concentrations of 5F-PB-22 in both Cortex and CPu. Data are expressed as mean percentage ± standard error of mean (SEM) against the control value with significance set at $p<0.05$. One-way ANOVA analysis.

Effect of increasing concentrations of 5F-AKB-48 on [^{3}H]MK-801 autoradiographic binding

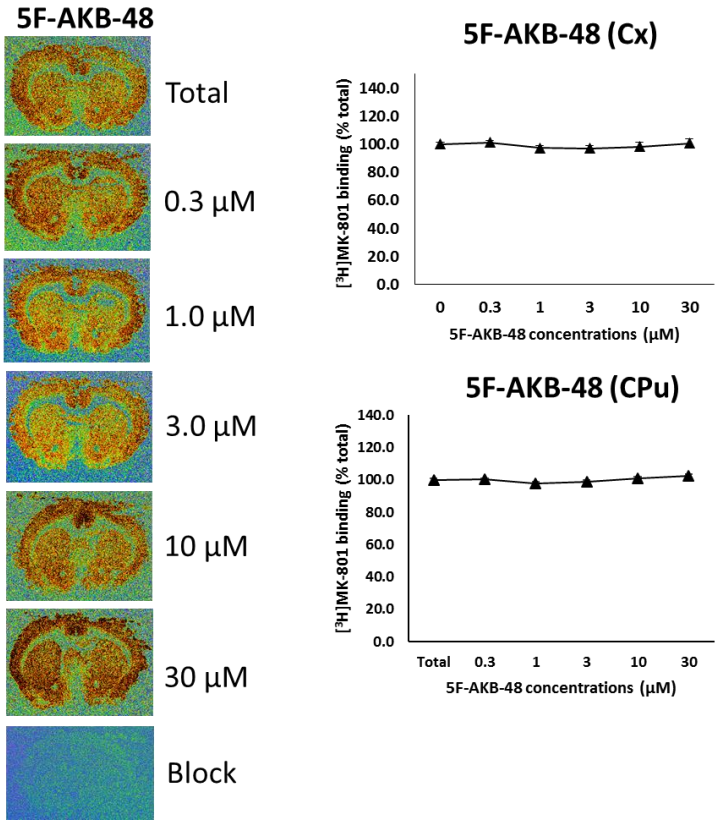

Figure 18: Representative computer-enhanced images of brain slices (on the left) and graphical representation of pooled data from 6 rats (on the right) showing the binding of [^{3}H]MK-801 to NMDAR in presence of increasing concentrations of 5F-AKB-48 in both Cortex and CPu. Data are expressed as mean percentage ± standard error of mean (SEM) against the control value with significance set at $p<0.05$. One-way ANOVA analysis.

Effect of increasing concentrations of STS-135 on [^{3}H]MK-801 autoradiographic binding

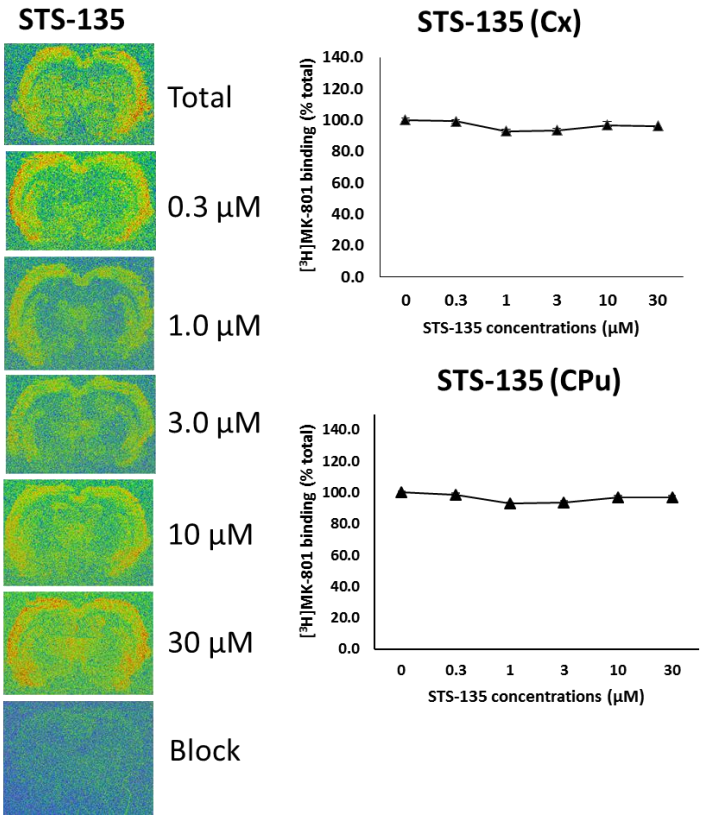

Figure 19: Representative computer-enhanced images of brain slices (on the left) and graphical representation of pooled data from 6 rats (on the right) showing the binding of [^{3}H]MK-801 to NMDAR in presence of increasing concentrations of STS-135 in both Cortex and CPu. Data are expressed as mean percentage ± standard error of mean (SEM) against the control value with significance set at $p<0.05$. One-way ANOVA analysis.

3.4.5) CB_1R and NMDAR autoradiography studies with SCs: discussion

The first aim of the present study was to investigate the potential binding properties of the SCs BB-22, 5F-PB-22, 5F-AKB-48 and STS-135 at the level of CB_1 receptors. As expected, our results confirmed that the investigated compounds behave as highly potent CB_1 receptor ligands able to compete with the radioligand [^{3}H]CP-55,940. Consistent with homogenate studies (De Luca et al., 2016), BB-22 and 5F-PB-22 showed similar levels of displacement compared to the control values at all concentrations tested in both areas, Cortex and CPu. Indeed, the post-hoc Tukey's test did not reveal any significant differences between these two drugs on the percentage of the radioligand bound, against the control value, in both areas (two-way ANOVA) (see Figure 11). Similar effects between these two drugs can be easily observed in the graphical representation of the radioligand bound in presence of increasing concentrations of the drugs where BB-22 and 5F-PB-22 curves mostly overlap (see Figure 11). On the other hand, 5F-AKB-48 and STS-135 showed lower ability to compete with the radioligand compared to BB-22 and 5F-PB-22. Specifically, significant differences between 5F-AKB-48 vs BB-22 and 5F-PB-22 effects were observed at low and high concentrations (0.3, 10.0 and 30.0 µM) in the Cortex, and at all concentrations tested except for 3.0 µM (at which no differences were observed against both drugs), and 30.0 µM (at which a significant difference was observed against 5F-PB-22 only) in the CPu. On the other hand, significant differences between STS-135 vs BB-22 and 5F-PB-22 effects were observed at low concentrations in the Cortex (0.3, 1.0, 3.0 µM). As regards to CPu, all concentrations of STS-135 except for 30.0 µM, were significantly different against 5F-PB-22, and only low concentrations (0.3, 1.0, 3.0 µM) showed significance against BB-22 (see Figure 11). To sum up, our results were consistent with previous homogenate study findings, by which all index SCs in our study were described as high-affinity agonists at CB_1 receptors, with BB-22 and 5F-PB-22 showing higher affinities compared to 5F-AKB-48 and STS-135.

The second aim of the present study was to investigate the potential binding properties of the same SCs at the level of glutamate NMDA receptors in order to discover the underlying pharmacological mechanism responsible for several hallucinogenic events experienced by SC users. According to our findings, all SCs tested were not able to compete with the NMDAR radioligand [^{3}H]MK-801 (see Figures 16, 17, 18, 19), rejecting the hypothesis of potential binding of these SCs to the NMDA receptors at all concentrations investigated, and leading us to consider alternative mechanisms responsible for hallucinogenic events. In this regard, two other main pharmacological models of hallucinations may be alternatively considered such as

the dopaminergic model which involves a stimulation of D_2 receptors in the limbic striatum and the serotoninergic model which involves the stimulation of $5HT_{2A}$ receptors on cortical neurons. Both these mechanisms cause an alteration of the functioning of the cortico-striato-thalamo-cortical loops, as already observed with the glutamatergic model (Rolland et al., 2014). In view of the above, further binding studies are needed to exclude the potential binding of SCs to serotoninergic and dopaminergic receptors. Anyway, although there has been much debate regarding the underlying exact pharmacological mechanism responsible for hallucinations and psychosis after SC use, the most commonly accepted mode of activity of this class seems to involve a pure CB_1 receptor mediated dis-inhibitory or inhibitory mechanism of other pathways (GABAergic, glutamatergic, dopaminergic) that ultimately may affect the functioning of the cortico-striato-thalamo-cortical loop responsible for altered perceptions and psychoses. Additionally, their high affinity and intrinsic activity at CB_1 receptors might partially explain their high potential to trigger psychotic-like symptoms (including hallucinations) (Fattore et al., 2016).

These outcomes confirmed that these SCs are able to enhance the function of the endogenous cannabinoid system, fully activating CB_1 receptors which are mainly sited in the central nervous system. Since the cannabinoid system is implicated in several physiological functions (e.g. pain, mood, appetite, memory, stress response, social behaviour, anxiety), the super-agonism of SCs at the CB_1 receptor highlights the potential side effects that can arise from their use (alteration of mood, agitation, vomiting, hallucinations, psychoses, seizures, convulsions, and panic attacks).

These more serious adverse effects in contrast to use of cannabis are potentially related to the full agonism showed by SCs at the CB_1 receptor compared to Δ9-THC which is only a partial agonist of this receptor and thus not able to activate and saturate all of the receptor population.

Our outcomes, along with cases of serious toxic effects, highlight the emergent clinical issues caused by the use of these drugs.

According to their high potential for abuse and their unpredictable serious side effects, novel SCs have no medical benefit and authorities have made it illegal to sell, buy, or possess some these chemicals (ACMD, 2016). Indeed, although some SCs have been shown to stimulate appetite, suppress nausea, and to have some benefits in the treatment of PTSD (Post-Traumatic Stress Disorder) (Fraser et al., 2009), they may also cause profound psychological and physical effects, highlighting their narrow therapeutic index (Seely et al., 2012).

Overall, the alarming popularity of SCs highlights the urgent need to plan effective tailored treatment strategies against the risks related to both acute intoxication and chronic use of SCs. Additional pharmacological and toxicological studies are needed to assess the long-term effects of these drugs (Cooper et al., 2016).

3.5 Synthetic stimulants and DAT autoradiography studies

Aims

5-(2-Aminopropyl)indole (5-API or 5-IT) and 2-DPMP are two synthetic stimulants belonging to the NPS class considered particularly harmful as a result of numerous toxicity events consistent with sympathomimetic toxidromes associated with their use. In detail, 5-IT is a tryptamine derivative and a substituted phenethylamine with stimulant and hallucinogenic properties, while desoxypipradrol also known as 2-diphenylmethylpiperidine (2-DPMP), is chemically related to methylphenidate and pipradrol and shares with them a similar pharmacology. Both entered the illicit market as MDMA replacements and have become quickly popular for their strong psychoactive effects. From a pharmacological point of view, a recent study confirmed that the clinical effects of 5-IT partly result from selective and reversible inhibition of MAO_A enzymes (Herraiz and Brandt, 2014) and from its full efficacy releasing activity at the level of DAT and NET. Additionally, a higher selectivity for DAT and NET compared to MDMA has been demonstrated (Marusich et al., 2016). As previously observed with other drugs of abuse, the high selectivity for DAT/NET versus SERT may account for the high abuse potential of 5-IT in humans and animals (Banks et al., 2014; Negus and Miller, 2014).

On the other hand, 2-DPMP is a synthetic stimulant with high abuse potential that may act as a potent DAT and NET inhibitor without releasing properties (Simmler et al., 2014) able to stimulate evoked dopamine efflux in NAc brain slices to a greater extent compared to cocaine (Davidson and Ramsey, 2012). Notably, the monoamine uptake transport inhibition and releasing properties of 5-IT were monitored using *in vitro* release assays in brain synaptosomes (Marusich et al., 2016) while 2-DPMP studies have been conducted in embryonic kidney 293 cells (HEK 293) (Simmler et al., 2014). In view of the above we decided to investigate the potential binding properties of these two stimulants to the dopamine transporter in rat brain slices using the autoradiography procedure.

The rationale behind the choice of these drugs was related to the numerous clinical implications, toxicity events and fatalities related to their use and potentially resulting from their peculiar pharmacodynamical profile.

The autoradiography procedure was performed in specific areas of coronal brain sections and we employed the competition binding essay by which increasing concentrations of 5-IT and 2-DPMP were tested for their ability to compete with a fixed concentration of the radio-labelled ligand [^{125}I]RTI-121 characterised by high affinity and selectivity for the target protein DAT (Strazielle et al., 1998). The target brain regions examined were the CPu and NAc shell which exhibit a high expression of dopamine transporters.

The concentration range used was in accordance with that employed in previous *in vitro* studies (10^{-10}- 10^{-4} M), although in our studies, only five concentrations were assessed (0.3, 1.0, 3.0, 10, 30 μM). The small number of concentrations assessed represented a limitation of our study, as a wider number of concentrations would have allowed us to calculate reliable concentration-effect curves and IC_{50} values. In view of the above, we limited the elaborations of our data to the statistical analysis and graphical representation of the binding data of [^{125}I]RTI-121 in presence of increasing concentrations of the synthetic stimulants in both CPu and NAc shell. The methods used were the same as those described by Strazielle et al. (1998).

3.5.1) Synthetic stimulants and DAT autoradiography studies: materials and methods

Brain cutting and slides preparation

Frozen brains from six adult Wistar rats (body weight: 250 grams) were coronally and serially sliced, using a cryostat (Bright instruments), into 20 nM sections in a rostro-caudal direction from +2.2 to +1.0 mm versus bregma, to harvest the NAc and the CPu. Afterwards, the slices were collected using glass polysine-coated slides (4 slices per slide) and then stored in deep freezer at −80 °C, until the day of the experiment. Two synthetic stimulants were tested (5-IT and 2-DPMP) at six different concentrations: 0 (or total), 0.3, 1, 3, 10, 30 μM on serial brain sections. Overall, 21 slides were prepared per drug (42 in total), individually containing 2 pairs of slices (84 pairs in total), each one destined at different concentrations of a drug (2 concentrations per slide) except for 3 slides destined for the binding block.

Chemicals used for DAT autoradiography experiment

The radioligand for dopamine transporters, [^{125}I]RTI 121 (specific activity 2200 Ci/mM) was purchased from Perkin Elmer (UK). All the other chemicals, including the synthetic stimulants (Desoxypipradrol hydrochloride solution: D-082, and 5-IT solution: A-107) were purchased from Sigma-Aldrich (UK).

Preincubation and incubation

On the day of the experiment the slides were removed from the deep freezer and allowed to thaw for three hours in trays. The sections were then preincubated for thirty minutes at room temperature in 0.5 ml of phosphate saline buffer (PBS) at pH 7.4 (137 mM NaCl, 2.7 mM KCl, 10.14 mM Na_2HPO_4, 1.76 mM K_2HPO_4). Different concentrations of the drugs were prepared from initial concentrations (5.7 mM for 5-IT and 3.5 mM for 2-DPMP) through serial dilution with the working ligand ([^{125}I]RTI-121 (20 pM) + phosphate-saline buffer). In detail, during incubation (60 minutes), 18 slides for drug were incubated in 0.5 ml of working ligand buffer in the absence of antagonist, while non-specific binding (block) was determined by incubating 3 slides per drug with 0.5 mL of buffer in the same way as described above but in the presence of nomifensine (400 μM) and in the absence of the tested drug. Following incubation, the slides were dipped in ice cold buffer two times for twenty minutes and left to dry overnight (Strazielle et al., 1998).

Apposition and film development

The day after the slides were apposed to an x-ray film (Kodak biomax MR film), left into x-ray cassettes and stored in a fridge (4 ºC) for three days (Strazielle et al., 1998). Afterwards, the films were developed, washed under running water for thirty minutes and left to dry overnight.

Image capturing and analysis

The images were captured and analysed. The means of optical density values from both sides of duplicate sections were calculated to assess the specific binding. Measurement of the optical densities was performed on both hemispheres in the CPu and NAc shell (regions of interest or ROIs) of each section. Changes in the optical densities were calculated as the average percentage of changes in adjacent brain sections against the control value (100%).

Synthetic stimulants and DAT autoradiography statistical analysis

Autoradiography data on radioligand binding were analysed using one- and three-way ANOVAs followed by post-hoc Tukey's tests. Data were expressed as mean percentage ± standard error of mean (SEM) against the control value with significance set at $p<0.05$. Binding of [^{125} I]RTI-121 was analysed in presence of increasing concentrations of the drugs in both CPu and NAc shell. Statistica (version 10) was used as the statistical software.

3.5.2) Synthetic stimulants and DAT autoradiography studies: results

The displacement of [^{125}I]RTI-121 was examined in both CPu and NAc shell. Figures 21 and 22 show autoradiograms of relevant brain sections labelled with this radioligand. According to our findings, both synthetic stimulants mediated a marked concentration-dependent reduction in the radioligand signal intensity in brain tissue, indicating competition between the synthetic stimulants and the radioligand. One-way ANOVA for each drug revealed (see Figure 20) a significant effect of synthetic stimulant concentrations in both CPu and NAc shell vs controls where no drugs were present (total binding). Notably, 2-DPMP was highly effective in reducing the radioligand signal intensity in both CPu and NAc shell, starting from the lowest concentration tested (0.3 µM); while 5-IT showed a significant competition with the radioligand starting from 1.0 µM ($p<0.05$) in the NAc shell and 3.0 µM ($p<0.01$) in the CPu. Moreover, three-way ANOVA of the binding data of both drugs in both areas (CPu and NAc shell) revealed a significant effect of the drug type ($p<0.0001$), drug concentrations ($p<0.0001$), and a significant effect of concentrations x drug ($p<0.0001$) and drug x per area interactions ($p<0.05$) (see Figure 20). In detail, post-hoc Tukey's test showed a significant difference between 5-IT CPu data vs 2-DPMP CPu data; and 5-IT NAc shell data vs 2-DPMP NAc shell data at 0.3, 1.0, 3.0 µM with 2-DPMP being more effective in displacing the radioligand compared to 5-IT (see Figure 20).

	1-way ANOVA			
Drugs	CPu		NAc shell	
5-IT	F(5,30)=35.82	p<0.0001	F(5,30)=33.12	p<0.0001
2-DPMP	F(5,30)=66.94	p<0.0001	F(5,30)=51.46	p<0.0001

	Three-way ANOVA		
Drugs	CPu, NAc shell		
5-IT , 2-DPMP	Concentrations	F (5, 5) = 169.2	p<0.0001
	Drug	F (1, 5) = 205.2	p<0.0001
	Area	F (1, 5) = 0.006299	p>0.05
	Concentrations x Drug	F (5, 5) = 11.58	p<0.0001
	Concentrations x Area	F (5, 5) = 0.5193	p>0.05
	Drug x Area	F (1, 5) = 6.599	p<0.05
	Concentrations x Drug x Area	F (5, 5) = 0.6091	p>0.05

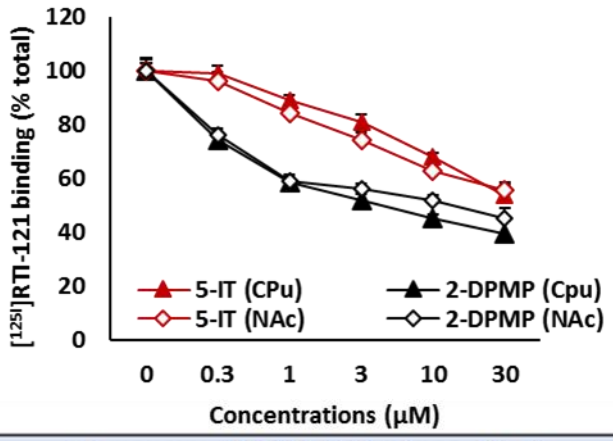

	Three-way ANOVA (Tukey's post hoc)				
	Comparisons			Significance	
0.3µM	5-IT (CPu)	vs	2-DPMP (CPu)	****	p<0.0001
	5-IT (NAc)	vs	2-DPMP (NAc)	***	p<0.001
1.0 µM	5-IT (CPu)	vs	2-DPMP (CPu)	****	p<0.0001
	5-IT (NAc)	vs	2-DPMP (NAc)	****	p<0.0001
3.0 µM	5-IT (CPu)	vs	2-DPMP (CPu)	****	p<0.0001
	5-IT (NAc)	vs	2-DPMP (NAc)	**	p<0.01

Figure 20: The tables on the top and on the bottom, show the statistical results of the binding data of [^{125}I]RTI-121 to DAT in presence of increasing concentrations of 5-IT and 2-DPMP in CPu and NAc shell (One-way and tree way-ANOVAs followed by post-hoc Tukey's tests). On the middle, graphical representation of pooled data from 6 rats showing the binding of [^{125}I]RTI-121 in presence of increasing concentrations of 5-IT and 2-DPMP in CPu and NAc shell.

Effect of increasing concentrations of 5-IT on [^{125}I]RTI-121 autoradiographic binding

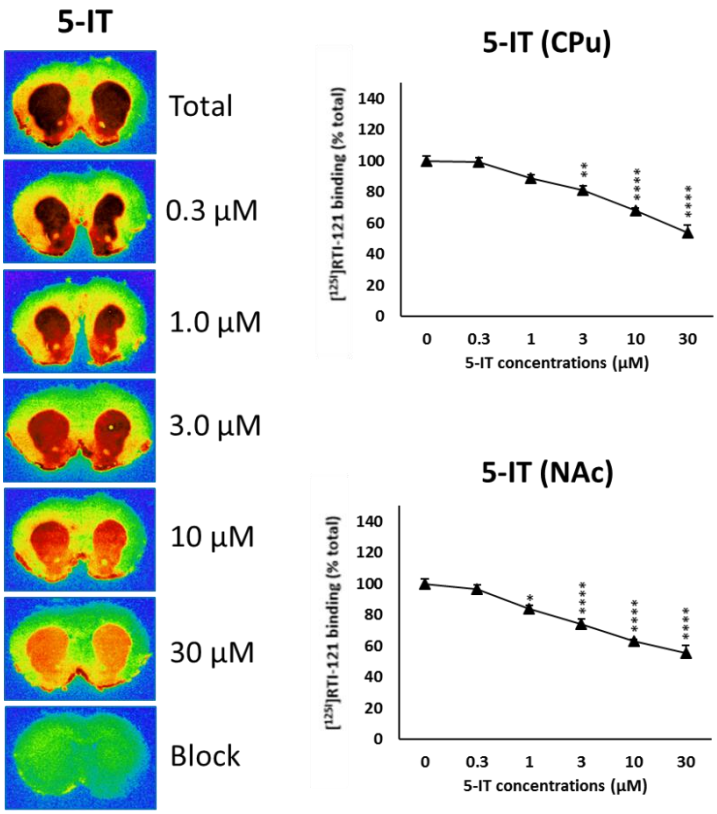

Figure 21: Representative computer-enhanced images of brain slices (on the left) and graphical representation of pooled data from 6 rats (on the right) showing the binding of [^{125}I]RTI-121 to DAT in presence of increasing concentrations of 5-IT in both NAc shell and CPu. Data are expressed as mean percentage ± standard error of mean (SEM) against the control value with significance set at $p<0.05$. One-way ANOVA analysis (****$p<0.0001$, **$p<0.01$, * $p<0.05$, post-hoc Tukey's tests).

Effect of increasing concentrations of 2-DPMP on [^{125}I]RTI-121 autoradiographic binding

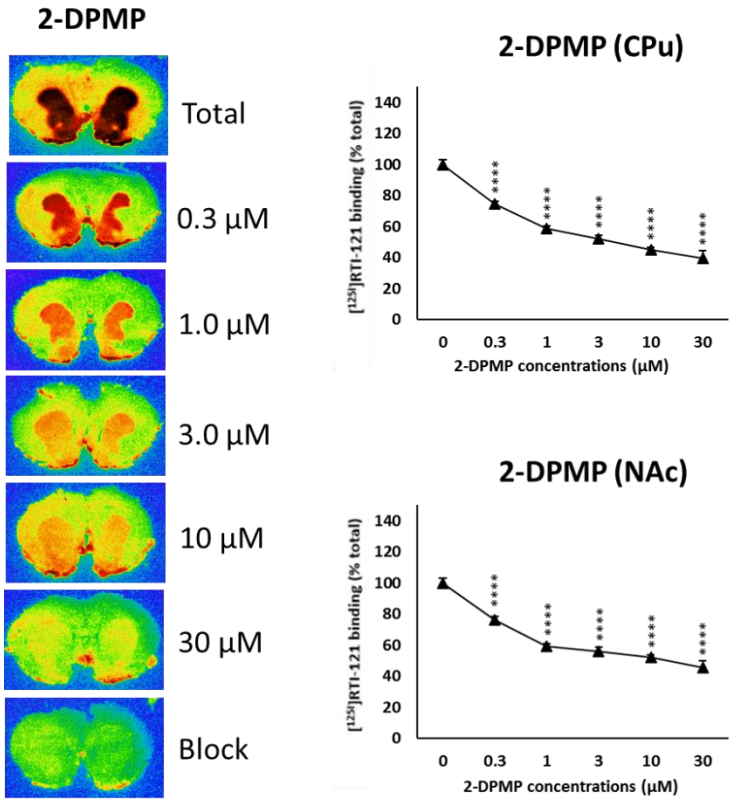

Figure 22: Representative computer-enhanced images of brain slices (on the left) and graphical representation of pooled data from 6 rats (on the right) showing the binding of [^{125}I]RTI-121 to DAT in presence of increasing concentrations of 2-DPMP in both NAc shell and CPu. Data are expressed as mean percentage ± standard error of mean (SEM) against the control value with significance set at $p<0.05$. One-way ANOVA analysis (****$p<0.0001$, post-hoc Tukey's tests).

3.5.3) Synthetic stimulants and DAT autoradiography studies: discussion

Consistent with previous *in vitro* studies, 5-IT and 2-DPMP behave as highly potent DAT ligands able to compete with the radioligand [^{125}I]RTI-121 in a concentration-dependent way in CPu and NAc brain slices. Notably, 2-DPMP could displace the radioligand in both cerebral regions, starting from lower concentrations (0.3 µM) compared to 5-IT (1.0 µM in the NAc shell and 3.0 µM in the CPu). On the other hand, larger concentrations of 5-IT (10 and 30 µM) in both areas caused a comparable displacement of the radioligand as 2-DPMP. The effect of these two drugs is notable, especially considering that a prototypical stimulant drug like cocaine is able to significantly displace [^{125}I]RTI-121 at higher concentrations (3, 10 and 30 µM) compared to 2-DPMP and 5-IT in NAc brain slices, under the same methods (Strazielle et al., 1998) and conditions (Opacka-Juffry et al., 2014).

As previously observed with other drugs of abuse, the high affinity for DAT may account for the high abuse potential of these drugs in humans and animals (Banks et al., 2014; Negus and Miller, 2014). Indeed, stimulants belonging to different classes share the ability to act at the level of DAT as pure inhibitors (like 2-DPMP) or releasing agent (such as 5-IT) influencing the duration and the extent of the dopaminergic signal in the reward system and producing positive effects such as pleasure, euphoria, increased energy and sociability. On the other hand, several sympathomimetic toxidromes can occur as a result of their activity at the level of monoamine transporters which, in the case of 5-IT, is furthermore coupled with inhibition of monoamine oxidase (MAO) activity.

Chapter 4: *In vitro* fast scan cyclic voltammetry studies

4.1) *In vitro* fast scan cyclic voltammetry overview

Fast-scan cyclic voltammetry (FSCV) is a powerful electrochemical analytical technique that has been used extensively to investigate drug mechanisms associated with neurotransmitter transmission in order to develop new strategies for therapeutic intervention in drug addiction. FSCV presents several advantages, including: real-time investigation of neurotransmitter concentrations, quantification of changes in neurotransmitter concentrations in the nanomolar to micromolar range, minimal tissue damage and high spatial resolution according to the micrometer size of the probe used (Boulton et al., 1995).

In detail, *in vitro* FSCV enables the monitoring of neurochemical release of electroactive neurotransmitters (e.g. monoamines) with a temporal resolution that allows pharmacological manipulation of neurotransmitter release in specific regions of brain slices enabling the discrimination between neurotransmitter release and uptake events (Garris and Wightman, 1995).

Studies using brain slices have been recognised as particularly advantageous in defining the mechanisms underlying neurotransmitter dynamics in different brain regions, and how these processes can be affected by pharmacological manipulation (Stamford et al., 1995; John, & Jones, 2007).

In detail, using brain slices provides several advantages:

- ✓ numerous slices can be made from each target brain region;
- ✓ one single animal can be used to obtain slices from different brain regions;
- ✓ electrode placement can be easily and carefully performed in specific anatomical areas, including very small regions;
- ✓ physiological parameters (pH, temperature, degree of oxygenation) can be constantly regulated and monitored;
- ✓ pharmacological activity of the drugs can be evaluated avoiding hepatic metabolism;
- ✓ unwanted drug interactions can be avoided (e.g. interactions with chemicals typically used to anesthetize animals);
- ✓ Drugs characterised by high toxicity or poor penetration through the blood-brain barrier can be tested (Stamford et al., 1995; John, & Jones, 2007).

However, using brain slices has some drawbacks:

- ✓ the usual input and output pathways present in the intact brain and the connections with the periphery are compromised;
- ✓ the tissue degrades at a faster rate than in the live animal;
- ✓ the *in vivo* activity patterns and dynamics are not totally reproduced (loss of hormonal regulations and blood circulation through the vascular system; loss of the peripheral degradation of the molecules);
- ✓ the tissue properties may be altered around the cutting surface, affecting the metabolic state of neurons;
- ✓ the effects of decapitation ischaemia on the health condition of the slice have not been well established (Schurr, 1986).

Electrodes used in Fast Scan Cyclic Voltammetry in rat brain slices

FSCV recordings are performed using an electrochemical system composed of four different electrodes: reference, auxiliary, stimulating and recording electrodes.

The reference electrode is a silver/silver chloride electrode made from a silver wire coated with a layer of silver chloride. The function of this electrode is to provide a stable voltage to which the working electrode potential is referenced.

The auxiliary electrode is an inert conductor and specifically a stainless-steel wire which records changes in the working electrode potential. Any electrochemical event in the working electrode is associated with an opposite electrochemical reaction in the auxiliary electrode.

The stimulating electrode is a bipolar steel electrode (A-M Systems, WA, USA) used to apply electric current to the tissue. It is made of two epoxy-insulated tungsten microelectrodes whose tips are properly tapered and sanded using abrasive paper in order to cause the minimal trauma to the tissue whilst allowing the passage of the required amount of the current.

The recording microelectrode is the electrode on which the reaction of interest takes place. The most common form of working electrode used in FSCV is a carbon fibre microelectrode which allows scans of wide potential windows (Boulton et al., 1995; Stamford et al., 1995).

Carbon fibre microelectrode preparation

Carbon fibre microelectrodes are made by aspirating a single carbon fibre (8 μm diameter) into a borosilicate glass capillary (10 cm length; 2.0 mm outer diameter, 1.16 mm inner diameter; Harvard Apparatus Ltd, Kent, UK) through vacuum suction. Each capillary is pulled into two electrodes using a microelectrode puller (P-30, Sutter Instruments Co., USA). The electrode is then thoroughly examined using a high-power microscope (100-200x magnification) in order to check if there is a good glass-carbon junction that indicates a good stability of the electrode. The exposed length of the carbon fibre is then trimmed to a length of approximately 75 μm using a scalpel under the guidance of a high-power microscope (100-200x magnification). Before use, microelectrodes are backfilled with artificial Cerebro-Spinal Fluid (aCSF) using a needle (25 gauge, 3.5 in., Becton–Dickinson and Co., Franklin Lakes, NJ) and a single thread of copper (Squires Electronics, Inc., Cornelius, OR) is then inserted and pushed into the electrode tip and used for connection to the headstage amplifier. An auxiliary electrode and a reference electrode are also connected to the headstage amplifier and located in the recording chamber in contact with the aCSF solution (John, & Jones, 2007; Brierley & Davidson, 2013). The tip of the carbon microelectrode is then left in the aCSF for a period during which scans are applied for 15 minutes before use and the noise level and the shape of the current signal is closely checked to predict the accuracy and sensitivity of the electrode. After this period, the microelectrode is left to equilibrate in aCSF for other 20 minutes before use ('frying process'). Good microelectrodes can be used for a few days and some precautions include: leaving the microelectrode in distilled water between experiments, manipulate them with care or sonicate them (application of sound energy to speed the removal of the brain tissue that occludes the electrodes' tips by breaking intermolecular interactions) (Boulton et al., 1995; Stamford et al., 1995).

4.2) Fast scan cyclic voltammetry principles

Typically, during the experiment, the carbon fibre microelectrode is inserted into specific brain regions of living brain slices and a voltage in a triangular wave fashion is applied allowing the oxidation and reduction of the neurotransmitter. For neurotransmitters like DA a -1.0 to +1.4 V (vs Ag/AgCl) waveform is typically used with a voltage scan rate of 480 V/s and multiple waveform repetitions that enable the monitoring of kinetic events (uptake and release) with high temporal resolution are applied (Hafizi et al., 1990). The waveforms are originated from a generator and applied to the potentiostat. The current output of the working electrode is amplified and displayed on a computer used to control an X-Y chart recorder and stored on a

disk for data analysis on a computer. In detail, pulses may be programmed using the CED 1401 AD converter and the peaks may be graphed using the Spike software (Stamford et al., 1995).

Low voltages applied to the carbon fibre microelectrode enable the electrolysis of the neurotransmitter and the electrons resulting from this process represent the current output of the working electrode. Digital subtraction of the background current signals generated at the microelectrode before and after stimulation is usually made in order to isolate the Faradaic (redox) current originated by the electrolysis of the neurotransmitter. The two signals are indeed superimposable except at the redox positions. The extraction of Faradaic signals requires high-resolution digital methods that rely on computer-based systems and are used in some laboratories to enhance the resolution of data acquisition. The current measured gives an indication of the number of molecules oxidized/reduced and thus detection of the neurotransmitter levels before and after pharmacological manipulation (Stamford et al., 1995; John, & Jones, 2007).

To provide information on transmitter kinetics, a sample and hold circuit is set to monitor the current at the oxidation potential of the transmitter and the signal is displayed on a y-t chart recorder in the computer. In detail, while the X-Y recorder displays the cyclic voltammogram, the y-t recorder shows changes in oxidation currents and thus in concentrations. For quantification of changes in neurotransmitter concentration over time, the current is measured real-time and provides an indication of the ability of the pharmacological agents in changing neurotransmitter uptake and release events (see Figure 23) (Stamford et al., 1995).

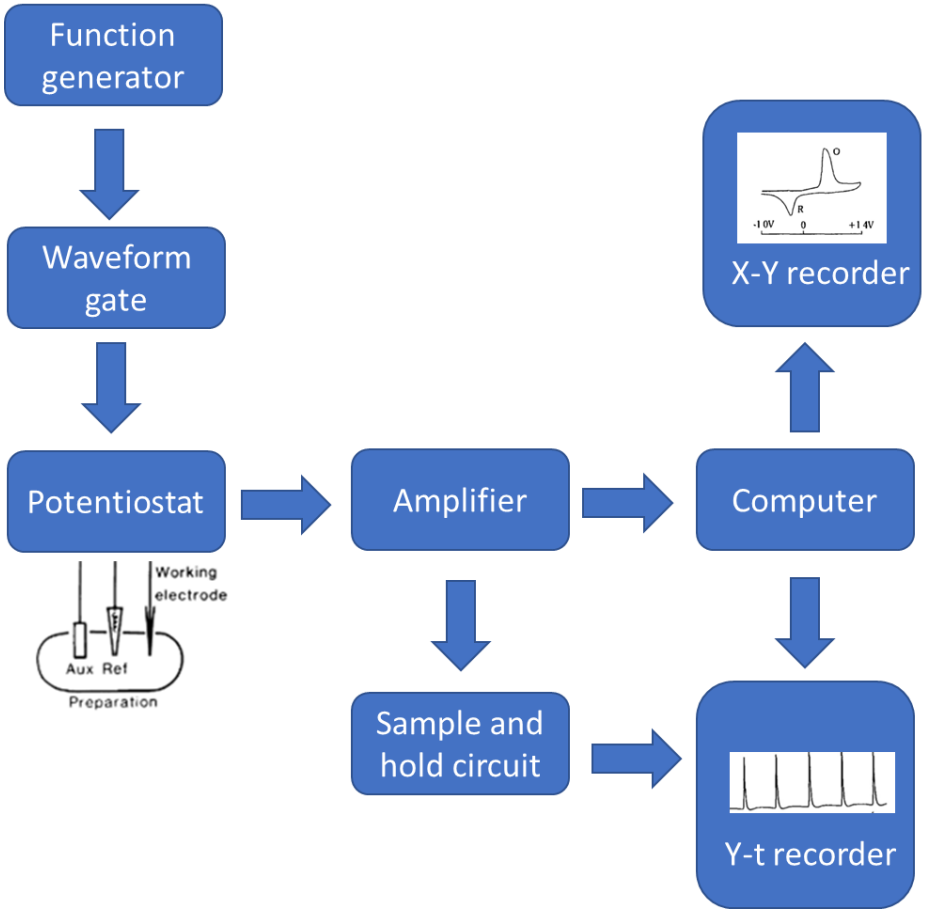

Figure 23: Fast Scan Cyclic Voltammetry set up (generator, waveform gate, potentiostat, amplifier, computer, sample and hold circuit, X-Y recorder, Y-t recorder). The picture was adapted from Stamford et al., 1995.

4.3) BB-22 and FSCV studies: aims

According to previous studies, the rewarding properties of synthetic cannabinoids involve the relative contributions of complex neuronal circuits (Lupica et al., 2004).

It is likely that the interaction of SCs with CB_1 receptors may promote the inhibition of GABA release onto DA neurons projecting from the VTA to the NAc (CB_1-mediated disinhibitory mechanism) and an increase of DA neuron-firing rate and DA neuron burst activity in the VTA with consequent enhance of terminal release of DA in the NAc. Furthermore, part of the rewarding actions of SCs seem to be mediated by actions occurring within the NAc, where SCs are thought to produce a disinhibition of the GABAergic output to the VTA and other brain structures (Lupica et al., 2004).

However, it has been discovered that many drugs of abuse have a direct effect on synaptic processes in the NAc and are self-administered by animals directly into the NAc (McBride et al., 1999). Based on these observations, we hypothesized that part of the rewarding actions of

these drugs could be mediated via direct interactions of SCs on synaptic processes within the NAc not necessarily mediated by CB_1 receptors. To this end, we studied the effects of BB-22 on evoked DA efflux and DA re-uptake half-life in brain slices containing the NAc, using the *in vitro* FSCV procedure. The rationale behind the choice of this drug was related to its highest affinity, potency and efficacy at the level of CB_1 receptors compared to the other synthetic cannabinoids tested (De Luca et al., 2016), and to the numerous health implications raised by using this drug over the recent years. *In vitro* FSCV was employed according to its ability to enable real-time investigation of dopamine dynamics before and after pharmacological manipulation in a specific region of brain slices (e.g. NAc shell), enabling discrimination between release and uptake events (Garris and Wightman, 1995). The NAc shell was selected as the target area in accordance with its role played in addiction. Indeed, typical drugs of abuse share the ability to activate the reward pathways and increase DA release preferentially in the NAc shell (Di Chiara and Imperato, 1988; Lecca et al., 2006). The mechanism responsible for this increase may depend on the effect of neuronal circuits inside or outside the NAc shell, highlighting the contributions of distinct pathways originating from different areas of the reward system. Using brain slices containing the NAc shell, limits the investigation of dopamine dynamics in this specific region, avoiding the potential influence of other regions of the reward system. Although this procedure does not reproduce the *in vivo* dynamics, it allows us to demonstrate whether BB-22 is able to increase DA release in the NAc shell without the contributions of other neuronal circuits (Lupica et al., 2004). Additionally, the pure pharmacological activity of BB-22 can be evaluated avoiding the potential influence of the periphery. The concentration range used (0, 0.03, 0.1, 0.3; 1.0 µm) and the strain of animals (Wistar rats) employed were in accordance with those used in *in vitro* autoradiography studies.

To sum up, our study aimed to investigate the effects of BB-22 on: basal dopamine levels; electrically-evoked DA peak efflux; and the time-constant of the dopamine decay phase (index of dopamine reuptake) in NAc shell brain slices.

4.4) BB-22 FSCV studies: materials and method

Preparation of the aCSF

The artificial cerebrospinal fluid (aCSF) closely matches the electrolyte concentrations of endogenous CSF and is prepared from high purity water and analytical grade reagents as previously described by Brierley and Davidson (2013). This media was used for storing brain slices after dissections, and for perfusing slices during electrophysiological recordings. The composition was as follows: NaCl 126 mM; KCl 4 mM; KH_2PO_4 1.4 mM; $MgSO_4$ 1.3 mM;

$NaHCO_3$ 26 mM; D-glucose 4 mM; $CaCl_2$ 2.4 mM in de-ionised water and oxygenated with 95% O_2/5% CO_2 at 32°C for at least 45 minutes before use. In order to prevent the precipitation of insoluble calcium salts, the calcium chloride was added after complete dissolution of the other salts.

Brain slices preparation

Wistar rats of eight weeks (body weight: 250 grams) were housed in the St George's University of London's animal house in groups of four per cage and kept under an inverted 12:12 hour light/dark cycle and at a constant temperature of 22 ± 2°C and humidity of about 60%. Tap water and standard food were available ad libitum in the home cage. The animals were sacrificed by cervical dislocation and quickly decapitated. Rats were treated in accordance with the UK Animals (Scientific Procedures) Act 1986 and UK Home Office regulations. No ethical protocol was required as brain slice studies are not covered by Home Office regulations. Their brains were rapidly removed and kept in ice cold oxygenated (95% O_2/5% CO_2) aCSF before being cut in 400 μm serial coronal sections in rostro-caudal direction (coordinates: from +1.0 to +2.2 mm versus bregma) (Paxinos and Watson, 2008) using the vibratome. The temperature of slicing was kept around 0 ± 1°C (with ice floes present in the aCSF solution) to reduce the energy demands of the tissue and to promote easy cutting (Stamford et al., 1995). Thereafter, the slices were left to equilibrate for one hour at room temperature on a plastic mesh in a slice saver filled with aCSF continuously bubbled with 95% O_2/5% CO_2. After equilibration, each slice was then transferred to the inner bath of a brain slice chamber provided with aCSF at a flow rate of 1 ml/min and temperature at 32.5 ± 0.5 °C and left to equilibrate in the new environment for about 40-45 minutes before applying electrical stimulation (Stamford et al., 1995). The temperature in the slice chamber was monitored using a CEM DT-613 digital thermometer. Low temperatures allow a long survival of the slice in healthier conditions and an optimal recording of the neurotransmitter dynamics. The environment of the inner chamber is regulated by an outer chamber containing distilled water continuously warmed by a heating coil in communication with a thermostatically heated water bath (Grant, Cambridgeshire, UK). The outer chamber allows the passage of oxygenated aCSF through a loop of tubing into the inner bath assuring that the liquid into the inner part is kept at a constant temperature. Artificial cerebrospinal fluid (aCSF) is constantly removed from the fluid surface through a syringe needle connected to a tube in communication with a vacuum pump which exercises a negative pressure. The auxiliary and reference electrodes are located away from the slice and immersed in the aCSF solution attached to a binding post on the top of the slice chamber (Davidson et al.,

2011). The recording microelectrode is placed in the NAc shell at the beginning of the equilibration period to monitor dopamine levels which could be affected by several factors like poor condition of the slice and high temperature (Davidson et al., 2011; Brierley and Davidson, 2013). All the electrodes (auxiliary, reference and recording) were connected to the headstage amplifier (NL 106).

Drugs

The synthetic cannabinoid BB-22 was purchased from an Internet source (www.researchchemist.co.uk) and its identity and purity were evaluated using nuclear magnetic resonance spectroscopy (NMR), gas chromatography mass spectrometry with electron ionisation (GC-EI-MS) and HPLC. The drug was solubilised in pure DMSO and five different concentrations of the drug were assessed: 0, 0.03, 0.1, 0.3; 1.0 μM. Each concentration was tested in six different brain slices from different animals except for BB-22 0.1μM which was tested in 7 different brain slices.

Electrical stimulation protocol

The electrical stimulation protocol was programmed into the Spike 7 data capture and sent to digital to analog and input–output interface boards (National Instruments, Austin, TX), which sends the stimulus to optical isolators (Neuro Log NL-800, Medical Systems, Greenvale, NY). After optical isolation, the stimulus is sent to the bipolar stimulating steel electrode (A-M Systems, WA, USA). The stimulating electrode was mounted on a micromanipulator and the tips were positioned on the surface of the slice. The carbon-fibre microelectrode (mounted on a separate micromanipulator) was positioned at a depth of 75 μm into the slice, and with a distance of 200 μm between the tips of the bipolar stimulating electrode in order to create an equilateral triangle. Prior electrical stimulation the stability and the health conditions of the brain slices were monitored as in the case of poor slice health large amounts of dopamine may be released and affect the experiment (Davidson et al., 2011). Electrode placement was performed using a stereo-microscope with a maximum magnification of 20x. According to previous studies, midbrain dopaminergic neurons in basal conditions fire at low frequencies of 5–10 Hz, but in the presence of rewarding stimuli they show more prevalent periodic short bursts of high-frequency activity (20 Hz) (Hyland et al., 2002). Accordingly, the stimulation protocol applied was conceived to mimic the burst firing typical of rodent dopaminergic neurons. A sequence of 10 × 1 ms 10 mA pulses was applied at a frequency of 20 Hz, with stimulus sequences applied every 5 min (Davidson & Stamford, 1993). Pulses were

programmed using the CED 1401 AD converter and the Spike software. The input voltage applied to the carbon electrode went from 0 to −1, up to +1.4, back to −1 and back to 0 V at 480 V/s. The whole voltage scan took 20 ms. Typically, the DA oxidation peak is at approximately 500–700 mV vs Ag/AgCl, while the single DA reduction peak is around −200 mV (John, & Jones, 2007; Brierley and Davidson, 2013).

Data acquisition and statistical analysis

Changes in recorded current in correspondence of the DA oxidation peak were graphed by the Spike software. Two parameters were calculated for each efflux episode: the peak height and the time constant of the half-life of the decay curve (analysed using Spike 7 software). In detail, stimulation events were applied every 5 minutes, the drug was added after three stable consecutive baseline events and its effect on dopamine dynamics was observed for one hour. All data were presented as percentages of the mean baseline data. Statistical analysis was conducted using Statistica (version 10) and performing two-way ANOVA. Data were expressed as mean ± standard error of mean (SEM), with significance set at $p<0.05$ (John, & Jones, 2007; Brierley and Davidson 2013).

4.5) BB-22 FSCV studies: results

According to our findings, BB-22 had no significant effect on evoked peak dopamine efflux at any concentrations tested. In this regard, although two-way ANOVA for repeated measures revealed a significant effect of the concentration: $F(4,26)=4.53$ $p<0.01$; of the time: $F(12,312)=1.97$ $p<0.05$; and a significant interaction time x concentration: $F(48,312)=1.74$ $p<0.005$; the post-hoc Tukey's test did not reveal any significant effect of BB-22 (0.03, 0.1, 0.3, 1 uM) in altering evoked dopamine efflux in the NAc shell in comparison to the control group (DMSO 1 µM) and any differences compared to the basal levels (see Figure 24). Additionally, BB-22 did not elicit any significant effect on the dopamine reuptake time-constant at any concentrations tested (figure not shown).

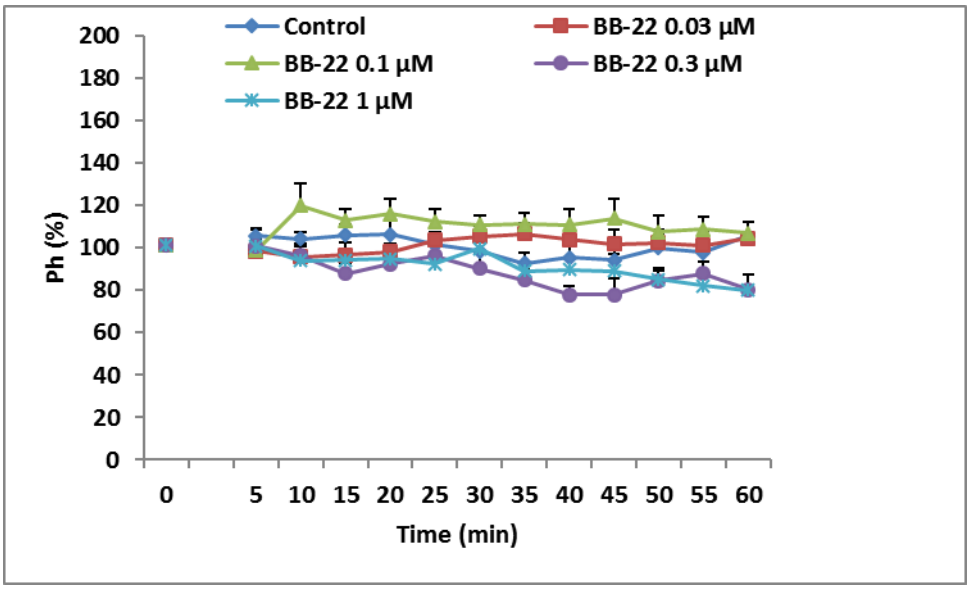

Figure 24: BB-22 FSCV studies. Dopamine Peak height (Ph) data after BB-22 exposure. The drug was added to the perfusion solution in contact with the brain slice after three stable consecutive baseline events and its effect on dopamine dynamics was observed for one hour. Data are expressed as percentage of basal values which are means ± SEM of at least three determinations (Control: n=6; BB-22 0.03µM, n=6; BB-22 0.1µM, n=7; BB-22 0.3µM, n=6; BB-22 1.0 µM, n=6). Two-way ANOVA, post-hoc Tukey's test.

4.6) BB-22 and FSCV studies: discussion

According to our findings, local application of the synthetic cannabinoid BB-22 in brain slices was unable to change evoked DA efflux and dopamine reuptake time-constant in the NAc shell at any doses tested.

Based on these observations, the results obtained would suggest the relative contributions of complex neuronal circuits, either within or outside the NAc, whose modulation would interfere with the interactions between BB-22 and dopaminergic neurons and represent critical pathways accounting for some of the rewarding properties of BB-22 exposure.

In this regard, although FSCV studies in brain slices may be advantageous to focus the investigation of dopamine dynamics in a specific brain region, they do not allow us to monitor and appreciate the potential influence of mechanisms involving other areas of the reward system (e.g. VTA) (Lupica et al., 2004).

It is indeed likely that BB-22, similarly to other SCs may disinhibit DA neurons projecting from the VTA to the NAc by promoting the inhibition of GABAergic neurons within the VTA (CB_1 disinhibitory mechanism) (Lupica et al., 2004).

Notably, this mechanism relies on the integrity of DAergic projections from the VTA to the NAc which is preserved in *in vivo* studies, and affected in NAc brain slices. As a result, the

increase of DA release mediated by BB-22 could not be appreciated in brain slices where all neuronal circuits outside the NAc have been lesioned.

Anyway, the findings obtained with this procedure allowed us to reject the hypothesis that part of the rewarding actions of BB-22 could be mediated via direct interactions on synaptic processes within the NAc without the contribution of external neuronal circuits. Additionally, the lack of effects on the dopamine reuptake time-constant, allowed us to discard the hypothesis of any direct action of BB-22 at the level of dopamine transporter in the NAc shell at the doses tested and to support the idea that neuronal circuits outside the NAc are indispensable to mediate DA increase in the NAc shell induced by BB-22.

Chapter 5: Microdialysis studies

5.1) Microdialysis overview

Microdialysis is a procedure widely used in neuropharmacology to allow continuous recovery and quantification of endogenous molecules (e.g. neurotransmitters, hormones, neuropeptides) from the extracellular fluid in the brain of freely moving animals (Chefer et al., 2009).

This procedure relies on the dialysis principle by which small-size molecules and water diffuse across a semipermeable membrane, driven by a concentration gradient between the extracellular fluid and the perfusion medium. The key element in microdialysis is the probe used as a tool to recover molecules from the extracellular space (Chefer et al., 2009). All probes are composed of a tubular dialysis membrane, continuously perfused with a liquid (artificial extracellular fluid) enabling the passage of compounds with suitable molecular masses according to the membrane cut-off. The perfusion liquid is infused slowly and continuously through the probe using microinfusion syringe pumps set up with perfusion rates ranging from 0.3 to 3 µl/min and connected to the probe through polyethylene tubes. Typical sample collection time ranges from 1 to 20 minutes. The dialysate fluid is analysed at specific time intervals using the High-performance Liquid Chromatography (HPLC) system equipped with an electrochemical detector (Chefer et al., 2009).

Microdialysis probe

Vertical probe (see Figure 25) is prepared according to the method of Tanda et al. (1996). It is composed of an inlet silica wire whose tip is shaped according to a 45-degree angle and by an outlet silica capillary whose extremity is modelled according to a truncated conical geometry. An inlet capillary is inserted into a stainless-steel tubing (22g) characterised by a sharp tip containing a small opening at one extremity, and a truncated conical geometry on the opposed side. A further hole is made 8 mm away from the sharp tip and serves as insertion point for the outlet capillary whose opposed extremity is surrounded from the metal outlet tubing. The lengths of silica capillaries protruding from the inlet stainless-steel tubing are adjusted and fixed with superglue (Super attack, Loctite) so that the difference between the inlet and outlet silica tube lengths corresponds to the desired extent of the active membrane. Inlet and outlet silica tips are covered by an artificial kidney membrane made of an acrylate copolymer of sodium-meta-allyl sulfonate (HOSPAL, outer diameter 310 µm and internal diameter 220 µm) which allows the passage of compounds with suitable molecular masses (400-600 Da) according to the membrane cut-off (Øe=310 µm; Øi=220 µm). The perfusion solution enters the probe passing through the inlet capillary, crosses the membrane and is then collected as a

dialysate from the outlet silica tubing. A circular-shaped polyethylene tube connected to the extremity of the stainless-steel outlet tubing, allows collection of the perfusate which is then injected in the HPLC system for analysis.

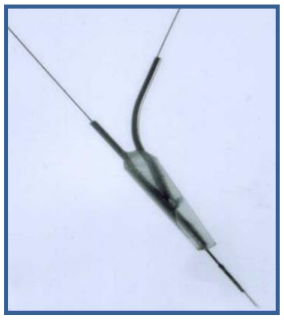

Figure 25: Picture of the microdialysis probe. The image was retrieved from the following website: http://slideplayer.it/slide/4250028/

Microdialysis surgery

Before starting surgery, stereotaxic coordinates for the target brain regions are determined using the rat brain Atlas of Paxinos and Watson (1998) which provides coordinates for the anterior-posterior (AP), lateral (L), and dorsal-ventral (DV) planes using as a reference point the bony landmark (bregma) on the skull's animal (Zapata et al., 2009). After anaesthesia, the animal is mounted onto the stereotaxic apparatus (see Figure 26) by placing and locking each ear bar in contact with each tympanic membrane into the auditory canals and securing the mouth with an anterior clamp so that the middle of the animal's scalp is positioned according to a 90° angle with respect to the stereotaxic instrument platform (Geiger et al., 2008). Using the point of a scalpel blade, a midline incision is made in order to expose the skull surface; the skin is retracted with haemostats to keep the incision open and the connective tissue is scraped away. Using sterile cotton swabs, the exposed skull surface is dried and the bregma (intersection between coronal and sagittal sutures) and lambda (intersection between occipital and sagittal sutures) positions are identified. The proper mounting of the animal onto the stereotaxic apparatus is confirmed by detection of bregma and lambda positions on the same horizontal plane according to which the brain atlas coordinates are based. Consistent with the atlas of Paxinos and Watson (1998), the coordinates used are as follows: NAc shell: Antero-Posteriority=+2.2, Laterality=±1.1 from bregma and Verticality=- 7.8 from dura; NAc Core: Antero-Posteriority =+1.6, Laterality =±1.8 from bregma and Verticality=-7.5 from dura; mPFCx: Anteriority=+3.7, Laterality=±0.8 from bregma and Verticality=-4.8 from dura; CPu:

Anteriority=+1.2, Laterality=±3.0 from bregma and Verticality=-5.5 from dura. Saline is applied to clean the skull surface and anterior-posterior and lateral coordinates of the bregma are determined after mounting the probe in the holder and positioning it over the bregma. Coordinates for probe placement are then determined by adding or subtracting designated values from bregma coordinates and a hole is drilled at this location using an up-and-down motion until the dura meninx is achieved. The probe is then brought down until flexion of the dura meninx at which the ventral coordinates are recorded, and designated values are subtracted for specific brain regions. A sterile needle is then used to gently puncture the meninges and allow unhampered insertion of the probe which is then lowered according to the designated ventral coordinates. Haemorrhage can be reduced by applying a small ice bag around the bleeding. The probe is then tightly fixed to the skull using plastic tips as supports around the probe and dental cement for adhesion to the bone. Once the cement has completely dried the animal is removed from the stereotaxic apparatus and housed in a plexiglass hemispheric bowl. The experiment of microdialysis is performed at least 24 hours after surgery to allow the complete recovery of the animal and the restoration of neurotransmitters basal levels on the brain (Zapata et al., 2009; Geiger et al., 2008).

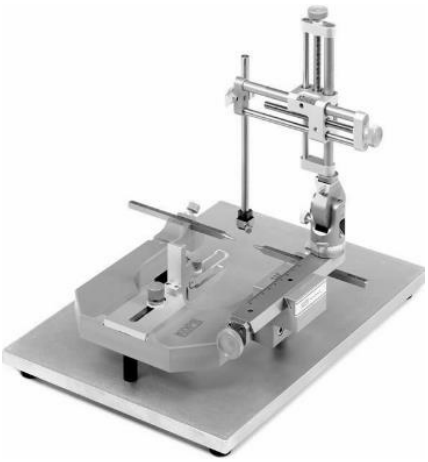

Figure 26: Picture of the stereotaxic apparatus. The image was retrieved from the following website: http://play.psych.mun.ca/~smilway/stereotax.htm

Microdialysis experiment

On the day of the experiment, animals are individually housed in plexiglass hemispheric bowls and their probes (aimed at specific brain regions) are connected to micro-infusion syringe pumps (CMA, Harvard Apparatus) through polyethylene tubes. The perfusion liquid (Ringer's solution) is infused slowly and continuously at constant rate of 1 μl/min and it mimics the

activity of the extracellular fluid present in the brain according to its chemical composition (147 mM NaCl, 4 mM KCl, 2.2 mM $CaCl_2$). The perfusion solution enters the probe passing through the inlet tubing, and endogenous solutes (neurotransmitters) cross the semipermeable membrane by passive diffusion from the extracellular fluid into the perfusion medium. The diffusion takes place as a result of a concentration gradient between the extracellular fluid of the brain and the artificial one (Ringer's solution) pumped at very low flow rate through the probe (Di Chiara, 1990). The dialysate leaving the probe through the outlet tube, is then collected through a circular-shaped polyethylene tube and analysed at certain time intervals using the HPLC system equipped with an electrochemical detector.

Sample analysis

During microdialysis experiments the dialysate samples are analysed for quantification of neurotransmitters using the direct injection of samples into a HPLC apparatus equipped with a reverse phase column and a coulometric detector (ESA, Coulochem II, Bedford, MA) (Imperato and Di Chiara, 1984). This method has been previously shown reliable for *in vivo* analysis of neurotransmitter release and their metabolites (Imperato and Di Chiara, 1984). The HPLC is a separation technique that involves the injection of a small volume of a sample (5 to 20 µL) into a reversed column (LC-18 DB, 15 cm, 5 µm particle size, Supelco) filled with a stationary phase (composed by tiny silica particles and long hydrocarbon chains attached to their surface) where the single components of the samples are forced through the column with a solvent (mobile phase) under high pressures (in the range of 400- to 600-bar) delivered by a pump (Cremella, LC, Italy). Normal flow rates in HPLC are in the 1- 2 ml/min range. A polar mobile phase is used (50 mM NaH_2PO_4, 0.1 mM Na_2-EDTA, 0.5 mM n-octylsodium sulfate, 15% (v/v) methanol, pH 5.5) to ensure a strong attraction between the polar solvent and polar molecules in the mixture, while non-polar compounds in the perfusate tend to interact with the hydrocarbon groups of the stationary phase to form van der Waals interactions.

Overall, mixture components are separated as a result of various chemical and/or physical interactions with the column's stationary phase and are quantified by an electrochemical detector whose output is analysed by a software program to provide the retention time (time of elution) of the sample components and their concentration levels (quantitative analysis) (Imperato and Di Chiara, 1984) (see Figure 25).

Electrochemical detection

Typically, coulochem detectors (e.g. ESA Coulochem II, Bedford, MA) present a standard cell containing two working electrodes (porous carbon electrodes) four auxiliary electrodes and four reference electrodes (Flanagan et al., 2005). The coulometric process is based on the complete electrolysis (complete oxidation/reduction) of the analyte at the porous electrode structure when a specific voltage is applied. The first electrode of the detector is set at + 125 mV (oxidation) and the second at - 175 mV (reduction). The electrons resulting from the oxidation/reduction processes are detected as current flows and the total charge passing through the electrochemical cell during electrolysis is proportional to the absolute amount of analyte. The coulometric detector can potentially be the most sensitive, accurate among many detectors available for quantitative analysis by HPLC. Overall, after separation and elution from the column, the analyte (e.g. dopamine) is oxidized at the first electrode of the detector and then reduced at the other electrode, with resulting production of a chromatographic peak. The peak is then compared to peaks of known sizes generated after injections of specific concentrations of dopamine (25, 50, 100 fentomoles) (Flanagan et al., 2005) (see figure 27).

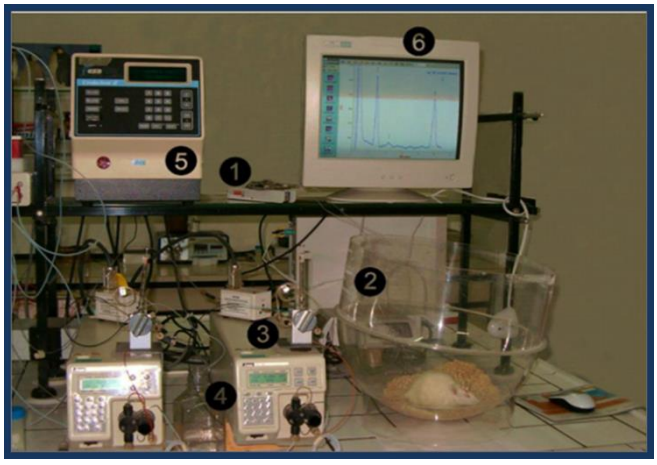

Figure 27: Picture of the microdialysis set-up: 1)perfusion pump; 2)Rat implanted with the probe; 3)Injector; 4)pump, column; 5)Detector; 6)Data analyser. This picture was retrieved from the following website: http://slideplayer.it/slide/4250028/

5.2) Synthetic cannabinoids and microdialysis studies

Aims

Over the years, the pharmacological effects of synthetic cannabinoids have been assessed in animals using different procedures focusing on different brain regions of the reward circuit. One common finding these studies share is the evidence for an enhancement in mesolimbic DA activity after intraperitoneal, intravenous administration or intracranial infusions of SCs. In the present study, four different synthetic cannabinoids (BB-22, 5F-PB-22, 5F-AKB-48 and STS-135), all belonging to the third-generation class, were selected to monitor DA release in specific areas of the reward system after their intravenous administration in freely moving rats. The rationale behind the choice of these drugs was related to the growing concern about the more serious health implications (e.g. toxicity events, fatalities, psychiatric consequences) raised using these new drugs and their higher abuse liability compared to the first-generation SC compounds. More serious clinical adverse effects and higher addiction-sustaining properties could be the expression of a distinct pharmacodynamical and pharmacological profile typical of these drugs. Indeed, as previously said, according to recent *in vitro* binding studies, all index SCs in the present study possess higher CB_1 affinity compared to the first-generation compound JWH-018; while only BB-22 and 5F-PB-22 show higher potency, with EC_{50} values significantly lower than JWH-018. Referring to their intrinsic activity, all of them except for STS-135, exhibit higher efficacy (E_{max}) compared to JWH-018 (De Luca et al., 2016).

In the present study, the effect of the compound with the highest CB_1 affinity, efficacy and potency, namely BB-22, was monitored in three different areas of the reward system (NAc shell, NAc core and mPFCx) and a wide pattern of dosages (0; 0.003; 0.01; 0.03; 0.1 mg/kg, i.v.) was tested and chosen in accordance with the K_i value found for this compound (De Luca et al., 2016). Additionally, the effect of a pre-treatment with the CB_1 inverse agonist/antagonist AM-251 (1 mg/kg, i.p.) was assessed, in order to establish the involvement of CB_1 receptors on the effect mediated by BB-22.

The other compounds were tested at a single dose level calculated considering their K_i values, and the ratio between the K_i value and the dose of BB-22 found effective in increasing DA release in the NAc shell. In view of the above, 5F-PB-22 was tested at 0.01 mg/kg, 5F-AKB-48 at 0.1 mg/kg and STS-135 at 0.15 mg/kg and their effects were monitored only in the NAc shell. An acute treatment was performed using the intravenous route of administration in the right jugular vein. This ROA was chosen among the others, because intravenous injection of

cannabinoids potentially leads to plasma profile similar to those observed after smoking (which is the most common way humans consume SCs) (Ohlsson et al., 1980). NAc shell, core and medial Prefrontal Cortex were selected as target areas in accordance with the role played by these regions in addiction. Indeed, typical drugs of abuse share the ability to activate the reward pathways and increase DA release preferentially in the NAc shell (Di Chiara and Imperato, 1988; Lecca et al., 2006). However, based on the type of drugs and dosages, an increase can be observed also in other regions of the reward system including mPFCx and NAc core (Moghaddam et al., 1989). The microdialysis procedure was employed in our study as a useful and reliable procedure for monitoring changes in DA levels in freely moving animals. Previous microdialysis studies have been performed to monitor the effect of JWH-018 in the mPFCx, NAc shell and NAc core. According to this study, JWH-018 increased DA selectively in the NAc shell (De Luca et al., 2015) similarly to Δ9-THC and WIN-55,212-2 (Tanda et al., 1997; Lecca et al., 2006). The maximal increase of dopamine was observed at 0.25 mg/kg, i.p., with a magnitude of about 65% over basal value. Notably, lower (0.125 mg/kg, i.p.) and higher doses (0.5 mg/kg, i.p.) were ineffective on DA release according to a concentration-dependent U-shaped curve as already observed in self-administration studies (De Luca et al., 2015). In our microdialysis experiments, we used the same strain of animals (Sprague-Dawley rats) and the same experimental design described in studies above mentioned focusing on JWH-018 (De Luca et al., 2015), aiming to avoid inter-strains variability. Overall, our study aimed to evaluate:

- whether the index SCs in our study share with JWH-018 the ability to stimulate DA transmission in the NAc shell;
- whether the synthetic cannabinoid BB-22 mediates DA transmission changes in other areas of the reward system, namely NAc core and mPFCx;
- the magnitude of DA change mediated by the index SCs in the present study;
- the involvement of CB_1 receptors on the effect mediated by the highest affinity, potency, efficacy compound BB-22.

No power calculations have been employed in this study and the experimental design was set up in accordance with previous studies conducted by the same team (De Luca et al., 2015), with the inclusion of some variations in terms of routes of administration and dosages which better addressed the aims of our analysis.

5.2.1) Synthetic cannabinoid microdialysis studies: materials and methods

Animals

Adult male Sprague-Dawley rats (body weight: 275-300 g; Harlan Laboratories, Italy) used for our experiments, were housed in groups of four per cage. The animal environment was kept under an inverted 12:12 hour light/dark cycle and at a constant temperature of 22 ± 2°C and humidity of about 60%. Tap water and standard food (Mucedola, Settimo Milanese, Italy) were available ad libitum in the home cage. All *in vivo* microdialysis experiments were conducted at the University of Cagliari (Italy) and carried out in accordance with the Guidelines for the Care and Use of Mammals in Neuroscience and Behavioural Research according to Italian (D.L. 116/92 and 152/06) and European Council directives (609/86 and 63/2010) and in compliance with the approved animal policies by the Ethical Committee for Animal Experiments (CESA, University of Cagliari) and the Italian Ministry of Health (Aut. N. 162/2016- PR). We made all efforts to minimize pain and suffering, and to reduce the number of animals used.

On the day before microdialysis experiment, animals underwent intravenous surgery followed by intracranial surgery.

Intravenous surgery

Before starting surgery, each animal was anesthetised with Equitesin (chloral hydrate 2.1 g, sodium pentobarbital 0.46 g, $MgSO_4$ 1.06 g, propylene glycol 21.4 ml, ethanol (90%) 5.7 ml, H_2O 3 ml; 3 ml/kg i.p.), shaved on the throat, and placed in the dorsal position on a surgical table. The legs were restrained to each side of the table and using a scalpel, a 2-cm incision was made right of the midline of the neck just over the right jugular vein. The connective tissue was stretched apart, and the jugular vein was exposed. The salivary and lymphatic tissues were separated and a section (5 mm) of the vessel was isolated. Using a silk suture, a loose tie was placed on both sides (cranial and caudal) of the vessel and using a small needle, an incision was made to pass the catheter in line with the vein. The catheter (Silastic, Dow Corning Corporation, Michigan, USA) was then inserted deeper into the vein towards the heart and secured tightening the cranial and caudal ligatures around the vessel. The other extremity of the catheter was exteriorised and fixed in the mid-scapular region of the back and the ventral incision was sutured (De Luca et al., 2016).

Intracranial Surgery

After intravenous surgery rats were surgically implanted with vertical dialysis probes aimed at the nucleus NAc shell, core and mPFCx. In detail, the animal was mounted onto the stereotaxic apparatus and a midline incision was made in order to expose the skull surface. Saline was applied to clean the skull surface and coordinates of probe placement were calculated using the bregma as a landmark. A hole was drilled, the meninge (dura mater) was gently punctured and the probe was lowered according to the designated ventral coordinates. At the end, the probe was tightly fixed to the skull using dental cement for adhesion to the bone. After surgery, experimental animals were removed from the stereotaxic apparatus and individually housed in plexiglass hemispheric bowls (Zapata et al., 2009; Geiger et al., 2008). According to the atlas of Paxinos and Watson (1998), the coordinates used to determine probe placement were the following: NAc shell: Antero-Posteriority=+2.2, Laterality=±1.1 from bregma and Verticality=-7.8 from dura; NAc Core: Antero-Posteriority =+1.6, Laterality =±1.8 from bregma and Verticality=-7.5 from dura; mPFCx: Anteriority=+3.7, Laterality=±0.8 from bregma and Verticality=-4.8 from dura (De Luca et al., 2016).

Microdialysis experiment

On the day of the experiment, the animals' probes were connected to micro-infusion syringe pumps (CMA, Harvard Apparatus) using polyethylene tubes. The perfusion liquid (Ringer's solution) was infused slowly and continuously at constant rate of 1 µl/min. Dialysate samples were collected every 10 minutes and the resulting specimens were injected into an HPLC system equipped with a coulometric detector (ESA; Coulochem II, Bedford, MA). The first electrode of the detector was set at +130 mV (oxidation) and the second at -175 mV (reduction). The composition of the mobile phase was: 50 mM NaH_2PO_4, 0.1 mM Na_2-EDTA, 0.5 mM n-octylsodium sulfate, 15% (v/v) methanol, pH 5.5. The sensitivity of the assay for DA was 5 fmol/sample. Dopamine recordings were performed for a total period of 180 minutes (De Luca et al., 2016).

Dissection and histology

Immediately after the microdialysis experiment, rats were sacrificed by injecting them with a lethal dose of anaesthetic; the probes were gently removed, and the brains were extracted and stored in formalin (8%). Later on, the hemisphere in which the probe was implanted was dissected and cut into coronal slices (100 µm of thickness) using a vibratome (Campden

Instruments, Biological Instruments, Besozzo, Italy). The slices were later transferred to multiwall plates and analysed under a microscope. Probe placement was evaluated according to the atlas of Paxinos and Watson (1998) (De Luca et al., 2016).

Statistical analysis

Data between different groups of treatment were analysed using Statistica for Windows (Version 10) and the differences in the levels of DA were analysed by ANOVA for repeated measures. Results obtained using ANOVA were then examined using the post-hoc Tukey's test (De Luca et al., 2016). ANOVA was used among other tests, because it is a reliable test to prove an assumed cause-effect relationship between independent variables (e.g. drug doses, time intervals) and dependent variables (e.g. dopamine levels) by comparing the mean scores within each group and among different groups based on different observations (variables). Specifically, the dependent variables represent measurements of the same variable (e.g. DA levels) at different times (measurements of DA levels on the same subject over time and under different dosages). The null hypothesis predicts that all data (e.g. all dopamine values) of all groups (e.g. all groups of animals that receive different drug dosages) have the same casual distribution and the difference between groups is casual. The null hypothesis is verified through the analysis of the F-value (ratio of two variances that are expected to be roughly equal under the null hypothesis). If the ratio of variances between groups and within groups (F value) is low, the group means are close together (low variability). By contrast, if the F-value is high, the group means are significantly different (high variability).

The post-hoc Tukey's test on the other hand, identifies the mean groups that are significantly different from each other. In our case, the post-hoc Tukey's test compares the means of each group of treatment to the means of every other group of treatment and it identifies any differences between means that are greater than the expected standard error. The formula for post-hoc Tukey's test is qs=YA-YB/SE, where YA=the larger of two means, YB=the smaller of two means, SE=standard error of the data in question. The qs value obtained is then compared to a q critical value (calculated on a population with normal distribution). Since the null hypothesis for Tukey's test predicts that the means being compared are from the same population, they should be normally distributed; thus, if qs value > q critical, the two means are critically different. At the end of analysis, both ANOVA for repeated measures and post-hoc Tukey's test provide the p-value (measure of evidence against the null hypothesis). When the threshold value assigned is p=0.05, p-value less than 0.05, indicates a significant difference

between means, by contrast, if the p-value is greater than 0.05, the null hypothesis cannot be rejected, and we cannot conclude that a significant difference between means exists.

Overall three distinct experiments were performed:

- Experiment 1: Effect of BB-22 administration on DA transmission in the NAc shell, core, and in the mPFC.
  Rats implanted in NAc shell, core and mPFCx were divided into different groups, one for each dose in each area. The doses of BB-22 tested were: 0 mg/kg; 0.003 mg/kg; 0.01mg/kg; 0.03mg/kg; 0.1 mg/kg (NAc shell, n= 29; NAc core, n= 27; mPFC, n= 21).

- Experiment 2: Role of CB_1 receptors on the NAc shell DA stimulation induced by BB-22.
  Rats implanted in NAc shell, were pre-treated intraperitoneally with the CB_1 antagonist/inverse agonist AM-251 (1.0 mg/kg) and injected intravenously with BB-22 (0.01 mg/kg) after thirty minutes (Veh n=6; AM-251 n=3).

- Experiment 3: Effect of 5F-PB-22, 5F-AKB-48, and STS-135 administration on DA transmission in the NAc shell.
  Rats implanted in NAc shell were divided into different groups, one for each drug at a specific dose: 5F-PB22 (0.01 mg/kg, n=6), 5F-AKB-48 (0.1 mg/kg, n=7) STS-135 (0.15 mg/kg, n=5). The vehicles were 17 in total.

5.2.2) Results for experiment 1: Effect of BB-22 administration on DA transmission in the NAc shell, core and in the mPFCx

In the first experiment the effect of a dose range of BB-22 (0.00, 0.003, 0.01, 0.03, 0.1, mg/kg i.v.) on DA transmission was assessed in the NAc shell and core, and mPFC. As shown in Figure 28, BB-22 (0.01 mg/kg, i.v.), caused an increase of DA levels selectively in the NAc shell. Notably, lower (0.003 mg/kg, i.v.) and higher doses (0.03, 0.1 mg/kg, i.v.) were ineffective on DA release according to a concentration-dependent U-shaped curve as already observed in previous microdialysis studies with JWH-018 (De Luca et al., 2015). Specifically, repeated measures three-way ANOVA revealed a significant effect of dose [$F(3,75)=4.46$; $p<0.01$], brain area [$F(2,75)=7.72$; $p<0.001$], and a significant dose x brain area interaction [$F(6,75)=6.46$; $p<0.0001$]. Furthermore, post-hoc Tukey's tests showed a significant increase

of DA, 20-40 and 90-120 minutes after BB-22 (0.01 mg/kg i.v.) injection compared to the basal value. Additionally, significant differences on DA dialysate were observed between:

- vehicle treated animals and 0.01 mg/kg i.v. treated animals implanted in NAc shell (90 min sample);
- 0.01 mg/kg i.v. treated animals implanted in NAc shell and 0.01 mg/kg i.v. treated implanted in NAc core (90 min sample);
- 0.01 mg/kg i.v. treated animals implanted in NAc shell and 0.01 mg/kg i.v. treated animals implanted in mPFC (30, 90 min sample) (see Figure 28).

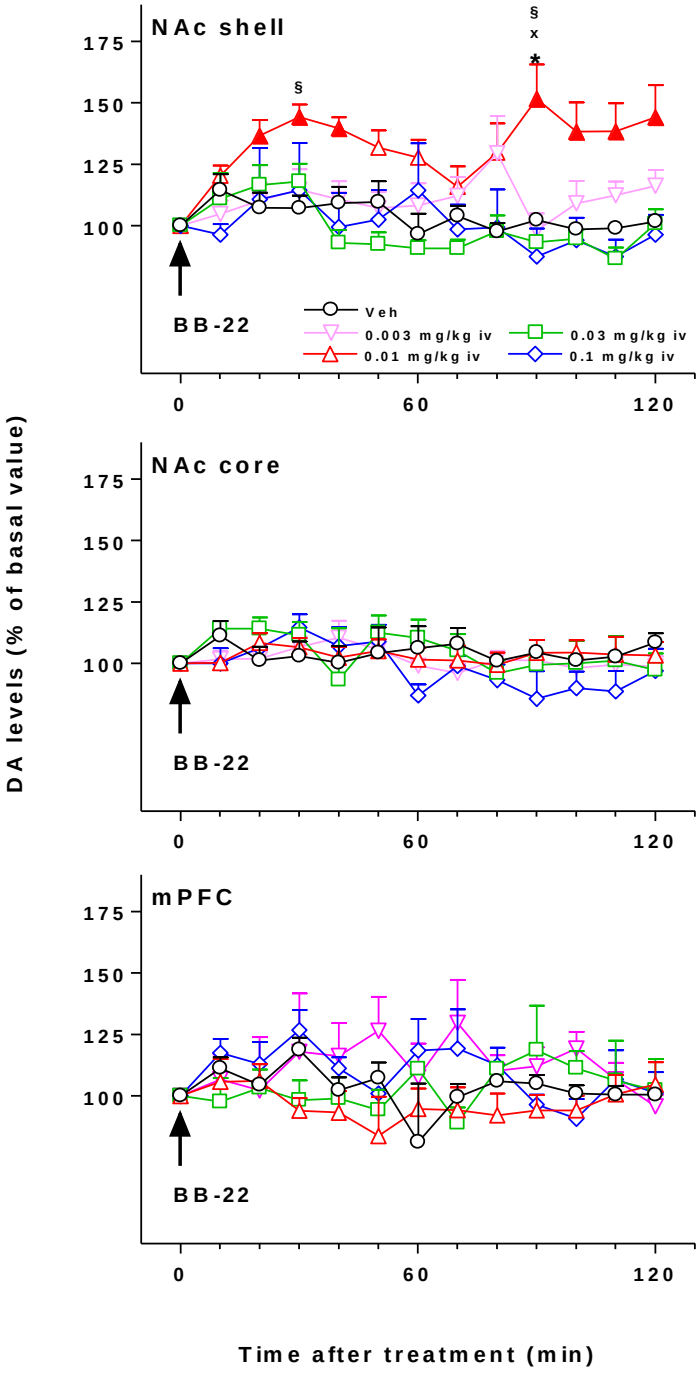

Figure 28*: In vivo* effect of BB-22 administration on DA transmission in the NAc shell, NAc core, and mPFC. Results are expressed as mean ± SEM of change in DA extracellular levels expressed as the percentage of basal values. The arrow indicates the moment of BB-22 i.v. injection at the dose of 0.003 mg/kg (magenta triangles), 0.01 mg/kg (red triangles), 0.03 mg/kg (green squares), 0.1 mg/kg (blue diamonds), or vehicle (black circles) in the NAc shell (A), NAc core (B), and mPFC (C). Solid symbol: $p < 0.05$ with respect to basal values; *$p < 0.05$ vs veh NAc shell group; × $p < 0.01$ vs 0.01 NAc core group; § $p < 0.01$ vs 0.01 mPFC group; (NAc shell n= 29; NAc core n= 27; mPFC n= 21) (Repeated measures three-way ANOVA, post-hoc Tukey's tests).

5.2.3) Results for experiment 2: Role mediated by CB_1 receptors on the increase of DA release in the NAc shell DA induced by BB-22

In the second experiment, we monitored whether the CB_1 inverse agonist/antagonist AM-251 (1 mg/kg, i.p.) was effective in reversing DA increase in the NAc shell mediated by BB-22 (0.01 mg/kg, i.v.) (see Figure 29). Two-way ANOVA showed a main effect of treatment [$F(1,11)=12.07$; $p< 0.005$], and treatment x time interaction [$F(18,198)=2.2$; $p < 0.005$] in animals pre-treated with the antagonist thirty minutes before BB-22 injection. Post-hoc Tukey's test showed the ability of AM-251 to significantly reduce dialysate DA in the NAc shell in comparison with rats pre-treated with the vehicle instead of the antagonist (90, 140, 150, 180 min sample).

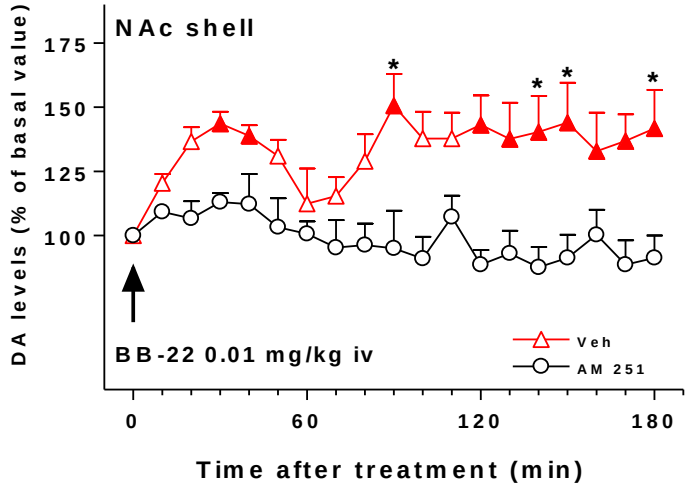

Figure 29: Blockade of BB-22 effect on the increase of DA transmission in the NAc shell mediated by AM-251. Results are expressed as mean ± SEM of change in DA extracellular levels expressed as the percentage of basal values. The arrow indicates the moment of BB-22 (0.01 mg/kg i.v.) injection in rats pre-treated with AM 251 (1.0 mg/kg i.p., 30 min before agonist) (circles) or vehicle (triangles). Solid symbol: $p < 0.05$ with respect to basal values; *$p < 0.05$ vs veh group. (veh n=6; AM-251 n=3) (Two-way ANOVA, post-hoc Tukey's test).

5.2.4) Results for experiment 3: Effect of 5F-PB-22, 5F-AKB-48, and STS-135 administration on DA transmission in the NAc shell

In this set of experiments, we studied the effect of 5F-PB-22 (0.01 mg/kg, i.v.), 5F-AKB-48 (0.1 mg/kg, i.v.) and STS-135 (0.15 mg/kg i.v.) on extracellular DA levels in the NAc shell. As shown in Figure 30, all the drugs increased DA levels in the NAc shell. Two-way ANOVA analysis showed the following significant effects: 5F-PB-22 treatment [$F(1,10)=15.97$; $p< 0.005$]; 5F-AKB-48 treatment [$F(1,11)=63.39$; $p< 0.001$], 5F-AKB-48 time x treatment [$F(18,198)=1.7$; $p< 0.05$]; STS-135 time [$F(18,144)=2.16$; $p<0.05$], STS-135 time x treatment

[F(18,144)=2.1; p< 0.005]. Furthermore, post-hoc Tukey's tests revealed significant differences on DA dialysate between:

- 5F-PB-22 (0.01 mg/kg, i.v.) treated-animals vs basal value (30, 40 min sample);
- 5F-AKB-48 (0.1 mg/kg, i.v.) treated-animals vs basal value (60, 100, 150 min sample) and vs vehicle treated animals (60, 100 min sample);
- STS-135 (0.15 mg/kg i.v.) treated-animals vs basal value and vs vehicle treated animals (60 min sample);

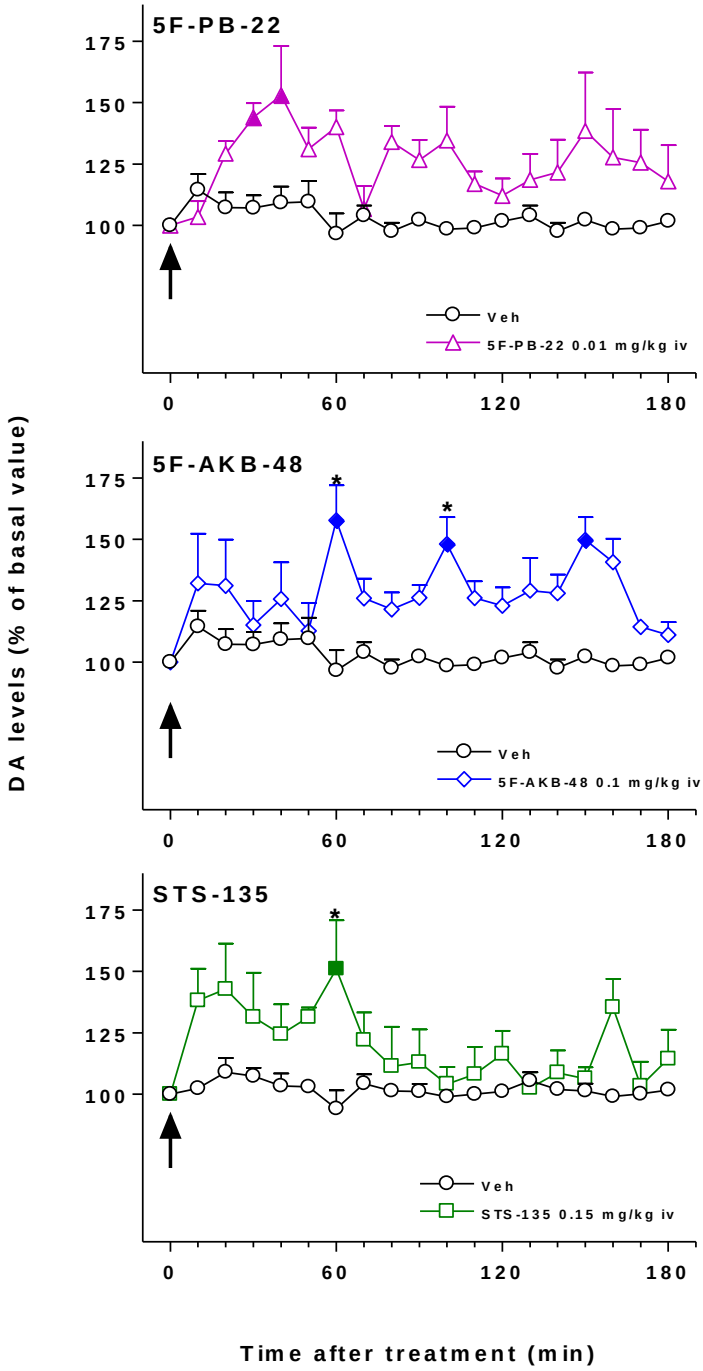

Figure 30: *In vivo* effect of 5F-PB-22, 5F-AKB-48, STS-135 administration on DA transmission in the NAc shell.

Results are expressed as mean ± SEM of change in DA extracellular levels expressed as the percentage of basal values. The arrow indicates the moment of synthetic cannabinoid i.v. injection: 5F-PB-22 0.01 mg/kg (triangles), 5F-AKB-48 0.1 mg/kg (diamonds), and STS-135 0.15 mg/kg (squares), or vehicle (circles) in the NAc shell. Solid symbol: $p < 0.05$ with respect to basal values; *$p < 0.05$ vs Veh group (5F-PB-22, n= 6; 5F-AKB-48, n= 7; STS-135 n= 5; Veh n=17) (Repeated measures three-way ANOVA, post-hoc Tukey's test).

5.2.5) Synthetic cannabinoids and microdialysis studies: discussion

According to the present findings, all synthetic cannabinoids tested could increase dopamine release in the NAc shell, while no changes were observed in other areas of the reward system, namely NAc core and mPFCx after BB-22 intravenous administration. This result is in line with previous research outcomes by which almost all drugs of abuse activate DA release preferentially in the NAc shell (Pontieri et al., 1995; Tanda et al., 1997; Cadoni and Di Chiara, 2000).

Among all index SCs in the present study, the compound with highest affinity, potency, efficacy, namely BB-22, was selected for a careful neurochemical evaluation. A wide pattern of dosages (0.00, 0.003, 0.01, 0.03, 0.1 mg/kg, i.v.) was tested in accordance with the K_i value found for this compound. The maximal increase of dopamine was observed at 0.01 mg/kg in the NAc shell, with a magnitude of about 50% over basal value and a loss of the effect at lower (0.003 mg/kg, i.v.) and higher doses (0.03, 0.1 mg/kg, i.v.) according to a concentration-dependent bell-shaped curve, as already observed with JWH-018 (De Luca et al., 2015 and 2016). The biphasic time-course of DA in the NAc shell is likely related to the degradation of the drug and the resulting formation of active metabolites acting as CB_1R agonists. However, further pharmacokinetic studies are needed to support this hypothesis.

Interestingly, the stimulation of dialysate DA in the NAc shell was elicited within a very narrow dose-range, similarly to Δ9-THC and differently from most drugs of abuse (Pontieri et al., 1995, Di Chiara et al., 2004).

Notably, the dose of BB-22 effective in stimulating DA release was around 10 times lower compared to that of JWH-018 able to stimulate DA release to the same extent (about 50% over basal). This finding was consistent with the evidence for different affinities exhibited by these two compounds at CB_1 receptors (BB-22, 0.11 nM; JWH-018, 3.38 nM) (De Luca et al., 2016).

Interestingly, the involvement of CB_1 receptors in the effect of BB-22, has been confirmed by inhibition of dopamine stimulation after pre-treatment with the CB_1 antagonist/inverse agonist AM-251 (1.0 mg/kg, i.p.).

Differently from the BB-22 study, all the other compounds were tested at a single dose (hypothesized to be effective according to their K_i value) and DA release was monitored in the same target region (NAc shell) on which DA output increase was observed after BB-22 (0.01 mg/kg, i.v.) administration. As expected, all the drugs caused an increase of DA levels with a magnitude comparable to that of BB-22 consistent with the dosage established in accordance

with their K_i values. Notably, the compound 5F-PB-22, elicited a 50% increase of DA release over basal levels at the same dosage (0.01, mg/kg, i.v.) observed with BB-22, while a dose of 5F-AKB-48 (0.1 mg/kg, i.v.) and STS-135 (0.15 mg/kg, i.v.) ten and fifteen times higher respectively, was necessary to obtain a 50% increase on DA release in the NAc shell. Notably, the same magnitude of increase was previously observed after administration of a dose 100 times higher of Δ9-THC (1 mg/kg, i.v.) (Pistis et al., 2002), providing circumstantial pre-clinical evidence for a greater putative abuse liability of SCs compared to the natural compound found in cannabis (Δ9-THC). However, additional behavioural studies (e.g. i.v. self-administration) are needed to support this hypothesis.

5.3) 2,4-Dinitrophenol (2,4-DNP) and microdialysis studies

Aims

Despite legal restrictions issued to contrast 2,4-DNP diffusion, this drug is still available over the Internet as a dieting aid according to its ability to increase basal metabolic rate, accelerate gluconeogenesis, promote fat mobilization and glycolysis. The underlying mechanism causing the abuse of this drug has been widely debated over the years with some researchers trying to find a rational explanation for its highly popular impact. Oxidative phosphorylation disruption is one of the principal mechanisms underlying the dieting aid properties of this compound, and it is also one of the principal mechanisms responsible for its highly toxicity potential, according to the small differences found between fat-burning and toxic dosages. Despite its ability to cross the blood-brain barrier has been widely documented (Perry et al., 2013), no published neurochemical studies up to now have described a central mediation of 2,4-DNP effects. However, in a study conducted in 1933 in humans, 2,4-DNP administration was demonstrated to be useful in the treatment of similar depressed metabolic states, characterised by mild depression, lethargy, apathy. In detail, 6 out of 18 patients orally treated for a 3-month period with 2,4-DNP (60 mg, 1 grain) every day, with the dose being increased 60 mg every third day, showed lightening of mood, increased activity and interest, which disappeared after drug discontinuation (Massermann and Goldsmith, 1933).

Other chemicals, like amphetamines, that share with 2,4-DNP the ability to uncouple oxidative phosphorylation, show an additional central mediation of the effects involving the reward pathways. In view of some analogies between 2,4-DNP and amphetamine mechanisms, we hypothesised that the oxidative phosphorylation was not the only underlying mechanism in common between amphetamines and 2,4-DNP and we further theorised that some alterations

could occur in the reward system following 2,4-DNP exposure. Since the NAc in particular is a terminal area of the mesolimbic dopaminergic system involved in several aspects of addiction, we aimed to monitor DA release in the NAc shell after acute intraperitoneal administration of 2,4-DNP using the microdialysis procedure in freely moving rats. DA release was additionally monitored in the CPu according to its involvement in some aspects of reward. In our microdialysis studies we used a single dose of 2,4-DNP (e.g. 20 mg/kg, i.p.) able to cause a moderate increase of temperature (e.g. $\Delta T=2.3 \pm 0.2$) without fatal complications (Gatz and Jones, 1970). Rat body temperature was monitored by means of a rectal digital thermometer during the microdialysis experiment. The intraperitoneal ROA was chosen instead of the oral one (common way to consume 2,4-DNP) because although the pharmacokinetics of substances administered intraperitoneally are similar to those observed after oral administration (the drug is primarily absorbed into the mesenteric vessels, and then gathered into the portal vein of liver), the bio-availability produced with the parenteral route of administration is higher (Turner et al., 2011). Note that, in our microdialysis experiments we used the same strain of animals (Sprague-Dawley rats) described in studies above mentioned focusing on the hyperthermia induced by 2,4-DNP (Gatz and Jones, 1970), aiming to avoid inter-strains variability. Overall, our study aimed to evaluate:

- whether 2.4-DNP (20 mg/kg, i.v.) shares with other drugs of abuse (e.g. amphetamine) the ability to stimulate DA transmission in the NAc shell and CPu;
- whether 2.4-DNP (20 mg/kg, i.v.) causes an increase of temperature comparable to that observed by Gatz and Jones (1970).

5.3.1) 2,4-DNP microdialysis studies: materials and methods

Animals

Twelve adult male Sprague-Dawley rats (body weight: 275-300 g; Harlan Laboratories, Italy) were housed in groups of six per cage. The animal environment was kept under an inverted 12:12 hour light/dark cycle and at a constant temperature of 22 ± 2°C and humidity of about 60%. Tap water and standard food were available ad libitum in the home cage. The microdialysis experiments were conducted in the University of Cagliari (Italy) and carried out in accordance with the Guidelines for the Care and Use of Mammals in Neuroscience and Behavioural Research according to Italian (D.L. 116/92 and 152/06) and European Council directives (609/86 and 63/2010) and in compliance with the approved animal policies by the Ethical Committee for Animal Experiments (CESA, University of Cagliari) and the Italian

Ministry of Health (Aut. N. 162/2016- PR). We made all efforts to minimize pain and suffering, and to reduce the number of animals used.

Surgery

Rats were anesthetized with Equitesin (chloral hydrate 2.1 g, sodium pentobarbital 0.46 g, $MgSO_4$ 1.06 g, propylene glycol 21.4 ml, ethanol (90%) 5.7 ml, H_2O 3 ml; 3 ml/kg i.p.), and implanted with vertical dialysis probes aimed at the NAc shell and CPu. According to the atlas of Paxinos and Watson (1998), the coordinates used were the following: NAc shell: Antero-Posteriority=+2.2, Laterality=±1.1 from bregma and Verticality=-7.8 from dura; CPu: Anteriority=+1.2, Laterality=±3.0 from bregma and Verticality=-5.5 from dura.

Microdialysis

On the day after surgery, an infusion pump constantly perfused with the Ringer's solution (rate: 1 μl/min) was connected to the probes. Dialysate samples were collected every 20 minutes and the resulting specimens were injected into an HPLC system equipped with a coulometric detector (ESA; Coulochem II, Bedford, MA). The parameters of the detector were the same used in the previous experiment with SCs. Dopamine recordings were performed every 20 minutes for a total period of 120 minutes.

Body Temperature measurement

Rat body temperature was monitored by means of a rectal digital thermometer. Recordings were performed during the microdialysis experiment every 15 minutes for a total period of 120 minutes after treatment.

Drug preparation

2,4-Dinitrophenol was intraperitoneally injected using a single dose of 20 mg/kg. The drug was dissolved in water. KOH 1N was added to the drug solution in order to neutralize the pH.

Groups of treatment

In preparation for the experiment, animals were divided into 4 groups:

- Rats implanted in CPu and treated with vehicle (n=3)
- Rats implanted in NAc and treated with vehicle (n=3)
- Rats implanted in CPu and treated with 2,4-DNP 20 mg/kg, i.p. (n=3)
- Rats implanted in NAc shell, and treated with 2,4-DNP 20 mg/kg, i.p. (n=3)

Dissection and histology

At the end of the experiment animals previously anesthetized, were sacrificed; the probes were gently removed, and the brains were cut in coronal slices using a vibratome. Fibre placement was determined consistent with the coordinates suggested in the atlas of Paxinos and Watson (1998).

Statistical analysis: All data were expressed as mean ± SEM. Data between different groups of treatment were analysed using Statistica for Windows (Version 10). Specifically, the differences in DA levels were analysed by ANOVA for repeated measures. Results obtained using ANOVA were then examined using the post-hoc Tukey's test with significance for $p < 0.05$.

5.3.2) 2,4-DNP microdialysis studies: results

Dopamine data

According to our findings, no significant effect of 2,4-DNP treatment on the percentage change of dialysate DA was found in the NAc shell compared to the vehicle group $F(1;4)=1.89$, $p>0.05$, along with no significant effect over time: $F(6;24)=0.96$, $p>0.05$ and no significant interaction time x treatment: $F(6;24)=0.95$, $p>0.05$ (two-way ANOVA) (figure not shown). Additionally, no significant effect of 2,4-DNP treatment on percentage change of dialysate DA was found in the CPu compared to the vehicle group: $F(1;4)=3.13$, $p>0.05$; along with no significant effect over time: $F(6;24)=1.97$, $p>0.05$ and no significant interaction time x treatment: $F(6;24)=2.39$ $p>0.05$ (two-way ANOVA) (figure not shown). Furthermore, no significant effect of 2,4-DNP treatment on percentage change of dialysate DA was found in the CPu compared to the shell: $F(1;4)=0.13$, $p>0.05$, along with no significant effect of the time: $F(6;24)=1.49$, $p>0.05$ and no significant interaction time x area: $F(6;24)=1.26$, $p>0.05$ (two-way ANOVA) (see Figure 31).

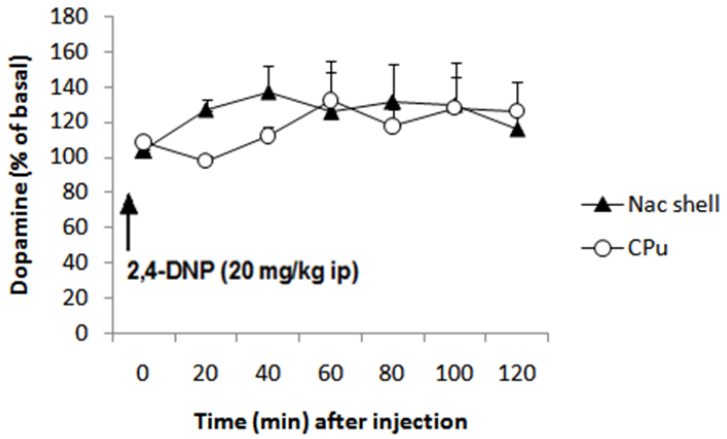

Figure 31: *In vivo* effect of 2,4-DNP (20 mg/kg, i.p.) administration on DA transmission in the NAc shell (n=3) and CPu (n=3). Results are mean ±SEM of DA extracellular levels expressed as the percentage of basal values.

Rectal temperature data

According to our findings, a significant effect of 2,4-DNP treatment on rectal temperature was observed compared to the vehicle: $F(1,10)=11.23$, $p<0.01$, with a significant effect of the time: $F(8,80)=6.76$, $p<0.0001$; and a significant interaction time x treatment: $F(8, 80)=2.85$, $p<0.01$ (2-way ANOVA; figure not shown).

Additionally, one-way ANOVA of the 2,4-DNP data over time, revealed a significant effect of the time on body temperature after 2,4-DNP treatment: $F(8,40)=12.11$, $p<0.0001$. Specifically, post-hoc Tukey's analysis showed a highly significant effect of 2,4-DNP on body temperature in the interval between 15 and 105 minutes after treatment ($p<0.0005$), with maximum observed average temperature increase of about 2.0 degrees Celsius 30 and 75 minutes after 2,4-DNP injection. The significance decreased 120 minutes after treatment ($p<0.005$) (see Figure 32).

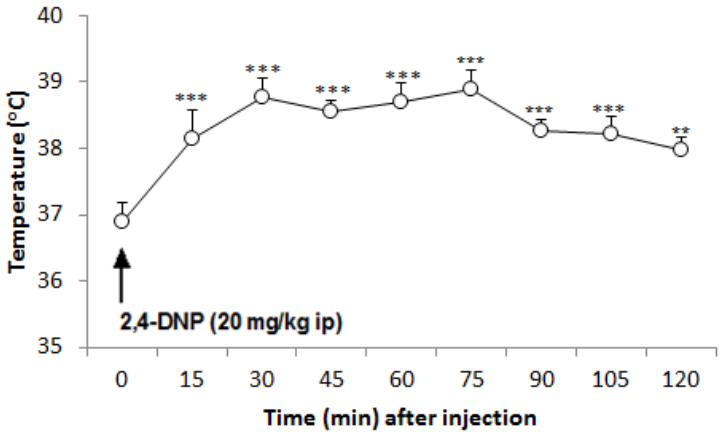

Figure 32: Effect of 2,4-DNP (20 mg/kg i.p.) administration on body temperature (n=6). Results are mean ±SEM of body temperature levels expressed in degrees Celsius. ***: p<0.0005; **: p<0.005 vs the respective basal values.

5.3.3) 2,4-DNP microdialysis studies: discussion

According to our findings, the acute treatment with 2,4-DNP (20 mg/kg, i.p.) did not cause any change in DA release in the NAc shell and CPu, rejecting the hypothesis of psychoactivity of this substance at this specific dose. Notably, this study showed some limitations. Firstly, one single dose of 2,4-DNP has been tested, and no dopamine output data have been recorded after acute administration of higher doses. This decision has been made according to an ethical approach by which animal's pain and suffering were minimized avoiding administration of larger doses that would have been extremely toxic for the rats. For the same ethical reason, we avoided any chronic treatment with 2,4-DNP, since repeated administrations would have potentially produced cardiovascular disturbances, liver and renal functions impairment, malignant hyperpyrexia that would have undoubtedly altered our neurochemical outcomes. An alternative approach would have engaged the use of lower doses of 2,4-DNP, but no pharmacological data up to date, have supported the hypothesis of a concentration-dependent U-shaped curve related to this drug. In view of the above, we concluded that there were not acceptable circumstantial reasons to proceed with any of these approaches. However, consistently with previous findings, our data confirmed that 2,4-DNP (20 mg/kg, i.p.) was able to cause hyperpyrexia in rats with a maximum observed average temperature increase of about 2.0 degrees Celsius, after 2,4-DNP injection. This compound is indeed known to be able to affect the energy production derived from the breakdown of fats and sugars by acting at the level of the inner mitochondrial membrane and shuttling protons between the inter-membrane space and the matrix. This mechanism increases the proton conductance of mitochondria and

affects the synthesis of adenosine triphosphate (ATP). As a result, the cellular energy is released as heat and produces thermogenesis (Harper et al., 2001; Ray et al., 2008).

Other anorectic drugs, like amphetamines, share with 2,4-DNP the ability to uncouple oxidative phosphorylation and increase body temperature. Therefore, the association of 2,4-DNP with these drugs may increase the risk of incurring fatal hyperthermia giving rise to a health emergency difficult to contain. Further studies are needed to elucidate 2,4-DNP pharmacological effects aiming at minimizing potential health arms related to its use/abuse.

5.4) 2-DPMP and D2PM microdialysis studies

Aims

2-DPMP and D2PM are two synthetic stimulants belonging to the pipradrol-derivative class that became popular as MDMA, and cocaine replacements. Their popularity in the UK quickly increased causing several toxic events and fatalities. Previous in *vitro* studies focusing on the effect of these drugs demonstrated that the pipradrol derivatives 2-DPMP and D2PM, were more potent DAT vs SERT inhibitors without releasing properties (Simmler et al., 2014). Furthermore, another *in vitro* fast scan cyclic voltammetry study demonstrated the ability of 2-DPMP (1, 3 or 10 μM) to increase evoked DA efflux and slowed DA reuptake to a greater extent compared to cocaine at the same doses, with a two-fold increase of DA efflux and a 3-fold reduction of DA reuptake activity with respect to cocaine (Davidson and Ramsey; 2012). All these data suggested that 2-DPMP and D2PM are potent DAT inhibitors and this mechanism accounts for their highly psychotogenic effects (Davidson and Ramsey, 2012). However, no studies have been conducted until now on the effect of these two drugs on DA release in target areas of the reward system in freely moving animals. As previously said, all drugs of abuse are able to cause an enhancement of mesolimbic DA activity. The magnitude of dopamine increase varies along with the dose, way of administration, and duration of treatment. In our study, the pipradrol derivatives 2-DPMP and D2PM were selected among other stimulants in order to monitor DA release in two different areas of the reward system: NAc shell, and CPu after their intravenous administration in rats. The rationale behind the choice of these drugs was related to the necessity to acquire some insights into the effect of these drugs in the reward pathways of the central nervous system, especially in view of the recent health emergencies raised by using these compounds and their highly psychotogenic effects.

In our microdialysis studies, a wide dose-range of these two stimulants was tested according to the k_i values found for 2-DPMP (0.007 ± 0.01 μM) and D2PM (0.07 ± 0.03 μM) at the level of DAT by Simmler et al. (2014). Specifically, the doses tested in the present study were as follows: 2-DPMP (0, 0.01, 0.1, 0.3, 0.5, 1.0 mg/kg, i.v.) and D2PM (0, 0.01, 0.1, 1.0, 3.0 mg/kg, i.v.). An acute treatment was performed using the intravenous route of administration because several reports described this ROA as a common practice to administer 2-DPMP and D2PM; additionally, intravenous injection is considered the most efficient means of delivering substances, as they are directly administered into blood vessels, avoiding the first-pass effect of hepatic metabolism (Turner et al., 2011). NAc shell and CPu were selected as target areas in accordance with the role played by these regions in addiction. Indeed, typical drugs of abuse share the ability to activate the reward pathways and increase DA release preferentially in the NAc shell (Di Chiara and Imperato, 1988; Lecca et al., 2006). Based on the type of drugs and dosages, an increase can be observed also in other regions of the reward system including CPu. Indeed, intravenous injection of stimulants like cocaine and amphetamine increases dopamine release in the dorsal striatum as well, however the magnitude of increase is greater in NAc shell than in the dorsal striatum (Lecca et al., 2006). The microdialysis procedure was employed among the others in our study, as a useful and reliable tool for monitoring changes of DA levels in freely moving animals. Note that, in our microdialysis experiments we used the same strain of animals (Wistar rats) described in *in vitro* fast scan cyclic voltammetry studies above mentioned, focusing on the effect of 2-DPMP on DA release in rat brain slices (Davidson and Ramsey, 2012), aiming to avoid inter-strains variability. Overall, our study aimed to:

- Evaluate whether the index synthetic stimulants in our study (2-DPMP, D2PM) share with other stimulants (e.g. cocaine) the ability to stimulate DA transmission in the NAc shell;
- Assess whether the synthetic stimulants tested, mediate DA transmission alteration in other areas of the reward system, namely dorsal striatum (CPu);
- Quantify the magnitude of DA change mediated by the index synthetic stimulants in the present study.

5.4.1) 2-DPMP and D2PM microdialysis studies: materials and methods

Animals

Adult male Wistar rats (body weight: 275-300 g; Envigo, Harlan Laboratories, Italy) destined for 2-DPMP and D2PM microdialysis experiments were housed in groups of four per cage.

The animal environment was kept under an inverted 12:12 hour light/dark cycle and at a constant temperature of 22 ± 2°C and humidity of about 60%. Tap water and standard food were available ad libitum in the home cage. All *in vivo* animal experiments were conducted in the University of Cagliari (Italy) and carried out in accordance with the Guidelines for the Care and Use of Mammals in Neuroscience and Behavioural Research according to Italian (D.L. 116/92 and 152/06) and European Council directives (609/86 and 63/2010) and in compliance with the approved animal policies by the Ethical Committee for Animal Experiments (CESA, University of Cagliari) and the Italian Ministry of Health (Aut. N. 162/2016- PR). We made all efforts to minimize pain and suffering, and to reduce the number of animals used.

Surgery

Rats were anesthetized with Equitesin (chloral hydrate 2.1 g, sodium pentobarbital 0.46 g, $MgSO_4$ 1.06 g, propylene glycol 21.4 ml, ethanol (90%) 5.7 ml, H_2O 3 ml; 3 ml/kg i.p.), and implanted with vertical dialysis probes aimed at the NAc shell and CPu. According to the atlas of Paxinos and Watson (1998), the coordinates used were the following: NAc shell: Antero-Posteriority=+2.2, Laterality=±1.1 from bregma and Verticality=-7.8 from dura; CPu: Anteriority=+1.2, Laterality=±3.0 from bregma and Verticality=-5.5 from dura.

Microdialysis experiment

On the day after surgery, infusion pumps constantly perfused with the Ringer's solution (rate: 1 µl/min) were connected to the probes. Dialysate samples were collected every 20 minutes and the resulting specimens were injected into an HPLC system equipped with a coulometric detector (ESA; Coulochem II, Bedford, MA). The parameters of the detector were the same used in the previous experiment with synthetic cannabinoids. Dopamine recordings were performed for a total period of 180 minutes in both experiments.

Drugs

Desoxypipradrol hydrochloride solution and Diphenyl-2-pyrrolidinemethanol powder were purchased from Sigma-Aldrich, Italy. 2-DPMP dilutions were directly prepared from the stock, while D2PM dilutions were performed after dissolving D2PM powder in a small amount of ethanol, HCl 2.4 mM, and distilled water.

2-DPMP microdialysis experiment

Groups of treatment

In preparation for the experiment, animals were divided into different groups:

- rats implanted in the NAc shell and treated with vehicle (n=4); 2-DPMP (0.01 mg/kg, i.v., n=3); (0.1 mg/kg, i.v., n=3); (0.3 mg/kg, i.v., n=3); (0.5 mg/kg, i.v., n=4); (1.0 mg/kg, i.v., n=3);
- rats implanted in CPu and treated with vehicle (n=4); 2-DPMP (0.01 mg/kg, i.v., n=4); (0.1 mg/kg, i.v., n=4); (0.3 mg/kg, i.v., n=3); (0.5 mg/kg, i.v., n=4); (1.0 mg/kg, i.v., n=3).

D2PM experiment

Groups of treatment:

- rats implanted in the NAc shell and treated with vehicle (n=4); D2PM (0.01 mg/kg, i.v., n=4); (0.1 mg/kg, i.v., n=5); (1.0 mg/kg, i.v., n=6); (3.0 mg/kg, i.v., n=5);
- rats implanted in the CPu and treated with vehicle (n=4); D2PM (0.01 mg/kg, i.v., n=3); (0.1 mg/kg, i.v., n=4); (1.0 mg/kg, i.v., n=3); (3.0 mg/kg, i.v., n=3)

Dissection and histology

At the end of the experiment animals previously anesthetized were sacrificed; the probes were gently removed, and the brains cut in coronal slices using a vibratome. Fibre placement was determined consistent with the coordinates suggested in the atlas of Paxinos and Watson (1998).

Statistical analysis

All data were expressed as mean ± SEM. Data between different groups of treatment were analysed using Statistica for Windows (Version 10). Specifically, the differences in DA levels were analysed by ANOVA for repeated measures. Results obtained using ANOVA were then examined using the post-hoc Tukey's test with significance for $p < 0.05$.

5.4.2) 2-DPMP microdialysis experiment: results

In this experiment the effect of a dose range of 2-DPMP (0.00, 0.01, 0.1, 0.3, 0.5, 1.0, mg/kg, i.v.) on DA transmission was assessed in the NAc shell and CPu in freely moving animals. Specifically, two-way ANOVA of DA data over time in NAc shell, revealed a significant effect of the dose [$F(5,14)=11.73$; $p<0.0005$], time [$F(9,126)=20.22$; $p<0.0001$], and a significant dose x time interaction [$F(45,126)=3.92$; $p<0.0001$]. Furthermore, post-hoc Tukey's test showed a significant increase of DA levels in the NAc shell 40 minutes after 2-DPMP (0.5

mg/kg, i.v.) injection, compared to the vehicle. Additionally, the highest dose (1.0 mg/kg, i.v.) caused a significant increase of DA release compared to the vehicle, 20 and 40 minutes after administration.

Significant differences on DA dialysate in the NAc shell were observed between: 2-DPMP (0.5 mg/kg, i.v.) treated animals vs basal value (40 min sample) and 2-DPMP (1.0 mg/kg, i.v.) treated animals vs basal value (20, 40 min sample) (see Figure 33).

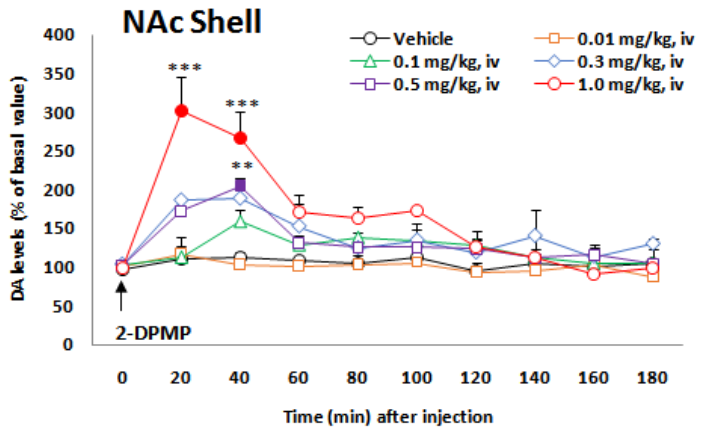

Figure 33: *In vivo* effect of 2-DPMP administration on DA transmission in the NAc shell. Results are expressed as mean ± SEM of change in DA extracellular levels expressed as the percentage of basal values. The arrow indicates the moment of 2-DPMP i.v. injection: vehicle (dark circles); 2-DPMP 0.01 mg/kg (orange squares); 2-DPMP 0.1 mg/kg (green triangles); 2-DPMP 0.3 mg/kg (blue diamonds); 2-DPMP 0.5 mg/kg (violet squares); 2-DPMP 1.0 mg/kg (red circles) in the NAc shell. Solid symbol: $p < 0.0001$ with respect to basal values; **$p < 0.001$; ***$p < 0.0001$ vs veh group (veh, n=4; 2-DPMP 0.01 mg/kg, n=3; 2-DPMP, 0.1 mg/kg, n=3; 2-DPMP 0.3 mg/kg, n=3; 2-DPMP 0.5 mg/kg, n=4; 2-DPMP 1.0 mg/kg, n=3) (Two-way ANOVA, post-hoc Tukey's test).

As regards to CPu, 2-way ANOVA of DA data over time, revealed a significant effect of the doses [$F(5,16)= 3.37$; $p<0.05$], a significant effect of the time [$F(9,144)= 30.35$; $p<0.0001$], and a significant dose x time interaction [$F(45,144)=4.58$; $p<0.0001$]. Furthermore, post-hoc Tukey's test showed a significant increase of DA levels in the CPu 20 and 40 minutes after 2-DPMP (0.5 and 1.0 mg/kg, i.v.) administration, compared to the vehicle. Additionally, significant differences on DA dialysate in the CPu were observed between: 2-DPMP (0.1 and 0.3 mg/kg, i.v.) treated animals vs basal value (40 min sample) and 2-DPMP (0.5 and 1.0 mg/kg, i.v.) treated animals vs basal value (20, 40 min sample) (see Figure 34).

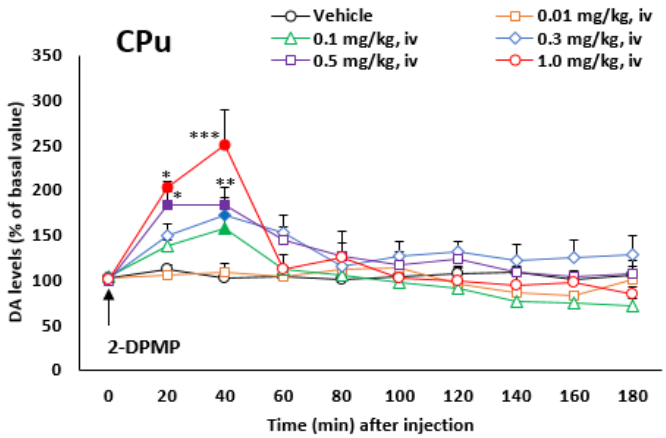

Figure 34: *In vivo* effect of 2-DPMP administration on DA transmission in the CPu. Results are expressed as mean ± SEM of change in DA extracellular levels expressed as the percentage of basal values. The arrow indicates the moment of 2-DPMP i.v. injection: vehicle (dark circles); 2-DPMP 0.01 mg/kg (orange squares); 2-DPMP 0.1 mg/kg (green triangles); 2-DPMP 0.3 mg/kg (blue diamonds); 2-DPMP 0.5 mg/kg (violet squares); 2-DPMP 1.0 mg/kg (red circles) in the CPu. Solid symbol: $p < 0.0001$ (violet squares and red circles), $p<0.01$ (blue diamonds), $p<0.05$ (green triangles) with respect to basal values; *$p < 0.05$; **$p < 0.01$, ***$p<0.0005$ vs veh group (veh, n=4; 2-DPMP 0.01 mg/kg, n=4; 2-DPMP 0.1 mg/kg, n=4; 2-DPMP 0.3 mg/kg, n=3; 2-DPMP 0.5 mg/kg, n=4; D2PM 1.0 mg/kg, n=3) (Two-way ANOVA, post-hoc Tukey's test).

Considering both areas, repeated measures three-way ANOVA revealed a significant effect of doses [$F(5,30)=10.82$; $p<0.0001$], brain area [$F(1,30)=6.56$; $p<0.05$], time [$F(9,270)=48.003$; $p<0.0001$] and a significant time x doses interaction [$F(45,270)=7.23$; $p<0.0001$]. Furthermore, post hoc Tukey's test showed a significant difference ($p<0.005$) of DA levels between NAc shell and CPu, 20 minutes after injection of 2-DPMP (1 mg/kg, i.v.).

5.4.3) D2PM microdialysis experiment: results

In this experiment the effect of a dose range of D2PM (0.00, 0.01, 0.1, 1.0, 3.0 mg/kg, i.v.) on DA transmission was assessed in the NAc shell and CPu in freely moving animals. Specifically, 2-way ANOVA of DA data over time in NAc shell, revealed a significant effect of the dose [$F(4,19)=7.84$; $p<0.0001$], and a significant dose x time interaction [$F(36,171)=1.51$; $p<0.05$]. Furthermore, post-hoc Tukey's test showed a significant increase of DA levels in the NAc shell 160 minutes after D2PM injection (3.0 mg/kg, i.v.) compared to the vehicle-treated group and basal value as well (see Figure 35).

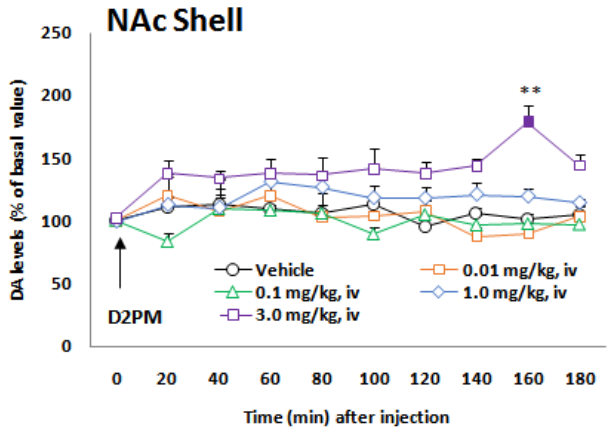

Figure 35: *In vivo* effect of D2PM administration on DA transmission in the NAc shell. Results are expressed as mean ± SEM of change in DA extracellular levels expressed as the percentage of basal values. The arrow indicates the moment of D2PM i.v. injection: vehicle (dark circles); D2PM 0.01 mg/kg (orange squares); D2PM 0.1 mg/kg (green triangles); D2PM 1.0 mg/kg (blue diamonds); D2PM 3.0 mg/kg (violet squares) in the NAc shell. Solid symbol: $p < 0.0001$ with respect to basal values; **$p < 0.005$ vs veh group (veh, n=4; D2PM 0.01 mg/kg, n=4; D2PM 0.1 mg/kg, n=5; D2PM 1.0, mg/kg, n=6; D2PM 3.0 mg/kg, n=5) (Two-way ANOVA, post-hoc Tukey's test).

As regards to CPu, 2-way ANOVA of DA data over time, revealed no significant effect of the doses [$F(4,12)= 2.80$; $p>0.05$], no effect of the time [$F(9,108)= 1.00$; $p>0.05$], and no significant dose x time interaction [$F(36,108)=1.13$; $p>0.05$] (see Figure 36).

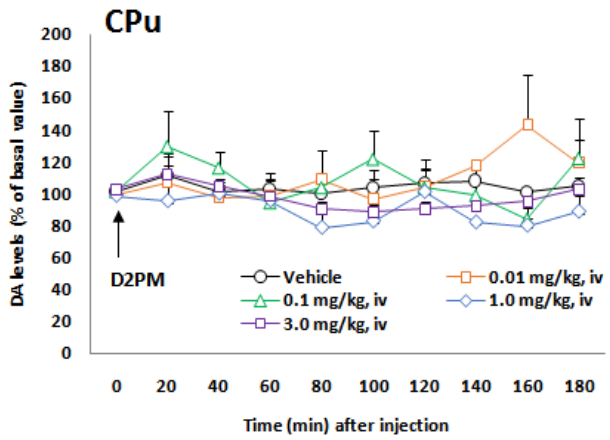

Figure 36: *In vivo* effect of D2PM administration on DA transmission in the CPu. Results are expressed as mean ± SEM of change in DA extracellular levels expressed as the percentage of basal values. The arrow indicates the moment of D2PM i.v. injection: vehicle (dark circles); D2PM 0.01 mg/kg (orange squares); D2PM 0.1 mg/kg (green triangles); D2PM 1.0 mg/kg (blue diamonds); D2PM 3.0 mg/kg (violet squares) in the CPu. Veh, n=4; D2PM 0.01 mg/kg, n=3; D2PM 0.1 mg/kg, n=4; D2PM 1.0 mg/kg, n=3; D2PM 3.0 mg/kg, n=3) (Two-way ANOVA, post-hoc Tukey's test).

Considering both areas, repeated measures three-way ANOVA revealed a significant effect of brain area [$F(1,31)=8.88$; $p<0.01$], a significant area x doses interaction [$F(4,31)=6.40$; $p<0.001$], and a significant time x area x doses interaction [$F(36,279)=1.77$; $p<0.01$]. Furthermore, post-hoc Tukey's test showed a significant difference ($p<0.01$) of DA levels between the NAc shell and the CPu 160 minutes after injection of D2PM (3 mg/kg, i.v.).

5.4.4) 2-DPMP and D2PM microdialysis experiments: discussion

In these experiments the effect of a dose range of 2-DPMP (0.00, 0.01, 0.1, 0.3, 0.5, 1.0, mg/kg, i.v.) and D2PM (0.00, 0.01, 0.1, 1.0, 3.0 mg/kg, i.v.) on DA transmission was assessed in the NAc shell and CPu of freely moving animals. According to our findings the acute treatment with 2-DPMP elicited a dose-dependent increase of DA release in the NAc shell with a fast onset of action and a short-lasting effect. The maximal peak effect (200% over basal levels) was observed between 20-40 minutes after the highest dose injection (1 mg/kg), with dopamine levels sharply decreasing at 60 minutes and achieving a plateau around the basal levels over the rest of the time. A similar DA time course was observed after injection of 2-DPMP (0.5 mg/kg), with the maximal increase occurring 40 minutes after injection and being much less pronounced (100% over basal levels) compared to that produced by the highest dose. Interestingly, lower doses were ineffective on DA release suggesting a dose-dependent related

effect of 2-DPMP. Notably, 2-DPMP elicited an increase of DA output in the CPu at the same dosages (0.5 mg/kg, i.v. and 1.0 mg/kg, i.v.) and with a percentage of increase comparable to that observed for the NAc shell at both doses.

Referring to D2PM, a dopamine release increase (78% over basal levels) was observed selectively in the NAc shell 160 minutes after injection of the highest dose (3.0 mg/kg, i.v.) with dopamine levels returning to the basal levels 180 minutes after injection. Interestingly, lower doses were ineffective on DA release in the NAc shell suggesting a dose-dependent related effect of D2PM. Notably, no doses caused any increase of DA levels in the CPu at any time.

The delayed onset of effect observed after D2PM injection in the NAc shell, could be likely related to the presence, in its structure, of the polar functional group -OH, likely responsible for its slow passage through the blood-brain-barrier (BBB); while the absence of polar groups in 2-DPMP chemical structure, may account for its rapid absorption through the BBB and its quick onset of effects.

Overall, these studies present some limitations. It is likely that larger doses of both drugs would have caused a higher dopamine peak effect in the target regions according to a dose-dependent effect. In view of this consideration, testing larger doses of both drugs, would have been useful to find the highest effective dose and to quantify the maximum DA peak effect. Furthermore, behavioural observations (e.g. motility, freezing, piloerection, grooming, sniffing, gnawing, rearing, scratching) during microdialysis studies, would have provided some additional information on the level of behavioural stimulation caused by these stimulants. In this regard, according to some preliminary observations in our laboratory, only high doses of 2-DPMP (0.5 and 1.0 mg/kg) seemed to produce stimulant behavioural effects; however, detailed preclinical studies are needed to better draft a behavioural profile of these drugs.

Chapter 6: Molecular modelling studies

6.1) Molecular modelling overview

Over the years, drug designers started to synthetise novel compounds intended to mimic the effects of controlled drugs, by introducing slight modifications to the chemical structure of illicit compounds in order to escape legal regulations (Liechti, 2015).

In this regard, the chemogenomics principles, which assume that structurally similar ligands share similar targets, allowed researchers to predict the possible effects of a drug on a set of targets by using the combination of molecular modelling with bioactivity databases available (Börjessonet al., 2005).

Computational chemistry and molecular modelling rely on the use of computers to simulate complex chemical systems including drug-target interactions in the central nervous system. These interactions can be represented by several variables using the principles of mathematics, chemistry, physics and computer science. The simulation studies by computer may be conducted in order to help researchers to either rationalize experimental observations and/or make predictions about what will happen in a real biological system at multiple levels (from atomistic to macroscopic modelling) and allowing scientists to save animals, time, money and materials (Young, 2009).

Against a background of increasing numbers of NPS used and their prevalence on the drug market, molecular modelling was utilized to postulate the mechanisms of action of novel compounds as the scientific literature was lacking to guide the design of experimental studies in humans and animals. The potential use of molecular modelling for the prediction and recognition of characteristic features of NPS (pharmacology, pharmacodynamics, toxicity, psychoactivity) has represented a step forward in biological science (Dargan and Wood, 2013).

Molecular modelling has become an integrated part of predicting and rationalising the properties of potential drug candidates as well as understanding the side-effects and toxicity of small molecules. From a clinical point of view, *in silico* studies use computer models to identify the potential target of novel drugs, and they may also prove useful in helping to predict the mechanism of action of a drug, driving the development of intervention strategies aimed to protect the public from the consequences of side effects and drug interactions (Dargan and Wood, 2013). Overall, these studies have the potential to speed up the rate of drug target discovery, reducing the number of failed expensive laboratory and clinical trials. However, *in silico* studies require constant experimental interplay with medicinal chemistry and biology to

validate the results predicted and provide structural context for NPS at specific targets relating them with their functional properties. Such approaches can be employed to assess addictive potential of NPS, and to plan new therapeutic strategies against their use/abuse (Dargan and Wood, 2013).

From a pragmatic point of view, several preliminary molecular modelling studies have been performed to get better understanding into binding properties and biological activities of some NPS at the level of specific targets (Menghani et al., 2016).

In this regard, *in silico* studies were performed to screen the activity of a range of N-benzyl phenethylamines (e.g. DOI NBOMe, 25H-NBOMe, 25I-NBOMe, etc) at the level of the 5-HT_{2A} receptor (Braden et al., 2006) and two highly conserved aromatic amino acids (Phe 339 and Phe 340) were identified as key residues involved in the recognition of these compounds (Roth et al., 1997). These data, along with experimental studies, may imply that these aromatic residues play a crucial role in agonist binding and signal transduction, offering molecular evidence of the mechanism of action of these drugs along with their potential pharmacological and clinical effects.

Further studies employed molecular modelling to explore the possible differences in the binding modes of the novel cathinones 4-MEC and 4-MePPP at DAT and SERT, and demonstrated that both compounds show analogous poses in DAT, while SERT is less able to accommodate 4-MePPP when compared with 4-MEC because of the steric hindrance caused by the bulky pyrrolidine ring structure of 4-MePPP. Overall, these results provide crucial clues about the pharmacology of these mephedrone analogues, and give information on the molecular requirements that drive drug selectivity at DAT vs SERT, providing new insights into the biological and pharmacological properties of these substances (Saha et al., 2015).

Other previous *in silico* studies, along with *in vitro* binding studies assessed the binding properties of the novel benzofuran 5-MAPB at DAT and demonstrated a binding mode for 5-MAPB that overlaps with the binding site of other stimulants such as amphetamine, MDMA, 5-APB, cocaine. These novel insights, offered by the interplay of computational methods with neurochemical procedures, relate these NPS to their functional properties at DAT, explaining their similarity in terms of pharmacological/clinical effects with other categories of stimulants (e.g. MDMA, cocaine) (Sahai et al., 2017).

Additional molecular modelling studies have been performed to assess the binding modes of the psychoactive compound of the Khat plant cathinone along with its metabolites

norephedrine and norpseudoephedrine at DAT (Kolodziejczyket al., 2016). These studies revealed all the conformers interact with an active binding pocket highly comparable with that of D-amphetamine, and suggested that the metabolites can have a crucial role in producing long-lasting effects after cathinone use.

Overall, these studies helped to elucidate the mechanism of action which may underlie the potential clinical and side-effects of a range of NPS, providing new insights into their biological activity for more successful abuse management and treatment plans against the use/abuse of these drugs.

Furthermore, molecular modelling studies have been also employed in drug discovery and structure-based drug design and have played a crucial role in the assessment of potential novel therapeutics in the treatment of a variety of diseases (Sliwoski et al., 2013).

In this respect, in a previous study, 10 thiourea derivatives were synthesized and assessed for the treatment of the Parkinson's disease psychosis and molecular docking studies were employed to screen their activity using a homology model of 5-$HT2_A$ receptor. Significant interactions between both thiourea NH groups and specific residues of the receptor were observed and provided new information related to their structural properties responsible for affinity towards the 5-$HT2_A$ receptor (Bielenica et al., 2016).

Further studies employed *in silico* simulations to screen the activity of a set of Risperidone derivatives using a homology model of the D2 receptor, in order to discover novel therapeutics for the treatment of the schizophrenia (Bhargava et al., 2014).

In another study, a series of novel quinazoline derivatives were synthesized and evaluated for their anti-inflammatory activity. To this aim *in silico* studies were performed to recognize the hypothetical binding mode of these compounds with the cyclooxygenase isoenzymes (COX-1 and COX-2) and specific substituents were regarded as responsible for affinity toward these enzymes (Balakumar et al., 2010).

Overall, computer-aided drug discovery and structure-based drug design allow researchers to save money and time, avoiding a large population of predicted inactive compounds and focusing resources on testing compounds likely to have any activity of interest in the treatment of a variety of diseases (Sliwoski et al., 2013).

Drug targets, focus on CB_1 receptors

The majority of drug targets are proteins (receptors, transporters, enzymes) having active binding sites usually with highly conserved amino acids. Natural substrates, as well as drugs and drugs candidates can establish a range of different types of interactions within the binding site (e.g. hydrogen bonds, π-system staking, ionic bonds, van der Waals interactions, electrostatic interactions) (Bull et al., 2015), allowing a protein to exert or modulate its function, respectively. In this regard, cannabinoids receptors (subtype 1) regulate a variety of physiological processes (appetite, mood, pain), while their pharmacological manipulations can lead to a range of clinical consequences.

The CB_1 receptor is a member of the superfamily of G-protein-coupled receptors (GPCRs), characterised by an intracellular C-terminal tail, seven transmembrane helices linked by three extracellular and three intracellular loops, and an extracellular N-terminal tail (Turu et al., 2010). It is the major cannabinoid receptor subtype found in the brain, but it also occurs in the peripheral nervous system (Castaneto et al., 2014; Howlett et al., 2002). It can interact with endogenous (e.g. anandamide, 2-AG) and exogenous cannabinoids which include structurally distinct classes of compounds such as: classical cannabinoid agonists (Δ9-THC), non-classical cannabinoid agonists (CP-55,940), aminoalkylindole agonists (AAI), CB_1 antagonists (rimonabant, AM-6358). CB_1 receptors are highly conserved among vertebrates and according to a comparative analysis, the human receptor presents 97% of identity at the amino acid level compared to the rodent CB_1 receptor and presents one less amino acid in the N- terminal (472 amino acids).

In response to ligand binding, the CB_1 receptor changes its conformation to activate the associated G-proteins and to promote a cascade of intracellular events including: decrease of cAMP level, inhibition of potassium, sodium, and N- and P/Q-type- calcium channels, inhibition of neurotransmitter release (Howlett et al., 2010).

Evaluation of binding modes of CB_1 receptor ligands using molecular modelling and mutation studies

Over the years, single-point mutagenesis and computational modelling studies on CB_1 receptors have provided valuable insights into the characterisation of the key residues involved in the recognition of specific ligands. In particular, mutation studies demonstrated that the binding pockets for classical (Δ9-THC), non-classical (CP-55,940) and endogenous cannabinoids (2-AG, Anandamide) is topologically different from that observed for aminoalkylindoles (JWH-018, WIN-55,212-2) although they spatially overlap (see Table 2).

Mutation of specific residues resulted in profound loss of affinity and recognition for these specific ligands, suggesting their crucial role in ligand binding (Song and Bonners 1996, Mc Allister et al., 2003; Shim and Howlett, 2006; Ahn et al., 2009; Shim, 2010; Shim et al., 2012; Hua et al., 2016; Shao et al., 2016).

More recently, the crystal structure of the human CB_1 receptor was synthesized and used in conjunction with computational molecular modelling to provide insights into the binding mode of the synthetic cannabinoid constituent of 'Spice' such as JWH-018 and other CB_1 agonists (e.g. anandamide, 2-AG, Δ9-THC, CP-55,940, WIN-55,212-2); and CB_1 antagonists (e.g. rimonabant, AM-6358, Otenabant, Taranabant) (Hua et al., 2016).

According to these studies, the CB_1 agonists mainly interact with the 3, 6, 7 helices and the N-terminal loop of the crystal structure of the CB_1 receptor; while the CB_1 antagonists mostly share interactions with the 2, 3, 6, 7 helices and ECL2 (extracellular loop 2). These findings were consistent with previous mutation study outcomes (see Table 2) (Mc Allister et al., 2003, Ahn et al., 2009).

CB_1R LIGANDS	CB_1R KEY INTERACTING RESIDUES
Aminoalkylindoles (e.g. WIN-55212,2)	$Phe^{3.36}$(200), $Tryp^{5.43}$(279), $Tryp^{6.48}$(356), $Tyr^{5.39}$ (275), $Asp^{2.50}$(163), $Tryp^{4.64}$ (255), $Val^{5.46}$ (282), $Phe^{3.25}$ (189), $Phe^{5.46}$ (197)
Endogenous cannabinoids (e.g. anandamide)	$Tyr^{5.39}$ (275), $Phe^{3.25}$ (189) and $Lys^{3.28}$ (192)
CB_1 antagonists (e.g. rimonabant)	$Leu^{3.29}$ (193), $Phe^{7.35}$ (379), $Phe^{2.57}$ (170), $Phe^{2.61}$ (174) $Phe^{3.36}$ (200), $Phe^{3.25}$ (189), $Tryp^{5.43}$ (279), $Cys^{7.43}$ (386) $Tryp^{6.48}$ (356), $Lys^{3.28}$ (192), $Cys^{7.43}$ (386), $Thr^{3.33}$ (197), $Met^{6.55}$ (363), $Phe^{3.36}$ (200), $Tryp^{5.43}$ (279), $Phe^{3.36}$ (200)
CB_1 antagonists (e.g. AM-6358)	$Phe^{3.36}$ (200), $Phe^{2.61}$ (174)
Non-classical cannabinoids (CP-55,940)	$Lys^{3.28}$ (192), $Tyr^{5.39}$ (275), $Phe^{2.61}$ (174), $Leu^{3.29}$ 193$Phe^{3.25}$ (189), $Ser^{7.39}$ (383)
Classical cannabinoids (Δ9-THC)	$Lys^{3.28}$ (192), $Phe^{2.61}$ (174), $Leu^{3.29}$ (193), $Ser^{7.39}$ (383)

Table 2: Key interacting residues crucial for CB_1 ligand binding recognition according to experimental mutation studies.

6.2) Homology modelling overview

The primary amino acid sequences for almost all human proteins are largely available. However, to assess the potential interactions between drugs and proteins, knowledge of the three-dimensional structure of the protein is required and crystallography is the most accurate way to predict and determine protein geometry (Engh and R. Huber, 1991).

Determination of appropriate protein crystallization is generally considered quite challenging and sometimes not feasible due to peculiar physicochemical characteristics of certain proteins and their high sensitivity to alterations of pH, temperature and ionic strength (Bergfors, 1999).

Considering that not all proteins have their crystal structure available, homology models represent the next best way of obtaining putative protein structures and may provide a good source for protein-ligand interaction studies (Young, 2009).

Given the complexity of drug mechanisms, it is important to consider that computational models are becoming increasingly useful in the pharmacology field as their predictions are validated by experimental findings. Overall, homology modelling predicts a three-dimensional structure from the sequence of a target protein with an accuracy that is often comparable to the best outcomes attained experimentally and it provides invaluable insights into the molecular basis of putative protein functions (Krieger et al., 2003).

Template identification, alignment, homology model building and validation

The homology model process includes several steps: template identification, template-target alignment, building of the homology model and model validation. Briefly, in homology modelling, the primary sequence of the target protein is compared with primary sequences of proteins for which crystal structures are available (templates) in order to find regions that are identical to the target protein. In this regard, homology modelling (or template-based protein modelling) relies on evolutionary relationships between a target protein and templates with known experimental structures to ultimately build the target three-dimensional model (Young, 2009). This principle is based on the fact that, during evolution, the three-dimensional structure of a protein has been more highly conserved than the associated amino acid sequence, so that similar evolutionary related sequences generally fold into similar structures and adopt comparable 3D structures (Chothia and Lesk, 1986). A crucial factor to consider in homology modelling is the sequence identity with the template, and the most accredited theory suggests that to obtain a reliable homology model, the sequence identity should be over 70% (Young, 2009). Of course, higher sequence identity between the model and the template leads to better expected quality models (Arnold et al., 2006). The crystallographic coordinates for several segments of known evolutionary-related proteins are then used to build the three-dimensional geometry of the protein and the homology model is validated with tools (e.g. Rampage and Procheck) based on a comparison of a range of stereo-chemical parameters with those of trusted reference structures (Arnold et al., 2006).

SWISS-MODEL: computational tool for template identification, alignment and homology model building

The online software 'SWISS-MODEL' provides a range of programmes and databases required for template identification; alignment; homology model building and access to updated protein sequence and structure databases (e.g. Protein Data Bank) (Arnold et al., 2006). In detail, the template structure database used by SWISS-MODEL (SMTL) is derived from the Protein Data Bank (Arnold et al., 2006). The sequence database search for template identification, provides an overview of the results organised in clusters of templates showing different percentages of identity. For each template, several information items are reported: PDB ID; name of the structure; experimental methods used to obtain the structure; resolution; the sequence identity to the target; the target sequence coverage; template search method used; oligomeric state; and description of ligands. The level of difficulty in identifying suitable templates for a target sequence may be low for well-characterised protein families or really high for proteins with unknown structure. To overcome this issue, SWISS-MODEL provides access to different methods to search for templates (BLAST, Iterative profile BLAST, HMM-based template library search) (Arnold et al., 2006).

'BLAST' is a Basic Local Alignment Search Tool that compares a query protein sequence with the SWISS-MODEL library of sequences extracted from PDB and identifies high scoring sequence alignments between the query sequence and the templates in the database using a specific algorithm. When no suitable templates are identified, two additional approaches are provided: PSI BLAST and HMM-based template library search.

'PSI BLAST' is a Position-Specific Iterative BLAST tool used to find more distant evolutionary templates compared to the query protein sequence. Initially, PSI BLAST produces a list of close evolutionary templates used to generate a 'profile sequence' which summarises significant analogies present in these templates. Then a query against the SWISS-MODEL library templates is performed using this 'profile sequence' and a wider group of proteins is identified. This group is then used to produce another 'sequence profile' and the process is repeated. This tool is more sensitive in identifying distant evolutionary relatives of the target sequence compared to BLAST (Arnold et al., 2006).

Alternatively, 'HMM-based template library search tool' finds all the sequence homologues that match the submitted sequence. These templates are then assembled and converted into a Hidden Markov Model (HMM) which is then scanned against the Hidden Markov model

library to find high score structural multiple alignments which are based only on geometric information of the proteins. Compared to PSI BLAST, this tool has higher sensitivity and generates more accurate alignments (Remmert et al., 2011). This tool may be use used as an alternative to PSI BLAST to identify distant evolutionary homologues of the target sequence.

The SWISS-MODEL server uses the improved HMM methods named Hidden 'HMM-HMM–based lightning-fast iterative sequence search' (HHblits; http://toolkit.genzentrum.lmu.de/hhblits/) (Remmert et al., 2011). HHBlits relies on the 'kClust tool' to cluster large protein sequence databases to below 30% sequence identity and it is ~1000 times quicker than BLAST (Hauser et al., 2013). In detail, the query sequence is firstly converted into a first HMM which is scanned against the HMM database (NR). Sequences from matched HMMs below a statistical defined expected value (E value) threshold (pre-filter), are then added to the query sequence from which another HMM for the next search iteration is built. The pre-filter reduces the number of full HMM-HMM alignments considerably (by ~2,500-fold) (Remmert et al., 2011).

When the sequence analysis is complete, and the alignment is corrected accordingly, the software proceeds with the generation of the model. The steps followed by SWISS-MODEL include: backbone generation, loop modelling, side chain modelling, and model optimization. Once the models have been built the server usually outputs an assessment of model quality. This section provides the three-dimensional structure of the model, the target-template alignment, and the model coordinates available in PDB format. Additional information about the selected templates, oligomeric state and bound ligands are provided. The global model quality is assessed calculating the QMEAN, Q-MEAN4, Q-MEAN4 Z-score functions (Benkert, et al., 2011). Regions that are poorly or highly modelled present different colours based on the QMEAN value, which is a scoring function referred to the geometrical properties of the entire structure and local regions of the model (each residue) and it consists of a combination of distinct structural parameters: torsion angle potential over three consecutive amino acids (local geometry); distance-dependent interaction potential among Cß in the polypeptide and among all atoms (long range-interactions); solvation potential and accessibility; terms reflecting the agreement between predicted and calculated secondary structure (Benkert et al., 2009). QMEAN4 score is the version of the scoring function based on normalised statistical potential scores. QMEAN4 Z-score is calculated by subtracting the normalized QMEAN4 from the average normalized QMEAN4 score described for high resolution proteins and divided by the standard deviation of the observed distribution.

Additionally, the SWISS-MODEL server generates a 'local quality plot' that shows the predicted similarity to the target for each residue, and a 'comparison plot' that provides a comparison of the quality scores (Q-MEAN Z-scores) of the model with those of experimental structures and indicates whether the quality of the model agrees with high-resolution crystal structures. Furthermore, the Global Model Quality Estimation (GMQE) score provided by SWISS-MODEL server, is an index of the accuracy of the model generated with a specific alignment (higher scores indicate higher quality estimation) (https://swissmodel.expasy.org/docs/help).

Rampage and Procheck: computational tools for model validation

Rampage

Rampage is a free software (http://mordred.bioc.cam.ac.uk/~rapper/rampage.php) that produces 2-D Ramachandran plots for evaluating the stereochemical quality of a protein by investigating whether the distribution of backbone bond dihedral angles (φ / ψ) agrees with that found in high resolution structures (Lovell et al., 2003). In detail, φ angle denotes rotation around Cα –N bond while ψ angle signifies rotation around the Cα-C bond in the polypeptide. Torsion angles control protein folding and specifically φ and ψ angles provide the flexibility required for the backbone to adopt a specific fold. Especially in recent years, φ / ψ plots for individual homology models have become crucial in structure validation, because they provide a sensitive indicator of geometrical local issues. The approximate location of the most favourable low-energy regions in a protein was largely accepted and these φ / ψ criteria have become a crucial aspect of protein structure validation (Lovell et al., 2003).

In detail, the input to Rampage is a single file containing the coordinates of the protein structure (PDB file). After analysis, the Rampage software produces φ / ψ plots for glycine, proline, pre-proline and all the other residues. The horizontal axis shows φ values, while the vertical shows ψ values. The plot is divided into three regions: favoured, allowed, and outlier regions. Different type of secondary structures (α-helices and β-sheets) present different ranges of dihedral angles and the Ramachandran plot allows clear regional distinction between these two structures, showing clustering of dots in two different low-energy regions. Theoretically, the average φ and ψ values for α-helices and β-sheets should be clustered around -57, -47 and -80, +150, respectively in the Ramachandran plot (Kumar et al., 2016). By contrast, outlier regions show residues involved in forbidden torsion angles due to steric hindrance. This type of deviation indicates issues with the structure since high resolution proteins tend to have better

clustering within the allowed regions and tend to fold according to specific secondary structures: α-helices and β-sheets.

φ / ψ plots for glycine proline, pre-proline residues are graphed separately because these amino acids do not follow the principle of clustering around the α- and β-regions. In this regard, the exceptional conformational flexibility of glycine and the unique conformational rigidity of proline make accessible otherwise forbidden dihedral angle distributions and affect the secondary structure of proteins. Glycine is indeed often found in loop regions, while proline typically functions as a helix disruptor and induces distortions that affect the pre-proline residues conformations as well (Lovell et al., 2003).

To sum up, in good quality homology models, the distribution of backbone bond dihedral angles (φ / ψ) in the Ramachandran plot must agree with that found in high resolution structures which are characterised by high clustering within the favoured and allowed regions. By contrast, torsion angles in disallowed regions of the Ramachandran plot may indicate problems with the structure (bad geometry) that should be carefully analysed (Lovell et al., 2003).

Procheck

The web server Procheck (http://services.mbi.ucla.edu/PROCHECK/) analyses the stereochemical quality of a given protein structure, by investigating whether specific stereochemical indicators agree with those found in well refined and high-resolution structures. The parameters analysed by this server include: dihedral angles, main chain bond lengths and angles, chi angles, disulphide bonds, non-bonded contact distances, hydrogen bonds, planarity, chirality. Distinct outputs are produced for all these parameters and all the plots are output in PostScript format (Laskowski et al., 1993).

Dihedral angles analysis: Similarly to Rampage, Procheck generates a Ramachandran plot showing the distribution of torsion angles (φ / ψ) for all residues in a protein. The plot is subdivided into core, allowed, generously allowed and disallowed regions. These regions are those described by Morris et al. (1992) who tested numerous protein structures at high resolutions and found that 97% of the φ / ψ distributions clustered in the core and allowed regions. Core regions were defined those with more than 100 residues per pixel, while allowed regions those with around eight residues per pixel.

In the Ramachandran plot, different colours highlight distinct regions and the darker the area the more favourable the φ / ψ distributions. In detail, red indicates low-energy regions (core), yellow allowed regions, cream the generously-allowed regions and white disallowed regions. Glycine residues are identified by triangles while the other residues are represented as squares. Ideally, the homology model should have over 90% of the residues clustered in the core regions A (right handed α-helices), B (β-sheets), L (left-handed α-helices). By contrast poor models have no clustering and present many outliers (Morris et al., 1992).

Main chain bond lengths and bond angles analysis: In protein structure, internal bond lengths and angles should conform to the stereochemical values described by Engh & Huber (1991) who performed a comprehensive analysis of around 80000 small-molecule structures. Differences greater than 0.05 Angstroms for bond lengths and 10 degrees for bond angles are highlighted (Laskowski et al., 1993).

Chi (χ) angles analysis: The side chain torsion angles are typically named as χ_1 (C_α-$C_ß$), χ_2 ($C_ß$-C_γ), χ_3 ($C\gamma$ -C_δ), etc. Steric hindrance between γ side chain and main chain restricts χ_1 angle. Preferred conformations of the side chain as a function of χ_1 (-60º, +180º, +60º) are gauche (+), trans and gauche (-). Procheck generates a χ_1 -χ_2 plot for each residue and ideally the values for each residue should cluster in nine ideal positions, resulting from the combinations of the three preferred conformations for each angle χ_1 and χ_2. Residues lying more than 3.0 standard deviations from ideal positions are labelled (Morris et al., 1992; Laskowski et al., 1993).

Disulphide bonds analysis: Disulphide bonds originate from interactions between the SH groups of two adjacent cysteine residues in the three-dimensional structure. Ideally, the S-S distance in each disulphide bond should be 2 Angstroms, while the χ_3 torsional angle defined by this bridge should be -85.8º in the left-handed conformation and 96.8º for a right-handed conformation. Significant deviations from these ideal values are highlighted (Laskowski et al., 1993; Morris et al., 1992).

Non-bonded contact distances analysis: Non-bonded atoms which are closer to 2.6 Angstroms (minimal accepted van der Waals separation) typically indicate bad contacts. This analysis excludes potential hydrogen bonding partners (H-bond acceptor and donors). Significant deviations from the ideal value are highlighted (Laskowski et al., 1993; Morris et al., 1992).

Hydrogen bond analysis: The analysis of main hydrogen energies is evaluated using the Kabsch & Sander (1983) method. Ideal values should be around -8.50 kJ mol^{-1}. Significant deviations

from this ideal value of -2.0 Kcal/mol are highlighted (Laskowski et al., 1993; Kabsch & Sander, 1983).

Planarity analysis: Residues with large planarity deviations indicate issues in the protein structure caused by bad geometry (e.g. incorrect backbone, misplaced chain positioning). For residues containing aromatic rings, root mean squared (RMS) distances greater than 0.03 Angstroms from the best fit plane are highlighted, while for the other residues the threshold value is 0.02 Angstroms. A negative value signalizes a D-amino acid. The planarity of the peptide bond is based on the measure of the ω torsion angles that ideally should be 180º (Laskowski et al., 1993; Morris et al., 1992).

Chirality analysis: This analysis evaluates potential Cα tetrahedral distortions and it is based on the measure of the rotational zeta torsion angle defined by the atoms: C_{α}, N, C, $C_{ß}$. The ideal value is 33.9 degrees. Significant deviations from this expected value are highlighted (Laskowski et al., 1993; Morris et al., 1992).

Proline φ torsion angle analysis: The cyclic structure of proline's side chain restricts the φ torsion angle to -65.4º. Proline along with glycine do not follow the Ramachandran plot. Significant deviations from this expected value are highlighted (Laskowski et al., 1993; Morris et al., 1992).

φ / ψ torsion angles in α-helix analysis: In the α-helix all the amino acids have negative φ / ψ torsion angles and specifically the ideal values are -65.3º and -39.4º. Significant deviations from this expected value are highlighted (Laskowski et al., 1993; Morris et al., 1992).

G-factor calculations: At the end of the analysis dihedral angles and main chain covalent forces are globally scored to produce G values. These G-factors are log-odds scores computed based on the observed mean and standard deviation values in the given structure compared to ideal values. G-factor values below -0.5 indicate unusual stereochemical properties of the model, while values below -1.0 indicate a highly unusual probability of conformation (Laskowski et al., 1993).

6.3) Molecular Docking overview

Molecular docking

In parallel to the incessant synthesis of novel compounds, the urge to identify structural information about potential drug-target interactions has increased greatly over the last few years.

In this regard, molecular docking is a method widely used to computationally simulate the molecular recognition process and to predict the "best-fit" orientation of two interacting partners (ligand-target). To determine the energetically most favourable binding modes, molecular docking generates different ligand binding poses and uses a scoring function to estimate the strength of binding interactions and rank the generated ligand poses (Sousa et al., 2006).

In order to perform computational drug-target docking experiments, a sizeable body of 3D structure information of novel drugs and relevant drug targets (e.g. receptors, transporter proteins) is necessary to predict the 3D structure of a drug-target complex. As regards to proteins, the most reliable sources are high-resolution crystal structures which are available in the Protein Data Bank (PDB). Alternatively, in the absence of experimental structures, good-quality homology models may be used. On the other hand, the 2D-structure of the ligands may be drawn using ChemDraw software and then converted into 3D structures using Avogadro software.

Docking approach

The docking approach simulates the actual docking process in which the ligand fits into the protein's binding site after a certain number of "moves" (translations, rotations, torsion angle rotations) and then the system's total energy is calculated.
Docking protocols employ a combination of a search algorithm and a scoring function. The search algorithms allow the degrees of freedom of the target–ligand system to be sampled in order to generate the best binding mode, while the scoring functions have been designed to rank different potential protein–ligand complexes based on the strength of their intermolecular interactions (Sousa et al., 2006).

Docking algorithm

Finding the best binding pose is crucial in a docking protocol and it is typically predicted by calculating the root-mean-square deviation (RMSD) between the experimentally observed atom positions of the ligands and the one(s) predicted by the algorithm. In this regard, the flexibility of the system and number of degrees of freedom included in the conformational search is a crucial aspect in the docking efficiency. Because of the huge number of degrees of freedom associated with the real biological system, the dimensionality of the issue is reduced through the application of different levels of approximations and different docking methods characterised by increasing complexity can be used:

- Rigid receptor and ligand approach: both the ligand and the receptor are treated as rigid entities and only the degrees of translational and rotational freedom are explored.
- Flexible ligand approach: the ligand is regarded as a flexible body while the receptor is kept rigid.
- Flexible ligand and receptor approach: both the ligand and the protein are treated as flexible entities and relies on the most complex algorithms that consider alternative conformational changes taking place between the ligand and the protein. Notably, the extent of flexibility of both protein and ligand is necessarily simplified (Sousa et al., 2006).

Specifically, three general categories of methods have been devised to treat ligand flexibility:

1. Systematic methods
2. Random or stochastic methods
3. Molecular Dynamics simulation methods (Sousa et al., 2006)

Systematic methods

Systematic docking methods can be divided into:

- ✓ Conformational search algorithm approach: all degrees of freedom in a molecule are explored by rotating all rotatable bonds in the ligand through 360° until the achievement and evaluation of possible combinations.
- ✓ Fragmentation approach: the ligand is initially fragmented into different rigid parts and then grown by placing each fragment in the active binding site. Alternatively, the fragments are docked into the binding site and then linked covalently to generate the initial ligand (Sousa et al.,2006).

Random or stochastic algorithm-based methods

Random algorithm-based methods sample the conformational space by applying random changes to the ligand. There are different types of methods based on random algorithms: Monte Carlo methods and Genetic Algorithm methods.

- ✓ Monte Carlo algorithm method: docking calculations consist of a number of independent runs starting from random conformations. Each of these steps involves a random perturbation of the conformation (random atomic movements) and a selection

in which the new conformation is evaluated according to the metropolis criterion (thermodynamical exploration characterised by simulation of changes in temperature) and checked against some probability of acceptance according to the Boltzmann probability distribution (by which a system at a low energy has a small probability of being at a high energy state).

If the random atomic movement causes a decrease in the energy of the system, then the new assembly is accepted. An example of a program that employs MC-based algorithm is Autodock Vina. In detail, this docking programme employs Monte Carlo algorithm to perform a global search and it additionally employs a local search (iterated global local optimizer) to increase the likelihood to find the global minimum of the conformers (Sousa et al., 2006).

- ✓ Genetic Algorithm method: according to this method, randomly-generated ligand poses are regarded as chromosomes; each state variable (translation, orientation, rotation) is treated as a gene, each ligand's state corresponds to the 'genotype' and ligand's atomic coordinates are regarded as 'phenotype'. Each ligand pose is then evaluated on the base of the 'fitness score' resulting from the total interaction energy (intermolecular energy, internal energy, torsional energy, unbound energy) of the protein-ligand system. Changes in state variables (mutations) are applied to the population of ligand poses (chromosomes) to sample a new pose space (offspring/descendant generation). Selection of specific new-generation ligand poses is based on the fitness score, by which ligand poses (chromosomes) with the best scores are preserved for propagation into new generation to enable the evolution of optimal solutions (correct binding modes) (Morris et al., 1998). An example of Genetic Algorithm-based docking program is Autodock 4.0. In detail, this docking program employs the Genetic Algorithm to perform a global search and it additionally employs a local search method based on the Amber force field to increase the likelihood to find the global minimum of the conformers.

Molecular dynamics simulation methods

Molecular dynamics methods are computer simulations where the molecules are allowed to interact for a specific period of time, in order to obtain a view of the dynamic evolution of the docking process. In this approach, forces between atoms/molecules and their energies are calculated using molecular mechanics force fields, while the trajectories of atoms and molecules are determined by employing Newton's equations of motion. Molecular dynamics simulations allow one to describe several events occurring in a dynamic molecular system: solvation of the molecules; motions of molecules at various temperatures and pressures; drug binding; conformational changes critical to protein function; membrane transport; local rearrangement of side chains; small motion of loops. The study of protein dynamics is a very challenging, expensive, and time-consuming process. However, different algorithms and force fields are being used to provide some insights on computational dynamic structural biology (Sousa et al., 2006).

Scoring functions

Scoring functions are mathematical methods used to identify the best binding pose of a ligand (goodness of fit) on the protein binding pocket by accurately predicting the binding free energy of the complex and the strength of the non-covalent interaction between two molecules (e.g. ligand and target). An important application of the scoring function is to identify the potential drug leads for a given protein target by searching a large NPS database (i.e. virtual database screening). A reliable scoring function should be able to rank NPS drugs according to their binding scores.

Since a very sophisticated scoring function would be computationally too expensive and too time-consuming, a number of simplifications and approximations are included with a natural cost in terms of accuracy (Sousa et al., 2006).

Scoring functions are typically classified as:

- ✓ force-field-based
- ✓ empirical-based
- ✓ knowledge-based

Force-field based scoring functions

Force-field scoring has long been employed in many successful docking programs including Autodock 4.0. The potential energy of the system is estimated by summing the strength of intermolecular van der Waals and electrostatic interactions between all atoms of the receptor and the ligand in the complex and the internal energy of the ligand and the protein using a force field. However, important contributions to the binding free energy such as solvation, entropic terms are often ignored or implicitly added, highlighting some traditional limitations of force field scoring functions (Sousa et al., 2006). The various contributions to binding can be written with the following equation:

$$\Delta G_{binding} = \Delta G_{solvent} + \Delta G_{int} + \Delta G_{conf} + \Delta G_{motion}$$

ΔG_{bind}= free energy of binding between a ligand and a receptor
$\Delta G_{solvent}$= desolvation free energy of both ligand and receptor upon binding
ΔG_{int}= interaction free energy involving direct contact of ligand with protein (e.g. van der Waals interactions, electrostatic interactions, and hydrogen bonds)
ΔG_{conf} = conformational strain loss upon binding
ΔG_{motion}= entropy loss upon binding (internal rotation and vibration) (Smith et al., 2009).

Docking programs such as Autodock 4.0 use a semi-empirical free energy force field to evaluate different conformations during docking simulations.
The force field is parameterized using a wide number of well-known protein-inhibitor complexes. The force field assesses binding in two steps: in the first step, the internal energies of the protein and ligand are estimated for the transition from the unbound states to the bound state; in the second step the intermolecular energies obtained combining the ligand and protein in their bound conformation are assessed (http://autodock.scripps.edu/faqs-help/manual/autodock-4-0-user-guide/AutoDock4.0_UserGuide.pdf).

The force field includes:

- ✓ six pair-wise assessments (V) where L refers to the "ligand" and P refers to the "protein"
- ✓ an estimation of the conformational entropy lost upon binding (ΔS_{conf}):

$$\Delta G = (V_{bound}{}^{L-L} - V_{unbound}{}^{L-L}) + (V_{bound}{}^{P-P} - V_{unbound}{}^{P-P}) + (V_{bound}{}^{P-L} - V_{unbound}{}^{P-L} + \Delta S_{conf})$$

Each of the pair-wise energetic terms includes assessments for dispersion/repulsion, electrostatics, hydrogen bonding terms and desolvation. In detail, van der Waals energy terms are described with a Lennard-Jones potential, while the electrostatic term is given by a Coulombic formulation.

Empirical Scoring Functions

Empirical scoring functions are based on empirical data and are used to determine the binding affinity between the ligand and the target. In detail, these scoring functions assume that binding energies can be approximated by a sum of several interaction terms derived from weighted structural parameters. The individual weights are obtained by fitting the scoring function to experimental binding parameters of a set of protein-ligand complexes with known structures (regression analysis). Several terms (e.g. hydrogen bonds, ionic and lipophilic interactions, loss of entropy upon binding) form the basis of the scoring functions. The various contributions to binding can be written with the following equation:

$$\Delta G = \Sigma_i W_i \Delta G_i$$

ΔG= free energy of binding

W_i= coefficient determined by fitting the binding affinity data of a set of well-known protein-ligand complexes

ΔGi= includes different energy terms (hydrogen bond, entropy, desolvation, electrostatics, hydrophobicity).

These scoring functions are fast, but their accuracy depends entirely on the experimental data set used in the parameterization process (Sousa et al., 2006)

Knowledge-based scoring function

This scoring function is based on statistical observations of intermolecular interactions of experimentally known complex structures and represent the binding affinity as a sum of protein-ligand atom pair interactions which are used to derive distance-dependent interaction free energies of protein-ligand atom pairs ("potentials of mean force"). This method is founded on the assumption that close intermolecular interactions that occur more frequently are likely to be energetically favourable and therefore contribute to binding affinity. In detail, pairwise

potentials are obtained from the frequency of occurrence of atom pairs in a database, according to the inverse Boltzmann relation.

In protein-ligand studies, the potentials are calculated by the following equation:

$wr=-K_bT\ ln[p(r)/p^*(r)]$

wr=pairwise potentials

Kb= Boltzmann constant

T=absolute temperature of the system

p(r)= number density of the protein-ligand atom pair at distance r

p*(r)= pair density in a reference state where the interatomic interactions are zero (Huang et al., 2010)

Some docking programs use a mix of different scoring functions. Autodock Vina for example uses hybrid empirical/ knowledge-based scoring functions to determine the binding affinity between the ligand and the target. Indeed, it uses empirical information from both the conformational preferences of the receptor-ligand complexes and the experimental affinity calculation (Trott and Olson, 2009).

Over the years, docking has been applied successfully in different types of virtual screening. Among them, PyRx 0.9.4 is a virtual screening with an easy-to-use user interface for AutoDock 4.0 and AutoDock Vina software, which makes it a valuable and popular tool in computational science as it does not require extensive expert and technical knowledge from users. This software is typically used to dock small molecules (e.g. drugs) to a macromolecule (e.g. receptor) to acquire some insights into the pharmacological activity of certain compounds (Dallakyan and Olson, 2015).

Computational docking programmes: Autodock 4.0 and Autodock Vina

Autodock 4.0 and Autodock Vina are computational docking programs that have been developed in parallel to answer to different needs. Different scoring functions (approximate mathematical methods) are used by these two programs to predict the strength of non-covalent interactions after docking and score each one of a set of different ligand binding poses.

In detail, Autodock uses semi-empirical force-field scoring functions based on physical atomic interactions (e.g. van der Waals interactions, electrostatic interactions, and bond

stretching/bending/torsional forces) derived from both experimental data and quantum mechanical calculations (Huang et al., 2010; Sousa et al., 2006).

On the other hand, Autodock Vina uses hybrid empirical/knowledge-based scoring functions that score ligand binding poses by applying rules based on preferred and non-preferred atom pair interactions found in experimentally determined protein-ligand complexes. These rules are then interpreted as scoring functions and used to score ligand binding poses (Mohan et al., 2005).

Autodock 4.0 and Autodock Vina both adopt the flexible ligand docking approach, but they use different algorithms to explore the potential rotation, translation and orientation space searches of the ligand being docked to generate the best binding pose (binding-mode of a ligand in a protein binding site). The number of degrees of freedom (number of independent motions) included in the conformational space is a challenging aspect that influences the searching efficiency (Sousa et al., 2006).

The specific search algorithm used by Autodock 4.0 is the random or stochastic Lamarckian genetic algorithm search. On the other hand, Autodock Vina relies on the Markov chains modified Monte Carlo algorithm.

The Lamarckian genetic algorithm search used by Autodock 4.0, is an algorithm based on the principle of evolution associated to a local search method during optimization that generates low-energy conformations and orientations of the ligand (Morris et al., 1998).

The local search method adopted during optimization, allows one to perform energy minimization by performing local energy assessments using a method based on the 'AMBER' force field. According to this method, energy calculations are performed by generating a three-dimensional grid within which the receptor protein is placed, and various ligand atoms are allowed to systematically visit every grid point. For each ligand's atom, different types of energies are calculated (hydrogen-bonding energies, electrostatic potentials, dispersion/repulsion energies) considering all receptor atoms near the grid points (8Å). Ligand atoms are given energy values which can later be sampled by the main docking programme to generate the best binding pose (Morris et al., 1998).

To enhance algorithm search performance, the local energy assessment is coupled with a conformational space search based on a genetic algorithm (Lamarckian genetic algorithm search).

Autodock Vina relies on the random approach method Markov chains modified Monte Carlo algorithm (simulated annealing) by which random changes in the ligand conformation are generated and a thermodynamical exploration of different states is performed in order to select energetically favourable states (global energy minimum) of the conformers. Changes in temperature are involved during the run for every conformation (Siavoush, 2016). To perform the local optimization, Vina employs the Iterated Global Local optimizer which uses multiple steps consisiting of a mutation followed by local optimization performed using the algorithm of Broyden-Fletcher-Goldfarb-Shanno (quasi-Newton method). This algorithm uses the value of the scoring function along with its gradient (multi-variable generalization of the derivatives of the scoring function with respect to orientation, position of the ligand and torsion of the rotatable bonds) and performs successive measurements of the gradient to find the global energy minimum of the conformers. By using multithreading (the ability of a central processing unit (CPU) to execute multiple processes or threads concurrently) the execution of the docking process in Vina is speeded up considerably (Trott and Olson, 2009).

6.4) SCs and *in silico* CB_1 receptor studies, aim and goals

The overall *in silico* CB_1 receptor study conducted by our research group, aimed at providing a rationale for different biological effects that a range of novel SCs exert by investigating their CB_1R binding properties. In detail, this study branched into two different analyses: docking of novel SCs against the homology model of the CB_1 receptor (Rattus Norvegicus) and docking of novel SCs against the crystal structure of the human CB_1 receptor.

- Docking of novel SCs against the homology model of the CB_1 receptor: since no crystal structure of the rodent CB_1 receptor was available at the time of our study, a homology model of this receptor was built and used for molecular docking investigations. In a first instance, the docking approach (Autodock Vina) was validated by performing a comparative analysis of the relevant binding interactions of a series of referent compounds against the homology model of the CB_1 receptor (Rattus Norvegicus) and those described in CB_1 receptor mutation studies. The compounds used for validation were the same as those used in the CB_1 computational study described by Hua et al., 2016 and included a range of CB_1 agonists (e.g. anandamide, 2-AG, Δ9-THC, CP-55,940, WIN-55,212-2, JWH-018) and CB_1 antagonists (e.g. rimonabant, AM-251, AM-6358, Otenabant, Taranabant). After validation, the same docking software (Autodock Vina) was engaged to explore and detect the crucial binding interactions of

a range of index novel SCs (BB-22, 5F-PB-22, 5F-AKB-48, STS-135) against the above-mentioned homology model.

- Docking of novel SCs against the crystal structure of the human CB_1 receptor: once the crystal structure of the human CB_1 receptor has been made available (Hua et al., 2016), the relevant key interactions of the above-mentioned referent compounds were investigated against the crystal structure of the human CB_1 receptor by employing two different docking software packages (Vina and Autodock 4.0). The docking methods were then validated by performing a critical comparative analysis of our findings against those obtained from available evidence-based literature on CB_1 receptor mutation studies. After validation, the same docking software packages were engaged to explore and detect the crucial binding interactions of the above-mentioned novel SCs against the crystal structure of the human CB_1 receptor. An additional comparative analysis of the outcomes produced by different docking software (Vina and Autodock 4.0) was undertaken, and the more consistent the results given by these software packages, the higher the reliability of their outcomes (further validation of the docking approach). Furthermore, relevant ligand interactions against the homology model (Rattus Norvegicus) and the crystal structure of the human CB_1 receptor were analytically compared and discussed.

6.5) CB_1 receptor homology modelling studies: methods

Template identification, alignment, homology model building and validation

The *in silico* homology model of the rodent CB_1 receptor was generated using the SWISS-MODEL server (https://swissmodel.expasy.org/ provides). This server was fully automated from the sequence search and alignment to structure generation and evaluation. X-ray structures of the proteins in the Protein Data Bank with highest sequence similarity were selected as template structures. An expected molecular model was generated and a global model quality estimation (GMQE) score was used by the SWISS-MODEL server for quality estimation of the generated model.

The primary sequence (FASTA) of the CB_1 receptor (Rattus Norvegicus) (Accession ID: NP_036916.1) was retrieved from the NCBI website (https://www.ncbi.nlm.nih.gov/protein) using the NCBI's own search engine 'Entrez' and it was used to build the model, according to the recognised evolutionary relationship between the Rattus Norvegicus species and the strains of laboratory rats employed in our preclinical studies (Hedrich, 2000).

According to SWISS-MODEL report, the template search was performed with Blast (Basic Local Alignment Search Tool) (Altschul et al., 1997) and HHblits ('HMM-HMM–based lightning-fast iterative sequence search') (Remmert et al., 2011) against the primary amino acid sequence contained in the Swiss-Model Template Library (SMTL) (last update: 2017-07-19, last included PDB release: 2017-07-14). An initial HHblits profile was built using the procedure outlined in Remmert et al. (2011), followed by one iteration of HHblits against NR (HMM database). The obtained profile was then searched against all profiles of the SMTL. The model was then built based on the target-template alignment using ProMod3 that generated the actual model coordinates according to the input alignment (Bienert et al., 2017). An insertion and deletion fragment modelling approach was performed using the fragment library; side chains were rebuilt, and loops were modelled with ProMod3. Finally, the geometry of the model was optimised by using a force field, and the global model quality was assessed calculating the QMEAN, Q-MEAN4, Q-MEAN4 Z-score functions (Benkert, et al., 2011).
To further investigate the stereochemical quality of our CB_1 receptor (Rattus Norvegicus) homology model, the PDB containing the coordinates of our protein structure was submitted to different structure assessment methods: Rampage (http://mordred.bioc.cam.ac.uk/~rapper/rampage.php) and Procheck (http://services.mbi.ucla.edu/PROCHECK).

6.6) CB_1 receptor homology modelling studies: results and discussion

Overall 36 highest quality templates ranked by a predicted global quality estimate, have been retrieved by the SWISS-MODEL server. Among them, the crystal structure (X-RAY diffraction 2.80 Å) of the monomer 5tgz.1.A (452 amino acids) (Human Cannabinoid receptor 1, flavodoxin) was selected to build the three-dimensional structure of the protein (sequence identity: 89.24%). After model building, the SWISS-MODEL server provided the target-template alignment (see Figure 37), a view of the three-dimensional structure of the model (see Figure 38), and the model coordinates available in PDB format. The resolution of our model was 1.5 Angstrom (high resolution) and the total number of residues was 312.

Figure 37: Target-template alignment : CB_1 receptor sequence (Rattus Norvegicus)-5TGZ1.A sequence

The Q-MEAN4 Z-score for the CB_1R homology model (Rattus Norvegicus) was satisfactory (-3.06), and indicated a tolerable geometry of the model (see Figure 38). From the analysis of the comparison plot emerged the fact that the structure of our homology model agreed with that of high-resolution proteins with a Q-MEAN Z-score>2 (light grey spots) while the majority of experimentally elucidated structures with high resolution shows a Q-MEAN Z-score<1 (dark spots). Notably, in this plot the algebraic signs of the calculated Z-scores were standardised (see Figure 38). From a general observation of the local quality plot, emerged that some residues presented score values below 0.6 which indicates low quality (see Figure 38). A detailed analysis using Rampage and Procheck was necessary to examine eventual issues related to these residues. Overall, the Global Quality Estimation (GMQE) calculated for our homology model was 0.6, which indicated an acceptable accuracy of the model.

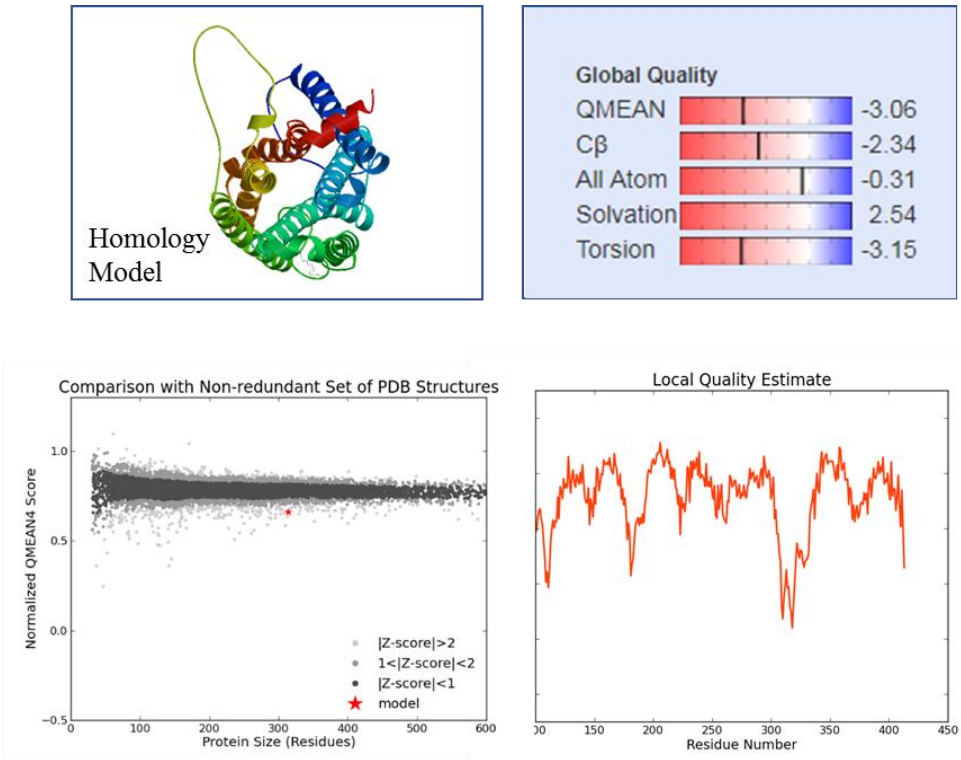

Figure 38: Top left: Three-dimensional structure of the CB_1 receptor homology model (Rattus Norvegicus); top right: global quality plot; bottom left: comparison plot; bottom right: local quality plot.

6.7) Quality estimation of the CB_1 receptor homology model

Rampage analysis: results and discussion

According to our findings, 97.4% of residues were found in favoured regions (304 amino acids, dark spots), 2.2% in allowed regions (Glu 107, Trp 256, Leu 271, Arg 308, Ser 317, Thr 322: orange squares and Gly 255: orange cross) and 0.3% in outlier regions (Lys 316, red square) (see Figure 39). Since the φ / ψ dihedral angle distributions were consistent with those found in high resolution structures (Lovell et al., 2003) these results suggested that the stereochemical quality of our model was acceptable. However, one single amino acid (Lys 316) showed torsion angle distributions in outlier regions of the Ramachandran plot, highlighting the presence of a local geometrical issue that was carefully examined using the Procheck assessment method.

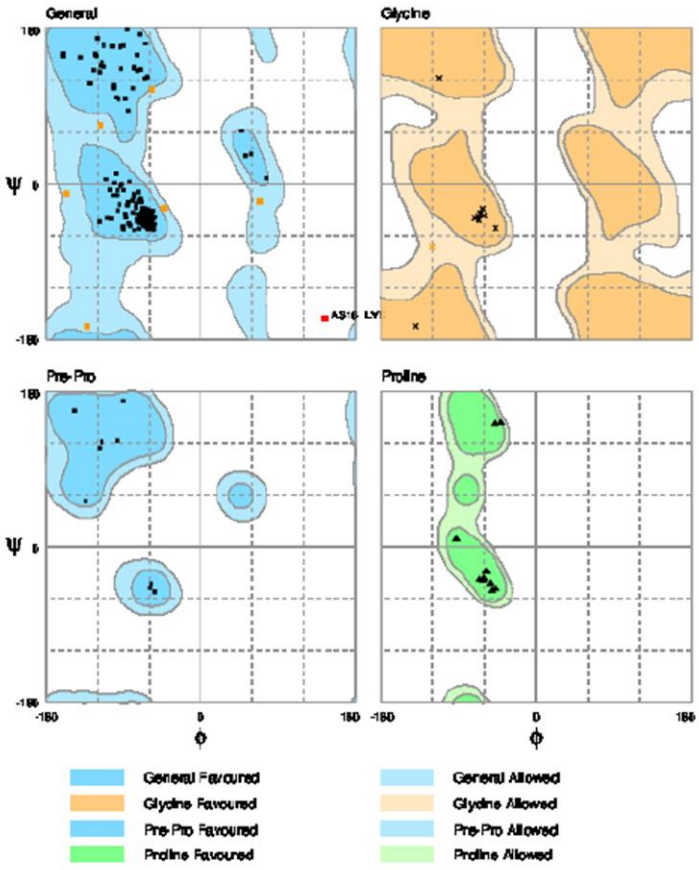

Evaluation of residues

```
Residue [A 107 :GLU] ( -42.68, -27.56) in Allowed region
Residue [A 255 :GLY] (-120.91, -72.36) in Allowed region
Residue [A 256 :TRP] ( -56.75, 110.21) in Allowed region
Residue [A 271 :LEU] (  68.42, -19.88) in Allowed region
Residue [A 308 :ARG] (-116.38,  68.72) in Allowed region
Residue [A 317 :SER] (-156.38, -10.57) in Allowed region
Residue [A 322 :THR] (-132.45,-164.44) in Allowed region
Residue [A 316 :LYS] ( 143.54,-155.21) in Outlier region
Number of residues in favoured region    (~98.0% expected)  :  304 ( 97.4%)
Number of residues in allowed region     ( ~2.0% expected)  :    7 (  2.2%)
Number of residues in outlier region                        :    1 (  0.3%)
```

Figure 39: Ramachandran plot, generated by Rampage server, of the CB_1 receptor homology model (Rattus Norvegicus).

Procheck analysis: results and discussion

Dihedral angles analysis outcomes: Similarly to Rampage, Procheck generated a Ramachandran plot showing the distribution of torsion angles (φ / ψ) for all residues in our homology model (see Figure 40). In detail:

- 95.5% of the residues were found in the most favoured regions marked with the letters A (right-handed alpha helices), B (beta strands), L (left-handed alpha helices) and indicated in red colour;
- 3.8% in allowed regions marked with the letters a (right-handed alpha helices), b (beta strands) l (left-handed alpha helices), p (allowed epsilon) and indicated in yellow;
- 0.3% in generously allowed regions marked with the letters ~a, ~b, ~l, ~p and indicated in cream (Leu 271);
- 0.3% in disallowed regions indicated in white (Lys 316).

These results were consistent with those obtained with Rampage, by which only one amino acid (Lys 316) was found in outlier regions. Additionally, the Ramachandran plots for all residue types, showed some residues found in unfavourable conformations (Lys 316, Gly 255, Leu 271 and Ser 317) that needed further examination. Overall, since our homology model showed over 90% of the residues clustered in the core regions A, B, L, it could be considered a good quality model.

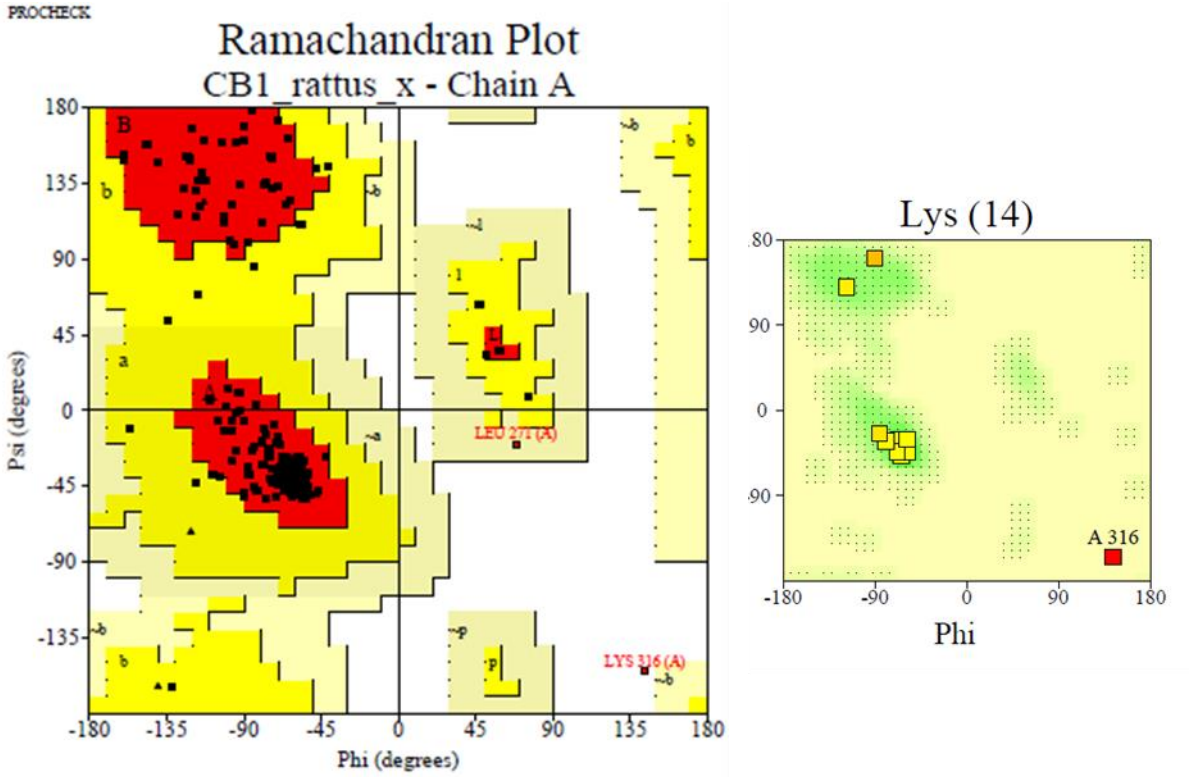

Figure 40: Ramachandran plot of the CB_1 receptor homology model (Rattus Norvegicus) generated by Procheck software.

Main chain parameters analysis: Overall, Procheck analyses five main chain properties of the structure (peptide bond planarity; measure of bad non-bonded interactions; alpha carbon tetrahedral distortion; hydrogen bond energies; overall G-factor) and generates plots for each parameter, making a comparison with main chain properties found in well refined structures (see Figure 41). The blue band in each plot represents the outcomes from well refined structures and the width of the band corresponds to a variation of one standard deviation from the mean. The plots in the Figure 41 shows the resolution of our homology model and other well-refined proteins against: the percentage of residues found in the most favoured regions; the planarity of the peptide bond (standard deviation of the ω torsion angle expressed in degrees); the number of bad contacts per 100 residues; the Cα tetrahedral distortion (standard deviation of the Z angle expressed in degrees); the standard deviation of the hydrogen bonds energies expressed in Kcal/mol. According to these analyses, our homology model (dark square) lies inside the band for each one of the five parameters considered. In detail, its position is indicated as 'better' (which specifies a variation from the mean<1 standard deviation) for all designed parameters and suggests a good agreement with well refined structures (see Figure 41).

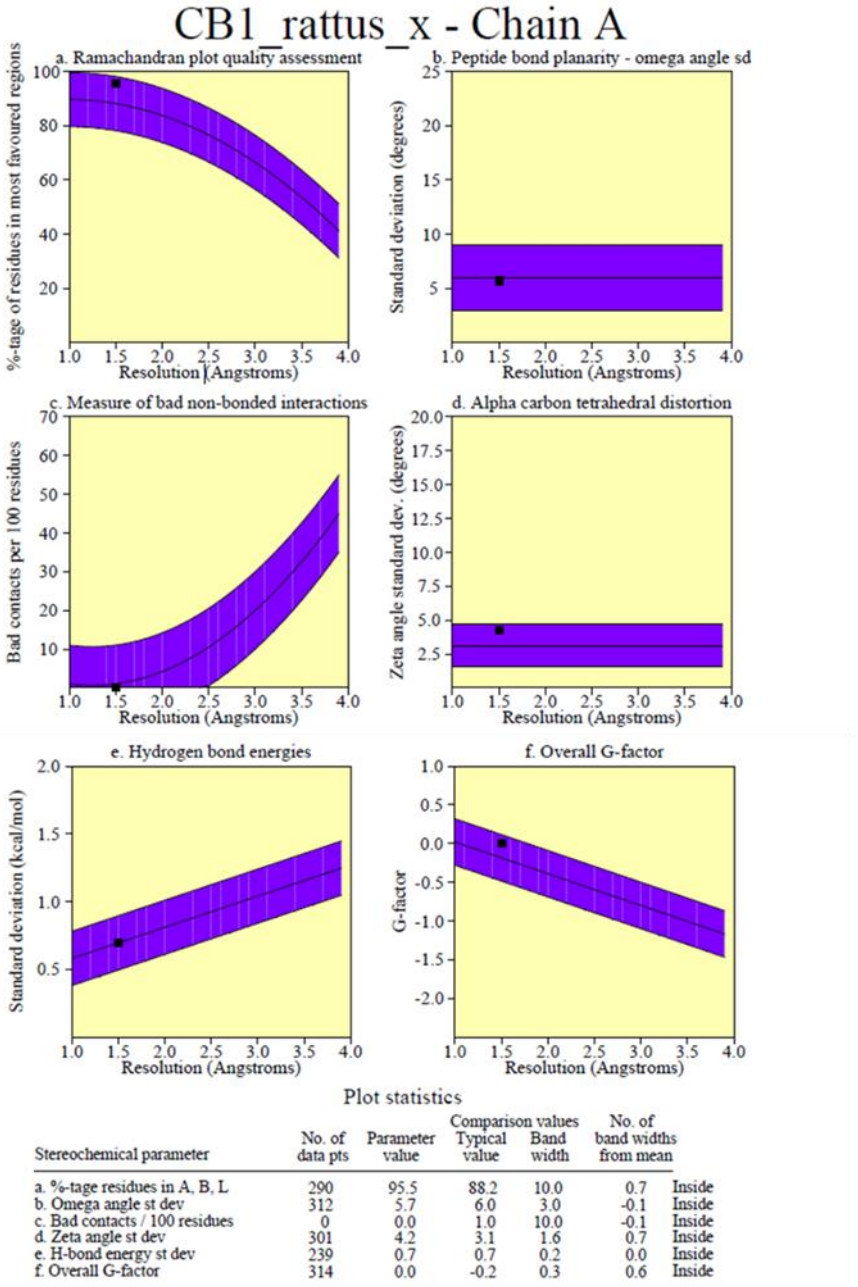

Plot statistics

Stereochemical parameter	No. of data pts	Parameter value	Comparison values Typical value	Band width	No. of band widths from mean	
a. %-tage residues in A, B, L	290	95.5	88.2	10.0	0.7	Inside
b. Omega angle st dev	312	5.7	6.0	3.0	-0.1	Inside
c. Bad contacts / 100 residues	0	0.0	1.0	10.0	-0.1	Inside
d. Zeta angle st dev	301	4.2	3.1	1.6	0.7	Inside
e. H-bond energy st dev	239	0.7	0.7	0.2	0.0	Inside
f. Overall G-factor	314	0.0	-0.2	0.3	0.6	Inside

Figure 41: Main chain parameters of the CB_1 receptor homology model (Rattus Norvegicus) generated by Procheck.

Residue by residue Chi (χ) angle analysis: As previously described, Procheck generates a χ1 - χ2 plot for each residue and preferably the values for each residue should cluster in nine ideal positions, resulting from the combinations of the three preferred conformations for each angle χ1 and χ2. The three preferred conformations are gauche (+), trans and gauche (-) (Morris et al., 1992; Laskowski et al., 1993). According to this analysis, four residues of our homology model (Asp 404, Ile 157, Leu 389, Trp 256) showed unfavourable conformations (score < -3.00) and needed careful examination.

Overall side chain properties analysis: Five different side chain properties are analysed by Procheck which ultimately generates different plots showing the resolution of our homology model and other well refined proteins against the standard deviation expressed in degrees of χ1 gauche (-), χ1 trans, χ1 gauche (+), pooled χ1 torsion angles and χ2 trans. According to these analyses, our homology model (dark square) lies inside the band and its position is indicated as 'better' for all designed parameters, suggesting a good consistency with well refined structures (see Figure 42).

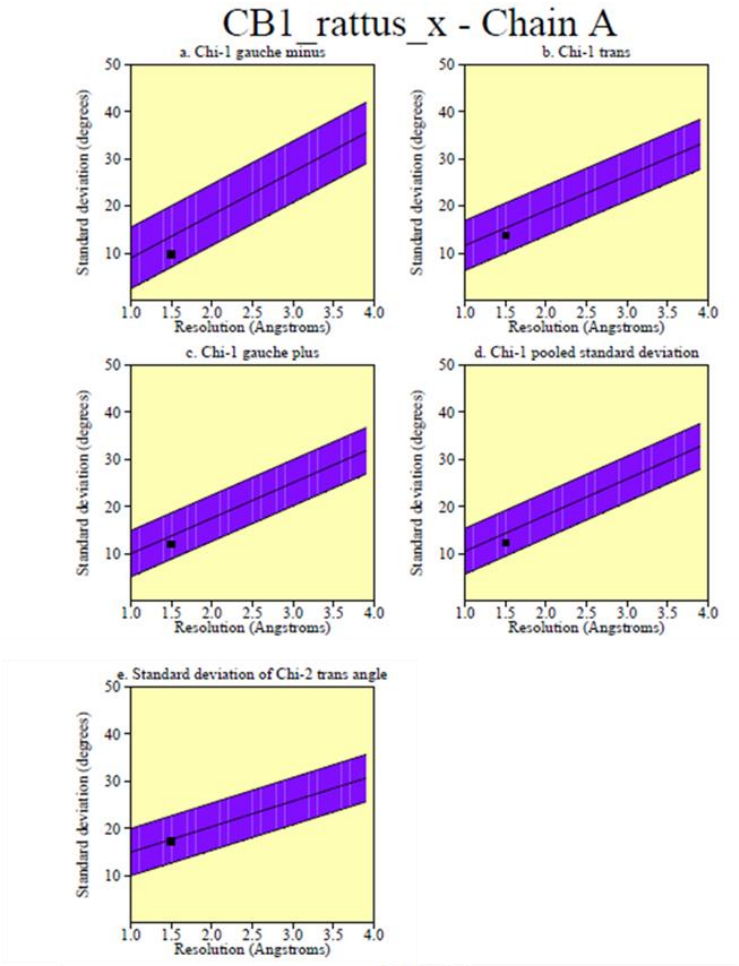

Plot statistics

Stereochemical parameter	No. of data pts	Parameter value	Comparison values Typical value	Band width	No. of band widths from mean	
a. Chi-1 gauche minus st dev	30	9.8	13.6	6.5	-0.6	Inside
b. Chi-1 trans st dev	93	13.7	15.3	5.3	-0.3	Inside
c. Chi-1 gauche plus st dev	147	11.9	13.8	4.9	-0.4	Inside
d. Chi-1 pooled st dev	270	12.3	14.3	4.8	-0.4	Inside
e. Chi-2 trans st dev	78	17.3	17.7	5.0	-0.1	Inside

Figure 42: Overall side chain properties of the CB_1 receptor homology model (Rattus Norvegicus) generated by Procheck.

Other residue by residue properties: Procheck for each residue, analyses other parameters including: (a) the absolute deviation from mean χ1 value; (b) absolute deviation from mean of omega torsion; (c) Cα chirality (absolute deviation of zeta torsion). Residues that deviate by more than 2 standard deviations from ideal values are indicated as red bars (see Figure 43). Additionally, the server generated (d) the schematic picture of the secondary structure, (e) the protein sequence along with the region of the Ramachandran plot where the residues are located, (f) each residue's maximum deviation from ideal values considering several parameters (see Figure 43). According to the residue by residue analysis 21 residues showed maximum deviation higher than 2 standard deviations from ideal values. In detail: Glu 101, Asp 185, Ala 306, His 321 (issues with the omega angle), Leu 148, Tyr 154, Phe 178, His 179, Arg 227, Leu 251, Leu 254, Leu 261, His 303, Leu 389, Arg 401 (issues with Phi helix), Arg 149, Tyr 154, His 179, Arg 227, Leu 251, Leu 254, Leu 261, His 303, Leu 389, Val 328 (issues with Psi helix), Leu 165, Leu 251, Arg 401, Arg 406 (issues with χ2 trans), Leu 254 (issues with χ1 gauche minus), Trp 256, Asn 257, Val 328 (issues with dihedral trans gauche plus), Ala 306 (issues with H bond energy), Lys 316 (issues with Cα chirality, D amino acid).

Bond length and bond angle analysis: From the bond length analysis, 99.9% of the residues were within limits and only one residue was highlighted (Gly 100: NCα length issue). As regards to the bond angles, 96.2% of the residues were within limits, while 3.8% were highlighted. Specifically, 24 residues showed bond angle values >2.0 standard deviations from mean including: Met 104, Glu 107, Asn 113, Thr 126, Arg 151, Asp 177, Ser 186, Arg 221, Arg 231, Leu 251, Pro 252, Asn 257, Phe 269, Asn 257, Phe 269, Thr 322, Arg 332, Ile 340, Gly 358, Asp 367, Val 368, Thr 392, Asn 394, Asp 404, Phe 413. These residues are worth investigating further.

Planarity analysis: Residues with large planarity deviations indicate issues in the protein structure caused by bad geometry. For residues containing aromatic rings, RMS distances greater than 0.03 Angstroms from the best fit plane are highlighted, while for the other residues the threshold value is 0.02 Angstroms. A negative value signals a D-amino acid (Laskowski et al., 1993; Morris et al., 1992). According to the analysis 84.9% of residues were within limits and 15.1% highlighted. Specifically, 12 amino acids showed distorted geometry, including: Tyr 154, His 155, Phe 175, Phe 190, Tyr 276, Trp 280, Phe 290, Tyr 293, Asp 339, Tyr 398 (see Figure 44).

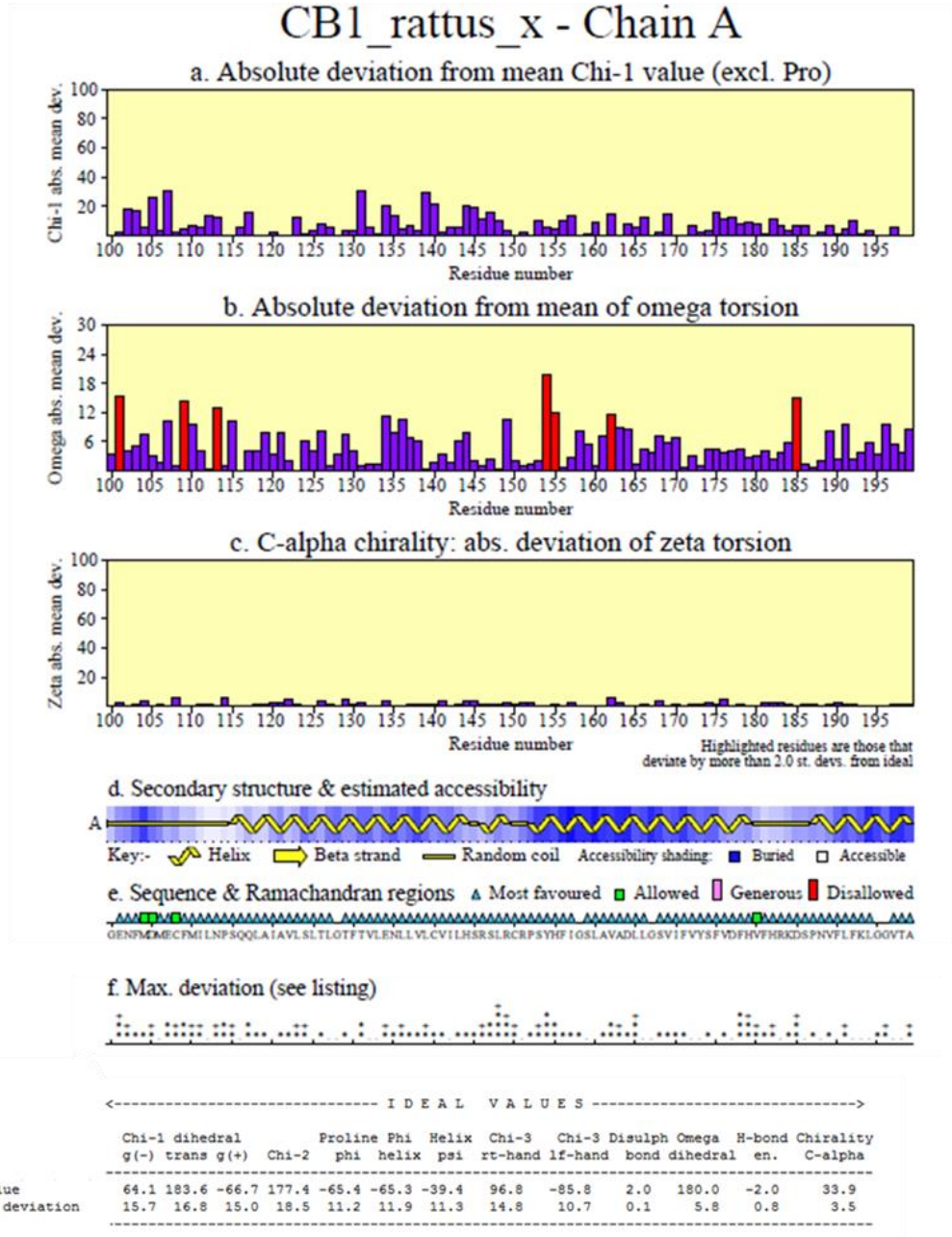

<----------- I D E A L V A L U E S ----------->

	Chi-1 dihedral g(-)	trans	g(+)	Chi-2	Proline phi	Phi helix	Helix psi	Chi-3 rt-hand	Chi-3 lf-hand	Disulph bond	Omega dihedral	H-bond en.	Chirality C-alpha
Ideal value	64.1	183.6	-66.7	177.4	-65.4	-65.3	-39.4	96.8	-85.8	2.0	180.0	-2.0	33.9
Standard deviation	15.7	16.8	15.0	18.5	11.2	11.9	11.3	14.8	10.7	0.1	5.8	0.8	3.5

Figure 43: Residue by residue properties of the CB_1 receptor homology model (Rattus Norvegicus) generated by Procheck.

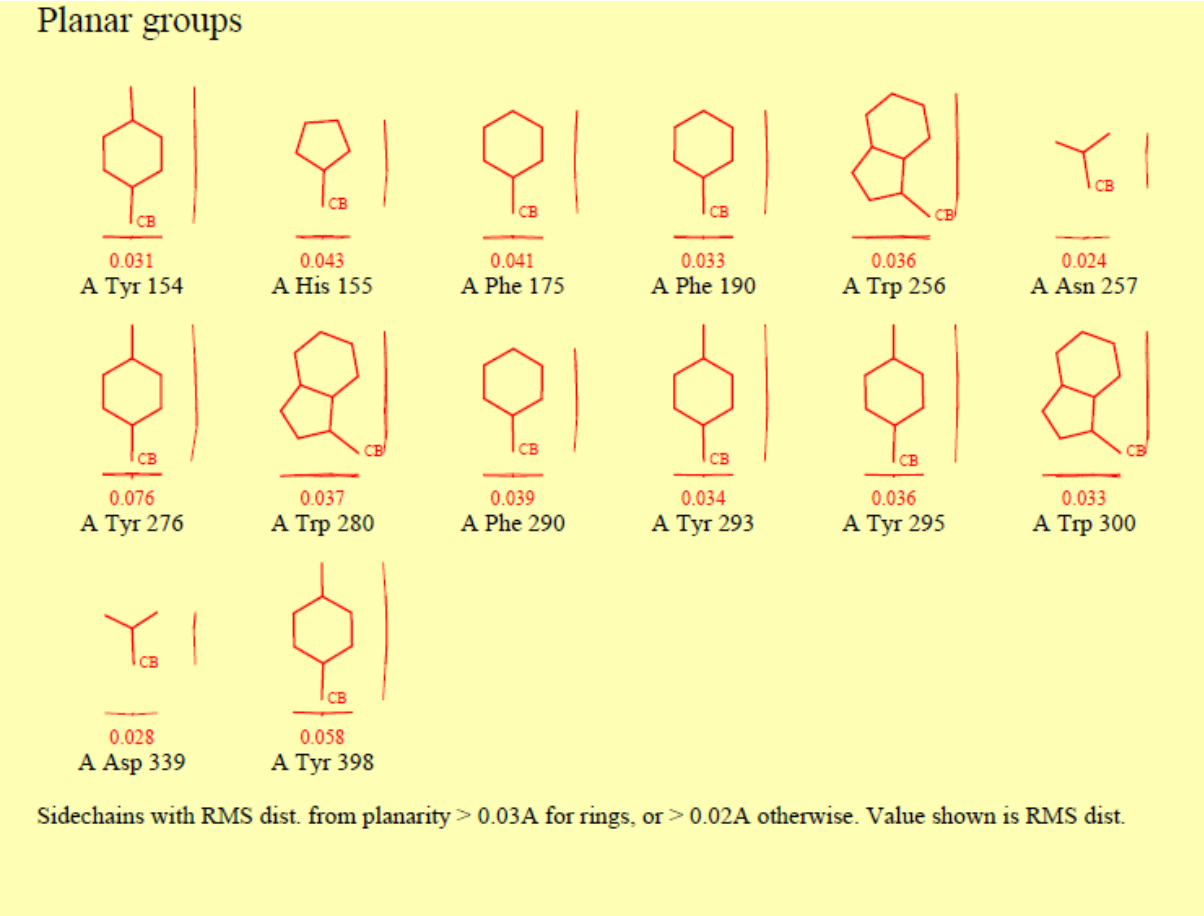

Figure 44: Residues of the CB_1 receptor homology model (Rattus Norvegicus) with planarity deviations according to Procheck.

G-factor calculations: At the end of analysis, Procheck generated G-factors which are log-odds scores computed based on the observed mean and standard deviation values in the given structure compared to ideal values. G-factor values for dihedral angles in our homology model was: -0.05, while for covalent bonds was: 0.04. Since, ideally scores should be above -0.5 (Laskowski et al., 1993), G-Factor values related to our homology model were acceptable.

6.8) Homology model refinement and preparation for docking process

Prior to docking, the homology model structure underwent some refinement operations. In detail, the protein was prepared using the protein preparation wizard tool in Maestro 10.4. (https://www.schrodinger.com/maestro). During this process, all hydrogens were added and protonation states of ionisable groups optimized for pH=7; water molecules were deleted, and issues associated with the workspace structure were fixed. After optimization, the PDB file was

converted into a format (.pdbqt) suitable for docking in the virtual screening software PyRx 0.9.4.

6.9) Ligand building and preparation for docking process

All ligands were prepared to create 3D geometries which were optimised prior to virtual screening. In detail, the SMILES (Simplified Molecular Input Line Entry System) of each ligand was retrieved from Pub Chem (https://www.ncbi.nlm.nih.gov/pccompound) and pasted into Chem Draw Professional 15.0 (http://www.cambridgesoft.com/Ensemble_for_Chemistry/ChemDraw/ChemDrawProfessional/) in order to obtain the 2D-structure (.mol file). The structure was then uploaded into Avogadro where the hydrogens were removed and added for pH=7.0 and the geometry was optimised using setup force field MMFS and number of steps: 10000 minimization steps. After optimization, each ligand was saved as mol.2 file and converted into a .pdbqt file format suitable for docking in the virtual screening PyRx 0.9.4. (https://sourceforge.net/p/pyrx/news/2016/02/pyrx-094-release-announcement/).

6.10) Docking of referent compounds against the homology model of the rodent CB_1 receptor, approach validation: methods

In the docking approach validation, the key binding interactions of a range of referent compounds against the homology model of the rodent CB_1 receptor were analysed. PyRx 0.9.4 was used as virtual screening software and the docking programme employed was Autodock Vina. This programme adopts a flexible ligand docking approach, and generates the best binding pose by comparing the root-mean-square deviation (RMSD) between the experimentally observed atom positions of the ligands and the one(s) predicted by the Markov chains modified Monte Carlo algorithm (Sousa et al., 2006). Vina search space coordinates used in our study were established according to previous experimental studies and were as follows: centre, X:41, Y:29, Z:317; dimensions, X: 25 Å, Y: 25 Å, Z: 25 Å. These parameters efficiently restricted where the movable atoms lay during the docking process. After docking, the ligand binding energy (Kcal/mol) and two variants of RMSD values were provided: rmsd/lb (RMSD lower bound) which matches identically labelled atoms and ignores any symmetry of the ligands, and rmsd/ub (RMSD upper bound) which considers alternative symmetric conformations of the ligands. The compounds used for validation were the same as those used in the CB_1 computational study described by Hua et al. (2016) and included a range of CB_1 agonists (e.g. anandamide, 2-AG, Δ9-THC, CP-55,940, WIN-55,212-2, JWH-018) and CB_1 antagonists (e.g. rimonabant, AM-251, AM-6358, Otenabant, Taranabant). Overall, eight

binding modes for each ligand were generated and the pose with the lowest binding energy (expressed in Kcal/mol) was selected to study the key binding interactions.

A comparative analysis of the relevant ligand binding interactions described in CB_1 receptor mutation studies and those found with our computational docking approach, was undertaken. The computational findings were then debated against the experimental ones and possible consistencies were highlighted to support our docking approach. For each referent compound, the lowest binding affinity values obtained using the docking programme Vina, were compared against the experimentally-obtained K_i values retrieved from the literature. Possible inconsistencies between computational and experimental binding affinity findings were analysed, and some limitations of the study were highlighted and discussed.

6.11) Docking of representative CB_1R agonists and antagonists against the CB_1 receptor (Rattus Norvegicus) homology model: results and discussion

Binding modes of representative CB_1 receptor agonists

According to the outcomes generated by the Vina docking programme, the indole group of the aminoalkylindole derivative JWH-018 (1-pentyl-3-(1-naphthoyl)indole) showed mainly hydrophobic interactions with residues placed on the N-terminal group of the protein (Met 105, Met 103, Phe 102); its pentyl tail formed mostly alkyl interactions with residues located on the helix 3 (Phe 189) and in the second extracellular loop (ECL2) (Phe 268, Pro 269); while its naphthoyl group interacted primarily through hydrophobic interactions with helix 2 (Phe 170), helix 3 (Val 196), helix 6 (Trp 356), helix 7 (Leu 387, Cys 386) (see Figures 45 and 46). The binding mode of JWH-018 was supported by mutation studies on helix 6 (Trp 356) and 3 (Phe 189) and structure–activity relationship (SAR) studies of N-alkyl chain length (Mc Allister et al., 2003; Shim et al., 2006; Aung et al., 2000).

The aminoalkylindole derivative WIN-55,212-2 (2,3-dihydro-5-methyl-3((4-morpholinyl)methyl)pyrrolo(1,2,3,-de)-1,4-benzoxazin-6-yl)-1-naphthalenyl methanone) formed mainly pi-sulphur interactions with residues placed on the N-terminal group of the receptor (Cys 107, Met 109); and hydrophobic and van der Waals interactions with the helix 7 (Met 384, Phe 381) and helix 2 (Phe 170, 174) (see Figures 44 and 46). The binding mode of this ligand was supported by relationship (SAR) study of N-alkyl chain length (Mc Allister et al., 2003) and computational studies where Phe 170 and Phe 174 (helix 2) were described as interacting residues for WIN-55,212-2 binding (Hua et al., 2016).

The endocannabinoids anandamide (N-arachidonoyl-2-hydroxyethylamide) and 2-AG (2-Arachidonylglycerol), adopted a C-shaped conformation forming interactions with the N-terminal loop and the ECL2, with their long aliphatic tails interacting with the 2, 3, 5, 6, 7 helices (see Figures 45 and 46). These results were in line with those described by Hua et al. (2016) and were in accordance with mutation studies by which Tyr 275 is a key residue for anandamide and 2-AG binding (Mc Allister et al., 2003).

Δ9-THC (Δ9-tetrahydrocannabinol) and CP-55,940 (3-(2-hydroxy-4-(1,1-dimethylheptyl)phenyl)-4-(3-hydroxypropyl)cyclohexanol) had their rings placed between the N-terminal loop and the extracellular loop (ECL2) (Phe 268). Other interacting residues were mainly located in the 3, 6, 7 helices (Δ9-THC and CP-55,940) and in the helix 5 (CP-55940) and formed mostly hydrophobic interactions with the ligands (see Figures 45 and 46). These results were supported by those described by Hua et al. (2016) and were in accordance with mutation studies by which Tyr 275, Phe 189, Ser 383, Phe 268, were described as key residues for CP-55,940 binding (Shim et al., 2006), while Ser 383 was described crucial for Δ9-THC recognition (Shao et al., 2016).

In this analysis, the residues were re-numbered according to the alignment with the target protein. The ligand protein interaction diagrams of the agonists complexed with the CB_1 receptor homology model are in the Figure 45. The lists of interactions observed between agonists and the CB_1 receptor (Rattus Norvegicus) homology model are in the Figure 46.

Binding modes of representative CB_1 receptor antagonists

Referring to the CB_1 antagonists, AM-251 (1-(2,4-dichlorophenyl)-5-(4-iodophenyl)-4-methyl-N-piperidin-1-ylpyrazole-3-carboxamide) principally interacted with residues placed in the N-terminal loop, in the ECL2, and in the 2, 3, 6, 7 helices of the homology model.

In detail, the dichlorophenyl group interacted with the 2, 6, 7 helices and the N-terminal loop; the iodophenyl group formed interactions with 3, 6, 7 helices and ECL2; and the pyrazole ring mainly interacted with the N-terminal loop (see Figures 47 and 48). Since AM-251 is structurally very close to rimonabant, it showed interactions with some residues considered crucial for rimonabant binding recognition, including: Phe 379, Phe 170, Cys 386, Phe 174, Trp 356 (Mc Allister et al., 2003; Shim, 2010; Shim et al., 2012).

The antagonist rimonabant (5-(4-chlorophenyl)-1-(2,4-dichlorophenyl)-4-methyl-N-piperidin-1-ylpyrazole-3-carboxamide) shared several identical interacting residues with AM-251 and

principally interacted with amino acids placed in the N-terminal loop, ECL2, and in the 3, 6, 7 helices, mainly through hydrophobic interactions. In detail, the chlorophenyl groups formed interaction with the 3, 6, 7 helices and ECL2, while the pyrazole ring mainly interacted with the N-terminal loop (see Figure 47 and 48). Consistent with mutation studies, rimonabant showed interactions with residues considered crucial for binding recognition, including Leu 193, Phe 170, Cys 386 (Shim, 2010; Mc Allister et al., 2003). Additionally, these results were in line with those described by Hua et al. (2016) by which Cys 386, Val 196, Phe 170, Phe 174, Trp 356, Leu 359, Ser 383 and Phe 268 directly interacted with rimonabant.

The antagonists otenabant (1-[8-(2-chlorophenyl)-9-(4-chlorophenyl)purin-6-yl]-4-(ethylamino)piperidine-4-carboxamide) and taranabant (N-(3-(4-chlorophenyl)-2-(3-cyanophenyl)-1-methylpropyl)-2-methyl-2((5(trifluoromethyl)pyridin2yl)oxy)propenamide), showed interactions with some residues considered crucial for rimonabant binding recognition (Shim, 2010; Mc Allister et al., 2003) and in line with those described by Hua et al. (2016), including Phe 268, Leu 359, Ser 383, Val 196, Trp 356, Phe 170, Phe 174, His 178 (otenabant interacting residues) and Cys 386, Val 196, Phe 170, Phe 174, Ser 383 (taranabant interacting residues) (see Figure 47 and 48).

The compound AM-6358 formed mainly hydrophobic interactions with the N-terminal loop, the ECL2 and the 2, 3, 5, 6, 7 helices; with the pyrazole ring interacting with the N-terminal, and the dichlorophenyl group mainly forming interactions with the 2 and 7 helices (see Figures 47 and 48). The interactions with Leu 387, Leu 359, Cys 386, Trp 356, Val 196, Gly 166, Ser 167, Phe 170, Phe 174, Ile 119, Met 384, Ile 105, Ser 383, Met 103, Phe 379, Phe 102, Phe 268, Leu 193, Thr 197 were in line with those described by Hua et al. (2016), and some of them were supported by previous studies by which mutagenesis of Phe170 and Phe 174 resulted in dramatically decreased functional affinity for AM-6538 (Mc Allister et al., 2003; Hua et al., 2016).

In this analysis, the residues were renumbered according to the alignment with the target protein. The ligand protein interaction diagrams of the antagonists complexed with the CB_1 receptor homology model are in the Figure 47. The lists of interactions observed between antagonists and the CB_1 receptor (Rattus Norvegicus) homology model are in the Figure 48.

6.12) Vina binding energies against experimental K_i values for representative CB_1 receptor agonists and antagonists

In our analysis, the lowest Vina binding energy (expressed in Kcal/mol) related to the best binding pose for each referent compound, was compared with the K_i value (expressed in nanomoles) obtained with experimental bioassay studies. The K_i value is reflective of the binding affinity and the smaller the K_i value, the greater the binding affinity of the compound; while the lowest the binding energy generated by the docking programme Vina, the higher the binding affinity.

As observed in the Table 3, there was no correlation between Vina binding energies and experimental K_i values (lower energies should be related to lower K_i values). The reasons for these inconsistencies could be related to the use of a homology model of the CB_1 receptor, characterised by some chemical and geometrical different features compared to the real CB_1 receptor, and to some limitations inherent to our docking approach.

First of all, the docking software Vina employs a simplified scoring function based on empirical free energies of binding with implicit hydrogens, no electrostatic contribution or atomic charges, to score poses more quickly; secondly, it reduces the conformational space search by employing a rigid model for the receptor which often leads to improper results. Additionally, it may be possible that scoring function needs to be optimized, especially for molecules containing fluorine or chlorine atoms, which may not be considered adequately (Forli et al., 2016). However, Vina docking software should perform sufficiently well for the prediction of bound complexes for drug-sized molecules, with errors on estimated energies around 2–3 Kcal/mol (Forli et al., 2016).

More advanced tools (such as molecular dynamics) with more sophisticated and computationally-intensive parameterizations of the system, are potentially needed to predict conformation and energy more accurately.

Referent compounds			
CB_1 receptor agonists			
Compounds	**Vina, binding energy (Kcal/mol)**	**Experimental K_i (nM)**	**Reference**
JWH-018	-8.7	9.0	Aung et al., 2000
ANANDAMIDE	-8.7	61.0	Lin et al., 1998
CP-55,940	-8.6	1.1	Melvin et al., 1993
2-AG	-8.3	45.0	Chen et al., 2008
WIN 55-212,2	-8.1	62.3	Felder et al., 1995
Δ9-THC	-7.7	41.0	Showalter et al., 1996
CB_1 receptor antagonists			
Compounds	**Vina, binding energy (Kcal/mol)**	**Experimental K_i (nM)**	**Reference**
AM-6358	-11.8	3.4	Hua et al., 2016
AM-251	-11.3	7.5	Südhof and Starke, 2007
RIMONABANT	-11.0	6.2	Soudijn et al., 2005
TARANABANT	-9.0	0.1	Shao et al., 2016
OTENABANT	-8.8	0.7	Hadcock et al., 2010

Table 3: Vina binding energies related to the best binding poses of representative CB_1R agonists and antagonists at the CB_1R homology model (Rattus Norvegicus) against experimental Ki values.

6.13) Conclusions of the docking approach validation

Overall, the outcomes generated by the docking programme Vina seemed to be sufficiently reliable in terms of ligand interactions, as most of the residues found to be involved in ligand binding were consistent with those considered crucial according to mutation studies and previous computational studies.

By contrast, in the light of the above-mentioned limitations of the docking approach, the binding energy values were approached with caution since no specific correlation between K_i values and binding energies was found.

The same methods were employed in the analysis of the binding interactions of the novel SCs BB-22, 5F-PB-22, 5F-AKB-48, STS-135 against the CB_1 receptor (Rattus Norvegicus) homology model. However, all the results were regarded as preliminary findings requiring further refinement and optimization with more sophisticated tools.

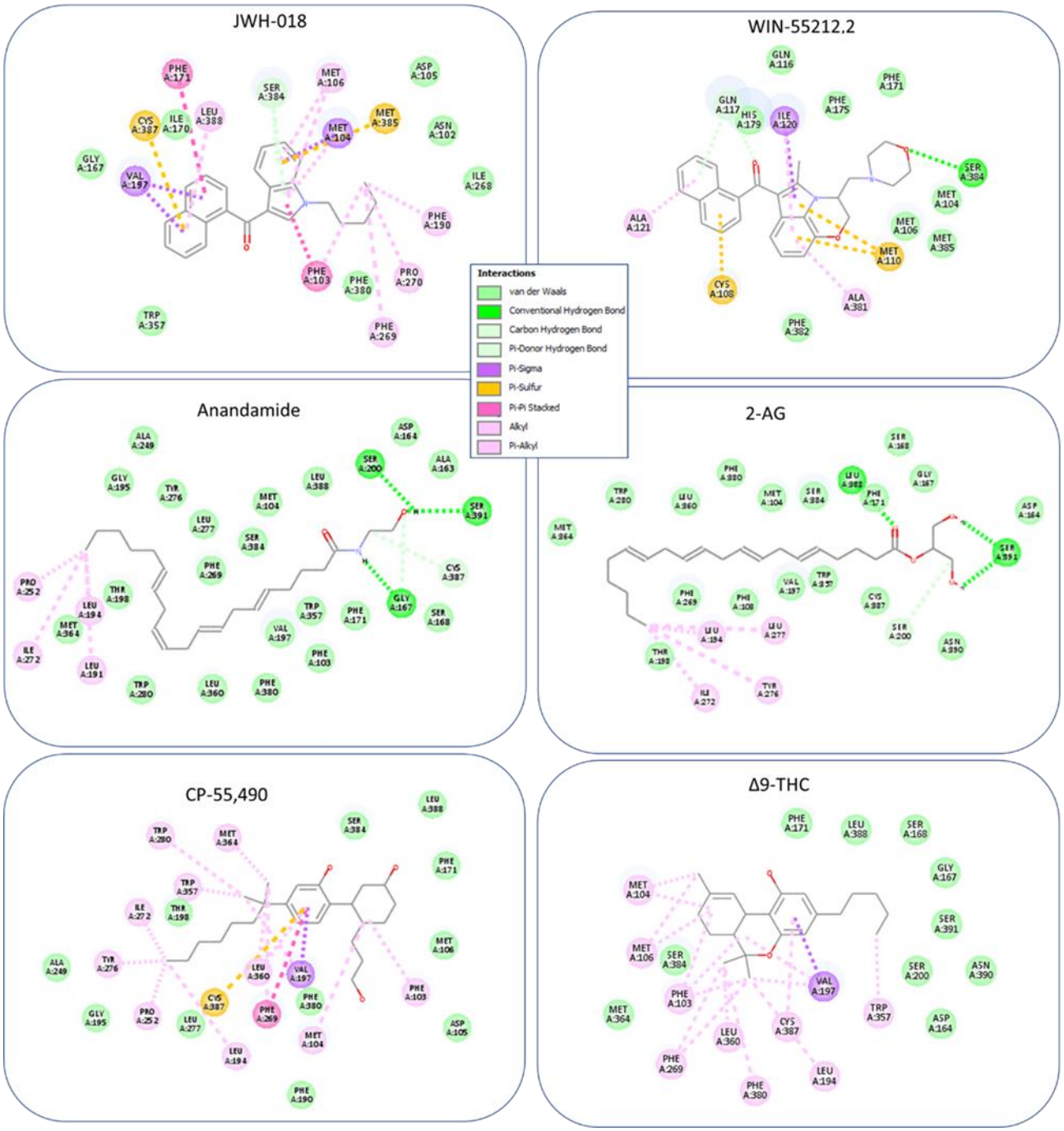

Figure 45: Ligand protein interaction diagrams of JWH-018, WIN-55,212-2, Anandamide, 2-AG, CP-55,940, Δ9-THC complexed with the CB_1R (Rattus Norvegicus) homology model. The complexes shown are the most favourable poses obtained using the molecular docking software Vina.

JWH-018		
Residues	Interactions	
After re-numbering	Type of interaction	Distance (Å)
SER 383	Pi-Donor Hydrogen Bond	3.46
MET 102	Pi-Sigma	3.82
VAL 196	Pi-Sigma	3.33
MET 384	Pi-Sulfur	5.42
CYS 386	Pi-Sulfur	5.61
PHE 170	Pi-Pi T-shaped	5.36
PHE 102	Pi-Pi T-shaped	5.03
PRO 269	Alkyl	4.82
PHE 102	Pi-Alkyl	5.07
PHE 189	Pi-Alkyl	4.79
PHE 268	Pi-Alkyl	5.36
MET 103	Pi-Alkyl	4.66
MET 105	Pi-Alkyl	5.11
LEU 387	Pi-Alkyl	5.48
Van der Waals interactions		
GLY 166, ILE 169, ASP 104, ASN 101, ILE 267, PHE 379, TRP 356		

2-AG		
Residues	Interactions	
After re-numbering	Type of interaction	Distance (Å)
LEU 387	Conventional Hydrogen Bond	3.10
SER 390	Conventional Hydrogen Bond	1.96
SER 199	Carbon Hydrogen Bond	3.55
LEU 193	Alkyl	4.09
ILE 271	Alkyl	4.05
LEU 276	Alkyl	5.13
TYR 275	Pi-Alkyl	5.18
Van der Waals interactions		
MET 363, TRP 279, LEU 359, PHE 379, MET 103, SER 383, SER 167, PHE 170, GLY 166, ASP 163, ASN 389, CYS 386, TRP 356, VAL 196, PHE 107, PHE 268, THR 197		

CP-55940		
Residues	Interactions	
After re-numbering	Type of interaction	Distance (Å)
VAL 196	Pi-Sigma	3.52
VAL 196	Alkyl	5.19
CYS 386	Pi-Sulfur	5.84
PHE 268	Pi-Pi Stacked	5.13
PHE 268	Pi-Alkyl	5.40
MET 103	Alkyl	5.19
LEU 359	Alkyl	4.41
MET 363	Alkyl	4.58
LEU 193	Alkyl	4.42
PRO 251	Alkyl	4.17
ILE 271	Alkyl	5.34
PHE 102	Pi-Alkyl	4.71
TYR 275	Pi-Alkyl	4.82
TRP 279	Pi-Alkyl	5.26
TRP 356	Pi-Alkyl	4.89
Van der Waals interactions		
ALA 248, THR 197, SER 383, PHE 170, MET 105, ASP 104, PHE 379, PHE 189, LEU 276, GLY 194, ALA 248		

WIN 55-212,2		
Residues	Interactions	
After re-numbering	Type of interaction	Distance (Å)
SER383	Conventional Hydrogen Bond	3.08
GLN116	Carbon Hydrogen Bond	3.11
GLN116	Pi-Donor Hydrogen Bond	4.05
ILE 119	Pi-Sigma	3.61
CYS 107	Pi-Sulfur	5.22
MET 109	Pi-Sulfur	5.09
ILE 119	Pi-Alkyl	4.56
ALA 380	Pi-Alkyl	5.05
ALA 120	Pi-Alkyl	5.33
Van der Waals interactions		
GLN 115, HIS 178, PHE 174, PHE 170, MET 103, MET 105, MET 384, PHE 381		

Anandamide		
Residues	Interactions	
After re-numbering	Type of interaction	Distance (Å)
SER 390	Conventional Hydrogen Bond	2.80
GLY 166	Conventional Hydrogen Bond	2.49
GLY 166	Carbon Hydrogen Bond	3.17
SER 199	Conventional Hydrogen Bond	2.15
CYS 386	Carbon Hydrogen Bond	3.64
LEU 190	Alkyl	4.31
LEU 193	Alkyl	3.95
PRO 251	Alkyl	4.39
ILE 271	Alkyl	5.29
Van der Waals interactions		
GLY 194, ALA 248, TYR 275, LEU 276, PHE 268, SER 383, MET 103, LEU 387, ASP 163, ALA 162, SER 167, PHE 170, TRP 356, VAL 196, PHE 102, PHE 379, LEU 359, TRP 279, THR 197, MET 363		

Δ9-THC		
Residues	Interactions	
After re-numbering	Type of interaction	Distance (Å)
VAL196	Pi-Sigma	3.67
VAL 196	Alkyl	4.12
MET 103	Alkyl	3.46
MET 105	Alkyl	4.04
LEU 193	Alkyl	5.04
LEU 359	Alkyl	4.02
PHE 102	Pi-Alkyl	5.01
PHE 268	Pi-Alkyl	4.48
TRP 356	Pi-Alkyl	4.57
PHE 379	Pi-Alkyl	4.85
CYS 386	Pi-Alkyl	4.95
Van der Waals interactions		
PHE 170, LEU 387, SER 167, GLY 166, SER 390, ASN 389, SER 199, ASP 163, MET 363, SER 383		

Figure 46: Lists of interactions observed between JWH-018, WIN-55,212-2, 2-AG, Anandamide, CP-55,940, Δ9-THC and the CB_1R (Rattus Norvegicus) homology model and obtained using the molecular docking software Vina.

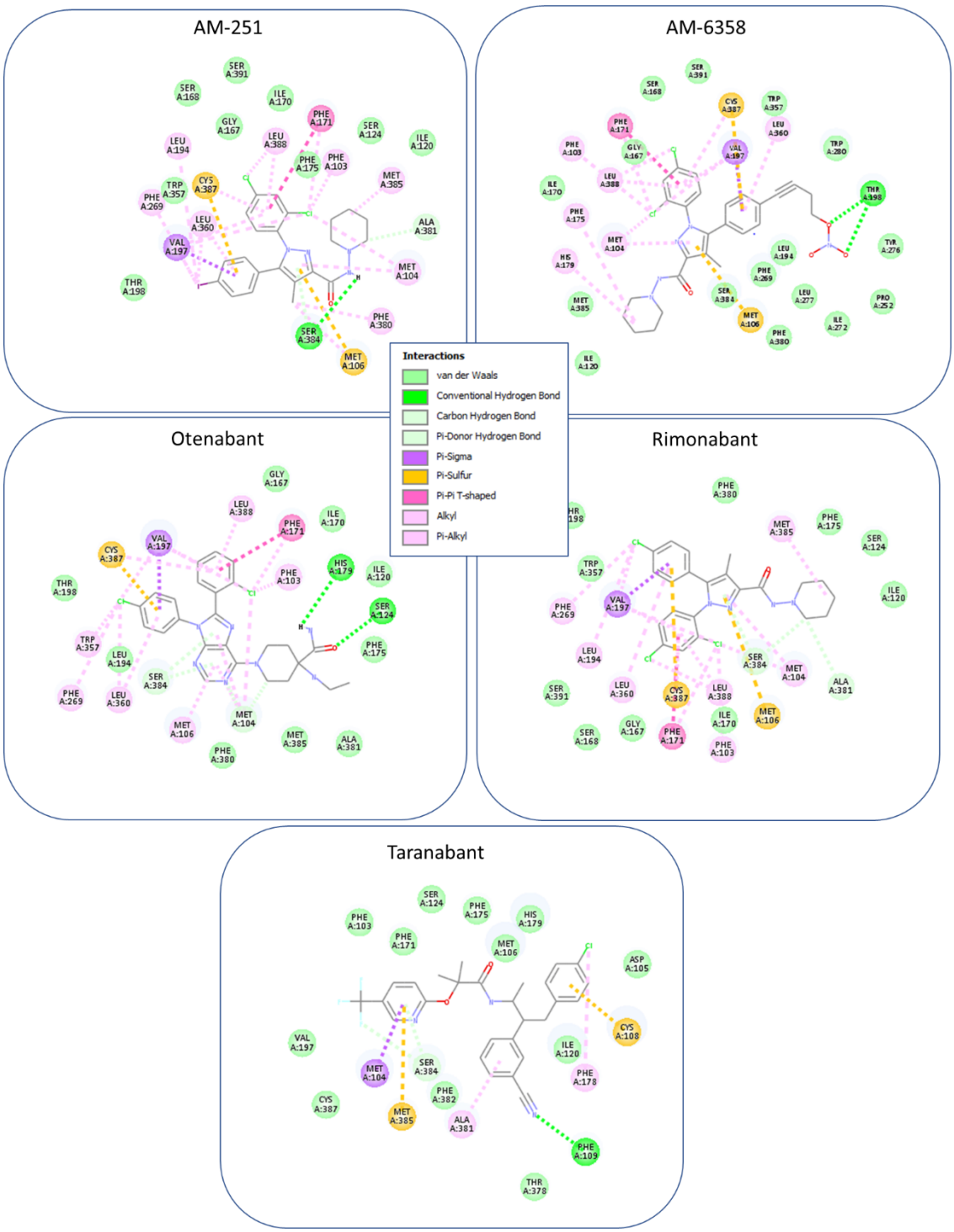

Figure 47: Ligand protein interaction diagrams of AM-251, AM-6358, Otenabant, rimonabant, taranabant complexed with the CB_1R (Rattus Norvegicus) homology model. The complexes shown are the most favourable poses obtained using the molecular docking software Vina.

AM-251		
Residues	Interactions	
After re-numbering	Type of interaction	Distance (Å)
ALA 380	Carbon Hydrogen Bond	3.31
CYS 386	Pi-Sulfur	5.82
CYS 386	Pi-Alkyl	5.34
LEU 193	Alkyl	5.40
LEU 359	Alkyl	5.26
LEU 359	Pi-Alkyl	5.21
LEU 387	Alkyl	5.17
LEU 387	Pi-Alkyl	5.17
MET 103	Alkyl	5.10
MET 103	Pi-Alkyl	4.99
MET 105	Pi-Sulfur	5.76
MET 105	Alkyl	4.78
MET 384	Alkyl	4.76
PHE 102	Pi-Alkyl	4.86
PHE 170	Pi-Alkyl	5.01
PHE 170	Pi-Pi T-shaped	5.32
PHE 268	Pi-Alkyl	5.07
PHE 379	Pi-Alkyl	4.85
SER 383	Conventional Hydrogen Bond	3.01
SER 383	Pi-Donor Hydrogen Bond	3.87
VAL 196	Pi-Sigma	3.67
VAL 196	Alkyl	4.27
VAL 196	Pi-Alkyl	4.47
Van der Waals interactions		
SER 167, SER 390, GLY 166, ILE 169, PHE 174, SER 123, ILE 119, THR 197, TRP 356		

Rimonabant		
Residues	Interactions	
After re-numbering	Type of interaction	Distance (Å)
SER 383	Carbon Hydrogen Bond	3.74
SER 383	Pi-Donor Hydrogen Bond	3.97
VAL 196	Pi-Sigma	3.64
MET 105	Pi-Sulfur	5.79
CYS 386	Pi-Sulfur	5.98
PHE 169	Pi-Pi T-shaped	5.37
MET 384	Alkyl	4.63
LEU 193	Alkyl	5.02
VAL 196	Alkyl	5.01
LEU 387	Alkyl	4.98
MET 103	Alkyl	5.25
VAL 196	Alkyl	4.15
PHE 102	Pi-Alkyl	4.88
PHE 170	Pi-Alkyl	5.10
PHE 268	Pi-Alkyl	4.85
MET 103	Pi-Alkyl	5.02
LEU 359	Pi-Alkyl	5.30
VAL 196	Pi-Alkyl	4.40
CYS 386	Pi-Alkyl	5.35
LEU 387	Pi-Alkyl	5.24
Van der Waals interactions		
THR 197, PHE 379, PHE 174, SER 123, ILE 119, ILE 169, GLY 166, SER 167, SER 390, TRP 356		

AM-6358		
Residues	Interactions	
After re-numbering	Type of interaction	Distance (Å)
CYS 386	Pi-Sulfur	5.80
CYS 386	Pi-Alkyl	5.39
HIS 178	Pi-Alkyl	5.27
LEU 359	Pi-Alkyl	5.12
LEU 387	Alkyl	4.71
LEU 387	Pi-Alkyl	5.11
MET 103	Alkyl	5.15
MET 103	Pi-Alkyl	5.07
MET 105	Pi-Sulfur	5.81
PHE 102	Pi-Alkyl	4.88
PHE 170	Pi-Pi T-shaped	5.25
PHE 170	Pi-Alkyl	5.03
PHE 174	Pi-Alkyl	5.42
THR 197	Conventional Hydrogen Bond	2.99
VAL 196	Pi-Sigma	3.59
VAL 196	Alkyl	4.24
VAL 196	Pi-Alkyl	4.51
Van der Waals interactions		
ILE 119, MET 384, ILE 169, GLY 166, SER 167, SER 390, TRP 356, TRP 279, TYR 275, PRO 251 ILE 271, LEU 276, LEU 193, PHE 268, PHE 379, SER 383		

Otenabant		
Residues	Interactions	
After re-numbering	Type of interaction	Distance (Å)
CYS 386	Pi-Sulfur	5.75
CYS 386	Pi-Alkyl	5.46
HIS 178	Conventional Hydrogen Bond	3.04
LEU 359	Alkyl	5.30
LEU 359	Pi-Alkyl	5.22
LEU 387	Pi-Alkyl	5.04
MET 103	Carbon Hydrogen Bond	3.70
MET 103	Alkyl	5.01
MET 103	Pi-Alkyl	4.67
MET 105	Pi-Alkyl	4.55
PHE 102	Pi-Alkyl	4.70
PHE 170	Pi-Pi T-shaped	5.10
PHE 170	Pi-Alkyl	5.12
PHE 268	Pi-Alkyl	5.48
SER 123	Conventional Hydrogen Bond	2.66
SER 383	Pi-Donor Hydrogen Bond	3.78
TRP 356	Pi-Alkyl	5.20
VAL 196	Pi-Sigma	3.44
VAL 196	Alkyl	4.26
VAL 196	Pi-Alkyl	4.62
Van der Waals interactions		
THR197, GLY 166, ILE 169, ILE 119, PHE 174, ALA 380, MET 384, PHE 379, LEU 193		

Taranabant		
Residues	Interactions	
After re-numbering	Type of interaction	Distance (Å)
PHE 108	Conventional Hydrogen Bond	3.16
SER 383	Carbon Hydrogen Bond	3.47
SER 383	Pi-Donor Hydrogen Bond	3.31
MET 103	Pi-Sigma	3.84
CYS 107	Pi-Sulfur	4.49
MET 384	Pi-Sulfur	4.93
PHE 177	Pi-Alkyl	5.13
ALA 380	Pi-Alkyl	4.42
Van der Waals interactions		
VAL 196, PHE 102, PHE 170, SER 123, PHE 174, MET 105, HIS 178, ASP 104, ILE 119, THR 377, PHE 381, CYS 386		

Figure 48: Lists of interactions observed between AM-251, AM-6358, otenabant, rimonabant, taranabant and the CB_1 receptor (Rattus Norvegicus) homology model obtained using the molecular docking software Vina.

6.14) Docking of a range of novel synthetic cannabinoids against the CB_1 receptor (Rattus Norvegicus) homology model: methods

In this analysis, the key binding interactions of a range of novel SCs (BB-22, 5F-PB-22, 5F-AKB-48, STS-135) against the homology model of the rodent CB_1 receptor were analysed. The methods used were the same applied with the referent compounds. In detail, PyRx 0.9.4 was used as virtual screening software and the docking programme employed was Vina. Search space coordinates used in our study were established according to previous experimental studies and were as follows: centre, X:41, Y:29, Z:317; dimensions, X: 25 Å, Y: 25 Å, Z: 25 Å. Overall, eight binding modes for each ligand were generated and the pose with the lowest binding energy (expressed in Kcal/mol) was selected to study the key binding interactions.
A comparative analysis of the relevant ligand binding interactions described in CB_1 receptor mutation studies and those found with our computational docking approach, was undertaken. The computational findings were then compared with the experimental ones and possible consistencies were highlighted to support our docking approach.

6.15) Docking of the novel synthetic cannabinoids against the CB_1 receptor (Rattus Norvegicus) homology model: results

According to Vina docking outcomes, the novel aminoalkylindole derivatives under study (BB-22, 5F-PB-22, 5F-AKB-48, STS-135) shared some identical interacting residues including: Leu 359 (helix 6), Met 103 (N-terminal loop), Phe 102 (N-terminal loop), Phe 170 (helix 2), Phe 268 (extracellular loop), Phe 379 (helix 7), Ser 383 (helix 7), Val 196 (helix 3). This evidence demonstrated that all novel SCs act at the level of the same binding pocket, showing mainly hydrophobic interactions with the 2, 3, 6, 7 helices, the ECL2 and the N-terminal loop (see Figures 49 and 50).

In detail, the indole group of BB-22 formed hydrogen bond and hydrophobic interactions with residues placed on the N-terminal loop; its cyclohexyl methyl group interacted through alkyl interactions with the 2, 3, 7 helices; while its quinolinyl group formed mostly hydrophobic interactions with ECL2 and with the N-terminal loop (see Figures 47 and 48).

On the other hand, the indole group of 5F-PB-22 interacted with the N-terminal loop through hydrogen bond and hydrophobic interactions; its fluorinated pentyl tail interacted with the 3, 5 and 6 helices; while its quinolinyl group formed hydrophobic interactions with helix 2 and the N-terminal loop (see Figures 49 and 50).

When complexed with the homology model, 5F-AKB-48 and STS-135 presented almost identical binding poses. In detail, their indazole and indole groups respectively, formed mainly hydrophobic interactions with the N-terminal group of the receptor and the helix 3; their fluorinated pentyl tail interacted mainly through alkyl interactions with the helix 6 and through van der Waals interactions with helix 7; while their adamantyl groups mostly formed alkyl interactions with the 3, 5 and 6 helices (see Figures 49 and 50).

Notably, some of the novel aminoalkylindole derivatives under study, interacted with residues that, according to mutation studies, were considered crucial for aminoalkylindole binding recognition (Mc Allister et al., 2003; Shim et al., 2006). Among them, Phe 200 (helix 3) interacted with 5F-PB-22 (pi-alkyl interaction); Trp 279 (helix 5) interacted with 5F-AKB-48, 5F-PB-22, STS-135 (pi-alkyl interactions); Trp 356 (helix 6) interacted with 5F-AKB-48, 5F-PB-22, STS-135 (pi-alkyl interactions) (see Figures 49 and 50).

Interestingly, all novel SCs under study, showed interactions with residues considered crucial for rimonabant binding recognition (Mc Allister et al., 2003, Shim et al., 2012). Specifically, BB-22 interacted with Phe 170 (helix 2), Phe 189 (helix 3), Phe 379, Cys 386 (helix 7); 5F-PB-22 interacted with Phe 170 (helix 2); Phe 189, Thr 197 and Phe 200 (helix 3); Trp 279 (helix 5), Trp 356 (helix 6), Phe 379 (helix 7); 5F-AKB-48 and STS-135 formed interactions with Phe 170, Thr 197, Leu 193, Trp 279, Trp 356, Phe 379, Cys 386.

In this analysis, the residues were renumbered according to the alignment with the target protein. The ligand protein interaction diagrams of the novel SCs complexed with the CB_1 receptor homology model are in the Figure 49. The lists of interactions observed between the novel SCs and the CB_1 receptor (Rattus Norvegicus) homology model are in Figure 50.

6.16) Vina binding energies against experimental K_i values for each third generation SC under study

According to the results generated by the Vina docking programme, BB-22 showed the lowest binding energy (-9.6 Kcal/mol) compared to the other novel compounds under study, while no relevant differences were observed among 5F-PB-22, 5F-AKB-48, STS-135 (see Table 4). These findings were partially supported by those obtained with experimental competition binding assay studies, by which BB-22 and 5F-PB-22 exhibited higher binding affinities compared to 5F-AKB-48 and STS-135. However, the experimental rank of order of CB_1 receptor affinity (BB-22, K_i 0.11) = (5F-PB-22, K_i 0.13)> (5F-AKB-48, K_i 0.87)> (STS-135, K_i 1.93) (De Luca et al., 2016), did not fully correlate with our computational findings (BB-

22, -9.6 Kcal/mol) > STS-135 (-9.0 Kcal/mol) ≃ 5F-PB-22 (-8.8 Kcal/mol) = 5F-AKB-48 (-8.8 Kcal/mol) (see Table 4).

Third generation synthetic cannabinoids		
Compounds	Vina, binding energy (Kcal/mol)	Experimental Ki (nM)
BB-22	-9.6	0.11
5F-PB-22	-8.8	0.13
5F-AKB-48	-8.8	0.87
STS-135	-9.0	1.93

Table 4: Vina binding energies related to the best binding poses of BB-22, 5F-PB-22, 5F-AKB-48, STS-135 at the CB_1R homology model (Rattus Norvegicus) against experimental K_i values.

The lack of correlation between Vina binding energies and experimental K_i values (lower energies should be related to lower K_i values) could be potentially related to:

- some different chemical, geometrical and three-dimensional features inherent to the homology model compared to the real CB_1 receptor;
- some limitations inherent to our docking approach (potential inability of the docking programme to detect small differences in terms of binding affinity; simplified scoring function, rigid model of the receptor, potential errors on estimated energies around 2–3 Kcal/mol, molecules containing atomic charges which may not be considered satisfactorily) (Forli et al., 2016) (see Chapter 6; Paragraph 12 for details).

Overall, the problem of predicting the affinity that a compound has for a protein is a challenging one in docking studies. The issue could have been potentially overcome employing a consensus scoring method (which is a more accurate method whereby the binding affinities are predicted by combining the results of several different scoring algorithms) (Houston and Walkinshaw, 2013), or by using more advanced tools (such as molecular dynamics) with more sophisticated parameterizations of the system (Forli et al., 2016).

Alternatively, we decided to perform further docking studies against the crystal structure of the human CB_1 receptor (made recently available in the protein data bank) and more accurate results were expected compared to those obtained with the CB_1R homology model. An additional comparative analysis of the outcomes produced by different docking software

packages (Vina and Autodock 4.0) was undertaken, and the more consistent the results given by these software packages, the higher the reliability of their outcomes.

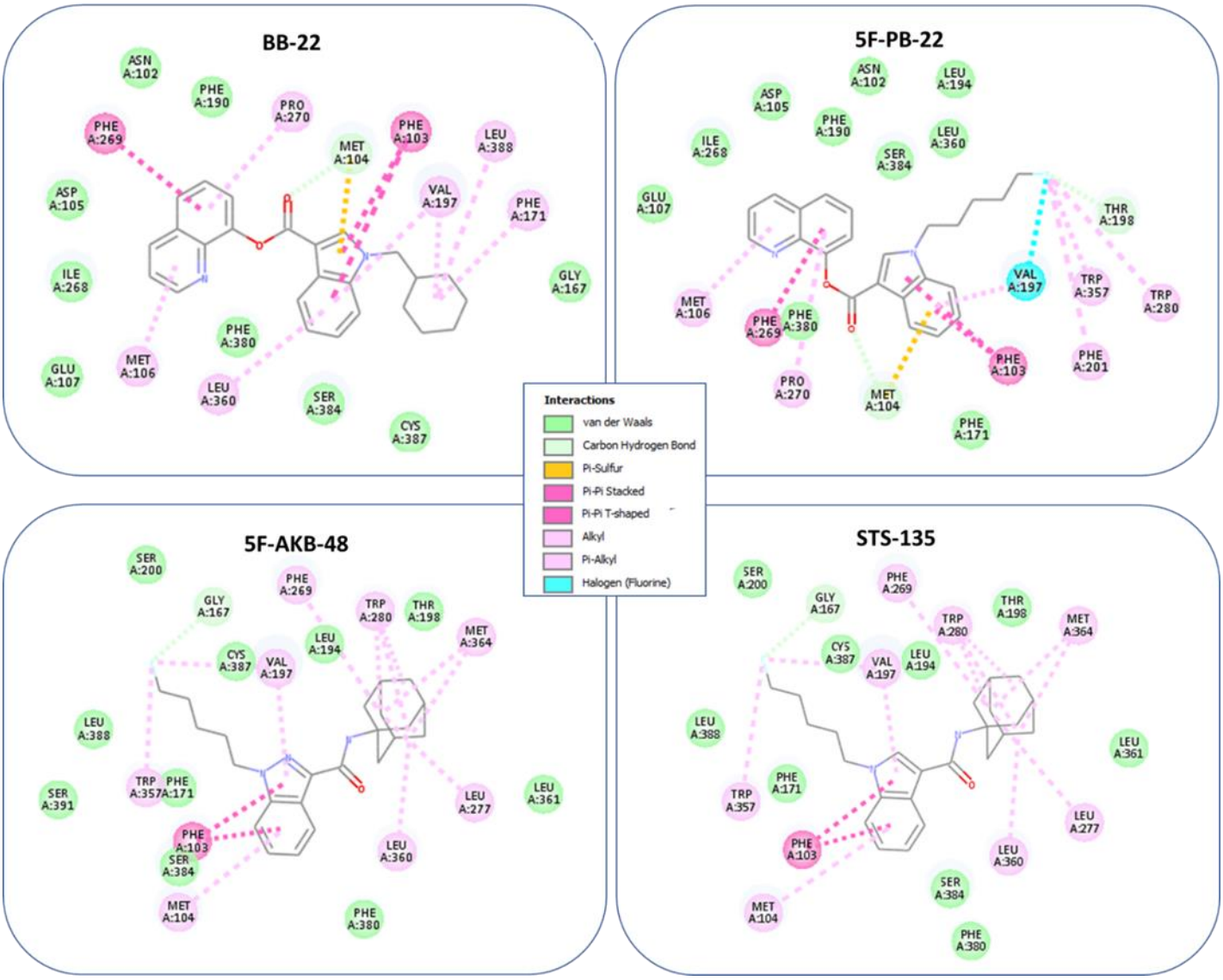

Figure 49: Ligand protein interaction diagrams of BB-22, 5F-PB-22, 5F-AKB-48, STS-135 complexed with the CB_1R (Rattus Norvegicus) homology model. The complexes shown are the most favourable poses obtained using the molecular docking software Vina.

BB-22		
Residues	Interactions	
After re-numbering	Type of interaction	Distance (Å)
MET 103	Carbon Hydrogen Bond	3.10
MET 103	Pi-Sulfur	6.00
PHE 102	Pi-Pi Stacked	4.51
PHE 268	Pi-Pi T-shaped	5.18
LEU 387	Alkyl	5.05
VAL 196	Alkyl	4.51
VAL 196	Pi-Alkyl	5.31
PHE 170	Pi-Alkyl	5.04
LEU 359	Pi-Alkyl	5.28
PRO 269	Pi-Alkyl	5.32
MET 105	Pi-Alkyl	4.91
Van der Waals interactions		
ASP 104, ASN 101, PHE 189, GLY 166, CYS 386, SER 383, PHE 379, GLU 106, ILE 268		

5F-AKB-48		
Residues	Interactions	
After re-numbering	Type of interaction	Distance (Å)
GLY 166	Carbon Hydrogen Bond;Halogen	3.52
PHE102	Pi-Pi Stacked	4.31
LEU 276	Alkyl	5.40
MET 363	Alkyl	4.15
LEU 359	Alkyl	4.59
VAL 196	Alkyl	3.91
VAL 196	Pi-Alkyl	4.27
PHE 268	Pi-Alkyl	4.67
TRP 279	Pi-Alkyl	4.50
TRP 356	Pi-Alkyl	4.89
MET 103	Pi-Alkyl	5.35
Van der Waals interactions		
SER 199, CYS 386, LEU 193, THR 197, LEU 360, PHE 379, SER 383, PHE 170, SER 390, LEU 387		

5F-PB-22		
Residues	Interactions	
After re-numbering	Type of interaction	Distance (Å)
MET 103	Pi-Sulfur	5.80
MET 103	Carbon Hydrogen Bond	3.38
THR 197	Carbon Hydrogen Bond;Halogen	3.25
VAL 196	Halogen (Fluorine)	3.67
PHE 102	Pi-Pi Stacked	4.60
PHE 102	Pi-Pi Stacked	4.94
PHE 268	Pi-Pi T-shaped	5.21
PHE 200	Pi-Alkyl	5.15
TRP 279	Pi-Alkyl	5.26
TRP 279	Pi-Alkyl	4.54
TRP 356	Pi-Alkyl	4.36
VAL 196	Pi-Alkyl	4.63
PRO 269	Pi-Alkyl	5.27
MET 105	Pi-Alkyl	4.89
Van der Waals interactions		
GLU 106, ILE 267, ASP 104, PHE 189, ASN 101, SER 383, LEU 359, LEU 193, PHE 170, PHE 379		

STS-135		
Residues	Interactions	
After re-numbering	Type of interaction	Distance (Å)
GLY 166	Carbon Hydrogen Bond;Halogen	3.40
PHE 102	Pi-Pi Stacked	4.32
LEU 276	Alkyl	5.35
MET 363	Alkyl	4.14
LEU 359	Alkyl	4.62
VAL 196	Alkyl	3.93
VAL 196	Pi-Alkyl	4.24
PHE 268	Pi-Alkyl	4.71
TRP 279	Pi-Alkyl	4.44
TRP 356	Pi-Alkyl	5.09
MET 103	Pi-Alkyl	5.35
Van der Waals interactions		
SER 199, CYS 386, LEU 193, THR 197, LEU 360, PHE 379, SER 383, PHE 170, LEU 387		

Figure 50: Lists of interactions observed between BB-22, 5F-PB-22, 5F-AKB-48, STS-135 and the CB_1R (Rattus Norvegicus) homology model obtained using the molecular docking software Vina.

6.17) Docking of representative CB_1R agonists and antagonists against the crystal structure of the human CB_1 receptor: approach validation

Methods

The crystal structure of the human CB_1 receptor (452 amino acids, 2.0 Angstroms of resolution) was retrieved from the Protein Data Bank (ID:5TGZ) and then underwent some refinement operations, while ligands were prepared to create 3D geometries which were optimised prior to virtual screening. The quality of the receptor structure employed plays a crucial role in determining reliable docking outcomes. In general, the higher the resolution of the crystal structure, the more reliable the docking results obtained (Mohan et al., 2005). The protein was prepared using the protein preparation wizard tool in Maestro 10.4. During this process, all hydrogens were displayed and optimized for pH=7; water molecules were deleted, issues associated with the workspace structure were fixed and bound ligands were removed. After optimization, the PDB file was converted into a format (.pdbqt) suitable for docking in the virtual screening PyRx 0.9.4.

The preparation phase of the ligands was the same described in the Chapter 6, Paragraph 9. After preparation, each ligand was converted into a .pdbqt file format suitable for docking. PyRx 0.9.4 was used as virtual screening software and Autodock Vina and Autodock 4.0 were the docking programs employed. Vina's search space coordinates were set as follows: centre, X:41, Y:29, Z:317; dimensions X: 25 Å, Y: 25 Å, Z: 25 Å. Overall, eight binding modes for each ligand were generated and the pose with the lowest binding energy (expressed in Kcal/mol) was selected to study the relevant key binding interactions. In Autodock 4.0, the search space coordinates used were the following: centre, X:41, Y:29, Z:317; number of points X: 184, Y: 230, Z: 294, spacing: 0.12 Å. For each pose the estimated free energy of binding resulted from the total interaction energy (intermolecular energy, internal energy, torsional energy, unbound energy) was calculated. In total, ten binding modes for each ligand were generated and the pose with the lowest estimated free energy of binding (expressed in Kcal/mol) was selected to study the relevant key binding interactions.

The key binding interactions of the same referent compounds used in our homology modelling studies were analysed against the crystal structure of the human CB_1 receptor (5TGZ).

6.18) Docking of representative CB_1R agonists and antagonists against the crystal structure of the human CB_1 receptor: results and discussion

Binding modes of representative CB_1 receptor agonists

Overall, Vina and Autodock 4.0 results were highly consistent for all referent compounds tested. In detail, according to both software docking programs, the indole group of the aminoalkylindole derivative JWH-018 (1-pentyl-3-(1-naphthoyl)indole) showed mainly hydrophobic and van der Waals interactions with residues placed on the N-terminal group of the protein (Ile 105, Met 103) and sulphur interactions with the helix 7 (met 384); its pentyl tail formed mostly alkyl interactions with residues located on the helix 3 (Phe 189) and on the second extracellular loop (ECL2) (Pro 269); while its naphthoyl group interacted primarily through hydrophobic interactions with the helix 2 and 3 (Phe 170, Val 196); van der Waals interactions with the helix 6 (Trp 356) and sulphur interactions with the helix 7 (Cys 386) (see Figures 51, 52, 53 and 54). The binding modes of JWH-018 obtained with both docking programs, were supported by mutation studies on helices 6 (Trp 356) and 3 (Phe 189) and structure–activity relationship (SAR) study of N-alkyl chain length (Mc Allister et al., 2003; Shim et al., 2006; Aung et al., 2000).

The aminoalkylindole derivative WIN-55,212-2 (2,3-dihydro-5-methyl-3((4-morpholinyl)methyl)pyrrolo(1,2,3,-de)-1,4-benzoxazin-6-yl)-1-naphthalenyl methanone) mainly formed interactions with residues placed on the N-terminal group of the receptor (Met 103, Ile/Met 105); and interactions with the helix 7 (Ser 383) and helix 2 (Phe 170) (Vina and Autodock 4.0 outcomes). Additionally, according to Autodock 4.0 findings, WIN-55,212-2 interacted with Phe 268 (ECL2) Trp 356 (helix 6), Phe 379 (helix 7), through hydrophobic interactions; while according to Vina outcomes, it interacted with Phe 174 (helix 2) as well (see Figures 51, 52, 53 and 54).The binding modes of this ligand were supported by relationship (SAR) study of N-alkyl chain length; mutation studies by which Trp 356 was described as a key residue for WIN-55,212-2 binding recognition (Mc Allister et al., 2003; Aung et al., 2000); and molecular modelling studies by which Phe 170, Phe 174 (helix 2) and Phe 379 (helix 7) were described as interacting residues for WIN-55,212-2 binding (Hua et al., 2016).

The agonists anandamide (N-arachidonoyl-2-hydroxyethylamide) and 2-AG (2-Arachidonylglycerol) formed interactions with the N-terminal group and the extracellular loop ECL2, and their long aliphatic tails interacted with the 3, 5, 6 and 7 helices (see Figures 51, 52, 53 and 54). These results were in line with those described by Hua et al. (2016) and were in accordance with mutation studies by which Tyr 275 (consistent with Vina and Autodock 4.0

outcomes) and Phe 189 (consistent with Autodock 4.0 outcome) were key residues for anandamide binding (Mc Allister et al., 2003).

Δ9-THC (Δ9-Tetrahydrocannabinol) and CP-55,940 (3-(2-hydroxy-4-(1,1-dimethylheptyl)phenyl)-4-(3-hydroxypropyl)cyclohexanol) had their rings placed between the N-terminal loop and the extracellular loop (ECL2) (Phe 268). Other interacting residues were mainly located in the 3, 6, 7 helices (Δ9-THC and CP-55,940) and in the helix 5 (CP-55940) and formed mostly hydrophobic interactions with these ligands (see Figures 51, 52, 53 and 54). These results were supported by those described by Hua et al. (2016) and were in accordance with mutation studies by which Phe 189, Ser 383, Phe 268 (consistent with Vina and Autodock 4.0 outcomes) and Ile 271, Tyr 275 (in line with Vina outcomes) were described as key residues for CP-55,940 binding; while Ser 383, Phe 174 (consistent with Vina and Autodock 4.0 outcomes) and Leu 193 (in line with Autodock 4.0 outcome) were reported to be crucial residues for Δ9-THC binding recognition (Shim et al., 2006; Shao et al., 2016).

The ligand protein interaction diagrams of the agonists complexed with the crystal structure of the CB_1 receptor obtained using the molecular docking software Vina and Autodock 4.0 are in the Figures 51 and 53 respectively. The lists of interactions observed between agonists and the CB_1 receptor (crystal structure) obtained using the molecular docking software Vina and Autodock 4.0, are in the Figures 52 and 54 respectively.

Binding modes of representative CB_1 receptor antagonists

As regards to the CB_1R antagonists, AM-251 (1-(2,4-dichlorophenyl)-5-(4-iodophenyl)-4-methyl-N-piperidin-1-ylpyrazole-3-carboxamide) principally interacted with residues placed in the N-terminal loop, in the ECL2, and in the 2, 3, 6, 7 helices. As expected, it showed interactions with some residues considered crucial for rimonabant binding recognition, including: Leu 193, Phe 379, Phe 170, Trp 356, Cys 386 (Vina and Autodock 4.0 outcomes) and Phe 189, Trp 279, Thr 197 (Autodock 4.0 outcomes) (see Figures 55, 56, 57, and 58).

The antagonist rimonabant (5-(4-chlorophenyl)-1-(2,4-dichlorophenyl)-4-methyl-N-piperidin-1-ylpyrazole-3-carboxamide) shared similar interacting residues with AM-251 and principally interacted with residues placed in the N-terminal loop, ECL2, and in the 2, 3, 6, 7 helices, forming mainly hydrophobic interactions. Consistent with mutation studies (Shim, 2010; Mc Allister et al., 2003), rimonabant showed interactions with residues considered crucial for rimonabant binding recognition, including Leu 193, Phe 379, Phe 170, Cys 386 (Vina and

Autodock 4.0 outcomes) and Phe 189, Trp 279 (Autodock 4.0 outcomes) (see Figures 55, 56, 57, and 58). Additionally, these results were in line with those described by Hua et al. (2016) by which Phe 268, Leu 359, Cys 386, Trp 356, Val 196, Ser 383, Phe 170, directly interacted with rimonabant.

The antagonist otenabant (1-[8-(2-chlorophenyl)-9-(4-chlorophenyl)purin-6-yl]-4-(ethylamino)piperidine-4-carboxamide) interacted with the same residues described by Hua et al. (2016), including Phe 268, Leu 359, Cys 386, Trp 356, Val 196, Ser 383, Phe 170, Phe 174, His 178, and it showed interactions with some residues considered crucial for rimonabant binding recognition (Vina and Autodock 4.0 outcomes) (Mc Allister et al., 2003; Shim et al., 2012) (see Figures see Figures 55, 56, 57, and 58).

Similarly to otenabant, the antagonist taranabant (N-(3-(4-chlorophenyl)-2-(3-cyanophenyl)-1-methylpropyl)-2-methyl-2((5(trifluoromethyl)pyridin2yl)oxy)propenamide) showed interactions with some residues considered crucial for rimonabant binding recognition (Shim, 2010; Mc Allister et al., 2003) and in line with those described by Hua et al. (2016) including Phe 268, Leu 359, Cys 386, Trp 356, Val 196, Ser 383, Phe 170, Phe 174, His 178 (Vina outcomes) and Phe 170, Phe 174, His 178 (Autodock 4.0 outcomes) (see Figures 55, 56, 57, and 58).

The antagonist AM-6358 formed mainly hydrophobic interactions with the N-terminal loop, the ECL2 and the 2, 3, 6, 7 helices. In detail, several interacting residues were in line with those described by Hua et al. (2016), and included: Leu 387, Leu 359, Cys 386, Trp 356, Val 196, Gly 166, Ser 167, Phe 170, Phe 174, Ile 119, Met 384, Ile 105, Ser 383, Met 103, Phe 379, Phe 102, Phe 268, Leu 193, Thr 197 (Vina and Autodock 4.0 outcomes) (see Figures 55, 56, 57, and 58).

The ligand protein interaction diagrams of the antagonists complexed with the crystal structure of the CB_1 receptor obtained using the molecular docking software programs Vina and Autodock 4.0 are in the Figures 55 and 57, respectively. The lists of interactions observed between antagonists and the CB_1 receptor (crystal structure) obtained using the molecular docking software Vina and Autodock 4.0, are in Figures 56 and 58, respectively.

6.19) Vina and Autodock 4.0 binding affinities against experimental K_i values for representative CB_1 receptor agonists and antagonists

In our analysis, the lowest Vina and Autodock 4.0 binding energies (expressed in Kcal/mol) related to the best binding pose for each referent compound, were compared with the K_i value (expressed in nanomoles) obtained with bioassay studies.

As observed in the Table 5, there is no correlation between Vina and Autodock 4.0 binding energies against experimental K_i values (lower energies should be related to lower K_i values). The reasons for these inconsistencies may be related to some limitations inherent to our docking approaches. Vina and Autodock 4.0 currently employ some simplifications that may affect the outcomes generated. Firstly, they both use a rigid receptor, and this may be a serious limitation if the real system includes significant receptor motion (Forli et al., 2016). To overcome this issue, we used a receptor structure taken from a receptor-ligand complex, where the receptor should be in the relevant conformation (Hua et al., 2016). Additionally, Vina and Autodock 4.0 scoring functions are highly approximated and the number of degrees of freedom for the ligands is necessarily limited (Forli et al., 2016). Furthermore, both methods require a simplified typing of atoms (identification of aromatic and aliphatic carbon atoms) and molecules containing fluorine or chlorine atoms may not be considered adequately. Obviously, better results would have been obtained employing more sophisticated and computationally-intensive programs or using complementary tools that would have helped to predict the binding energies more accurately. This improvement could represent the next goal in our study.

Referent compounds				
CB_1R agonists				
	Vina	Autodock 4.0		
Compounds	Binding energy (Kcal/mol)	Binding energy (Kcal/mol)	Experimental K_i (nM)	Reference
JWH-018	-9.5	-10.2	9.0	Aung et al., 2000
CP-55,940	-8.7	-9.1	1.1	Melvin et al., 1993
WIN 55-212,2	-8.7	-11.5	62.3	Felder et al., 1995
ANANDAMIDE	-8.5	-9.3	61.0	Lin et al., 1998
Δ9-THC	-8.1	-9.8	41.0	Showalter et al., 1996
2-AG	-7.9	-6.7	45.0	Chen et al., 2008
CB_1R antagonists				
	Vina	Autodock 4.0		
Compounds	Binding energy (Kcal/mol)	Binding energy (Kcal/mol)	Experimental K_i (nM)	Reference
AM-6358	-12.0	-13.1	3.4	Hua et al., 2016
OTENABANT	-11.4	-11.5	0.7	Hadcock et al., 2010
AM-251	-11.4	-13.3	7.5	Südhof and Starke, 2007
RIMONABANT	-11.3	-12.6	6.2	Soudijn et al., 2005
TARANABANT	-9.7	-7.9	0.1	Shao et al., 2016

Table 5: Vina and Autodock 4.0 binding energies related to the best binding poses of representative CB_1R agonists and antagonists at the CB_1R crystal structure, against experimental K_i values.

6.20) Conclusions of the docking approach validation

Globally, the outcomes generated by the docking programs employed, were considered reliable in terms of ligand interactions, as most of the residues found to be involved in ligand binding were in line with those considered crucial in previous mutation studies and computational analyses.

By contrast, since no specific correlation between K_i values and binding energies was found, the binding energy values were approached with caution. The same methods were employed in the analysis of the binding interactions of the index SCs BB-22, 5F-PB-22, 5F-AKB-48, STS-135 against the crystal structure of the human CB_1 receptor. However, all the results were regarded as preliminary findings requiring further optimization with more sophisticated tools.

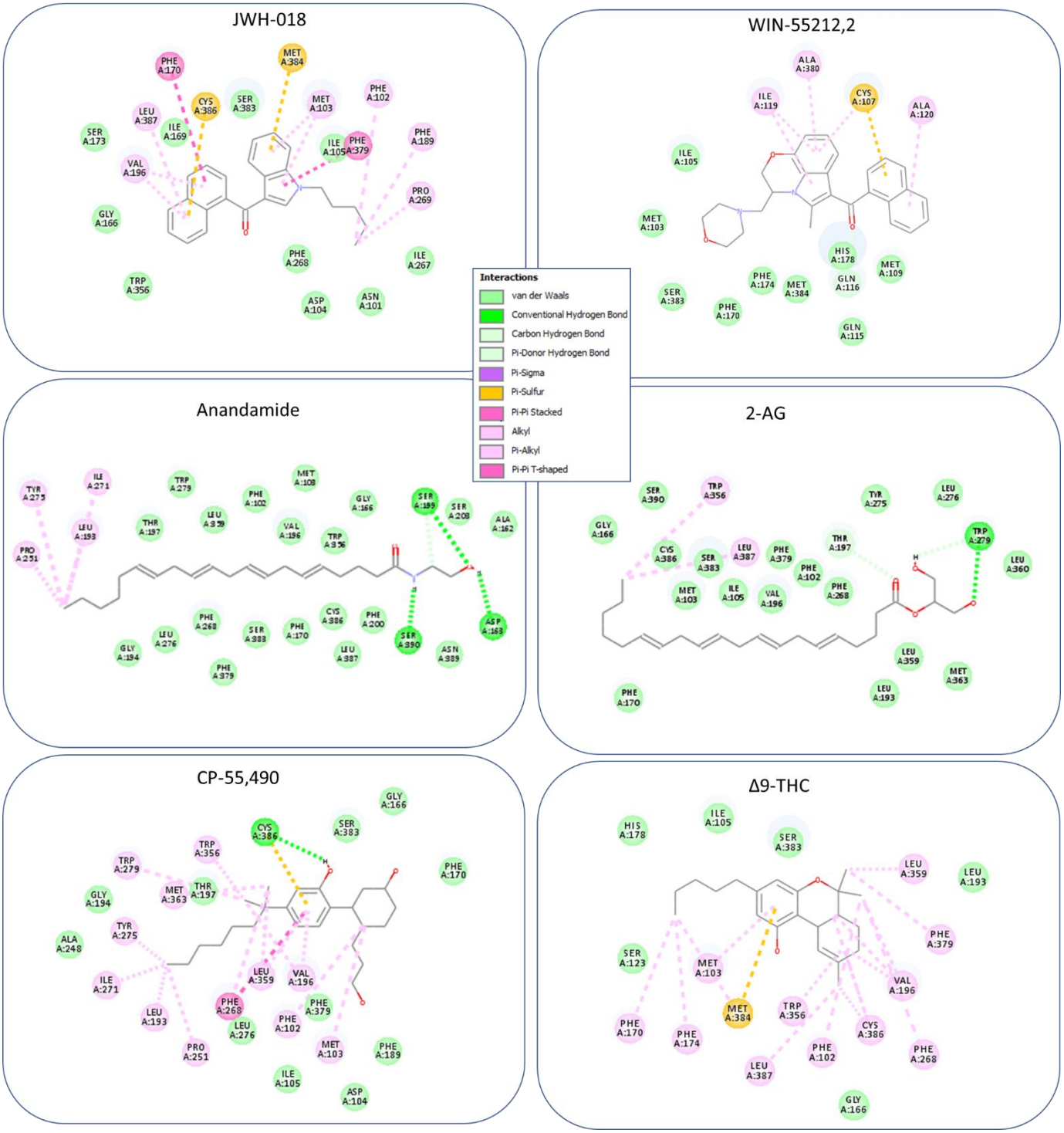

Figure 51: Ligand protein interaction diagrams of JWH-018, WIN-55,212-2, Anandamide, 2-AG, CP-55,940, Δ9-THC complexed with the CB_1R crystal structure. The complexes shown are the most favourable poses obtained using the molecular docking software Vina.

JWH-018		
VINA	Interactions	
Residues	Type of interaction	Distance (Å)
MET 384	Pi-Sulfur	5.63
CYS 386	Pi-Sulfur	5.50
PHE 170	Pi-Pi T-shaped	5.37
PHE3 79	Pi-Pi T-shaped	5.68
PRO 269	Alkyl	4.70
PHE 102	Pi-Alkyl	5.26
PHE 189	Pi-Alkyl	4.86
MET 103	Pi-Alkyl	4.32
VAL 196	Pi-Alkyl	3.83
LEU 387	Pi-Alkyl	5.47
Van der Waals interactions		
ILE 169, SER 383, ILE 105, ILE 267, ASN 101, SER 173,PHE 268, ASP 104, TRP 356, GLY 166		

2-AG		
VINA	**Interactions**	
Residues	**Type of interaction**	**Distance (Å)**
LEU 387	Alkyl	5.28
THR 197	Carbon Hydrogen Bond	2.42
TRP 279	Conventional Hydrogen Bond	2.34
TRP 279	Pi-Donor Hydrogen Bond	2.52
TRP 356	Pi-Alkyl	5.30
Van der Waals interactions		
GLY 166, SER 390, CYS 386, MET 103, ILE 105, PHE 379, SER 383 VAL 196, PHE 102, PHE 268, TYR 275, LEU 276, LEU 360, MET 363, LEU 359, LEU 193, PHE 170		

CP-55,940		
VINA	**Interactions**	
Residues	**Type of interaction**	**Distance (Å)**
CYS 386	Conventional Hydrogen Bond	2.96
CYS 386	Pi-Sulfur	5.76
PHE 268	Pi-Pi Stacked	5.10
MET 103	Alkyl	5.17
VAL 196	Alkyl	5.35
LEU 359	Alkyl	4.42
MET 363	Alkyl	4.38
LEU 193	Alkyl	4.37
PRO 251	Alkyl	4.22
ILE 271	Alkyl	5.38
PHE 102	Pi-Alkyl	4.67
PHE 268	Pi-Alkyl	5.20
TYR 275	Pi-Alkyl	4.85
TRP 279	Pi-Alkyl	5.13
TRP 356	Pi-Alkyl	5.02
VAL 196	Pi-Alkyl	4.30
LEU 359	Pi-Alkyl	5.05
Van der Waals interactions		
ALA 248, GLY 194, THR 197, SER 383, GLY 166, PHE 170, PHE 189,PHE 379, ASP 104, ILE 105, LEU 276		

WIN-55,212-2		
VINA	Interactions	
Residues	Type of interaction	Distance (Å)
ALA 120	Pi-Alkyl	5.36
ALA 380	Pi-Alkyl	4.83
CYS 107	Pi-Sulfur	5.14
CYS 107	Pi-Alkyl	5.36
GLN 116	Carbon Hydrogen Bond	2.32
ILE 119	Pi-Alkyl	4.76
Van der Waals interactions		
MET 103, ILE 105, SER 383, PHE 170, PHE 174, MET 384, PHE 174, PHE 170, SER 383		

ANANDAMIDE		
VINA	**Interactions**	
Residues	**Type of interaction**	**Distance (Å)**
ASP 163	Conventional Hydrogen Bond	2.17
ILE 271	Alkyl	4.71
LEU 193	Alkyl	4.06
PRO 251	Alkyl	4.28
SER 199	Conventional Hydrogen Bond	2.93
SER 199	Carbon Hydrogen Bond	2.72
SER 390	Conventional Hydrogen Bond	2.00
TYR 275	Pi-Alkyl	4.91
Van der Waals interactions		
THR 197, TRP 279, LEU 359, PHE 102, VAL 196, MET 103 TRP 356, GLY 166, SER 208, ALA 162, GLY 194, LEU 276, PHE 268, PHE 379, SER 383, PHE 170, CYS 386, LEU 387, PHE 200, ASN 389		

Δ9-THC		
VINA	**Interactions**	
Residues	**Type of interaction**	**Distance (Å)**
CYS 386	Alkyl	4.29
LEU 359	Alkyl	4.76
LEU 387	Alkyl	4.09
MET 103	Pi-Alkyl	4.43
MET 384	Pi-Sulfur	5.39
MET 384	Alkyl	4.53
PHE 102	Pi-Alkyl	4.72
PHE 170	Pi-Alkyl	5.19
PHE 174	Pi-Alkyl	4.84
PHE 268	Pi-Alkyl	5.13
PHE 379	Pi-Alkyl	5.01
TRP 356	Pi-Alkyl	5.31
VAL 196	Alkyl	4.37
VAL 196	Alkyl	4.27
Van der Waals interactions		
SER 123, HIS 178, ILE 105, SER 383, LEU 193, GLY 166		

Figure 52: Lists of interactions observed between JWH-018, WIN-55,212-2, 2-AG, Anandamide, CP-55,940, Δ9-THC and the CB_1R crystal structure and obtained using the molecular docking software Vina.

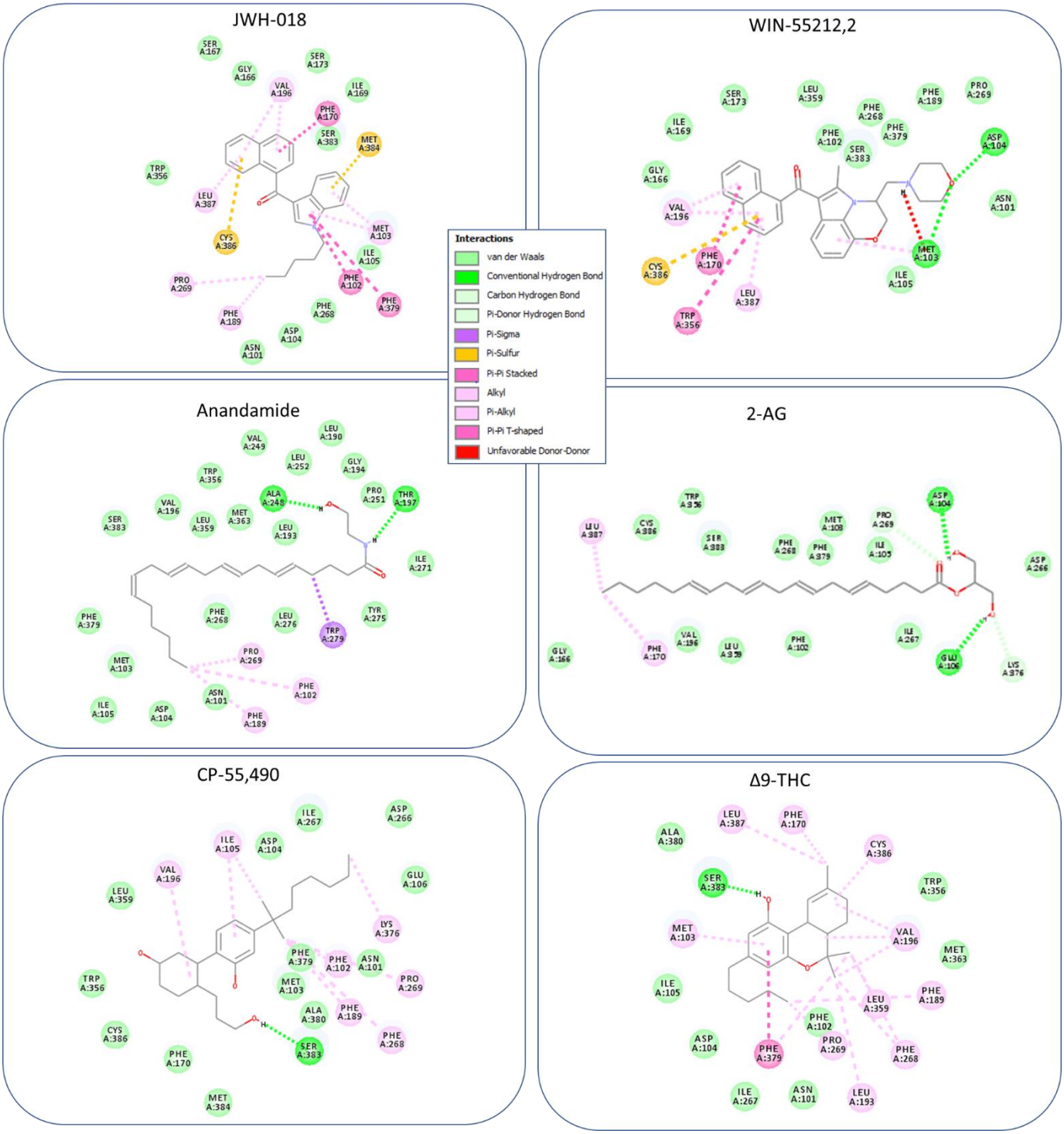

Figure 53: Ligand protein interaction diagrams of JWH-018, WIN-55,212-2, Anandamide, 2-AG, CP-55,940, Δ9-THC complexed with the CB_1R crystal structure. The complexes shown are the most favourable poses obtained using the molecular docking software Autodock 4.0.

JWH-018		
AUTODOCK 4.0	**Interactions**	
Residues	**Type of interaction**	**Distance (Å)**
CYS 386	Pi-Sulfur	5.78
LEU 387	Pi-Alkyl	5.04
MET 103	Pi-Alkyl	4.43
MET 384	Pi-Sulfur	5.48
PHE 102	Pi-Pi T-shaped	5.22
PHE 170	Pi-Pi T-shaped	5.26
PHE 189	Pi-Alkyl	4.65
PHE 379	Pi-Pi T-shaped	5.74
PRO 269	Alkyl	4.15
VAL 196	Pi-Alkyl	3.91
Van der Waals interactions		
TRP 356, SER 167, GLY 166, SER 173, ILE 169, SER 383, ILE 105, PHE 287, ASP 104, ASN 101		

WIN 55,212-2		
AUTODOCK 4.0	**Interactions**	
Residues	**Type of interaction**	**Distance (Å)**
ASP 104	Conventional Hydrogen Bond	2.12
CYS 386	Pi-Sulfur	5.61
LEU 387	Pi-Alkyl	5.44
MET 103	Conventional Hydrogen Bond	2.50
MET 103	Pi-Alkyl	4.60
MET 103	Unfavourable donor-donor	2.19
PHE 170	Pi-Pi T-shaped	5.36
TRP 356	Pi-Pi Stacked	5.88
VAL 196	Pi-Alkyl	3.72
Van der Waals interactions		
GLY 166, ILE 169, SER 173, LEU 359, PHE 102, SER 383, PHE 268, PHE 379, PHE 189, PRO 269, ASN 101, ILE 105		

2-AG		
AUTODOCK 4.0	**Interactions**	
Residues	**Type of interaction**	**Distance (Å)**
GLU 106	Conventional Hydrogen Bond	2.25
ASP104	Conventional Hydrogen Bond	2.12
PRO 269	Carbon Hydrogen Bond	2.95
LYS 376	Carbon Hydrogen Bond	2.50
LEU 387	Alkyl	4.20
PHE 170	Pi-Alkyl	5.41
Van der Waals interactions		
GLY 166, CYS 386, TRP 356, SER 383, PHE 268, PHE 379, MET 108, ILE 105, ASP 266, ILE 267, PHE 102, LEU 358, VAL 196, GLY 166		

ANANDAMIDE		
AUTODOCK 4.0	**Interactions**	
Residues	**Type of interaction**	**Distance (Å)**
THR 197	Conventional Hydrogen Bond	2.01
ALA 248	Conventional Hydrogen Bond	1.88
TRP 279	Pi-Sigma	3.29
PRO 269	Alkyl	4.62
PHE 102	Pi-Alkyl	5.30
PHE 189	Pi-Alkyl	4.82
Van der Waals interactions		
SER 383, VAL 196, LEU 359, TRP 356, MET 363, LEU 193, VAL 249, LEU 252, LEU 190, GLY 194, PRO 251, ILE 271, TYR 275, LEU 276, ASN 101, PHE 268, ASP 104, MET 103, ILE 105, PHE 379		

CP-55, 940		
AUTODOCK 4.0	**Interactions**	
Residues	**Type of interaction**	**Distance (Å)**
ILE 105	Alkyl	3.91
ILE 105	Pi-Alkyl	5.40
LYS 376	Alkyl	5.06
PHE 102	Pi-Alkyl	4.78
PHE 189	Pi-Alkyl	4.87
PHE 268	Pi-Alkyl	5.26
PRO 269	Alkyl	5.09
SER 383	Conventional Hydrogen Bond	1.98
VAL 196	Alkyl	5.34
Van der Waals interactions		
LEU 359, ASP 104, ILE 267, ASP 266, GLU 106, ASN 101, PHE 379, MET 103, ALA 380, MET 384, PHE 170, CYS 386, TRP 356		

Δ9-THC		
AUTODOCK 4.0	**Interactions**	
Residues	**Type of interaction**	**Distance (Å)**
CYS 386	Alkyl	4.41
LEU 193	Alkyl	4.99
LEU 359	Alkyl	3.94
LEU 387	Alkyl	4.37
MET 103	Pi-Alkyl	5.29
PHE 170	Pi-Alkyl	4.39
PHE 189	Pi-Alkyl	4.85
PHE 268	Pi-Alkyl	4.63
PHE 379	Pi-Pi T-shaped	5.24
PHE 379	Pi-Alkyl	5.00
PRO 269	Alkyl	4.19
SER 383	Conventional Hydrogen Bond	1.82
VAL 196	Alkyl	4.08
Van der Waals interactions		
ALA 380, TRP 356, MET 363, PHE 102, ASN 101, ILE 267, ASP 104, ILE 105		

Figure 54: Lists of interactions observed between JWH-018, WIN-55,212-2, 2-AG, Anandamide, CP-55,940, Δ9-THC and the CB_1R crystal structure and obtained using the molecular docking software Autodock 4.0.

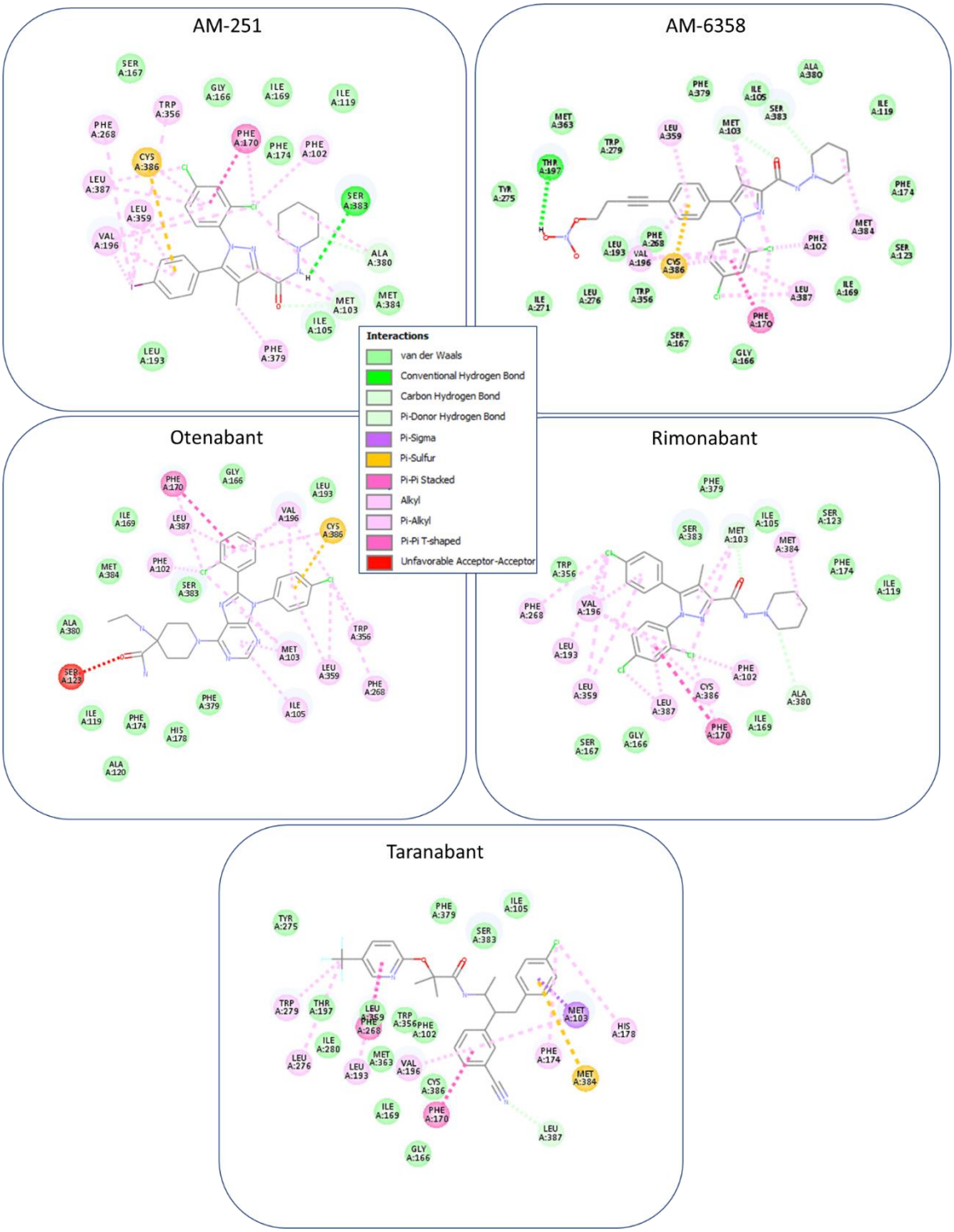

Figure 55: Ligand protein interaction diagrams of AM-251, AM-6358, otenabant, rimonabant, taranabant complexed with the CB_1R crystal structure. The complexes shown are the most favourable poses obtained using the molecular docking software Vina.

AM-251		
VINA	Interactions	
Residues	Type of interaction	Distance (Å)
ALA 380	Carbon Hydrogen Bond	3.18
ALA 380	Alkyl	4.97
CYS 386	Pi-Sulfur	5.64
CYS 386	Pi-Alkyl	5.20
LEU 359	Alkyl	5.29
LEU 359	Pi-Alkyl	5.22
LEU 387	Alkyl	4.76
LEU 387	Pi-Alkyl	5.13
MET 103	Carbon Hydrogen Bond	2.54
MET 103	Alkyl	4.90
MET 103	Pi-Alkyl	5.01
PHE 102	Pi-Alkyl	4.75
PHE 170	Pi-Pi T-shaped	5.24
PHE 170	Pi-Alkyl	5.09
PHE 268	Pi-Alkyl	5.31
PHE 379	Pi-Alkyl	4.69
SER 383	Conventional Hydrogen Bond	2.59
TRP356	Pi-Alkyl	5.35
VAL 196	Alkyl	4.39
VAL 196	Pi-Alkyl	4.38
Van der Waals interactions		
SER 167, GLY 166, ILE 169, ILE 119, PHE 174, MET 384, ILE 105, LEU 193		

OTENABANT		
VINA	Interactions	
Residues	Type of interaction	Distance (Å)
CYS 386	Pi-Sulfur	5.55
CYS 386	Pi-Alkyl	5.43
ILE 105	Pi-Alkyl	5.10
LEU 359	Alkyl	5.23
LEU 359	Pi-Alkyl	5.22
LEU 387	Pi-Alkyl	5.03
MET 103	Alkyl	4.82
MET 103	Pi-Alkyl	4.85
PHE 102	Pi-Alkyl	4.50
PHE 170	Pi-Pi T-shaped	5.04
PHE 170	Pi-Alkyl	5.30
PHE 268	Pi-Alkyl	5.33
SER 123	Unfavorable Acceptor-Acceptor	2.76
TRP 356	Pi-Alkyl	5.20
VAL 196	Alkyl	4.34
VAL 196	Pi-Alkyl	4.33
Van der Waals interactions		
ALA 380, MET 384, ILE 169, SER 383, GLY 166, LEU 193, PHE 379, HIS 178, PHE 174, ALA 120, ILE 119		

AM-6358		
VINA	Interactions	
Residues	Type of interaction	Distance (Å)
CYS 386	Pi-Sulfur	5.71
CYS 386	Pi-Alkyl	5.14
LEU 359	Pi-Alkyl	5.23
LEU 387	Alkyl	4.87
LEU 387	Pi-Alkyl	5.15
MET 103	Carbon Hydrogen Bond	2.63
MET 103	Alkyl	5.14
MET 103	Pi-Alkyl	5.08
MET 384	Alkyl	4.88
PHE 102	Pi-Alkyl	5.00
PHE 170	Pi-Alkyl	5.00
PHE 170	Pi-Pi T-shaped	5.43
SER 383	Carbon Hydrogen Bond	3.79
THR 197	Conventional Hydrogen Bond	2.56
VAL 196	Alkyl	4.32
VAL 196	Pi-Alkyl	4.34
Van der Waals interactions		
TYR 275, MET 363, TRP 279, PHE 379, ILE 105, ALA 380, ILE 119, PHE 174, SER 123, ILE 169, GLY 166, SER 167, TRP 356, LEU 276, ILE 271, LEU 193, PHE 268		

RIMONABANT		
VINA	Interactions	
Residues	Type of interaction	Distance (Å)
ALA 380	Carbon Hydrogen Bond	3.45
CYS 386	Pi-Alkyl	5.21
LEU 193	Alkyl	5.00
LEU 359	Alkyl	5.47
LEU 359	Pi-Alkyl	5.36
LEU 387	Alkyl	4.77
LEU 387	Pi-Alkyl	5.15
MET 103	Carbon Hydrogen Bond	2.74
MET 103	Alkyl	5.09
MET 103	Pi-Alkyl	4.92
MET 384	Alkyl	4.83
PHE 102	Pi-Alkyl	4.88
PHE 170	Pi-Pi T-shaped	5.29
PHE 170	Pi-Alkyl	5.09
PHE 268	Pi-Alkyl	4.75
VAL 196	Alkyl	4.29
VAL 196	Pi-Alkyl	4.42
Van der Waals interactions		
TRP 356, SER 383, PHE 379, ILE 105, SER 123, PHE 174, ILE 119, ILE 169, GLY 166, SER 167		

TARANABANT		
VINA	Interactions	
Residues	Type of interaction	Distance (Å)
HIS 178	Pi-Alkyl	4.44
LEU 193	Pi-Alkyl	5.21
LEU 276	Alkyl	5.00
LEU 387	Carbon Hydrogen Bond	2.74
MET 103	Pi-Sigma	2.73
MET 103	Pi-Sulfur	4.46
MET 103	Pi-Alkyl	5.46
MET 384	Pi-Sulfur	4.86
PHE 170	Pi-Pi T-shaped	4.96
PHE 174	Pi-Alkyl	4.85
PHE 268	Pi-Pi Stacked	5.00
TRP 279	Pi-Alkyl	3.94
TRP 279	Pi-Alkyl	4.83
VAL 196	Pi-Alkyl	4.36
Van der Waals interactions		
TYR 275, PHE 379, SER 383, ILE 105, GLY 166, ILE 169, CYS 386, MET 363, PHE 102, TRP 356, LEU 359, ILE 280, THR 197		

Figure 56: Lists of interactions observed between AM-251, AM-6358, otenabant, rimonabant, taranabant and the CB_1 receptor crystal structure obtained using the molecular docking software Vina.

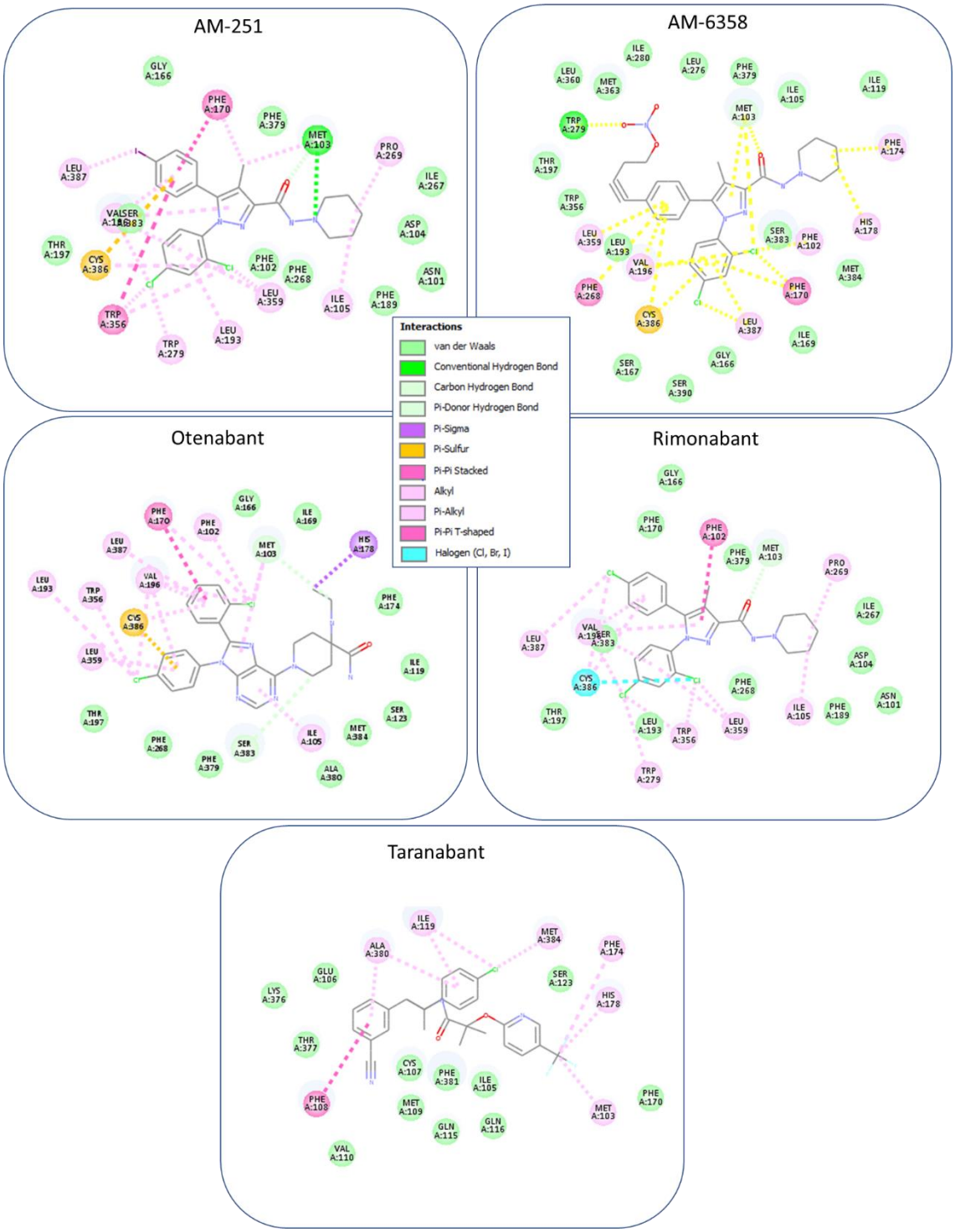

Figure 57: Ligand protein interaction diagrams of AM-251, AM-6358, Otenabant, rimonabant, taranabant complexed with the CB_1R crystal structure. The complexes shown are the most favourable poses obtained using the molecular docking software Autodock 4.0.

AM-251		
AUTODOCK 4.0	Interactions	
Residues	Type of interaction	Distance (Å)
CYS 386	Pi-Sulfur	5.67
CYS 386	Alkyl	3.87
ILE 105	Alkyl	5.30
LEU 193	Pi-Alkyl	5.43
LEU 359	Alkyl	3.55
LEU 359	Pi-Alkyl	5.39
LEU 387	Alkyl	4.43
MET 103	Conventional Hydrogen Bond	2.19
MET 103	Carbon Hydrogen Bond	2.10
MET 103	Alkyl	3.73
PHE 170	Pi-Pi T-shaped	5.93
PHE 170	Pi-Alkyl	5.45
PRO 269	Alkyl	4.84
TRP 279	Pi-Alkyl	5.21
TRP 356	Pi-Alkyl	4.83
TRP 356	Pi-Pi Stacked	5.96
VAL 196	Alkyl	5.30
VAL 196	Pi-Alkyl	3.93
Van der Waals interactions		
GLY 166, PHE 379, ILE 267, ASP 104, ASN 101, PHE 189, PHE 268, PHE 102, SER 383, THR 197		

AM-6358		
AUTODOCK 4.0	Interactions	
Residues	Type of interaction	Distance (Å)
CYS 386	Pi-Sulfur	5.57
CYS 386	Pi-Alkyl	5.14
HIS 178	Pi-Alkyl	5.16
LEU 359	Pi-Alkyl	5.25
LEU 387	Alkyl	4.39
LEU 387	Pi-Alkyl	4.90
MET 103	Carbon Hydrogen Bond	2.51
MET 103	Alkyl	5.20
MET 103	Pi-Alkyl	5.04
PHE 102	Pi-Alkyl	5.11
PHE 170	Pi-Pi T-shaped	5.22
PHE 170	Pi-Alkyl	4.94
PHE 174	Pi-Alkyl	5.14
PHE 268	Pi-Pi Stacked	5.51
TRP 279	Conventional Hydrogen Bond	1.80
VAL 196	Alkyl	4.32
VAL 196	Pi-Alkyl	4.17
Van der Waals interactions		
LEU 360, MET 363, ILE 280, LEU 276, PHE 379, ILE 105, ILE 119 MET 384, ILE 169, GLY 166, SER 390, SER 167, LEU 193, TRP 356, SER 383, THR 197		

OTENABANT		
AUTODOCK 4.0	Interactions	
Residues	Type of interaction	Distance (Å)
CYS 386	Pi-Sulfur	5.58
CYS 386	Pi-Alkyl	5.41
HIS 178	Pi-Sigma	3.37
ILE 105	Pi-Alkyl	5.26
LEU 193	Alkyl	5.30
LEU 359	Pi-Alkyl	5.24
LEU 387	Pi-Alkyl	5.11
MET 103	Carbon Hydrogen Bond	3.59
MET 103	Alkyl	4.68
MET 103	Pi-Alkyl	5.40
PHE 102	Pi-Alkyl	4.58
PHE 170	Pi-Pi T-shaped	5.18
PHE 170	Pi-Alkyl	5.13
SER 383	Carbon Hydrogen Bond	2.78
TRP 356	Pi-Alkyl	5.34
VAL 196	Alkyl	4.53
VAL 196	Pi-Alkyl	4.18
Van der Waals interactions		
GLY 166, ILE 169, PHE 174, ILE 119, SER 123, MET 384, ALA 380, PHE 379, PHE 268, THR 197		

RIMONABANT		
AUTODOCK 4.0	Interactions	
Residues	Type of interaction	Distance (Å)
CYS 386	Halogen (Cl, Br, I)	3.40
CYS 386	Alkyl	3.53
CYS 386	Pi-Alkyl	4.93
ILE 105	Alkyl	5.40
LEU 359	Alkyl	3.62
LEU 359	Pi-Alkyl	5.33
LEU 387	Alkyl	4.21
MET 103	Carbon Hydrogen Bond	1.96
PHE 102	Pi-Pi Stacked	4.47
PRO 269	Alkyl	4.77
TRP 279	Pi-Alkyl	5.23
TRP 356	Pi-Alkyl	4.74
VAL 196	Alkyl	5.36
VAL 196	Pi-Alkyl	3.95
Van der Waals interactions		
PHE 170, GLY 166, PHE 379, ILE 267, ASP 104, ASN 101, PHE 189, PHE 268, LEU 193, THR 197, SER 383		

TARANABANT		
AUTODOCK 4.0	Interactions	
Residues	Type of interaction	Distance (Å)
ALA 380	Pi-Alkyl	4.02
ALA 380	Pi-Alkyl	4.78
HIS 178	Pi-Alkyl	4.72
ILE 119	Alkyl	4.58
ILE 119	Pi-Alkyl	4.59
MET 384	Alkyl	3.53
MET 103	Alkyl	3.83
PHE 108	Pi-Pi Stacked	5.56
PHE 174	Pi-Alkyl	4.95
Van der Waals interactions		
LYS 376, GLU 106, SER 123, PHE 170, GLN 116, ILE 105, PHE 381, GLN 115 CYS 107, MET 109, VAL 110, THR 377		

Figure 58: Lists of interactions observed between AM-251, AM-6358, otenabant, rimonabant, taranabant and the CB_1 receptor crystal structure obtained using the molecular docking software Autodock 4.0.

6.21) Docking of a range of novel synthetic cannabinoids against the crystal structure of the human CB_1 receptor: methods

In this analysis, the key binding interactions of a range of novel SCs (BB-22, 5F-PB-22, 5F-AKB-48, STS-135) against the crystal structure of the human CB_1 receptor were analysed. The methods used were the same applied with the referent compounds. PyRx 0.9.4 was used as virtual screening software and Autodock Vina and Autodock 4.0 were the docking programmes employed. Vina's search space coordinates were set as follows: centre, X:41, Y:29, Z:317; dimensions X: 25 Å, Y: 25 Å, Z: 25 Å. Overall, eight binding modes for each ligand were generated and the pose with the lowest binding energy (expressed in Kcal/mol) was selected to study the relevant key binding interactions. In Autodock 4.0, the search space coordinates used were the following: centre, X:41, Y:29, Z:317; number of points X: 184, Y: 230, Z: 294, spacing: 0.12 Å. For each pose the estimated free energy of binding resulted from the total interaction energy (intermolecular energy, internal energy, torsional energy, unbound energy) was calculated. In total, ten binding modes for each ligand were generated and the pose with the lowest estimated free energy of binding (expressed in Kcal/mol) was selected to study the relevant key binding interactions.

6.22) Docking of a range of novel synthetic cannabinoids with the crystal structure of the human CB_1 receptor: results and discussion

According to Vina findings, the novel aminoalkylindole derivatives under study (BB-22, 5F-PB-22, 5F-AKB-48, STS-135) shared some identical interacting residues including: Ile 105, Met 103, Phe 102 (N-terminal loop), Phe 170 (helix 2), Phe 379, Ser 383 (helix 7). However, according to the outcomes generated by Autodock 4.0, the interacting residues shared by all novel SCs, were many more and included: Ile 105, Met 103, Phe 102, (N-terminal loop), Phe 170, Phe 268, Pro 269 (helix 2), Phe 189, Val 196 (helix 3), Phe 379, Ser 383 (helix 7), Ile 267 (ECL2) (see Figures 57, 58, 59 and 60).

Referring to Vina outcomes, the indole core of BB-22 formed alkyl interactions with the N-terminal loop; its quinolinyl group formed a sulphur interaction with helix 7 (Cys 386), and alkyl interactions with helix 3 (Val 196) and helix 7 (Leu 387); while its cyclohexyl methyl group interacted with both, the ECL2 (Phe 268) and the N-terminal loop (Ile 105) through alkyl interactions. On the other hand, the best binding pose of BB-22 generated by Autodock 4.0 programme, showed slight different type of interactions, with its indole group forming pi-pi and sulphur interactions with helix 7 (Phe 379, Cys 386 respectively); its cyclohexyl methyl group forming alkyl interactions with the 2, 3, 7 helices and its quinolinyl group interacting

with both, the ECL2 (pi-pi interactions) and the N-terminal loop (alkyl and hydrogen bond interactions) of the receptor (see Figures 59, 60, 61 and 62).

According to Vina outcomes, the indole group of 5F-PB-22, interacted mainly with the N-terminal loop of the protein through pi-pi (Phe 102) and sulphur interactions (Met 103); its quinolinyl group formed primarily alkyl interactions with the N-terminal loop and the ECL2; while its fluorinated pentyl tail interacted mainly with the 2, 3, 5, 6 and 7 helices of the receptor. On the other hand, the best binding pose of 5F-PB-22 generated by Autodock 4.0 programme, showed slight different type of interactions, with the indole group interacting with the N-terminal loop and ECL2; the quinolinyl group forming mainly alkyl interactions with helix 3 and van der Waals interactions with helix 7; and the fluorinated pentyl tail interacting with the N-terminal loop, the ECL2 and helix 7 (see Figures 59, 60, 61 and 62).

Referring to Vina outcomes, the indazole and indole groups of 5F-AKB-48 and STS-135 respectively, interacted mainly with the N-terminal loop; their adamantyl groups formed mostly hydrophobic interactions with the 2 and 7 helices; while their fluorinated pentyl tails formed halogen interactions with the helix 7 (Ser 383) (Vina outcomes). On the other hand, the best binding poses of 5F-AKB-48 and STS-135 generated by Autodock 4.0 programme, showed slight different type of interactions, with the indole group of 5F-AKB-48 interacting with the helix 3 and the N-terminal loop; and the indazole group of STS-135 forming interactions with the N-terminal loop, and the 3 and 7 helices. Additionally, their adamantyl groups primarily interacted with the ECL2 ant the N-terminal loop, while the fluorinated pentyl tails mainly interacted with the 3 and 6 helices (see Figures 59, 60, 61 and 62).

Notably, according to Vina outcomes, only the novel aminoalkylindole derivatives BB-22 and 5F-PB-22 interacted with residues that, according to mutation studies, were considered crucial for aminoalkylindole binding recognition (Mc Allister et al., 2003, Shim et al., 2006). In this regard, Phe 200 (helix 3) and Trp 279 (helix 5) interacted with 5F-PB-22 (pi-alkyl interaction); while Trp 356 (helix 6) interacted with both BB-22 and 5F-PB-22 (van der Waals and pi-alkyl interactions respectively). On the other hand, according to Autodock 4.0 outcomes, only STS-135 interacted with a residue (Trp 356) referred as crucial for aminoalkylindole binding recognition (see Figures 59, 60, 61 and 62).

Interestingly, the index novel SCs in our study, showed interactions with residues considered crucial for rimonabant binding recognition (Mc Allister et al., 2003; Shim et al., 2012).

The ligand protein interaction diagrams of the novel SCs complexed with the CB_1R crystal structure according to Vina and Autodock 4.0 programs are in the Figures 59 and 61 respectively, while the lists of interactions are in the Figures 60 and 62.

6.23) Vina and Autodock 4.0 binding affinities against experimental K_i values for each novel SC under study

According to the results generated by the docking programme Vina, BB-22, STS-135, 5F-AKB-48, 5F-PB-22 showed comparable binding energies (-9.6, -9.6, -9.5, -9.1 Kcal/mol respectively). On the other hand, according to Autodock 4.0 outcomes, the rank of order of the estimated free energy of binding was as follows: BB-22 (-11.48 kcal/mol), STS-135 (-11.2 Kcal/mol), 5F-AKB-48 (-10.93 Kcal/mol), and 5F-PB-22 (-9.53 kcal/mol) (see Table 6). Overall, there was no correlation between both Vina and Autodock 4.0 binding energies against experimental K_i values (lower energies should be related to lower K_i values). The reasons for these inconsistencies may be related to some limitations inherent to our docking approaches (for details see paragraph 6.19).

Third generation synthetic cannabinoids			
	VINA	AUTODOCK 4.0	Experimental results
Molecule	Binding affinity (Kcal/mol)	Binding energy (Kcal/mol)	Ki (nM)
BB-22	-9.6	-11.48	0.11
5F-PB-22	-9.1	-9.53	0.13
5F-AKB-48	-9.5	-10.93	0.87
STS-135	-9.6	-11.2	1.93

Table 6: Vina and Autodock 4.0 binding energies related to the best binding poses of BB-22, 5F-PB-22, 5F-AKB-48, STS-135 at the CB_1R crystal structure, vs experimental K_i values.

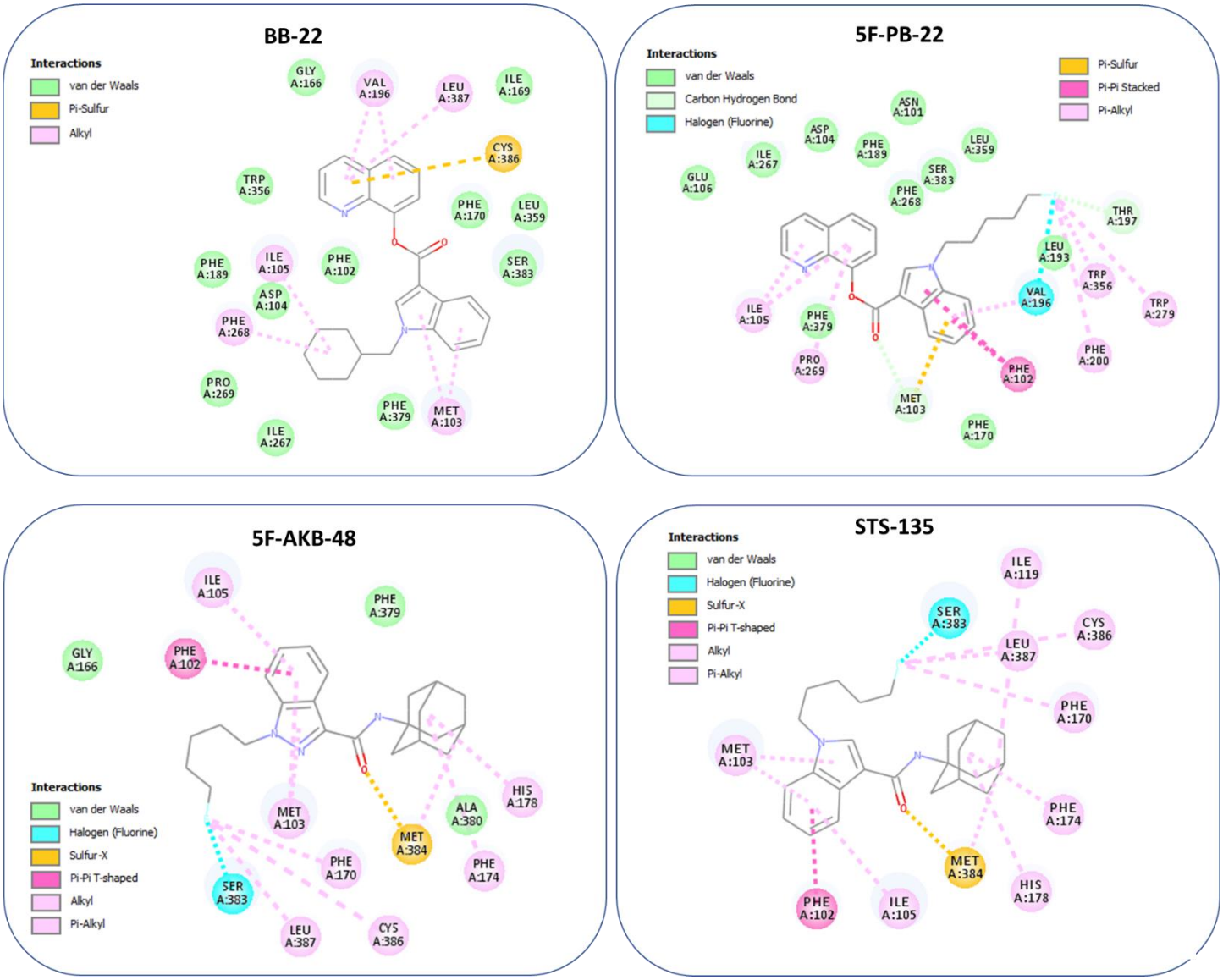

Figure 59: Ligand protein interaction diagrams of BB-22, 5F-PB-22, 5F-AKB-48, STS-135 complexed with the CB_1R crystal structure. The complexes shown are the most favourable poses obtained using the molecular docking software Vina.

BB-22		
VINA	**Interactions**	
Residues	**Type of interaction**	**Distance (Å)**
CYS 386	Pi-Sulfur	5.66
ILE 105	Alkyl	5.23
PHE 268	Pi-Alkyl	4.75
MET 103	Pi-Alkyl	4.35
VAL 196	Pi-Alkyl	3.79
LEU 387	Pi-Alkyl	5.29
Van der Waals interactions		
PRO 269, PHE 189, ASP 104, PHE 102, TRP 356, GLY 166, ILE 169, PHE 170, LEU 359, SER 383, PHE 379, ILE 267		

5F-AKB-48		
VINA	**Interactions**	
Residues	**Type of interaction**	**Distance (Å)**
CYS 386	Alkyl	5.13
HIS 178	Pi-Alkyl	5.05
ILE 105	Pi-Alkyl	5.40
LEU 387	Alkyl	3.88
MET 103	Pi-Alkyl	4.36
MET 384	Sulfur-X	3.32
MET 384	Alkyl	4.67
PHE 102	Pi-Pi T-shaped	4.95
PHE 170	Pi-Alkyl	4.41
PHE 174	Pi-Alkyl	5.11
SER 383	Halogen (Fluorine)	3.49
Van der Waals interactions		
GLY 166, PHE 379, ALA 380		

5F-PB-22		
VINA	**Interactions**	
Residues	**Type of interaction**	**Distance (Å)**
ILE 105	Pi-Alkyl	4.38
MET 103	Carbon Hydrogen Bond	2.56
MET 103	Pi-Sulfur	5.67
PHE 102	Pi-Pi Stacked	4.55
PHE 200	Pi-Alkyl	4.95
PRO 269	Pi-Alkyl	5.25
THR 197	Carbon Hydrogen Bond;Halogen (Fluorine)	2.23
TRP 279	Pi-Alkyl	4.46
TRP 356	Pi-Alkyl	4.31
VAL 196	Halogen (Fluorine)	3.62
VAL 196	Pi-Alkyl	4.73
Van der Waals interactions		
GLU 106, ILE 267, ASP 104, PHE 189, ASN 101,PHE 268, SER 383, LEU 359, LEU 193 PHE 170, PHE 379		

STS-135		
VINA	**Interactions**	
Residues	**Type of interaction**	**Distance (Å)**
SER 383	Halogen (Fluorine)	3.31
MET 384	Sulfur-X	3.27
PHE 102	Pi-Pi T-shaped	4.96
ILE 119	Alkyl	5.46
MET 384	Alkyl	4.64
CYS 386	Alkyl	5.10
LEU 387	Alkyl	3.95
PHE 170	Pi-Alkyl	4.40
PHE 174	Pi-Alkyl	5.11
HIS 178	Pi-Alkyl	5.09
MET 103	Pi-Alkyl	4.34
ILE 105	Pi-Alkyl	5.45

Figure 60: Lists of interactions observed between BB-22, 5F-PB-22, 5F-AKB-48, STS-135 and the CB_1R crystal structure obtained using the molecular docking software Vina.

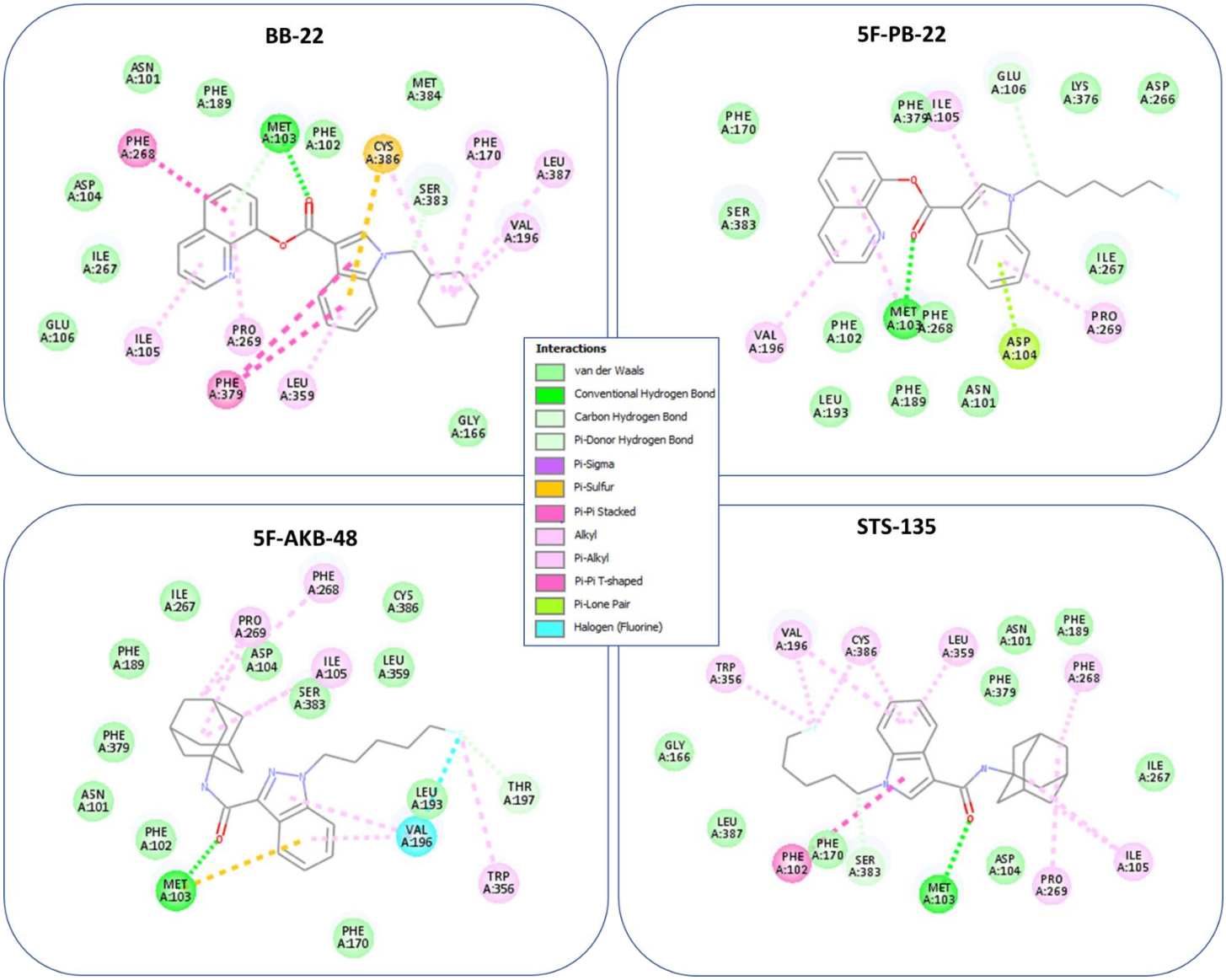

Figure 61: Ligand protein interaction diagrams of BB-22, 5F-PB-22, 5F-AKB-48, STS-135 complexed with the CB_1R crystal structure. The complexes shown are the most favourable poses obtained using the molecular docking software Autodock 4.0.

BB-22		
AUTODOCK 4.0	**Interactions**	
Residues	**Type of interaction**	**Distance (Å)**
CYS 386	Pi-Sulfur	5.40
CYS 386	Alkyl	5.37
ILE 105	Pi-Alkyl	4.33
LEU 359	Pi-Alkyl	5.04
LEU 387	Alkyl	5.13
MET 103	Conventional Hydrogen Bond	2.24
MET 103	Carbon Hydrogen Bond	2.16
MET 103	Pi-Donor Hydrogen Bond	3.11
PHE 170	Pi-Alkyl	5.07
PHE 268	Pi-Pi T-shaped	4.95
PHE 379	Pi-Pi T-shaped	5.53
PRO 269	Pi-Alkyl	5.40
SER 383	Carbon Hydrogen Bond	2.96
VAL 196	Alkyl	4.75
Van der Waals interactions		
ASP 104, ASN 101, PHE 189, PHE 102, MET 384, GLY 166, GLU 106, ILE 267		

5F-PB-22		
AUTODOCK 4.0	**Interactions**	
Residues	**Type of interaction**	**Distance (Å)**
ASP 104	Pi-Lone Pair	2.98
GLU 106	Carbon Hydrogen Bond	3.46
ILE 105	Pi-Alkyl	4.15
MET 103	Conventional Hydrogen Bond	1.97
MET 103	Pi-Alkyl	4.20
PRO 269	Pi-Alkyl	4.39
VAL 196	Pi-Alkyl	5.25
Van der Waals interactions		
PHE 170, PHE 379, LYS 376, ASP 266, ILE 267, ASN 101, PHE 189, PHE 268, PHE 102, LEU 193, SER 383		

5F-AKB-48		
AUTODOCK 4.0	**Interactions**	
Residues	**Type of interaction**	**Distance (Å)**
ILE 105	Alkyl	3.95
MET 103	Conventional Hydrogen Bond	2.56
MET 103	Carbon Hydrogen Bond	2.74
MET 103	Pi-Sulfur	5.75
PHE 268	Pi-Alkyl	4.66
PRO 269	Alkyl	4.86
THR 197	Carbon Hydrogen Bond;Halogen (Fluorine)	2.48
TRP 356	Pi-Alkyl	4.61
VAL 196	Halogen (Fluorine)	3.23
VAL 196	Alkyl	3.95
VAL 196	Pi-Alkyl	4.44
Van der Waals interactions		
PHE 379, PHE 189, ILE 267, ASP 104, CYS 386, SER 383, LEU 359, LEU 193, PHE 170, PHE 102, ASN 101		

STS-135		
AUTODOCK 4.0	**Interactions**	
Residues	**Type of interaction**	**Distance (Å)**
CYS 386	Alkyl	3.68
CYS 386	Pi-Alkyl	4.94
ILE 105	Alkyl	4.08
LEU 359	Pi-Alkyl	4.86
MET 103	Conventional Hydrogen Bond	2.62
MET 103	Carbon Hydrogen Bond	2.61
PHE 102	Pi-Pi Stacked	5.56
PHE 268	Pi-Alkyl	4.59
PRO 269	Alkyl	4.75
SER 383	Carbon Hydrogen Bond	3.24
TRP 356	Pi-Alkyl	3.95
VAL 196	Alkyl	4.33
VAL 196	Pi-Alkyl	5.15
Van der Waals interactions		
GLY 166, PHE 379, ASN 101, PHE 189, ILE 267, ASP 104, PHE 170, LEU 387		

Figure 62: Lists of interactions observed between BB-22, 5F-PB-22, 5F-AKB-48, STS-135 and the CB_1R crystal structure obtained using the molecular docking software Autodock 4.0.

6.24) Comparison among docking outcomes obtained using the CB_1 receptor homology model (Rattus Norvegicus) and the crystal structure of the human CB_1 receptor

Binding modes of representative CB_1 receptor agonists

Overall, the type of interactions and the binding poses generated for each agonist, changed slightly according to the docking programme used (Vina or Autodock 4.0) and the receptor involved (CB_1 homology model or crystal structure). However, the consistency obtained using the same docking program Vina and different receptors (CB_1 homology model or crystal structure) seemed higher compared to that obtained using different docking programs (Vina and Autodock 4.0) and the same receptor (CB_1R crystal structure).

According to Vina outcomes, the indole group of JWH-018 interacted through pi-sigma and alkyl interactions with residues placed on the N-terminal group (Met 103, Met 105) of the homology model (see Figures 45 and 46); and through alkyl and van der Waals interactions with amino acids (Met 103, Ile 105) placed on the N-terminal group of the crystal structure (see Figures 51 and 52). Additionally, the residue Ser 383 of either receptor (homology model or crystal structure) formed hydrogen bond or van der Waals interactions with the indole group of the ligand; while the same type of interaction (pi-sulphur) was observed between Met 384 and the indole group of the ligand in both ligand-protein complexes. Additionally, the pentyl tail of JHW-018 formed alkyl interactions with the helix 3 (Phe 189) and the ECL2 (Pro 269) of either protein; while its naphthoyl group formed hydrophobic interactions with the helix 2 (Phe 170); van der Waals interactions with Trp 356 and alkyl/pi-sulphur interactions with other residues placed on the helix 7 of either receptor. Furthermore, the type of interactions with Val 196 (helix 3) was different (pi-sigma interaction or alkyl interaction) according to the protein involved (homology model or crystal structure respectively) (see Figures 45, 46, 51 and 52).

As regards to Autodock 4.0 outcomes, the binding pose of JWH-018 and the type of interactions with the protein (crystal structure) were slightly different compared to those obtained with Vina docking programme. In detail, alkyl interactions were observed with Met 103, Phe 189, Pro 269 and Val 196; van der Waals interactions with Ile 105, Ser 383 and Trp 356; pi-sulphur interactions with Met 384; and pi-pi T-shaped interactions with Phe 170 (see Figures 53 and 55).

Overall, the binding modes of JWH-018 were supported by mutation studies on the helix 6 (Trp 356) and 3 (Phe 189) and structure–activity relationship (SAR) studies of N-alkyl chain length (Mc Allister et al., 2003; Aung et al., 2000).

According to Vina docking outcomes, when complexed with either receptor (homology model or crystal structure) the agonist WIN-55,212-2, formed pi-sulphur and van der Waals interactions with residues placed on the N-terminal group (Cys 107, Ile/Met 105, Met 103) and helix 2 (Phe 170, Phe 174). Other shared interactions were observed with Ala 380, Ser 383, Met 384, although the nature of interactions was different according to the protein involved (alkyl, hydrogen bond and van der Waals interactions referring to the homology model; and alkyl, van der Waals interactions referring to the crystal structure) (see Figures 45, 46, 51 and 52).

On the other hand, according to Autodock 4.0 outcomes, WIN-55,212-2 showed van der Waals and hydrogen bond interactions with residues placed on the N-terminal group (Ile 105, Met 103) and hydrophobic and van der Waals interactions with amino acids placed on the helix 2 (Ile 169, Phe 170) of the crystal structure. Additionally, other interactions were observed with residues placed on the helix 6 (Trp 356, pi-pi staked) and helix 7 (Phe 379, van der Waals interactions), which were considered crucial for WIN-55,212-2 binding, and were not detected with Vina docking programme (see Figures 53 and 54).

The binding modes of WIN-55,212-2 were supported by relationship (SAR) studies of N-alkyl chain length (Mc Allister et al., 2003) and computational studies where Phe 170 and Phe 174 (helix 2) and Trp 356 (helix 6) were described as interacting residues for WIN-55,212-2 binding (Hua et al., 2016).

According to Vina outcomes, the endocannabinoids anandamide and 2-AG, when complexed with either, the homology model or the crystal structure, shared interactions with the N-terminal loop (Phe 102, met 103) and the ECL2 (Phe 268); while their long aliphatic tails mostly interacted through van der Waals or hydrogen bond interactions with helix 2 (Gly 166, Phe 170) and helix 3 (Thr 197, Val 196). The type of interaction with Tyr 275 (helix 5) was different based on the receptor involved. In detail, anandamide formed van der Waals or alkyl interactions when complexed with either the homology model or crystal structure; while 2-AG formed alkyl, or van der Waals interactions when complexed with either protein. Other van der Waals interactions were observed with residues placed on the helix 6 (Leu 359) and helix 7 (Ser 383, Phe 379) on both ligand-protein complexes (see Figures 45, 46, 51 and 52).

According to Autodock 4.0 results, the compounds anandamide and 2-AG, complexed with the crystal structure, mainly formed hydrophobic interactions with residues placed on the N-

terminal loop (Phe 102, Met 103), the ECL2 (Phe 268) and the 3, 5, 6 and 7 helices, consistent with those obtained with the docking programme Vina. By contrast, no interactions were observed with the helix 2 and an additional relevant alkyl interaction was observed between Phe 189 and anandamide which was not detected with Vina docking programme (see Figures 53 and 54). Overall, these results were in line with those described by Hua et al. (2016) and were in accordance with mutation studies by which Tyr 275 (consistent with Vina and Autodock 4.0 outcomes) and Phe 189 (consistent with Autodock 4.0 outcome) were key residues for anandamide binding (Mc Allister et al., 2003).

According to Vina docking outcomes, Δ9-THC and CP-55,940 complexed with either, the homology model or the crystal structure, had their rings placed between the N-terminal loop and the second extracellular loop (ECL2), and they shared hydrophobic interactions with Met 103, Phe 102, Met/Ile 105 and Phe 268. Other van der Waals interactions were observed between CP-55,940 and the 3 and 7 helices (Phe 189; Ser 383), while hydrophobic interactions were detected with the helix 2 (Phe 170) and helix 5 (Tyr 275). Referring to the crystal structure-Δ9-THC complex, van der Waals and alkyl interactions were observed with some residues considered crucial for ligand binding (Ser 383 and Phe 174), while no interaction with Phe 174 was detected on the complex with the homology model (Vina outcomes) (see Figures 45, 46, 51, 52).

On the other hand, according to Autodock 4.0 results, CP-55,940 complexed with the crystal structure, showed relevant alkyl interactions with Phe 189 and Phe 268 and hydrogen bond interactions with Ser 383; while Δ9-THC formed crucial alkyl interactions with Leu 193 as well (see Figures 53 and 54).

These results were supported by those described by Hua et al. (2016) and were in accordance with mutation studies by which Phe 189, Ser 383, Phe 268, Ile 271, Tyr 275 were described as key residues for CP-55,940 binding; while Ser 383, Phe 174 and Leu 193 were reported to be crucial residues for Δ9-THC binding recognition (Shim et al., 2006; Shao et al., 2016).

Binding modes of representative CB_1 receptor antagonists

Referring to the CB_1 antagonists, the docking outcomes slightly changed according to the docking programme used (Vina or Autodock 4.0) and the receptor involved (CB_1R homology model or crystal structure).

According to Vina outcomes, AM-251 complexed with either, the homology model or the crystal structure, showed alkyl interactions with residues placed on the N-terminal loop (Phe

102, Met 103) and pi-sulphur or van der Waals interactions with |Met/Ile 105 according to the protein involved (CB_1R homology model or crystal structure). In detail, the dichlorophenyl group of AM-251 complexed with either protein, interacted through hydrophobic and van der Waals interactions with the helix 2 (Phe 170, Phe 174); and through alkyl interactions with Leu 359 (helix 6), Leu 387 (helix 7) and the N-terminal loop (Phe 102). Additionally, the iodophenyl group of the ligand formed alkyl and hydrophobic interactions, or van der Waals and alkyl interactions with Leu 193 and Val 196, when the ligand was complexed with either the homology model or the crystal structure; while alkyl interactions with Leu 359 and Phe 268 and pi-sulphur interactions with Cys 386 (helix 7) were observed on both ligand-protein complexes. The type of interaction with Trp 356 (helix 6) was different based on the receptor involved. In detail, the iodophenyl group of AM-251 formed van der Waals or alkyl interactions when the ligand was complexed with either the homology model or the crystal structure. Additionally, the pyrazole ring of AM-251 interacted through hydrogen bond interactions and alkyl interactions with Ser 383 and Phe 379 (helix 7) of both proteins; and formed pi-sulphur and alkyl interactions or van der Waals and hydrogen bond interactions with the N-terminal group (Met/Ile 105, Met 103) according to the type of protein complexed with the ligand (homology model or crystal structure) (see Figures 47, 48, 55 and 56).

On the other hand, Autodock 4.0 outcomes obtained with the crystal structure, were slightly different compared to those obtained with Vina docking programme. In detail, the dichlorophenyl group of AM-251 did not interact with the helix 2 and showed alkyl and van der Waals interactions with the helix 3 (Leu 193, Thr 197), while forming alkyl interactions with the helix 5 (Trp 279). Additionally, some interacting residues were the same detected with Vina docking programme and included Leu 359 (alkyl interaction), Cys 386 (sulphur interaction), Phe 102 (van der Waals interaction). On the other hand, the interactions with the iodophenyl group of AM-251 were different compared to those detected with Vina docking programme and involved hydrophobic and van der Waals interactions with the helix 2 (Phe 170, Gly 166), alkyl interaction with the 3, 7 helices (Val 196, Leu 387), and hydrophobic interactions with the helix 6 (Trp 356); while the pyrazole ring, consistently with Vina outcomes, mainly interacted with the N-terminal loop through alkyl interactions (Met 103) and with the helix 7 (Phe 379) through van der Waals interactions (see Figures 57 and 58).

According to the high structural similarity of AM-251 with Rimonabant, several interactions considered crucial for rimonabant binding recognition (Mc Allister et al., 2003; Shim et al., 2012) were detected and involved the following residues: Leu 193, Phe 379, Phe 170, Trp 356,

Cys 386 (Vina and Autodock 4.0 outcomes); Phe 189, Trp 279, Thr 197 (Autodock 4.0 outcomes); Phe 174 (Vina outcomes).

According to Vina outcomes obtained with either protein (CB_1 receptor homology model or crystal structure), the antagonist rimonabant shared several identical interacting residues with AM-251 and principally interacted through hydrophobic interactions, with amino acids placed in the N-terminal loop, the ECL2, and the 3, 6, 7 helices. In detail, when the ligand was complexed with the homology model, the chlorophenyl group formed pi-sigma and alkyl interactions with the helix 3 (Leu 193, Val 196), van der Waals interactions with the helix 6 (Trp 356), hydrogen bond interactions with the helix 7 (Ser 383), and alkyl interactions with the ECL2 (Phe 268). Slightly different type of interactions involving the same residues, were observed when the ligand was complexed with the crystal structure. In detail, alkyl interactions were detected with the helix 3 (Leu 193, Val 196), van der Waals interactions with the 6 and 7 helices (Trp 356, Ser 383) and alkyl interactions with the ECL2 (Phe 268). Additionally, the pyrazole ring mainly interacted with the N-terminal loop (Met 103) through alkyl interactions on both complexes, while sulphur or van der Waals interactions were detected with Met/Ile 105, based on the protein involved (homology model or crystal structure). Moreover, the dichlorophenyl group of rimonabant, primarily interacted through pi-pi interactions with the helix 2 (Phe 170) and alkyl interactions with the helix 7 (Leu 387), on either complex (rimonabant-homology model or rimonabant-crystal structure) (see Figures 47, 48, 55 and 56).

Autodock 4.0 results were slightly different from Vina outcomes. In detail, the chlorophenyl group of rimonabant formed van der Waals interactions with Phe 170 and Ser 383, and alkyl interactions with Val 196 and Leu 387; its dichlorophenyl group formed van der Waals interactions with Leu 193, alkyl interactions with Trp 279, Trp 356, Leu 359 and halogen interaction with Cys 386; while its pyrazole ring mainly interacted with the N-terminal loop (Phe 102, pi-pi hydrophobic interaction) and the ECL2 (Phe 268, van der Waals interactions). (see Figures 57 and 58).

Overall, consistent with mutation studies (Shim, 2010; Mc Allister et al., 2003), rimonabant showed interactions with residues considered crucial for rimonabant binding recognition, including Leu 193, Phe 379, Phe 170, Cys 386 (Vina and Autodock 4.0 outcomes) and Phe 189, Trp 279 (Autodock 4.0 outcomes). Additionally, these results were in line with those described by Hua et al. (2016) by which Phe 268, Leu 359, Cys 386, Trp 356, Val 196, Ser 383, Phe 170, directly interacted with rimonabant.

According to Vina outcomes, the antagonists otenabant and taranabant complexed with either, the homology model or the crystal structure, shared relevant interactions with some residues considered crucial for rimonabant binding recognition (Shim, 2010; Mc Allister et al., 2003) and in line with those described by Hua et al. (2016). In detail, otenabant complexed with either protein, the homology model or the crystal structure, shared alkyl interactions with Phe 268, Leu 359, Trp 356; hydrophobic interactions with Val 196, Phe 170 and van der Waals interactions with Phe 174. By contrast, the type of interactions with Ser 383 and His 178 were different (hydrogen bonds or van der Waals interactions) depending on the protein involved (homology model or crystal structure). On the other hand, taranabant when complexed with the homology model, formed van der Waals interactions with Cys 386, Val 196, Phe 170, Phe 174 and a hydrogen bond interaction with Ser 383; while, when complexed with the crystal structure, it formed van der Waals interactions with Cys 386; pi-alkyl interactions with Val 196 and Phe 174; pi-pi hydrophobic interactions with Phe 170; and van der Waals interactions with Ser 383 (see Figures 47, 48, 55 and 56). Autodock 4.0 outcomes related to otenabant and taranabant, were quite different from Vina outcomes. However, Phe 170, Phe 174, His 178 seemed to be interacting residues for both compounds, consistently with Vina outcomes and previous computational studies (Hua et al., 2016). In detail, otenabant formed hydrophobic interactions with Phe 170 and van der Waals interactions with Phe 174; while taranabant interacted through alkyl interactions with His 178 and Phe 174, and through van der Waals interactions with Phe 170 (see Figures 57 and 58).

Referring to Vina outcomes, the compound AM-6358 formed alkyl and pi-sulphur interactions with the N-terminal group (Met 103, Met/Ile 105) when complexed with the homology model, and van der Waals and hydrogen bond interactions with the same residues when complexed with the crystal structure. Additionally, AM-6358 complexed with either protein, the homology model or the crystal structure, shared hydrophobic and van der Waals interactions with the helix 2 (Phe 170, Phe 174, Gly 166, Ile 271), hydrogen bond and van der Waals interactions with the helix 3 (Thr 197, Leu 193); van der Waals interactions with helix 5 (Tyr 275, Trp 279), alkyl interactions and van der Waals interactions with the helix 6 (Leu 359, Trp 356); sulphur interactions with the helix 7 (Cys 386); van der Waals interactions with the ECL2 (Phe 268, Ile 271) (see Figures 47, 48, 55 and 56). On the other hand, Autodock 4.0 results (ligand interactions and binding pose) were slightly different from Vina outcomes. In detail, AM-6358 formed alkyl, hydrogen bond and van der Waals interactions with the N-terminal loop (Met 103, Ile 105); hydrophobic and alkyl interactions with the helix 2 (Phe 170, Phe 174), alkyl and

van der Waals interactions with the helix 3 (Val 196, Leu 193); hydrogen bond interactions with the helix 5 (Trp 279); pi-alkyl and van der Waals interactions with the helix 6 (Leu 359, Trp 356); sulphur interactions with the helix 7 (Cys 386) and hydrophobic interactions with the ECL2 (Phe 268) (see Figures 57 and 58).

Overall, most of the interacting residues obtained with Vina and Autodock 4.0 programs, were in line with those described by Hua et al. (2016) and these docking results were supported by previous studies by which mutagenesis of Phe 170 and Phe 174 caused a dramatic decrease of functional affinity for AM-6538 (Mc Allister et al., 2003; Hua et al., 2016).

Binding modes of novel synthetic cannabinoids

Referring to Vina outcomes, when complexed with the CB_1R homology model, the indole group of BB-22 formed hydrogen bond and hydrophobic interactions with residues placed on the N-terminal loop (Met 103, Phe 102, respectively); its cyclohexyl methyl group interacted through alkyl interactions with the helix 2 (Phe 170), helix 3 (Val 196), helix 7 (Leu 387); while its quinolinyl group formed alkyl and hydrophobic interactions with the ECL2 (Pro 269, Phe 268); and alkyl and van der Waals interactions with the N-terminal loop (Met 105, Glu 106, Asp 104, Asn 101) (see Figures 49 and 50). On the other hand, when complexed with the CB_1R crystal structure, BB-22 showed several interactions with the same residues as those observed on the complex with the homology model; although the types of interactions were slightly different. In detail, the indole group of BB-22 interacted through alkyl and van der Waals interactions with residues placed on the N-terminal loop of the receptor (Met 103, Phe 102, respectively); its cyclohexyl methyl group formed alkyl and van der Waals interactions with the ECL2 (Phe 268, Pro 269, respectively) and the N-terminal loop (Asp 104); its quinolinyl group formed alkyl interactions with the helix 3 (Val 196) and helix 7 (Leu 387); van der Waals interactions with the helix 6 (Trp 356, Leu 359, respectively) and helix 2 (Phe 170, Ile 169), and pi-sulphur interactions with the helix 7 (Cys 386) of the crystal structure (see Figures 59 and 60).

On the other hand, Autodock 4.0 results (ligand interactions and binding pose) were slightly different from Vina outcomes. In detail, the indole group of BB-22 interacted through hydrophobic and pi-sulphur interactions with the helix 7 (Phe 379, Cys 386, respectively) and alkyl interactions with the helix 3 (Leu 359); its cyclohexyl methyl group interacted through alkyl interactions with the helix 3 (Val 196), helix 2 (Phe 170) and helix 7 (Leu 387); while its quinolinyl group formed mainly interactions with the helix 2 (Phe 268, Pro 269) and van der

Waals interactions with the N-terminal loop (Asn 101, Asp 104, Glu 106) (see Figures 61 and 62).

According to Vina outcomes obtained with either protein (CB_1 receptor homology model or crystal structure), the indole group of 5F-PB-22 interacted with the N-terminal loop through hydrogen bond and hydrophobic interactions (Met 103, Phe 102), its fluorinated pentyl tail interacted with the helix 3 (Val 196; halogen interaction), and helices 5 and 6 (Trp 279, Trp 356; alkyl interactions); while its quinolinyl group formed hydrophobic interactions with the helix 2 (Pro 269) and the N-terminal loop (Met/ile 105; alkyl interactions) (See figures 49, 50, 59 and 60). On the other hand, Autodock 4.0 results (ligand interactions and binding pose) were slightly different from Vina outcomes. Specifically, the indole group and the pentyl tail of the ligand mainly interacted with the ECL2 (Ile 267, Pro 269) and the N-terminal loop (Asp 104, Ile 105, Glu 106); while the quinolinyl group formed alkyl interactions with the helix 3 (Val 196), and van der Waals interactions with the helices 2 (Phe 170) and 7 (Phe 379, Ser 383) (see Figures 61 and 62).

Referring to Vina outcomes, 5F-AKB-48 and STS-135, when complexed with the homology model, presented almost identical binding poses. In detail, their indazole and indole groups formed mainly hydrophobic interactions with the N-terminal group of the receptor (Phe 102, Met 103) and the helix 3 (Val 196); their fluorinated pentyl tail interacted mainly through alkyl interactions with the helix 6 (Trp 356) and through van der Waals interactions with the helix 7 (Cys 386, Leu 387); while their adamantyl groups mostly formed alkyl interactions with the helix 6 (Leu 359, Met 363) and helix 5 (leu 276, Trp 279) and van der Waals interactions with the helix 3 (Thr 197) (see Figures 49 and 50).

When complexed with the crystal structure, 5F-AKB-48 and STS-135 binding poses were slightly different between each other, and showed similar interactions as those observed with the homology model. In detail, their indazole and indole groups mainly interacted with the N-terminal loop through hydrophobic interactions (Met 103, Phe 102, Ile 105); their fluorinated pentyl tails interacted primarily through alkyl interactions with the helix 2 (Phe 170) and helix 7 (Leu 387, Cys 386); while their adamantyl groups formed alkyl interactions with the helix 2 (Phe 174, His 178) (see Figures 59 and 60).

On the other hand, Autodock 4.0 results were slightly different from Vina outcomes. In detail, the indazole group of 5F-AKB-48 interacted with the N-terminal loop (met 103: pi-sulphur interaction) and the helix 3 (Val 196: alkyl interaction); its fluorinated pentyl tail formed

interactions with the helix 3 (Leu 193, Val 196, Thr 197) and helix 6 (Trp 356); while the adamantyl group formed mostly alkyl interaction with the helix 2 (Phe 268, Pro 269) and van der Waals interactions with the helix 7 (Phe 379, Ser 383). Referring to STS-135, the indole group interacted with the N-terminal loop (Phe 102: hydrophobic interaction), while its fluorinated pentyl tail showed alkyl interactions with the helix 3 (Val 196), helix 6 (Trp 356) and helix 7 (Cys 386). Furthermore, the adamantyl group of the ligand formed mostly alkyl interactions with the helix 2 (Phe 268, Pro 269) (See Figures 61 and 62).

Notably, the novel aminoalkylindole derivatives under study, interacted with some residues belonging to the same binding pocket observed for other aminoalkylindoles such as WIN-55,212-2, and described for the antagonist/inverse agonist Rimonabant (Mc Allister et al., 2003, Shim et al., 2006; Shim et al., 2012).

6.25) Vina and Autodock binding energies against experimental K_i values: comparison between outcomes obtained with the CB_1R homology model and the crystal structure

According to our findings, the binding energies obtained with Vina and Autodock 4.0 programs, did not correlate with the experimental K_i values, regardless which protein was employed in our docking studies (homology model or crystal structure). The results of this studies highlighted some limitations and shortcomings that can be ascribed to a combination of factors. In detail, both Vina and Autodock 4.0, do not include receptor motion during docking process and docking accuracy could be affected by the fact that upon ligand binding, the binding site may undergo a conformational change that these docking programs are not able to predict. Additionally, they employ simplified scoring functions and the number of degrees of freedom applied to the ligands is necessarily limited with errors on estimated binding energies around 2–3 Kcal/mol (Forli et al., 2016).

Referring to Vina only, some other limitations include the use of implicit hydrogens and spherically symmetric hydrogen bond potentials, while no electrostatic contribution or atomic charges are considered. On the other hand, Autodock 4.0, unlike Vina, includes explicit polar hydrogens and electrostatics; and uses a directional hydrogen-bonding term (Forli et al., 2016), however several limitations are encountered when ligands contain more than about eight torsion angles. More advanced tools and scoring function optimization could be necessary to predict binding energies more accurately (Forli et al., 2016).

6.26) SCs and CB_1 receptor docking studies: Conclusions

In the past decades, the high-speed synthesis of NPS has revolutionized the drug scenario, raising the urge to identify potential drug targets and investigate drug-target protein chemical interactions aiming to provide a rationale for different biological effects that specific NPS exert. Not surprisingly, molecular docking has been successfully used in recent years to predict the 3D structure of a range of drug-target complexes in order to find a biological/chemical explanation behind the pharmacological effects of specific drugs. In our initial studies, the index novel SCs were docked against a homology model, and the highest-ranking poses were analysed for ligand interactions. Subsequently, the CB_1 receptor crystal structure was released and the docking screen and ligand interaction analysis were repeated. The opportunity to investigate how homology model interacted with these compounds compared to crystal structure, and how different docking programme packages (Vina and Autodock 4.0) modify the results, allowed us to predict drug-target complex 3D structures and related intermolecular interactions, with appreciable accuracy. Notably, in view of some limitations inherent to our docking approaches, all results must be regarded as preliminary findings requiring further optimization with more sophisticated tools.

Initially, our docking approach was validated by the evidence that the binding properties of representative CB_1 receptor agonists and antagonists were consistent with those described in previous mutation and molecular modelling studies. However, the lack of correlation between binding energies (obtained with both docking programmes and both receptors) and experimental K_i values highlighted some limitations inherent to our docking approach, leading us to regard our outcomes as preliminary evidences that must to be approached with caution, and from which other insights may be conceived.

According to our findings, the docking programme Vina generated similar binding poses against the homology model and the crystal structure, suggesting that both models were useful for scoring and pose selection for virtual screening. On the other hand, slightly different interactions were observed with the docking programme Autodock 4.0, highlighting some differences in binding pose calculations.

Despite the binding poses of each compound slightly changed according to the docking programme used and the protein involved (homology model, crystal structure), they were characterised by common interactions with amino acid residues that participate as interacting

residues, suggesting with some approximation, the putative potential binding mode and properties of these compounds.

Based on the docking results, the novel aminoalkylindole derivatives under study (BB-22, 5F-PB-22, 5F-AKB-48, STS-135), all share the same binding pocket and formed mainly hydrophobic interactions with residues placed on the helices 2, 3, 6, 7, the ECL2 and the N-terminal loop. Common interacting residues detected with both docking programmes and both proteins, included Met 103, Phe 102, Phe 170, Phe 379, Ser 383; while all novel SCs, except for 5F-PB-22 formed interactions with Cys 386.

On the other hand, the agonists analysed, showed different interactions according to their chemical properties. Notably, the agonists belonging to the aminoalkylindole class, such as JWH-018 and WIN-55,212-2, shared some interacting residues (e.g. Met 103, Phe 170, Ser 383) with the index SCs in our study; while agonists belonging to the endocannabinoid class like anandamide, showed additional crucial interactions with the helix 5 (Tyr 275) that were not observed with the aminoalkylindole class compounds. On the same path, the agonist CP-55,940 (non-classical SC) showed interactions with Ile 271, which, according to mutation studies, is a crucial residue for CP-55,940 (Shao et al., 2016), but not for AAI recognition. Notably, this key interaction was detected only by the docking programme Vina, suggesting that it seemed to perform better compared to Autodock 4.0.

Referring to the antagonists, some interacting residues detected for rimonabant, AM-251, AM-6358, were the same as those observed for the novel SCs under study (e.g. Met 103, Phe 170, Ser 383), with the evidence of additional interactions with residues such as Leu 193, Phe 379, Trp 356, considered key residues for rimonabant binding and analogues (Mc Allister et al., 2003; Shim et al., 2012).

Overall, our docking outcomes provided new insights into the binding properties of the index SCs in our study, and suggested the evidence of a shared CB_1R binding pocket, composed by residues considered crucial for AAI recognition, and which overlaps to some extent, with that observed for other CB_1 agonists and antagonists. Additionally, it was found that using different proteins (homology model and crystal structure) produced consistent Vina outcomes; while Autodock 4.0 findings were slightly different compared to Vina results. Further advanced studies are needed to better predict the correct binding pose and ligand interactions for all compounds detected.

Chapter 7: Web-based study on 4,4′-Dimethylaminorex misuse

Role played by the internet on NPS marketing and use

The internet and social media play a key role in the distribution and marketing of NPS drugs. The anarchic nature of online markets is gradually changing the illegal drug scenario due to the availability of several communicative and interactive tools (e.g. blogs and fora) which allow the easy distribution of drugs with convincing and attractive marketing approaches, and provide novel opportunities for individuals all over the world to share information and experiences related to NPS. The fast-growing popularity of online drug market-places has been fuelled by a convergence of factors, including: relative anonymity, wide variety of available drugs, interactivity, online large-scale distribution, facilitation of multi-media news. Internet purchase has been reported as a crucial factor that drives users to consume NPS and represents a challenge for control policies and enforcements as the huge size and ever-changing content of the Internet interferes with the constant monitoring of drug-related websites (Dargan and Wood, 2013).

Among the social media users, the 'psychonauts' possess large levels of technical and/or pharmacological knowledge regarding NPS and share information on their patterns of use, reasons for using them, desirable effects, dosages, routes of administrations, drug sourcing mechanisms etc. (Orsolini et al., 2015). However, many of these sites include claims from enthusiasts that give poor advice and misjudge risks (Khey et al., 2013). Although social communities are virtual they can influence many aspects of the members' behaviour including initiation of use, altered perceptions, modification of favourite drugs (Kozinets, 2002; Loi et al., 2017). The virtual communities in general are conceived as a new aspect of social existence, characterised by its own distinctive style of interaction, and mode of personal communication. The interest in online communities has given rise to a new qualitative method called 'netnography', devised specifically to investigate the cultures and behaviours present on the Internet (Kozinets, 2016). The netnography approach may be really useful to gain some insights into some clinical and psychopharmacological aspects pertaining to the NPS drugs.

7.1) Web-based study on 4,4′-Dimethylaminorex misuse: aim

Our study aimed at describing, through an assessment of related anecdotal online reports, a range of clinical and pharmacological issues related to 4,4'-DMAR misuse, additionally reviewing the available evidence-based literature on this topic (Loi et al., 2017).

7.2) Web-based study on 4,4′-Dimethylaminorex misuse: methods

Peer-reviewed papers and online reports focused on 4,4′-DMAR misuse issues, were identified by performing a wide-range search on the Embase, Google Scholar, Scopus; and Pubmed/Medline databases typing the following key words: (4,4′-DMAR) AND (abuse OR misuse OR poisoning OR dependence OR addiction). The search focused on both preclinical and clinical data and covered the period up to November 15, 2016 (Loi et al., 2017). An additional web-based qualitative/observational approach was undertaken to identify information on 4,4′-DMAR misusers' first-hand experiences. To this end, between March and October 2016, multiple qualitative Google searches were carried out, using key words such as '4,4′-DMAR and abuse', '4,4′-DMAR and misuse'; '4,4′-DMAR and experience'; 'Serotoni and forum'; 'Speckled Cherry forum'; 'Speckled Cross forum'; 'Para-Methyl-4-Methylaminorex forum'; '4-methyl-euphoria forum'; '4-methyl-U4Eu forum'; '4,4-dimethylaminorex forum'. The first two pages/20 hits per keyword were considered and a range of websites was later excluded, because not pertinent; being duplicates; or requiring a registration or payment procedure (Loi et al., 2017). Overall, six websites hosting forum activity on 4,4′-DMAR use were identified: https://www.chemsrus.com; https://www.reddit.com; https://www.ukchemicalresearch.org; http://www.bluelight.org; http://www.psychonaut.com/forum.php; and https://drugs-forum.com. In total, 20 detailed posts focusing on 4,4′-DMAR use were found and individually analysed by identifying the common topics of discussion including: routes of administration (ROAs) and doses; desired effects; adverse effects; comparisons with other substances; concurrent intake with other drugs; medication use to counteract 4,4′-DMAR action; overall impression; and availability of harm-reduction messages (Loi et al., 2017).

7.3) Web-based study on 4,4′-Dimethylaminorex misuse: results

Literature identification analysis

The critical analysis was undertaken on 13 peer-reviewed papers and 3 reports (ACMD, 2014[c]; EMCDDA and Europol, 2014) identified with the comprehensive literature search above described. According to the evidence-based literature, the most widely used routes of administration (ROAs) were nasal insufflation and ingestion, followed by inhalation and injection; while commonly reported desired effects included: euphoria, disinhibition, increased energy and confidence (ACMD, 2014[c]; EMCDDA and Europol, 2014; Loi et al., 2017). Oral dosages were reported ranging from 10 to 200 mg, while the insufflated ones varied from 10

to 65 mg (ACMD, 2014; Coppola and Mondola, 2015). Reported untoward effects included: hyperthermia, sweating, tachycardia, nausea, dysphoria, psychosis (Coppola and Mondola, 2015; Cosbey et al., 2014; Glanville et al., 2015); while desired and undesired effects were often compared to those produced by stimulant drugs such as ecstasy or amphetamine (Schifano et al., 2015 and 2016). 4,4′-DMAR long-lasting stimulants' effects (12–16 hours) were commonly reversed using sedative and anxiolytics (Glanville et al., 2015; Schifano et al., 2016), while combination with other drugs was described causing several intoxication events and fatalities (EMCDDA and Europol, 2014; Glanville et al., 2015; Hentig, 2016). Social cohesion, and harm-reduction advice have been widely described among NPS users (Soussan & Kjellgren, 2016).

Self-reported ROAs and dosages

According to our analysis, dosages and routes of administration were widely debated, with users describing dosages; eventual redosing; and suggesting the optimal combination of ROAs to achieve the pursuit 'high level'. Specifically, dosages and ROAs were reported by 85% of users, with 76% of them describing oral use and dosages ranging from 10 to 120 mg; 12% reporting the intranasal ROA or vaping with dosages in the 10-to 60-mg range; and 12% describing an oral ingestion followed by the intranasal route, or by snorting and vaping (multiple redosing practice). Powder and pellets were the mostly described formulations (Loi et al., 2017).

Self-reported desired and untoward effects

Overall, 70% of users described a range of positive effects including stimulation, energy increase, euphoria, relaxation, increased sociability, empathy, disinhibition, and arousal. By contrast, a range of adverse effects was described by 55% of users and included hallucinations, altered perceptions, insomnia, queasiness, jaw clenching or tension or bruxism, blurry vision, nystagmus, psychosis, confusion, nausea, sweatiness, increased heart rate, and hyperthermia.

The effects of 4,4′-DMAR were compared with those associated with other stimulant consumptions (e.g., 4FA, MDMA, 6-APB, APB, 3-MMC, 4-MMC, MDPV a-PVP, 4-MMA, and MDMA) by 50% of the users (Loi et al., 2017).

Association with other recreational drugs

Understanding the effects of 4,4'-DMAR is complicated by the phenomenon of polydrug use. According to our analysis, some 30% (6/20) of users associated 4,4'-DMAR with other drugs, including alcohol (66%), 6-APB (17%) and phenylpiracetam (17%). The most reported reason

for using alcohol or 6-APB along with 4,4'-DMAR, was the necessity to cope with social anxiety issues (Loi et al., 2017).

Medication(s) self-administered to revert 4,4'-DMAR action

Some users described having trouble falling asleep after using 4,4'-DMAR, and some 20% of users reported the necessity to reverse the long-lasting stimulant effects of 4,4'-DMAR by using sedatives or anxiolytics (e.g., diazepam, zolpidem, trazodone, baclofen, flubromazepam, and etizolam) (Loi et al., 2017).

Overall impression

Some 50% of fora users provided their peers with a positive or a negative overall evaluation of their 4,4'-DMAR personal experiences, aiming at promoting or denigrating the use of this drug. Indeed, most of them described their personal experience as 'awesome', 'clear', 'enjoyable', 'comfortable', 'nice'; while others considered it 'disappointing' compared to their expectations. Other users described their experience using a technical language that involved a reference to the molecule's pharmacodynamics; pharmacokinetics; or addictive liability levels (Loi et al., 2017).

Harm reduction advice

Some 30% of users posted discussions and a range of advices characterised by a general concern for safety and social support aimed at minimizing/preventing drug-related harms, including avoiding polydrug use; being careful about the dosages and the tendency of re-dosing; and being aware of the intensity of the psychoactive effects of 4,4'-DMAR (Loi et al., 2017).

Limitations of the study

This study is characterised by a range of methodological limitations. In detail, only public websites of the surface web were analysed here and further analysis of the deep Web and 'dark net' materials would have provided a wider range of information on this topic (Orsolini et al., 2015); a multilingual analysis approach of a wider sample would have allowed the identification of further data of interest; there is no certainty that multiple discussions were posted by different individuals and an independent verification of the information provided by the fora communities is needed as it cannot completely trusted (Loi et al., 2017).

Ethical considerations

Our research involved the analysis of already existing reports published on public Internet fora. A discrete approach was undertaken, and no interactions with fora members and purchase attempts were made. Users' pseudonyms were not mentioned, and the quotes were slightly changed and not integrally reported to preserve the anonymity of fora members.

Ethics' approval for the observational web-based study on 4,4'-DMAR was granted by the University of Hertfordshire School of Pharmacy Ethics Committee, on December 15th, 2010 (reference code PHAEC/10-42), with a further 5-year extension of the approval having been granted in November 2013.

7.4) Web-based study on 4,4′-Dimethylaminorex misuse: discussion

4,4′-DMAR diffusion in several countries may be associated with its wide web-based distribution and its sought-after stimulant psychoactive effects (EMCDDA and Europol, 2014). Several factors may contribute to the public health threat posed by 4,4′-DMAR use, including drug quality, purity, and concomitant use with other recreational drugs (alcohol, entactogens, stimulants) (EMCDDA and Europol, 2014). A discrete amount of knowledge on 4,4'-DMAR originates from discussions posted by recreational users in widely available online fora, who used these platforms to share information and experiences related to drugs. According to previous published reports (ACMD, 2014; EMCDDA and Europol, 2014), oral ingestion and nasal insufflation were the most widely described way of administrations with dosages in the 10 to 200 mg-range and 10 to 65 mg-range, respectively, and injection practice having been rarely described. In the present study, fora users widely shared their personal 4,4'-DMAR related experiences, with most of the discussions dating back to 2013, before control legislation, and in parallel with the first seizures in the Europe. From 2015 and after control legislation, the online discussion sharply disappeared from the surface Web suggesting the potential move of 4,4′-DMAR-related illicit activities into the "deep Web," as already observed with other controlled substances (Orsolini et al., 2015). Overall, fora users described oral ingestion of powder and pellets at dosages (10-120 mg) consistent with those described in the evidence-based literature; while vaping and snorting ROAs were described in a context of multiple redosing practice, which is considered a quite popular approach according to the literature (Coppola & Mondola, 2015; Cosbey et al., 2014; Glanville et al., 2015). Most of the users in this study had a previous history of drug misuse, while possessing high levels of technical knowledge on drugs (psychonaut profile). The present investigation confirmed that 4,4'-DMAR is a recreational drug with stimulant properties (feelings of stimulation, euphoria,

energy, alertness, and increasing confidence) and pro-social effects (e.g. increased empathy, feelings of friendliness, interpersonal closeness, and openness), closely resembling those of other stimulants (EMCDDA and Europol, 2014). Consistent with previous published reports, the onset of the action seemed to be quite slow (peaking in 2–5 hr) and the stimulant effects quite long-lasting (e.g. 12–16 hr) (Glanville et al., 2015). Adverse effects being described (nausea, dysphoria, agitation, confusion, aggression, sweating, increased heart rate, hyperthermia, dilated pupils, psychosis, hallucinations, insomnia, jaw clench or jaw, tension or bruxism, blurry vision, and nystagmus) were consistent with those reported in previous studies (Glanville et al., 2015) and with 4,4′-DMAR being a MDMA-like compound. Poly-drug use was described by 30% of users, arising a reason for particular concern, resulting from the ingestion of 4,4'-DMAR with other serotonergic or dopaminergic compounds (Coppola & Mondola, 2015) and potentially responsible for disturbingly high rate of 4,4′-DMAR fatalities (EMCDDA and Europol, 2014). Notably, to counteract the long-lasting stimulant effects, 20% of users here, used a range of sedatives, potentially adding further health risks to the already risky practice of consuming 4,4′-DMAR (Loi et al., 2017).

Overall this study suggested that fora users cooperate in sharing an extensive range of information on 4,4'-DMAR, having sometimes detrimental consequences on people who may not be fully aware of the potential medical consequences of the compound being ingested. Additionally, the polydrug intake practice may potentially add further health risks, as the pharmacokinetic interactions of 4,4′-DMAR with other substances are not known. Further pharmacological analyses should be performed to better draft a risk profile for this drug and prevention strategies should be developed and promoted (Loi et al., 2017).

Chapter 8: Overall discussion of the PhD project

Over the last decades, the phenomenon of NPS has been constantly evolving and expanding, posing a healthcare challenge over the world. While some legislative interventions have attempted to curb the availability/marketing/abuse of these substances; scientists have tried to gather as much information as possible to gain some understanding into the complex multi-faceted phenomenon of NPS. The integration of knowledge resources coming from different areas of expertise has been providing valuable support against the NPS challenge; however, keeping pace with this highly-dynamic phenomenon turned out to be quite challenging despite the valuable efforts made by competent and experienced professionals.

The present project adopted a multi-disciplinary approach, involving a range of methodologies from different areas of expertise (neurobiology, pharmacology, chemistry, netnography) all engaged to gain some understanding into the complex phenomenon of NPS abuse.

The overall aim of this project was to gain insights into pharmacological, neurochemical and molecular properties of selected NPS in order to provide a reliable background needed for detection, assessment, management of NPS-related harms.

Different substances have been selected as targets for the present project according to their worldwide pattern of diffusion; the numerous toxicity events associated to their use and the lacking scientific knowledge available about them. In detail, the substances under study included the synthetic cannabinoids BB-22, 5F-PB-22, 5F-AKB-48 and STS-135; the synthetic stimulants 2-DPMP, D2PM, 5-IT, 4,4'-DMAR; and the dieting aid compound 2,4'-DNP.

The methods employed were *in vitro* quantitative autoradiography*, in vitro* fast scan cyclic voltammetry*; in vivo* microdialysis*; in silico* molecular docking, and the web-based analysis approach (netnography). The overall studies conducted by our group, branched into different analyses, each one characterised by specific goals and approaches.

Synthetic cannabinoids and CB_1R autoradiography studies: In the present study, the potential binding properties of BB-22, 5F-BP-22, 5F-AKB-48 and STS-135 at the level of CB_1 receptors were investigated. The binding properties of these drugs have been recently fully investigated on tissue homogenates (rat cortical membranes) using the radiolabelled competition binding assay (De Luca et al., 2016). However, the originality of our study lied in the methodological approach used in the binding analysis of the novel SCs. In detail, we employed the ARG procedure which is a refined method used to establish the anatomical distribution of drug-target interactions in specific areas of coronal brain sections (cortex and CPu) with the advantage of

preserving tissue architecture. Consistent with the experiments performed on cortical tissue homogenates, competition binding assay studies have been performed. As expected, our results were consistent with previous homogenate study findings, by which all index SCs in our study were described as high-affinity agonists at CB_1 receptors, with BB-22 and 5F-PB-22 showing higher affinities compared to 5F-AKB-48 and STS-135.

The quantitative image-based data of the binding of these drugs at the level of CB_1 receptors from intact brain tissue (brain slices), provided a support and a further contribution to the existing knowledge-base with additional information on the anatomical distribution of the radioligand displacement mediated by these SCs, and allowed a comparative analysis of the displacement in different cerebral regions of the brain sections (Cortex and CPu).

Synthetic cannabinoids and NMDAR autoradiography studies: In this study, the potential binding properties of the same SCs at the level of glutamate NMDA receptors were investigated in cortical and striatal brain slices. The rationale behind this study was related to the necessity to discover the underlying pharmacological mechanism responsible for several hallucinogenic events experienced by SC users. Hallucinations may indeed result from NMDAR dysfunction, which has been previously described as a potential and specific hallucinatory mechanism (Rolland et al., 2014). The originality of our study lays in the fact that no published information was available, at the time of our study, on the activity of these novel SCs at the level of the NMDAR. According to our findings, all synthetic cannabinoids tested were not able to compete with the high affinity and selectivity NMDAR radioligand, rejecting the hypothesis of potential binding of these SCs to the NMDA receptors at all concentrations investigated. These findings provide a valuable contribution to the existing knowledge-base, leading us to consider alternative mechanisms responsible for hallucinogenic events (serotoninergic, dopaminergic, or pure CB_1 mediated dis-inhibitory or inhibitory mechanisms of other pathways). Further investigations are needed to determine which one of these hypotheses would be the most valid one.

Synthetic stimulants and DAT autoradiography studies: This study aimed to investigate the potential binding properties of 5-IT and 2-DPMP at the level of the DAT, in rat brain slices using the autoradiography procedure. Previous *in vitro* studies confirmed that 5-IT can cause a reversible inhibition of MAO_A enzymes (Herraiz and Brandt, 2014) and it behaves as a full efficacy releasing agent at the level of DAT and NET (Marusich et al., 2016). Additionally, 2-DPMP was found to be a potent dopamine and norepinephrine reuptake inhibitor without releasing properties (Simmler et al., 2014) able to stimulate evoked dopamine efflux in NAc

brain slices to a greater extent compared to cocaine (Davidson and Ramsey, 2012). Notably, the monoamine uptake transport inhibition and releasing properties of 5-IT were monitored using *in vitro* release assays in brain synaptosomes (Marusich et al., 2016), while 2-DPMP studies have been conducted in embryonic kidney 293 cells (HEK 293) (Simmler et al., 2014) and in brain slices using the FSCV procedure (Davidson and Ramsey, 2012). The originality of our study lays in the methodological approach used. The binding properties of these drugs were indeed investigated for the first time in brain slices using the autoradiography procedure rather than the brain synaptosome-based approach (Marusich et al., 2016) or the embryonic kidney 293 cells-based analysis (Simmler et al., 2014). To this aim, we decided to perform the ARG procedure in specific areas of coronal brain sections and we employed the competition binding assay approach. The target regions examined were the striatum and NAc shell which exhibit a high expression of dopamine transporters.

Consistent with previous *in vitro* studies, 5-IT and 2-DPMP behaved as highly potent DAT ligands able to compete with the radioligand of [^{125}I]RTI-121 in a concentration-dependent way in CPu and NAc brain slices. Notably, 2-DPMP could displace the radioligand in both cerebral regions, starting from lower concentrations (0.3 µM) compared to 5-IT (1 µM in the NAc shell and 3.0 µM in the CPu). On the other hand, higher concentration of 5-IT (10 and 30 µM) in both areas caused a comparable displacement as 2-DPMP. The quantitative image-based analysis of the binding of these drugs at the level of DAT from intact brain tissue (brain slices), provided a support and a further contribution to the existing knowledge-base with additional information on the anatomical distribution of the radioligand displacement mediated by these synthetic stimulants, and allowing a comparative analysis of the displacement in different cerebral regions of the brain sections (CPu and NAc shell).

BB-22 fast scan cyclic voltammetry studies: This study aimed to investigate the effects of BB-22 on evoked DA efflux and DA re-uptake half-life in brain slices containing the NAc. Using brain slices limited the investigation of dopamine dynamics in the NAc shell, avoiding the potential influence of other regions of the reward system. The originality of this study lays in the rationale of our purpose of research based on the hypothesis that part of the rewarding actions of BB-22 could be mediated via direct interactions on synaptic processes within the NAc shell not necessarily mediated by CB_1 receptors. According to our findings, local application of the synthetic cannabinoid BB-22 in brain slices was not able to change evoked DA efflux and dopamine reuptake time-constant in the NAc shell at any doses tested. This finding would suggest the relative contributions of complex neuronal circuits, either within or

outside the NAc, that may represent critical pathways accounting for some of the rewarding properties of BB-22 exposure. Notably, this mechanism would potentially rely on the integrity of DAergic projections from the VTA to the NAc which is affected in NAc brain slices. These findings contributed to the existing body of knowledge, allowing us to support the idea that neuronal circuits outside the NAc are indispensable to mediate *in vivo* DA increase in the NAc shell induced by BB-22; and to discard the hypothesis of any direct action of BB-22 at the level of dopamine transporter in the NAc shell at the doses tested.

SC microdialysis studies: These studies aimed to monitor DA release in three different areas of the reward system (NAc shell, core, and medial PFCx) after acute intravenous administration of BB-22 and only in the NAc shell after acute intravenous administration of 5F-PB-22, 5F-AKB-48 and STS-135, in freely moving adult rats. These specific brain regions were selected as target areas in accordance with their role played in addiction. The originality of this study lays in the type of compounds analysed (third generation SCs) along with the technical procedure employed (*in vivo* microdialysis) and the target cerebral regions assessed. At the time of our studies, no analyses had been performed before, using the same combinations of variables; indeed, our study was the first one to analyse specific aspects of the rewarding properties of these compounds, providing more conceptual thinking and practical proposals in the pharmacological and clinical fields. According to our findings, all SCs tested were able to increase dopamine release in the NAc shell. These results were in line with previous research according to which almost all drugs of abuse are able to increase DA release in the NAc shell (Pontieri et al., 1995; Tanda et al., 1997; Cadoni et al., 2000). Notably, BB-22 and 5F-PB-22, elicited a 50% increase of DA release over basal at the dose of 0.01, mg/kg, i.v., while a dose of 5F-AKB-48 and STS-135 ten and fifteen times higher respectively, was necessary to obtain the same extent of increase on DA release in the NAc shell. Importantly, the same magnitude of increase was previously observed after administration of a dose 100 times higher of Δ9-THC (1 mg/kg, i.v.) (Pistis et al., 2002). Overall, these findings provided the first circumstantial pre-clinical evidence for a greater putative abuse liability of the third generation SCs compared to the natural compound found in Cannabis (Δ9-THC) and this evidence could make a significant contribution to the existing body of knowledge. Researchers and clinicians could indeed use this new data as valid background to develop further experimental analyses (e.g. on behavioural and reinforcing aspects of SC use) and valid strategies (e.g. more suitable therapeutic approaches) against use/abuse of these substances.

2,4-DNP microdialysis studies: These studies aimed to monitor DA release in two different areas of the reward system (CPu and NAC shell) after acute intraperitoneal administration of the dieting aid compound 2,4-DNP. The underlying mechanism causing the abuse of this drug has been widely debated over the years. Despite the widespread use of 2,4'-DNP, no published neurochemical studies up to now have described a central mediation of 2,4-DNP effects (Perry et al., 2013). In view of the above, we hypothesised that some alterations could occur in the reward system following 2,4-DNP exposure. To this end, we used a unique dose of 2,4-DNP (e.g. 20 mg/kg, i.p.) able to cause a moderate increase of temperature without fatal complications (Gatz and Jones, 1970). According to our findings, the acute treatment with 2,4-DNP (20 mg/kg i.p.) did not cause any change in DA release in the NAc shell and CPu, rejecting the hypothesis of psychoactivity of this substance at this specific dose. Although being characterised by some methodological limitations, this study suggested that the abuse of this drug could be simply driven by its dieting aid properties rather than being centrally mediated. The originality of this study lays in the fact that it represented the first attempt to explain the abuse of this drug assuming its potential central activity at the level of the reward system. Although our hypothesis was rejected, our findings represent a valuable contribution to the body of knowledge, because a preliminary evidence of non-psychoactivity has been provided for this drug. However, further neurochemical and pharmacological analyses are needed to confirm this evidence.

D2PM and 2-DPMP microdialysis studies: In our study the pipradrol derivatives 2-DPMP and D2PM, were selected among other stimulants to monitor DA release in two different areas of the reward system: NAc shell, and CPu after their intravenous administration in freely moving rats. Previous *in vitro* pharmacological studies focusing on the effect of these drugs have been performed in brain slices (Davidson and Ramsey, 2012) and in embryonic kidney 293 cells (HEK 293) (Simmler et al., 2014). However, the originality of our study lays in the fact that no *in vivo* studies had been conducted before ours, on the effect of these two drugs on DA release in target areas of the reward system, in freely moving animals. According to our findings, the acute treatment with 2-DPMP (0.5 and 1 mg/kg) elicited a comparable increase of DA release in the NAc shell and CPu, while a dopamine release increase was observed selectively in the NAc shell after injection of the highest dose (3.0 mg/kg, i.v.) of D2PM. These findings provided circumstantial preclinical evidence for a putative effect of these drugs in specific areas of the reward system and may provide a further contribute to the body of knowledge that can

be used to plan new tailored strategies for a more successful abuse management and treatment against the use/abuse of these drugs.

In silico molecular docking studies: These studies aimed to evaluate the intermolecular interactions of the synthetic cannabinoids BB-22, 5F-PB-22, 5F-AKB-48 and STS-135, and other referent compounds (CB_1 agonist and antagonists) within a homology model of the rodent CB_1 receptor and the crystal structure of the human CB_1 receptor. The originality of these studies lays in the fact that no published docking studies were available at the time of our studies on these target drugs (BB-22, 5F-PB-22, 5F-AKB-48 and STS-135) using the same docking approach. These studies contributed to the existing body of knowledge, because they demonstrated that the SCs BB-22, 5F-PB-22, 5F-AKB-48 and STS-135 interact with rodent and human CB_1 receptor residues that, according to previous mutation and computational studies, are considered crucial for aminoalkylindole derivative binding recognition.

The web-based analysis approach: This study aimed at analysing the information provided by the fora communities on 4,4'-DMAR use, additionally critically reviewing the available evidence-based literature on this topic. The originality of this study lays in the fact that no published studies were available at the time of our studies on this topic, using the same methodological approach. According to our findings, fora members co-operate in exchanging an extensive body of knowledge about this drug, and the recurring topics of discussion include: routes of administration and dosages, desired and undesired effects, comparison and association with other drugs and medications, overall impression, provision of harm reduction advice. This approach has contributed to the existing body of knowledge, providing further insights into the clinical and psychopharmacological issues pertaining to 4,4'-DMAR, on which little is known in terms of use/abuse, pharmacology, pharmacodynamics, pharmacokinetics.

To sum up:

- our analytical studies allowed the characterisation of the NPS binding sites providing a detailed and reliable anatomical distribution of the radioligand displacement mediated by the index drugs;
- our neurochemical studies provided some new knowledge into the biological mechanisms of NPS addiction and contributed to our understanding of how these drugs alter functional dopaminergic transmission in the neural systems;

- our docking studies provided new insights into the binding properties of the index SCs in our study, and suggested the evidence of a shared CB_1R binding pocket composed by residues considered crucial for AAI recognition, and which overlaps to some extent, with that observed for other CB_1 agonists and antagonists;
- our web-based studies provided further insights into the clinical and psychopharmacological issues pertaining to the NPS object of our study.

8.1) Conclusions

Overall, drugs of abuse may alter the brain's normal level of biochemical activity through a variety of different mechanisms, complicating the understanding of the role of biology and neurochemistry in drug use and abuse. Specifically, they may affect the synthesis, degradation, release, or reuptake of a neurotransmitter, and mimic or block the action of a neurotransmitter at a receptor in the brain. Since NPS use/abuse is a complex phenomenon involving a complex interaction of biological, neurochemical, environmental factors, the individual analysis of these aspects was crucial to gain a better and wider comprehension on this topic.

Globally, the findings of our study provided some preliminary understandings on:

- how the index drugs work in specific brain regions;
- how they interact with their targets;
- why certain drugs have the potential for abuse;
- what are their psychopharmacological and untoward effects.

All these aspects, provided some insights into neurobiological and pharmacological aspects of the index NPS and helped us to better understand the mechanisms of drug action in the brain. Overall, this knowledge represents a valuable background useful to develop valid strategies against NPS use/abuse.

8.2) Summary of the methodologies employed and analysis of the findings obtained for each drug assessed

BB-22, 5F-PB-22, 5F-AKB-48, STS-135: The biological activity of these synthetic cannabinoids was assessed using autoradiography, *in silico* docking and microdialysis procedures. While the autoradiography studies confirmed the super agonism of the index compounds at the CB_1 receptors and their inactivity at the NMDA receptors, the *in silico*

docking studies provided detailed information on the intermolecular interactions between the novel SCs and the CB_1 receptor, highlighting that crucial residues involved in ligand binding and the active binding pocket at which these drugs display their agonist activity are comparable to those observed for other aminoalkylindole derivatives (e.g. JWH-018). On the other hand, microdialysis studies demonstrated the ability of these drugs to increase DA release in the NAc shell, suggesting the underlying biological mechanism responsible for their putative and addictive properties. *In vitro* FSCV studies have been employed only in the neurochemical analysis of the highest potency, affinity and intrinsic activity CB_1R agonist BB-22. These studies confirmed that the rewarding effects of this drug are highly related to the complex interplay among neural pathways originating from different cerebral areas of the reward system, and no effect can be observed in brain slices where most of these projections have been lesioned. Overall, these outcomes can provide a biological background needed for developing efficient therapeutic approaches finalised to cope with the untoward effects caused by their activity at the level of specific pathways.

2-DPMP and D2PM: The biological activity of the pipradrol derivative 2-DPMP has been assessed using autoradiography and microdialysis procedures. The competition binding data demonstrated that this compound acts at the level of DAT in the NAc, starting from lower concentrations (0.3 μM) compared to D2PM (1 μM) and cocaine (3 μM). This outcome highlights the extreme dangerousness of this drug according to its high abuse potential and monoaminergic activity. Considering these data, clinical interventions can be planned to address sympathomimetic toxidromes and to cope with the persistent duration of the extent of DA signal in the brain caused by this drug. On the other hand, the neurochemical activity of D2PM was assed only using the microdialysis procedure and a DA release was observed selectively in the NAc shell with a delayed onset of effects probably resulting from the presence in its structure of a polar functional group likely responsible for its slow passage through the BBB. Additionally, the involvement of psychoactive metabolites in its central activity cannot be excluded. Although additional studies are needed to better draft a pharmacological profile of these drugs, these preliminary studies can direct prevention strategies towards specific tailored interventions in order to limit the untoward effects caused by the interaction of this drug at the level of DAT.

5-IT: The neurobiological activity of the tryptamine derivative 5-IT has been assessed only using the ARG procedure. According to these studies, a binding of this drug at DAT has been demonstrated, and its effect was notable especially considering that lower

concentrations of 5-IT (1 μm) compared to cocaine (3 μm) were able to displace the radioligand in the NAc. These outcomes highlighted the potential clinical effects caused by this drug which are furthermore exacerbated by its additional activity as inhibitor of MAO activity. Serious sympathomimetic toxidromes may result from its use/abuse and the urge to cope therapeutically with these non-fatal and fatal toxicity events is needed.

2,4-DNP: the neurochemical effect of this dieting aid compound was hypothesised and monitored only using the microdialysis procedure. The absence of psychoactive effects found for this compound suggests that the clinical effects produced by this drug are mainly related to its ability to cause oxidative phosphorylation disruption rather than being centrally mediated. The fatal hyperthermia which can arise after its use, represents a challenging clinical issue and clinicians are currently trying to address this threat by planning tailored therapeutic interventions.

4,4'-DMAR: The psychopharmacological effects of this aminoindane derivative were analysed through a careful observational approach of web fora reports published by 4,4'-DMAR first-hand users. Several topics of discussion (e.g. dosages, ROAs, desired/undesired effects, concomitant use with other drugs/medications, overall impression, harm reduction advice) were identified associated to the use of this substance, and a comparative critical approach was undertaken in view of the existing literature on this topic. Pharmacological effects being described were consistent with 4,4'-DMAR being a monoaminergic releasing agent, and a poly-drug intake practice was described and advised by several users. Detailed recipes with dosages, ROAs and effects over time have been posted. However, some users showed some concerns about the potential harmful effects of this drug and harm reduction advice was observed in several reports along with an overall impression about the effect of this drug. Overall, this study suggested that social communities can have some detrimental effects on members' behaviour and prevention strategies towards the diffusion of misleading information over the Internet should be developed and promoted.

8.3) Future studies

NPS use/abuse/addiction is a phenomenon that cannot be reproduced in a laboratory setting without limitations. However, some of the behavioural characteristics of this drug abuse and addiction can be satisfactorily modelled in laboratory animals and may contribute to the understanding of the neurobiological basis of drug taking behaviour. To this aim, future studies

may employ a drug self-administration model to test whether animals will work (in general, this means to lever press) to obtain the substance and to evaluate the reinforcing properties of the index NPS; a drug discrimination procedure which is a behavioural paradigm based on specific perceptions experienced by animals after drug administration and which helps to predict drug abuse properties and subjective feeling in humans; a conditioned place-preference paradigm that provides information on reward/aversion effects associated to tested drugs in animals. Additional locomotor activity studies may be conducted to provide some information on the level of behavioural stimulation/inhibition caused by the index NPS.

Overall, these studies may help to explain the neurobiological and molecular mechanisms underlying the addictive and reinforcing properties of NPS and are also excellent tools for the investigation of therapeutic agents against NPS use/abuse/addiction.

References

Abouchedid, R., Hudson, S., Thurtle, N., Yamamoto, T., Ho, J. H., Bailey, G., … Dargan, P. I. (2017). Analytical confirmation of synthetic cannabinoids in a cohort of 179 presentations with acute recreational drug toxicity to an Emergency Department in London, UK in the first half of 2015. *Clinical Toxicology*, *55*(5), 338–345. https://doi.org/10.1080/15563650.2017.1287373

ACMD (2009). Consideration of the major cannabinoid agonists - GOV.UK. Retrieved 20 October 2016, from www.gov.uk/.../file/119149/acmd-report-agonists.pdf

ACMD (2010). ACMD advice on 'Ivory Wave'. GOV.UK. Retrieved 12 December 2016, from www.gov.uk/.../file/119135/advice-ivory-wave.pdf

ACMD (2012). Further consideration of the synthetic cannabinoids - GOV.UK. Retrieved 20 October 2016, from https://www.gov.uk/government/publications/acmd-further-consideration-of-the-synthetic-cannabinoid

ACMD (2014[a]). NPS report: tryptamines - GOV.UK. Retrieved 12 December 2016, from https://www.gov.uk/government/publications/nps-reports-on-tryptamines-and-ah-7921

ACMD (2014[b]). 'Third generation' synthetic cannabinoids - GOV.UK. Retrieved 20 October 2016, from https://www.gov.uk/government/publications/third-generation-synthetic-cannabinoids

ACMD (2014[c]). Report summary: synthetic stimulant 4,4'-DMAR - GOV.UK. Retrieved 12 April 2017, from https://www.gov.uk/government/publications/report-summary-synthetic-stimulant-44-dmar

ACMD (2016). 'The Misuse of Drugs (Designation) (Amendment) (England, Wales and Scotland), Order 2016- GOV.UK. Retrieved 20 March 2017, from http://www.tihs.org.uk/strips/14.12.16.html

Agency for Toxic Substances and Disease Registry (1995). Toxicological Profile for Dinitrophenol. Retrieved 14 April 2016, from http://www.atsdr.cdc.gov/toxprofiles/tp64.pdf

Ahn, K. H., Bertalovitz, A. C., Mierke, D. F., & Kendall, D. A. (2009). Dual Role of the Second Extracellular Loop of the Cannabinoid Receptor 1: Ligand Binding and Receptor Localization. *Molecular Pharmacology*, *76*(4), 833–842. https://doi.org/10.1124/mol.109.057356

Alger, B. E. (2002). Retrograde signaling in the regulation of synaptic transmission: focus on endocannabinoids. *Progress in Neurobiology*, *68*(4), 247–286.

Altschul, S. F., Madden, T. L., Schäffer, A. A., Zhang, J., Zhang, Z., Miller, W., & Lipman, D. J. (1997). Gapped BLAST and PSI-BLAST: a new generation of protein database search programs. *Nucleic Acids Research*, *25*(17), 3389–3402.

Ameri, A. (1999). The effects of cannabinoids on the brain. *Progress in Neurobiology*, *58*(4), 315–348. https://doi.org/10.1016/S0301-0082(98)00087-2

Arbo, M. D., Bastos, M. L., & Carmo, H. F. (2012). Piperazine compounds as drugs of abuse. *Drug and Alcohol Dependence*, *122*(3), 174–185. https://doi.org/10.1016/j.drugalcdep.2011.10.007

Arnold, K., Bordoli, L., Kopp, J., & Schwede, T. (2006). The SWISS-MODEL workspace: a web-based environment for protein structure homology modelling. *Bioinformatics*, *22*(2), 195–201. https://doi.org/10.1093/bioinformatics/bti770

Aung, M. M., Griffin, G., Huffman, J. W., Wu, M., Keel, C., Yang, B., … Martin, B. R. (2000). Influence of the N-1 alkyl chain length of cannabimimetic indoles upon CB(1) and CB(2) receptor binding. *Drug and Alcohol Dependence*, *60*(2), 133–140.

Autodock 4.0 manual. Retrieved 15 December 2016, from http://autodock.scripps.edu/faqs-help/manual/autodock-4-0-user-guide/AutoDock4.0_UserGuide.pdf.

Balakumar, C., Lamba, P., Pran Kishore, D., Lakshmi Narayana, B., Venkat Rao, K., Rajwinder, K., … Narsaiah, B. (2010). Synthesis, anti-inflammatory evaluation and docking studies of some new fluorinated fused quinazolines. *European Journal of Medicinal Chemistry*, *45*(11), 4904–4913. https://doi.org/10.1016/j.ejmech.2010.07.063

Banister, S. D., Stuart, J., Kevin, R. C., Edington, A., Longworth, M., Wilkinson, S. M., … Kassiou, M. (2015). Effects of Bioisosteric Fluorine in Synthetic Cannabinoid Designer Drugs JWH-018, AM-2201, UR-144, XLR-11, PB-22, 5F-PB-22, APICA, and STS-135. *ACS Chemical Neuroscience*, *6*(8), 1445–1458. https://doi.org/10.1021/acschemneuro.5b00107

Banks, M. L., Bauer, C. T., Blough, B. E., Rothman, R. B., Partilla, J. S., Baumann, M. H., & Negus, S. S. (2014). Abuse-related effects of dual dopamine/serotonin releasers with varying potency to release norepinephrine in male rats and rhesus monkeys. *Experimental and Clinical Psychopharmacology*, *22*(3), 274–284. https://doi.org/10.1037/a0036595

Bartlett, J., Brunner, M., & Gough, K. (2010). Deliberate poisoning with dinitrophenol (DNP): an unlicensed weight loss pill. *Emergency Medicine Journal*, *27*(2), 159–160. https://doi.org/10.1136/emj.2008.069401

Baumann, M. H., & Volkow, N. D. (2016). Abuse of New Psychoactive Substances: Threats and Solutions. *Neuropsychopharmacology*, *41*(3), 663–665. https://doi.org/10.1038/npp.2015.260

Behonick, G., Shanks, K. G., Firchau, D. J., Mathur, G., Lynch, C. F., Nashelsky, M., … Meroueh, C. (2014). Four Postmortem Case Reports with Quantitative Detection of the Synthetic Cannabinoid, 5F-PB-22. *Journal of Analytical Toxicology*, *38*(8), 559–562. https://doi.org/10.1093/jat/bku048

Belayev, L., Busto, R., Watson, B. D., & Ginsberg, M. D. (1995). Post-ischemic administration of HU-211, a novel non-competitive NMDA antagonist, protects against blood-brain barrier disruption in photochemical cortical infarction in rats: a quantitative study. *Brain Research*, *702*(1), 266–270.

Bellucci, G. (1955). [(2-Diphenylmethyl-piperidine hydrochloride and the methyl ester of 2-chloro-2-phenyl-2-(2-piperidyl)-acetic acid), drugs with waking effect in anesthesia]. *Minerva Anestesiologica*, *21*(6), 125–128.

Benkert, P., Biasini, M., & Schwede, T. (2011). Toward the estimation of the absolute quality of

individual protein structure models. *Bioinformatics*, *27*(3), 343–350. https://doi.org/10.1093/bioinformatics/btq662

Benkert, P., Künzli, M., & Schwede, T. (2009). QMEAN server for protein model quality estimation. *Nucleic Acids Research*, *37*(suppl_2), W510–W514. https://doi.org/10.1093/nar/gkp322

Bergfors, T. M. (1999). *Protein Crystallization: Techniques, Strategies, and Tips: a Laboratory Maual*. Internat. Univ. Line.

Bhargava, K., Nath, R., Seth, P. K., Pant, K. K., & Dixit, R. K. (2014). Molecular Docking studies of D2 Dopamine receptor with Risperidone derivatives. *Bioinformation*, *10*(1), 8–12. https://doi.org/10.6026/97320630010008

Bielenica, A., Kędzierska, E., Koliński, M., Kmiecik, S., Koliński, A., Fiorino, F., … Struga, M. (2016). 5-HT 2 receptor affinity, docking studies and pharmacological evaluation of a series of 1,3-disubstituted thiourea derivatives. *European Journal of Medicinal Chemistry*, *116*, 173–186. https://doi.org/10.1016/j.ejmech.2016.03.073

Bienert, S., Waterhouse, A., de Beer, T. A. P., Tauriello, G., Studer, G., Bordoli, L., & Schwede, T. (2017). The SWISS-MODEL Repository—new features and functionality. *Nucleic Acids Research*, *45*(D1), D313–D319. https://doi.org/10.1093/nar/gkw1132

Bluelight - The Front Page. Retrieved 15 December 2016, from http://www.bluelight.org/vb/content/

Börjesson, U. (2005). *Chemogenomics in Drug Discovery. Methods and Principles in Medicinal Chemistry, Vol. 22. Edited by Hugo Kubinyi and Gerhard Müller*. Wiley Online Library.

Boulton, A. A., Baker, G. B., & Adams, R. (1995). *Voltammetric Methods in Brain Systems* (Vol. 27). New Jersey: Humana Press. Retrieved from http://link.springer.com/10.1385/0896033120

Boulton, A. A., Baker, G. B., & Bateson, A. N. (1998). *Cell Neurobiology Techniques* (Vol. 33). New Jersey: Humana Press. Retrieved from http://link.springer.com/10.1385/0896035107

Braden, M. R., Parrish, J. C., Naylor, J. C., & Nichols, D. E. (2006). Molecular Interaction of

Serotonin 5-HT2A Receptor Residues Phe339(6.51) and Phe340(6.52) with Superpotent N-Benzyl Phenethylamine Agonists. *Molecular Pharmacology*, *70*(6), 1956–1964. https://doi.org/10.1124/mol.106.028720

Brandes, J. L., Kudrow, D., Stark, S. R., O'Carroll, C. P., Adelman, J. U., O'Donnell, F. J., … Lener, S. E. (2007). Sumatriptan-Naproxen for Acute Treatment of Migraine: A Randomized Trial. *JAMA*, *297*(13). https://doi.org/10.1001/jama.297.13.1443

Brandt, S. D., Baumann, M. H., Partilla, J. S., Kavanagh, P. V., Power, J. D., Talbot, B., … Cosbey, S. H. (2014). Characterization of a novel and potentially lethal designer drug *(±)-cis-para* -methyl-4-methylaminorex (4,4'-DMAR, or 'Serotoni'): Characterization of (±)-cis- and (±)-*trans-para* -methyl-4-methylaminorex (4,4'-DMAR). *Drug Testing and Analysis*, *6*(7-8), 684–695. https://doi.org/10.1002/dta.1668

Brierley, D. I., & Davidson, C. (2013). Harmine augments electrically evoked dopamine efflux in the nucleus accumbens shell. *Journal of Psychopharmacology*, *27*(1), 98–108. https://doi.org/10.1177/0269881112463125

Bull, S. C., & Doig, A. J. (2015). Properties of Protein Drug Target Classes. *PLOS ONE*, *10*(3), e0117955. https://doi.org/10.1371/journal.pone.0117955

Cadoni, C., & Di Chiara, G. (2000). Differential changes in accumbens shell and core dopamine in behavioral sensitization to nicotine. *European Journal of Pharmacology*, *387*(3), R23–25.

Carson, J. R., Poos, G. I., & Almond Jr, H. R. (1965). 2-Amino-5-aryl-2-oxazolines. Tautomerism, stereochemistry, and an unusual reaction. *The Journal of Organic Chemistry*, *30*(7), 2225–2228.

Castaneto, M. S., Gorelick, D. A., Desrosiers, N. A., Hartman, R. L., Pirard, S., & Huestis, M. A. (2014). Synthetic cannabinoids: Epidemiology, pharmacodynamics, and clinical implications. *Drug and Alcohol Dependence*, *144*, 12–41. https://doi.org/10.1016/j.drugalcdep.2014.08.005

Castellanos, D., & Thornton, G. (2012). Synthetic Cannabinoid Use: Recognition and Management.

Journal of Psychiatric Practice, *18*(2), 86–93. https://doi.org/10.1097/01.pra.0000413274.09305.9c

Cheer, J. F., Kendall, D. A., & Marsden, C. A. (2000). Cannabinoid receptors and reward in the rat: a conditioned place preference study. *Psychopharmacology*, *151*(1), 25–30.

Chefer, V. I., Thompson, A. C., Zapata, A., & Shippenberg, T. S. (2009). Overview of Brain Microdialysis. In J. N. Crawley, C. R. Gerfen, M. A. Rogawski, D. R. Sibley, P. Skolnick, & S. Wray (Eds.), *Current Protocols in Neuroscience*. Hoboken, NJ, USA: John Wiley & Sons, Inc. Retrieved from http://doi.wiley.com/10.1002/0471142301.ns0701s47

ChemDraw Professional – PerkinElmer Informatics Desktop Software. Retrieved 24 February 2017, from http://www.cambridgesoft.com/Ensemble_for_Chemistry/ChemDraw/ChemDrawProfessional/

Chen, J.-K., Chen, J., Imig, J. D., Wei, S., Hachey, D. L., Guthi, J. S., … Harris, R. C. (2008). Identification of Novel Endogenous Cytochrome P450 Arachidonate Metabolites with High Affinity for Cannabinoid Receptors. *Journal of Biological Chemistry*, *283*(36), 24514–24524. https://doi.org/10.1074/jbc.M709873200

Chen, J. P., Paredes, W., Li, J., Smith, D., Lowinson, J., & Gardner, E. L. (1990). Delta 9-tetrahydrocannabinol produces naloxone-blockable enhancement of presynaptic basal dopamine efflux in nucleus accumbens of conscious, freely-moving rats as measured by intracerebral microdialysis. *Psychopharmacology*, *102*(2), 156–162.

Chothia, C., & Lesk, A. M. (1986). The relation between the divergence of sequence and structure in proteins. *The EMBO Journal*, *5*(4), 823–826.

Cimino, G., & De Stefano, S. (1978). Chemistry of Mediterranean gorgonians: Simple indole derivatives from Paramuricea chamaeleon. *Comparative Biochemistry and Physiology Part C: Comparative Pharmacology*, *61*(2), 361–362. https://doi.org/10.1016/0306-

4492(78)90070-9

Colman, E. (2007). Dinitrophenol and obesity: An early twentieth-century regulatory dilemma. *Regulatory Toxicology and Pharmacology*, *48*(2), 115–117. https://doi.org/10.1016/j.yrtph.2007.03.006

Cooper, Z. D. (2016). Adverse Effects of Synthetic Cannabinoids: Management of Acute Toxicity and Withdrawal. *Current Psychiatry Reports*, *18*(5), 52. https://doi.org/10.1007/s11920-016-0694-1

Coppola, M., & Mondola, R. (2013). 5-Iodo-2-aminoindan (5-IAI): Chemistry, pharmacology, and toxicology of a research chemical producing MDMA-like effects. *Toxicology Letters*, *218*(1), 24–29. https://doi.org/10.1016/j.toxlet.2013.01.008

Coppola, M., & Mondola, R. (2015). 4,4′-DMAR: Chemistry, Pharmacology and Toxicology of a New Synthetic Stimulant of Abuse. *Basic & Clinical Pharmacology & Toxicology*, *117*(1), 26–30. https://doi.org/10.1111/bcpt.12399

Corazza, O., Valeriani, G., Bersani, F. S., Corkery, J., Martinotti, G., Bersani, G., & Schifano, F. (2014). 'Spice,' 'kryptonite,' 'black mamba': an overview of brand names and marketing strategies of novel psychoactive substances on the web. *Journal of Psychoactive Drugs*, *46*(4), 287–294. https://doi.org/10.1080/02791072.2014.944291

Corkery, J., Claridge, H., Loi, B., Goodair, C., & Schifano, F. (2014). *Drug-related deaths in the UK: January-December 2012: Annual report 2013*. International Centre for Drug Policy. Retrieved 10 April 2016 from http://uhra.herts.ac.uk/handle/2299/12818

Corkery, J. M., Elliott, S., Schifano, F., Corazza, O., & Ghodse, A. H. (2012). 2-DPMP (desoxypipradrol, 2-benzhydrylpiperidine, 2-phenylmethylpiperidine) and D2PM (diphenyl-2-pyrrolidin-2-yl-methanol, diphenylprolinol): A preliminary review. *Progress in Neuro-Psychopharmacology and Biological Psychiatry*, *39*(2), 253–258. https://doi.org/10.1016/j.pnpbp.2012.05.021

Corkery, J. M., Elliott, S., Schifano, F., Corazza, O., & Ghodse, A. H. (2013). MDAI (5,6-methylenedioxy-2-aminoindane;6,7-dihydro-5H-cyclopenta[f][1,3]benzodioxol-6-amine; ‘sparkle’; ‘mindy’) toxicity: a brief overview and update: MDAI toxicity: brief review and update. *Human Psychopharmacology: Clinical and Experimental*, *28*(4), 345–355. https://doi.org/10.1002/hup.2298

Cosbey, S., Kirk, S., McNaul, M., Peters, L., Prentice, B., Quinn, A., … Archer, R. P. (2014). Multiple Fatalities Involving a New Designer Drug: Para-Methyl-4-Methylaminorex. *Journal of Analytical Toxicology*, *38*(6), 383–384. https://doi.org/10.1093/jat/bku031

Council on Pharmacy and Chemistry (1935). Dinitrophenol not acceptable for New and Nonofficial Remedies, reports of the Council. *JAMA* 105:31e3.

Cutting, W. C., Mehrtens, H. G., & Tainter, M. L. (1933). Actions and uses od dinitrophenol: promising metabolic applications. *Journal of the American Medical Association*, *101*(3), 193. https://doi.org/10.1001/jama.1933.02740280013006

Dallakyan, S., & Olson, A. J. (2015). Small-Molecule Library Screening by Docking with PyRx. In J. E. Hempel, C. H. Williams, & C. C. Hong (Eds.), *Chemical Biology* (Vol. 1263, pp. 243–250). New York, NY: Springer New York. Retrieved from http://link.springer.com/10.1007/978-1-4939-2269-7_19

Dalton, V. S., & Zavitsanou, K. (2010). Cannabinoid effects on CB_1 receptor density in the adolescent brain: An autoradiographic study using the synthetic cannabinoid HU210. *Synapse*, *64*(11), 845–854. https://doi.org/10.1002/syn.20801

Dargan, P. I., and Wood, D. M. (Eds.) (2013). In *Novel Psychoactive Substances*. Boston: Academic Press. Retrieved from http://www.sciencedirect.com/science/article/pii/B9780124158160000183

Davenport, A. P. (2005). *Receptor Binding Techniques*. Springer Science & Business Media.

Davenport, A. P., & Russell, F. D. (1996). Radioligand binding assays: theory and practice. *Current*

Directions in Radiopharmaceutical Research and Development. Amsterdam: Kluwer, 169–179.

Davidson, C., Chauhan, N. K., Knight, S., Gibson, C. L., & Young, A. M. J. (2011). Modelling ischaemia in vitro: Effects of temperature and glucose concentration on dopamine release evoked by oxygen and glucose depletion in a mouse brain slice. *Journal of Neuroscience Methods*, *202*(2), 165–172. https://doi.org/10.1016/j.jneumeth.2011.05.019

Davidson, C., & Ramsey, J. (2012). Desoxypipradrol is more potent than cocaine on evoked dopamine efflux in the nucleus accumbens. *Journal of Psychopharmacology*, *26*(7), 1036–1041. https://doi.org/10.1177/0269881111430733

Davidson, C., & Stamford, J. A. (1993). Neurochemical evidence of functional A10 dopamine terminals innervating the ventromedial axis of the neostriatum: in vitro voltammetric data in rat brain slices. *Brain Research*, *615*(2), 229–239.

De Luca, M. A., Bimpisidis, Z., Melis, M., Marti, M., Caboni, P., Valentini, V., … Di Chiara, G. (2015). Stimulation of in vivo dopamine transmission and intravenous self-administration in rats and mice by JWH-018, a Spice cannabinoid. *Neuropharmacology*, *99*, 705–714. https://doi.org/10.1016/j.neuropharm.2015.08.041

De Luca, M. A., Castelli, M. P., Loi, B., Porcu, A., Martorelli, M., Miliano, C., … Di Chiara, G. (2016). Native CB1 receptor affinity, intrinsic activity and accumbens shell dopamine stimulant properties of third generation SPICE/K2 cannabinoids: BB-22, 5F-PB-22, 5F-AKB-48 and STS-135. *Neuropharmacology*, *105*, 630–638. https://doi.org/10.1016/j.neuropharm.2015.11.017

Deligianni, E., Corkery, J. M., Schifano, F., & Lione, L. A. (2017). An international survey on the awareness, use, preference, and health perception of novel psychoactive substances (NPS). *Human Psychopharmacology: Clinical and Experimental*, *32*(3), e2581. https://doi.org/10.1002/hup.2581

Di Chiara, G. (1990). In-vivo brain dialysis of neurotransmitters. *Trends in Pharmacological Sciences*, *11*(3), 116–121.

Di Chiara, G., Bassareo, V., Fenu, S., De Luca, M. A., Spina, L., Cadoni, C., … Lecca, D. (2004). Dopamine and drug addiction: the nucleus accumbens shell connection. *Neuropharmacology*, *47*, 227–241. https://doi.org/10.1016/j.neuropharm.2004.06.032

Di Chiara, G., & Imperato, A. (1988). Drugs abused by humans preferentially increase synaptic dopamine concentrations in the mesolimbic system of freely moving rats. *Proceedings of the National Academy of Sciences of the United States of America*, *85*(14), 5274–5278.

EMCDDA (2014). Report on the risk assessment of 5-(2-aminopropyl)indole in the framework of the Council Decision on new psychoactive substances. Retrieved 12 March 2016, from http://www.emcdda.europa.eu/publications/risk-assessment/5-IT_en

EMCDDA (2015). European Drug Report 2015: Trends and Developments. Retrieved 14 February 2017, from http://www.emcdda.europa.eu/publications/edr/trends-developments/2015

EMCDDA (2016). European Drug Report 2016: Trends and Developments. Retrieved 19 October 2017, from http://www.emcdda.europa.eu/publications/edr/trends-developments/2016

EMCDDA (2017). European Drug Report 2017: Trends and Developments. Retrieved 19 March 2017, from http://www.emcdda.europa.eu/publications/edr/trends-developments/2017

EMCDDA–Europol (2014). Joint Report on a new psychoactive substance: 4,4'-DMAR (4-methyl-5-(4-methylphenyl)-4,5-dihydrooxazol-2-amine) | www.emcdda.europa.eu. Retrieved 12 May 2016, from http://emcdda.europa.eu/publications/joint-reports/4-4-DMAR_en

Engh, R. A., & Huber, R. (1991). Accurate bond and angle parameters for X-ray protein structure refinement. *Acta Crystallographica Section A: Foundations of Crystallography*, *47*(4), 392–400.

ESPAD Report 2015 — Results from the European School Survey Project on Alcohol and Other

Drugs. Retrieved 15 March 2017, from http://www.emcdda.europa.eu/publications/joint-publications/emcdda-espad-report_en

Fantegrossi, W. E., Moran, J. H., Radominska-Pandya, A., & Prather, P. L. (2014). Distinct pharmacology and metabolism of K2 synthetic cannabinoids compared to Δ9-THC: Mechanism underlying greater toxicity? *Life Sciences*, *97*(1), 45–54. https://doi.org/10.1016/j.lfs.2013.09.017

Fantegrossi, W. E., Murnane, K. S., & Reissig, C. J. (2008). The behavioral pharmacology of hallucinogens. *Biochemical Pharmacology*, *75*(1), 17–33. https://doi.org/10.1016/j.bcp.2007.07.018

Fattore, L. (2016). Synthetic cannabinoids—further evidence supporting the relationship between cannabinoids and psychosis. *Biological Psychiatry*, *79*(7), 539–548.

Fattore, L., & Fratta, W. (2011). Beyond THC: The New Generation of Cannabinoid Designer Drugs. *Frontiers in Behavioral Neuroscience*, *5*. https://doi.org/10.3389/fnbeh.2011.00060

Felder, C. C., Joyce, K. E., Briley, E. M., Mansouri, J., Mackie, K., Blond, O., … Mitchell, R. L. (1995). Comparison of the pharmacology and signal transduction of the human cannabinoid CB1 and CB2 receptors. *Molecular Pharmacology*, *48*(3), 443–450.

Flanagan, R. J., Perrett, D., & Whelpton, R. (2005). *Electrochemical Detection in HPLC: Analysis of Drugs and Poisons*. Royal Society of Chemistry.

Flash Eurobarometer Report (March 2016) - European Commission. Retrieved 10 April 2017, from https://ec.europa.eu/growth/content/flash-eurobarometer-report-march-2016-0_en

Follath, F., Burkart, F., & Schweizer, W. (1971). Drug-induced Pulmonary Hypertension? *BMJ*, *1*(5743), 265–266. https://doi.org/10.1136/bmj.1.5743.265

Food Standards Agency (2003). Alert over DNP 'fat burner' capsules. Retrieved 20 March 2016, from http://webarchive.nationalarchives.gov.uk/20101210015936/http://www.food.gov.uk/news/ne

wsarchive/2003/jun/dnpfatburner

Food Standards Agency (2012). Warning about 'fat-burner' substances containing DNP. Retrieved 20 March 2016, from http://www.food.gov.uk/news-updates/news/2012/nov/dnp-warning#.Ul1f9dKsgk0

Forli, S., Huey, R., Pique, M. E., Sanner, M. F., Goodsell, D. S., & Olson, A. J. (2016). Computational protein–ligand docking and virtual drug screening with the AutoDock suite. *Nature Protocols*, *11*(5), 905–919. https://doi.org/10.1038/nprot.2016.051

Fraser, G. A. (2009). The Use of a Synthetic Cannabinoid in the Management of Treatment-Resistant Nightmares in Posttraumatic Stress Disorder (PTSD). *CNS Neuroscience & Therapeutics*, *15*(1), 84–88. https://doi.org/10.1111/j.1755-5949.2008.00071.x

Freund, T. F., Katona, I., & Piomelli, D. (2003). Role of Endogenous Cannabinoids in Synaptic Signaling. *Physiological Reviews*, *83*(3), 1017–1066. https://doi.org/10.1152/physrev.00004.2003

Fujita, Y., Koeda, A., Fujino, Y., Onodera, M., Kikuchi, S., Niitsu, H., … Inoue, Y. (2016). Clinical and toxicological findings of acute intoxication with synthetic cannabinoids and cathinones: Synthetic cannabinoids and cathinone toxicity. *Acute Medicine & Surgery*, *3*(3), 230–236. https://doi.org/10.1002/ams2.182

Gandhi, A. S., Wohlfarth, A., Zhu, M., Pang, S., Castaneto, M., Scheidweiler, K. B., & Huestis, M. A. (2015). High-resolution mass spectrometric metabolite profiling of a novel synthetic designer drug, N-(adamantan-1-yl)-1-(5-fluoropentyl)-1H-indole-3-carboxamide (STS-135), using cryopreserved human hepatocytes and assessment of metabolic stability with human liv: Metabolite profiling of STS-135 using human hepatocytes. *Drug Testing and Analysis*, *7*(3), 187–198. https://doi.org/10.1002/dta.1662

Gardner, E. L. (2002). Addictive potential of cannabinoids: the underlying neurobiology. *Chemistry and Physics of Lipids*, *121*(1-2), 267–290.

Garris, P. A., & Wightman, R. M. (1995). Regional Differences in Dopamine Release, Uptake, and Diffusion Measured by Fast-Scan Cyclic Voltammetry. In A. A. Boulton, G. B. Baker, & R. Adams, *Voltammetric Methods in Brain Systems* (Vol. 27, pp. 179–220). New Jersey: Humana Press. Retrieved from http://link.springer.com/10.1385/0-89603-312-0:179

Gatz, E. E., & Jones, J. R. (1970). Haloperidol antagonism to the hyperpyrexic and lethal effects of 2,4-dinitrophenol in rats. *Anesthesia and Analgesia*, *49*(5), 773–780.

Geiger, B. M., Frank, L. E., Caldera-Siu, A. D., & Pothos, E. N. (2008). Survivable stereotaxic surgery in rodents. *Journal of Visualized Experiments: JoVE*, (20).

Gessa, G. L., Melis, M., Muntoni, A. L., & Diana, M. (1998). Cannabinoids activate mesolimbic dopamine neurons by an action on cannabinoid CB1 receptors. *European Journal of Pharmacology*, *341*(1), 39–44.

Glanville, J., Dargan, P. I., & Wood, D. M. (2015). 4-Methyl-5-(4-methylphenyl)-4,5-dihydrooxazol-2-amine (4,4′-DMAR, 4,4′-dimethylaminorex): availability, prevalence of use, desired effects and acute toxicity: 4,4′-DMAR: Availability, Use and Effects. *Human Psychopharmacology: Clinical and Experimental*, *30*(3), 193–198. https://doi.org/10.1002/hup.2472

Global Drug Survey (2012). Key finding report. Retrieved 4 April 2016, from https://www.globaldrugsurvey.com/

Global Drug Survey (2017). Key finding report. Retrieved 4 October 2017, from https://www.globaldrugsurvey.com/

Grundlingh, J., Dargan, P. I., El-Zanfaly, M., & Wood, D. M. (2011). 2,4-Dinitrophenol (DNP): A Weight Loss Agent with Significant Acute Toxicity and Risk of Death. *Journal of Medical Toxicology*, *7*(3), 205–212. https://doi.org/10.1007/s13181-011-0162-6

Gunderson, E. W., Haughey, H. M., Ait-Daoud, N., Joshi, A. S., & Hart, C. L. (2012). 'Spice' and 'K2' Herbal Highs: A Case Series and Systematic Review of the Clinical Effects and Biopsychosocial Implications of Synthetic Cannabinoid Use in Humans: Synthetic

Cannabinoid Case Series Systematic Review. *The American Journal on Addictions*, *21*(4), 320–326. https://doi.org/10.1111/j.1521-0391.2012.00240.x

Gurtner, H. P. (1985). Aminorex and pulmonary hypertension. A review. *Cor et Vasa*, *27*(2-3), 160–171.

Hadcock, J. R., Griffith, D. A., Iredale, P. A., Carpino, P. A., Dow, R. L., Black, S. C., … Scott, D. O. (2010). In vitro and in vivo pharmacology of CP-945,598, a potent and selective cannabinoid CB1 receptor antagonist for the management of obesity. *Biochemical and Biophysical Research Communications*, *394*(2), 366–371. https://doi.org/10.1016/j.bbrc.2010.03.015

Hafizi, S., Kruk, Z. L., & Stamford, J. A. (1990). Fast cyclic voltammetry: improved sensitivity to dopamine with extended oxidation scan limits. *Journal of Neuroscience Methods*, *33*(1), 41–49.

Harper, J. A., Dickinson, K., & Brand, M. D. (2001). Mitochondrial uncoupling as a target for drug development for the treatment of obesity. *Obesity Reviews*, *2*(4), 255–265.

Hauser, M., Mayer, C. E., & Söding, J. (2013). kClust: fast and sensitive clustering of large protein sequence databases. *BMC Bioinformatics*, *14*, 248. https://doi.org/10.1186/1471-2105-14-248

Hedrich, H. J. (2000). History, Strains and Models. In *The Laboratory Rat* (pp. 3–16). Elsevier. Retrieved from http://linkinghub.elsevier.com/retrieve/pii/B9780124264007500406

Hentig, N. V. (2016). Potential drug interactions between cART and new psychoactive substances. *Journal of Antivirals & Antiretrovirals*, *8*(2). http://dx.doi.org/10.4172/jaa.1000e131

Herraiz, T., & Brandt, S. D. (2014). 5-(2-Aminopropyl)indole (5-IT): a psychoactive substance used for recreational purposes is an inhibitor of human monoamine oxidase (MAO): MAO inhibition studies with 5-(2-aminopropyl)indole. *Drug Testing and Analysis*, *6*(7-8), 607–613. https://doi.org/10.1002/dta.1530

Hoffman, A. F., & Lupica, C. R. (2000). Mechanisms of cannabinoid inhibition of GABA(A)

synaptic transmission in the hippocampus. *The Journal of Neuroscience: The Official Journal of the Society for Neuroscience*, *20*(7), 2470–2479.

Home Office (2012). Circular: a change to the Misuse of Drugs Act 1971 - GOV.UK. Retrieved 6 June 2017, from https://www.gov.uk/government/publications/a-change-to-the-misuse-of-drugs-act-1971-control-of-pipradrol-related-compounds-and-phenazepam

Houston, D. R., & Walkinshaw, M. D. (2013). Consensus Docking: Improving the Reliability of Docking in a Virtual Screening Context. *Journal of Chemical Information and Modeling*, *53*(2), 384–390. https://doi.org/10.1021/ci300399w

Howlett, A. C., Barth, F., Bonner, T. I., Cabral, G., Casellas, P., Devane, W. A., … Pertwee, R. G. (2002). International Union of Pharmacology. XXVII. Classification of cannabinoid receptors. *Pharmacological Reviews*, 54(2), 161–202.

Howlett, A., Blume, L., & Dalton, G. (2010). CB1 Cannabinoid Receptors and their Associated Proteins. *Current Medicinal Chemistry*, *17*(14), 1382–1393. https://doi.org/10.2174/092986710790980023

Hoyte, C. O., Jacob, J., Monte, A. A., Al-Jumaan, M., Bronstein, A. C., & Heard, K. J. (2012). A Characterization of Synthetic Cannabinoid Exposures Reported to the National Poison Data System in 2010. *Annals of Emergency Medicine*, *60*(4), 435–438. https://doi.org/10.1016/j.annemergmed.2012.03.007

Hsiao, A. L., Santucci, K. A., Seo-Mayer, P., Mariappan, M. R., Hodsdon, M. E., Banasiak, K. J., & Baum, C. R. (2005). Pediatric fatality following ingestion of dinitrophenol: postmortem identification of a 'dietary supplement'. *Clinical Toxicology (Philadelphia, Pa.)*, *43*(4), 281–285.

Hua, T., Vemuri, K., Pu, M., Qu, L., Han, G. W., Wu, Y., … Liu, Z.-J. (2016). Crystal Structure of the Human Cannabinoid Receptor CB 1. *Cell*, *167*(3), 750–762.e14. https://doi.org/10.1016/j.cell.2016.10.004

Huang, S.-Y., Grinter, S. Z., & Zou, X. (2010). Scoring functions and their evaluation methods for protein–ligand docking: recent advances and future directions. *Physical Chemistry Chemical Physics*, *12*(40), 12899. https://doi.org/10.1039/c0cp00151a

Hyland, B. I., Reynolds, J. N. J., Hay, J., Perk, C. G., & Miller, R. (2002). Firing modes of midbrain dopamine cells in the freely moving rat. *Neuroscience*, *114*(2), 475–492.

Imperato, A., & Di Chiara, G. (1984). Trans-striatal dialysis coupled to reverse phase high performance liquid chromatography with electrochemical detection: a new method for the study of the in vivo release of endogenous dopamine and metabolites. *The Journal of Neuroscience: The Official Journal of the Society for Neuroscience*, *4*(4), 966–977.

INTERPOL (2015). Global alert for the potentially lethal illicit diet drug 2,4-DNP. Retrieved 15 April 2016, from https://www.interpol.int/News-and-media/News/2015/N2015-050

Iversen, L., White, M., & Treble, R. (2014). Designer psychostimulants: Pharmacology and differences. *Neuropharmacology*, *87*, 59–65. https://doi.org/10.1016/j.neuropharm.2014.01.015

James, D.A., Potts, S., Thomas, S.H.L., Chincholkar, V.M., Clarke, S., Dear, J. (2011). Clinical features associated with recreational use of 'ivory wave' preparations containing desoxypipradrol Abstract 12. *Clinical Toxicology* 49:197–269 (Abstract. The 2011 International Congress of the European Association of Poisons Centres and Clinical Toxicologists. Dubrovnik, Croatia).

John, C. E., & Jones, S. R. (2007). Fast Scan Cyclic Voltammetry of Dopamine and Serotonin in Mouse Brain Slices. In A. C. Michael & L. M. Borland (Eds.), *Electrochemical Methods for Neuroscience*. Boca Raton (FL): CRC Press/Taylor & Francis. Retrieved from http://www.ncbi.nlm.nih.gov/books/NBK2579/

Johnson, M. P., Conarty, P. F., & Nichols, D. E. (1991). [^{3}H]monoamine releasing and uptake inhibition properties of 3,4-methylenedioxymethamphetamine and p-chloroamphetamine

analogues. *European Journal of Pharmacology*, *200*(1), 9–16.

Kabsch, W., & Sander, C. (1983). Dictionary of protein secondary structure: Pattern recognition of hydrogen-bonded and geometrical features. *Biopolymers*, *22*(12), 2577–2637. https://doi.org/10.1002/bip.360221211

Kalix, P. (1990). Pharmacological properties of the stimulant khat. *Pharmacology & Therapeutics*, *48*(3), 397–416.

Kamour, A., George, N., Gwynnette, D., Cooper, G., Lupton, D., Eddleston, M., … Thomas, S. H. L. (2015). Increasing frequency of severe clinical toxicity after use of 2,4-dinitrophenol in the UK: a report from the National Poisons Information Service. *Emergency Medicine Journal*, *32*(5), 383–386. https://doi.org/10.1136/emermed-2013-203335

Khey, D. N., Stogner, J., & Miller, B. L. (2013). *Emerging Trends in Drug Use and Distribution*. Springer Science & Business Media.

Knoche, H. W. (1991). *Radioisotopic methods for biological and medical research*. New York, N.Y.: Oxford University Press.

Kolodziejczyk, W., Kar, S., Hill, G. A., & Leszczynski, J. (2016). A comprehensive computational analysis of cathinone and its metabolites using quantum mechanical approaches and docking studies. *Structural Chemistry*, *27*(4), 1291–1302. https://doi.org/10.1007/s11224-016-0779-9

Korde, A. S., Pettigrew, L. C., Craddock, S. D., & Maragos, W. F. (2005). The mitochondrial uncoupler 2,4-dinitrophenol attenuates tissue damage and improves mitochondrial homeostasis following transient focal cerebral ischemia. *Journal of Neurochemistry*, *94*(6), 1676–1684. https://doi.org/10.1111/j.1471-4159.2005.03328.x

Kozinets, R. V. (2002). The field behind the screen: Using netnography for marketing research in online communities. *Journal of Marketing Research*, *39*(1), 61–72.

Kozinets, R. V. (2016). Netnography: understanding networked communication society. *The SAGE Handbook of Social Media Research Methods*.

Krieger, E., Nabuurs, S. B., & Vriend, G. (2003). Homology modeling. *Methods of Biochemical Analysis*, *44*, 509–524.

Kumar, R., Singh, B. R., Kukreja, R., Feltrup, T., & Cai, S. (2016). *Protein Toxins in Modeling Biochemistry*. Springer.

Kurt, T. L., Anderson, R., Petty, C., Bost, R., Reed, G., & Holland, J. (1986). Dinitrophenol in weight loss: the poison center and public health safety. *Veterinary and Human Toxicology*, *28*(6), 574–575.

Laskowski, R. A., MacArthur, M. W., Moss, D. S., & Thornton, J. M. (1993). PROCHECK: a program to check the stereochemical quality of protein structures. *Journal of Applied Crystallography*, *26*(2), 283–291. https://doi.org/10.1107/S0021889892009944

Lecca, D., Cacciapaglia, F., Valentini, V., & Di Chiara, G. (2006). Monitoring extracellular dopamine in the rat nucleus accumbens shell and core during acquisition and maintenance of intravenous WIN 55,212-2 self-administration. *Psychopharmacology*, *188*(1), 63–74. https://doi.org/10.1007/s00213-006-0475-3

Lee, H. C. H., Law, C. Y., Chen, M. L., Lam, Y. H., Chan, A. Y. W., & Mak, T. W. L. (2014). 2,4-Dinitrophenol: A threat to Chinese body-conscious groups. *Journal of the Chinese Medical Association*, *77*(8), 443–445. https://doi.org/10.1016/j.jcma.2014.05.003

Lee, K.-W., Kim, H.-C., Lee, S.-Y., & Jang, C.G. (2011). Methamphetamine-sensitized mice are accompanied by memory impairment and reduction of N-methyl-d-aspartate receptor ligand binding in the prefrontal cortex and hippocampus. *Neuroscience*, *178*, 101–107.

Lidder, S., Dargan, P., Sexton, M., Button, J., Ramsey, J., Holt, D., & Wood, D. (2008). Cardiovascular toxicity associated with recreational use of diphenylprolinol (diphenyl-2-pyrrolidinemethanol [D2PM]). *Journal of Medical Toxicology: Official Journal of the American College of Medical Toxicology*, *4*(3), 167–169.

Liechti, M. (2015). Novel psychoactive substances (designer drugs): overview and pharmacology of

modulators of monoamine signaling. *Swiss Medical Weekly*. https://doi.org/10.4414/smw.2015.14043

Lin, S., Khanolkar, A. D., Fan, P., Goutopoulos, A., Qin, C., Papahadjis, D., & Makriyannis, A. (1998). Novel Analogues of Arachidonylethanolamide (Anandamide): Affinities for the CB1 and CB2 Cannabinoid Receptors and Metabolic Stability. *Journal of Medicinal Chemistry*, *41*(27), 5353–5361. https://doi.org/10.1021/jm970257g

Loi, B., Zloh, M., De Luca, M. A., Pintori, N., Corkery, J., & Schifano, F. (2017). 4,4′-Dimethylaminorex ('4,4′-DMAR'; 'Serotoni') misuse: A Web-based study. *Human Psychopharmacology: Clinical and Experimental*, *32*(3), e2575. https://doi.org/10.1002/hup.2575

López-Arnau, R., Martínez-Clemente, J., Pubill, D., Escubedo, E., & Camarasa, J. (2012). Comparative neuropharmacology of three psychostimulant cathinone derivatives: butylone, mephedrone and methylone: Neuropharmacology of cathinone derivatives. *British Journal of Pharmacology*, *167*(2), 407–420. https://doi.org/10.1111/j.1476-5381.2012.01998.x

Lovell, S. C., Davis, I. W., Arendall, W. B., de Bakker, P. I., Word, J. M., Prisant, M. G., … Richardson, D. C. (2003). Structure validation by Cα geometry: ϕ, ψ and Cβ deviation. *Proteins: Structure, Function, and Bioinformatics*, *50*(3), 437–450

Lovett, D. P., Yanes, E. G., Herbelin, T. W., Knoerzer, T. A., & Levisky, J. A. (2013). Structure elucidation and identification of a common metabolite for naphthoylindole-based synthetic cannabinoids using LC-TOF and comparison to a synthetic reference standard. *Forensic Science International*, *226*(1-3), 81–87. https://doi.org/10.1016/j.forsciint.2012.12.012

Lupica, C. R., Riegel, A. C., & Hoffman, A. F. (2004). Marijuana and cannabinoid regulation of brain reward circuits. *British Journal of Pharmacology*, *143*(2), 227–234. https://doi.org/10.1038/sj.bjp.0705931

Maestro 10.4 | Schrödinger. Retrieved 20 January 2016, from https://www.schrodinger.com/Maestro

Martinotti, G., Lupi, M., Acciavatti, T., Cinosi, E., Santacroce, R., Signorelli, M. S., … di Giannantonio, M. (2014). Novel Psychoactive Substances in Young Adults with and without Psychiatric Comorbidities. *BioMed Research International*, *2014*, 1–7. https://doi.org/10.1155/2014/815424

Marusich, J. A., Antonazzo, K. R., Blough, B. E., Brandt, S. D., Kavanagh, P. V., Partilla, J. S., & Baumann, M. H. (2016). The new psychoactive substances 5-(2-aminopropyl)indole (5-IT) and 6-(2-aminopropyl)indole (6-IT) interact with monoamine transporters in brain tissue. *Neuropharmacology*, *101*, 68–75. https://doi.org/10.1016/j.neuropharm.2015.09.004

Masserman, J. H., & Goldsmith, H. (1934). Dinitrophenol: its therapeutic and toxic actions in certain types of psychobiologic underactivity. *Journal of the American Medical Association*, *102*(7), 523–525.

McAllister, S. D., Rizvi, G., Anavi-Goffer, S., Hurst, D. P., Barnett-Norris, J., Lynch, D. L., … Abood, M. E. (2003). An Aromatic Microdomain at the Cannabinoid CB $_1$ Receptor Constitutes an Agonist/Inverse Agonist Binding Region. *Journal of Medicinal Chemistry*, *46*(24), 5139–5152. https://doi.org/10.1021/jm0302647

McBride, W. J., Murphy, J. M., & Ikemoto, S. (1999). Localization of brain reinforcement mechanisms: intracranial self-administration and intracranial place-conditioning studies. *Behavioural Brain Research*, *101*(2), 129–152.

McIlroy, G., Ford, L., & Khan, J. M. (2016). Acute myocardial infarction, associated with the use of a synthetic adamantyl-cannabinoid: a case report. *BMC Pharmacology and Toxicology*, *17*(1). https://doi.org/10.1186/s40360-016-0045-1

McLaughlin, G., Morris, N., Kavanagh, P. V., Power, J. D., Twamley, B., O'Brien, J., … Baumann, M. H. (2015). Synthesis, characterization, and monoamine transporter activity of the new psychoactive substance 3′,4′-methylenedioxy-4-methylaminorex (MDMAR): Newly emerging psychoactive substances. *Drug Testing and Analysis*, *7*(7), 555–564.

https://doi.org/10.1002/dta.1732

Melvin, L. S., Milne, G. M., Johnson, M. R., Subramaniam, B., Wilken, G. H., & Howlett, A. C. (1993). Structure-activity relationships for cannabinoid receptor-binding and analgesic activity: studies of bicyclic cannabinoid analogs. *Molecular Pharmacology*, *44*(5), 1008–1015.

Menghani, S., Kerzare, D., Rarokar, N., & Khedekar, P. (2016). Molecular Docking, Synthesis and Evaluation of Antianxiety and Anticonvulsant potential of some Novel 3-(substituted benzylidene)-5-phenyl-7-nitro-1, 3-dihydro-1H, 3H-1, 4-Benzodiazepine-2-one. *American Journal of PharmTech Research*, 6(6).

Miliano, C., Serpelloni, G., Rimondo, C., Mereu, M., Marti, M., & De Luca, M. A. (2016). Neuropharmacology of New Psychoactive Substances (NPS): Focus on the Rewarding and Reinforcing Properties of Cannabimimetics and Amphetamine-Like Stimulants. *Frontiers in Neuroscience*, *10*. https://doi.org/10.3389/fnins.2016.00153

Moghaddam, B., & Bunney, B. S. (1989). Differential effect of cocaine on extracellular dopamine levels in rat medial prefrontal cortex and nucleus accumbens: Comparison to amphetamine. *Synapse*, *4*(2), 156–161. https://doi.org/10.1002/syn.890040209

Mohan, V., Gibbs, A., Cummings, M., Jaeger, E., & DesJarlais, R. (2005). Docking: Successes and Challenges. *Current Pharmaceutical Design*, *11*(3), 323–333. https://doi.org/10.2174/1381612053382106

Morris, A. L., MacArthur, M. W., Hutchinson, E. G., & Thornton, J. M. (1992). Stereochemical quality of protein structure coordinates. *Proteins: Structure, Function, and Genetics*, *12*(4), 345–364. https://doi.org/10.1002/prot.340120407

Morris, G. M., Goodsell, D. S., Halliday, R. S., Huey, R., Hart, W. E., Belew, R. K., & Olson, A. J. (1998). Automated docking using a Lamarckian genetic algorithm and an empirical binding free energy function. *Journal of Computational Chemistry*, *19*(14), 1639–1662.

https://doi.org/10.1002/(SICI)1096-987X(19981115)19:14<1639::AID-JCC10>3.0.CO;2-B

Musselman, M. E., & Hampton, J. P. (2014). ‘ Not for Human Consumption”: A Review of Emerging Designer Drugs’. *Pharmacotherapy: The Journal of Human Pharmacology and Drug Therapy*, *34*(7), 745–757. https://doi.org/10.1002/phar.1424

Negus, S. S., & Miller, L. L. (2014). Intracranial Self-Stimulation to Evaluate Abuse Potential of Drugs. *Pharmacological Reviews*, *66*(3), 869–917. https://doi.org/10.1124/pr.112.007419

Nelson, M. E., Bryant, S. M., & Aks, S. E. (2014). Emerging Drugs of Abuse. *Emergency Medicine Clinics of North America*, *32*(1), 1–28. https://doi.org/10.1016/j.emc.2013.09.001

Nichols, D. E. (2004). Hallucinogens. *Pharmacology & Therapeutics*, *101*(2), 131–181. https://doi.org/10.1016/j.pharmthera.2003.11.002

Nichols, D. E., Johnson, M. P., & Oberlender, R. (1991). 5-Iodo-2-aminoindan, a nonneurotoxic analogue of p-iodoamphetamine. *Pharmacology, Biochemistry, and Behavior*, *38*(1), 135–139.

NPIS (2017). Annual Report. National Poisons Information Service. Retrieved 20 September 2017, from http://www.npis.org/annualreports.html

OFDT (2014). New psychoactive substances: user profiles and practices. Retrieved 12 June 2017, from https://en.ofdt.fr/BDD/publications/docs/eftaacw4.pdf

Ohlsson, A., Lindgren, J. E., Wahlen, A., Agurell, S., Hollister, L. E., & Gillespie, H. K. (1980). Plasma delta-9 tetrahydrocannabinol concentrations and clinical effects after oral and intravenous administration and smoking. *Clinical Pharmacology and Therapeutics*, *28*(3), 409–416.

Onaivi, E. S., Ishiguro, H., Gong, J.-P., Patel, S., Meozzi, P. A., Myers, L., … Uhl, G. R. (2008). Brain neuronal CB2 cannabinoid receptors in drug abuse and depression: from mice to human subjects. *PloS One*, *3*(2), e1640. https://doi.org/10.1371/journal.pone.0001640

Opacka-Juffry, J., Pinnell, T., Patel, N., Bevan, M., Meintel, M., & Davidson, C. (2014). Stimulant

mechanisms of cathinones — Effects of mephedrone and other cathinones on basal and electrically evoked dopamine efflux in rat accumbens brain slices. *Progress in Neuro-Psychopharmacology and Biological Psychiatry*, *54*, 122–130. https://doi.org/10.1016/j.pnpbp.2014.04.009

Orsolini, L., Papanti, G. D., De Berardis, D., Guirguis, A., Corkery, J. M., & Schifano, F. (2017). The 'Endless Trip' among the NPS Users: Psychopathology and Psychopharmacology in the Hallucinogen-Persisting Perception Disorder. A Systematic Review. *Frontiers in Psychiatry*, *8*, 240. https://doi.org/10.3389/fpsyt.2017.00240.

Orsolini, L., Papanti, G. D., De Berardis, D., Guirguis, A., Corkery, J. M., & Schifano, F. (2017). The 'Endless Trip' among the NPS Users: Psychopathology and Psychopharmacology in the Hallucinogen-Persisting Perception Disorder. A Systematic Review. *Frontiers in Psychiatry*, *8*, 240. https://doi.org/10.3389/fpsyt.2017.00240.

Orsolini, L., Papanti, G. D., Francesconi, G., & Schifano, F. (2015). Mind Navigators of Chemicals' Experimenters? A Web-Based Description of E-Psychonauts. *Cyberpsychology, Behavior, and Social Networking*, *18*(5), 296–300. https://doi.org/10.1089/cyber.2014.0486

Palamar, J. J., Acosta, P., Sherman, S., Ompad, D. C., & Cleland, C. M. (2016). Self-reported use of novel psychoactive substances among attendees of electronic dance music venues. *The American Journal of Drug and Alcohol Abuse*, *42*(6), 624–632. https://doi.org/10.1080/00952990.2016.1181179

Pehek, E. A., Schechter, M. D., & Yamamoto, B. K. (1990). Effects of cathinone and amphetamine on the neurochemistry of dopamine in vivo. *Neuropharmacology*, *29*(12), 1171–1176.

Parascandola, J. (1974). Dinitrophenol and bioenergetics: an historical perspective. *Molecular and Cellular Biochemistry*, *5*(1-2), 69–77.

Paxinos, G., & Watson, C. (1998). *The rat brain in stereotaxic coordinates.* 3rd edition. *Vol*. Academic Press, San Diego.

Perkins, R. G. (1919). A Study of the Munitions Intoxications in France. *Public Health Reports (1896-1970), 34*(43), 2335. https://doi.org/10.2307/4575357

Perry, R. J., Kim, T., Zhang, X.-M., Lee, H.-Y., Pesta, D., Popov, V. B., … Shulman, G. I. (2013). Reversal of Hypertriglyceridemia, Fatty Liver Disease, and Insulin Resistance by a Liver-Targeted Mitochondrial Uncoupler. *Cell Metabolism*, *18*(5), 740–748. https://doi.org/10.1016/j.cmet.2013.10.004

Pertwee, R. G. (2005). Pharmacological actions of cannabinoids. *Handbook of Experimental Pharmacology*, (168), 1–51.

Pintori, N., Loi, B., & Mereu, M. (2017). Synthetic cannabinoids: the hidden side of Spice drugs. *Behavioural Pharmacology*, *28*(6), 409–419. https://doi.org/10.1097/FBP.0000000000000323

Pistis, M., Ferraro, L., Pira, L., Flore, G., Tanganelli, S., Gessa, G. L., & Devoto, P. (2002). Δ9-Tetrahydrocannabinol decreases extracellular GABA and increases extracellular glutamate and dopamine levels in the rat prefrontal cortex: an in vivo microdialysis study. *Brain Research*, *948*(1-2), 155–158. https://doi.org/10.1016/S0006-8993(02)03055-X

Pontieri, F. E., Tanda, G., & Di Chiara, G. (1995). Intravenous cocaine, morphine, and amphetamine preferentially increase extracellular dopamine in the 'shell' as compared with the 'core' of the rat nucleus accumbens. *Proceedings of the National Academy of Sciences*, *92*(26), 12304–12308.

Poos, G. I., Carson, J. R., Rosenau, J. D., Roszkowski, A. P., Kelley, N. M., & Mcgowin, J. (1963). 2-amino-5-aryl-2-oxazolines. Potent new anorectic agents. *Journal of Medicinal Chemistry*, *6*, 266–272.

PROCHECK. Retrieved 23 March 2017, from http://services.mbi.ucla.edu/PROCHECK/

Protein - NCBI. Retrieved 20 March 2017, from https://www.ncbi.nlm.nih.gov/protein

PubChem Compound - NCBI. Retrieved 20 February 2016, from

https://www.ncbi.nlm.nih.gov/pccompound

PyRx - Virtual Screening Tool / News: PyRx 0.9.4 Release Announcement. Retrieved 24 February 2016, from https://sourceforge.net/p/pyrx/news/2016/02/pyrx-094-release-announcement/

RAMPAGE: Ramachandran Plot Assessment. Retrieved 23 March 2017, from http://mordred.bioc.cam.ac.uk/~rapper/rampage.php

Ray, S., & Peters, C. A. (2008). Changes in microbiological metabolism under chemical stress. *Chemosphere*, *71*(3), 474–483. https://doi.org/10.1016/j.chemosphere.2007.10.026

Ray, T. S. (2010). Psychedelics and the Human Receptorome. *PLoS ONE*, *5*(2), e9019. https://doi.org/10.1371/journal.pone.0009019

Remmert, M., Biegert, A., Hauser, A., & Söding, J. (2011). HHblits: lightning-fast iterative protein sequence searching by HMM-HMM alignment. *Nature Methods*, *9*(2), 173–175. https://doi.org/10.1038/nmeth.1818

Reuter, P., & Pardo, B. (2017). New psychoactive substances: Are there any good options for regulating new psychoactive substances? *International Journal of Drug Policy*, *40*, 117–122. https://doi.org/10.1016/j.drugpo.2016.10.020

Richardson, J. B., St. Vil, C., Wish, E., & Cooper, C. (2016). 'On papers': perceptions of synthetic cannabinoid use among black males under criminal justice supervision. *Health & Justice*, *4*(1). https://doi.org/10.1186/s40352-016-0032-z

Robbe, D., Alonso, G., Duchamp, F., Bockaert, J., & Manzoni, O. J. (2001). Localization and mechanisms of action of cannabinoid receptors at the glutamatergic synapses of the mouse nucleus accumbens. *The Journal of Neuroscience: The Official Journal of the Society for Neuroscience*, *21*(1), 109–116.

Rolland, B., Jardri, R., Amad, A., Thomas, P., Cottencin, O., & Bordet, R. (2014). Pharmacology of Hallucinations: Several Mechanisms for One Single Symptom? *BioMed Research International*, *2014*, 1–9. https://doi.org/10.1155/2014/307106

Roth, B. L., Gibbons, S., Arunotayanun, W., Huang, X.-P., Setola, V., Treble, R., & Iversen, L. (2013). The Ketamine Analogue Methoxetamine and 3- and 4-Methoxy Analogues of Phencyclidine Are High Affinity and Selective Ligands for the Glutamate NMDA Receptor. *PLoS ONE*, *8*(3), e59334. https://doi.org/10.1371/journal.pone.0059334

Roth, B. L., Shoham, M., Choudhary, M. S., & Khan, N. (1997). Identification of conserved aromatic residues essential for agonist binding and second messenger production at 5-hydroxytryptamine 2A receptors. *Molecular Pharmacology*, *52*(2), 259–266.

Saha, K., Partilla, J. S., Lehner, K. R., Seddik, A., Stockner, T., Holy, M., … Baumann, M. H. (2015). 'Second-Generation' Mephedrone Analogs, 4-MEC and 4-MePPP, Differentially Affect Monoamine Transporter Function. *Neuropsychopharmacology*, *40*(6), 1321–1331. https://doi.org/10.1038/npp.2014.325

Sahai, M. A., Davidson, C., Khelashvili, G., Barrese, V., Dutta, N., Weinstein, H., & Opacka-Juffry, J. (2017). Combined in vitro and in silico approaches to the assessment of stimulant properties of novel psychoactive substances – The case of the benzofuran 5-MAPB. *Progress in Neuro-Psychopharmacology and Biological Psychiatry*, *75*, 1–9. https://doi.org/10.1016/j.pnpbp.2016.11.004

Sainsbury, P. D., Kicman, A. T., Archer, R. P., King, L. A., & Braithwaite, R. A. (2011). Aminoindanes-the next wave of 'legal highs'? *Drug Testing and Analysis*, *3*(7-8), 479–482. https://doi.org/10.1002/dta.318

Sanders, B., Lankenau, S. E., Bloom, J. J., & Hathazi, D. (2008). 'Research Chemicals': Tryptamine and Phenethylamine Use Among High-Risk Youth. *Substance Use & Misuse*, *43*(3-4), 389–402. https://doi.org/10.1080/00952990701202970

Schifano, F., Orsolini, L., Papanti D., G., & Corkery, J. M. (2015). Novel psychoactive substances of interest for psychiatry. *World Psychiatry*, *14*(1), 15–26. https://doi.org/10.1002/wps.20174

Schifano, F., Orsolini, L., Papanti, D., & Corkery, J.M. (2016). NPS: Medical Consequences

Associated with Their Intake. In M. H. Baumann, R. A. Glennon, & J. L. Wiley (Eds.), *Neuropharmacology of New Psychoactive Substances (NPS)* (Vol. 32, pp. 351–380). Cham: Springer International Publishing. Retrieved from http://link.springer.com/10.1007/7854_2016_15

Schifano, F., Papanti, G. D., Orsolini, L., & Corkery, J. M. (2016). Novel psychoactive substances: the pharmacology of stimulants and hallucinogens. *Expert Review of Clinical Pharmacology*, *9*(7), 943–954. https://doi.org/10.1586/17512433.2016.1167597

Schultes, R. E. (1979). Hallucinogenic plants: their earliest botanical descriptions. *Journal of Psychedelic Drugs*, *11*(1-2), 13–24.

Schurr A. (1986). Brain Slice Preparation in Electrophysiology. Retrieved 27 October 2017, from https://scholar.google.it/scholar?hl=it&as_sdt=0%2C5&q=Brain+Slice+Preparation+In+Electrophysiology&btnG=

Seely, K. A., Lapoint, J., Moran, J. H., & Fattore, L. (2012). Spice drugs are more than harmless herbal blends: A review of the pharmacology and toxicology of synthetic cannabinoids. *Progress in Neuro-Psychopharmacology and Biological Psychiatry*, *39*(2), 234–243. https://doi.org/10.1016/j.pnpbp.2012.04.017

Seetohul, L. N., & Pounder, D. J. (2013). Four fatalities involving 5-IT. *Journal of Analytical Toxicology*, *37*(7), 447–451. https://doi.org/10.1093/jat/bkt053

Shao, Z., Yin, J., Chapman, K., Grzemska, M., Clark, L., Wang, J., & Rosenbaum, D. M. (2016). High-resolution crystal structure of the human CB1 cannabinoid receptor. *Nature*, *540*(7634), 602–606. https://doi.org/10.1038/nature20613

Shim, J.Y. (2010). Understanding functional residues of the cannabinoid CB1. *Current Topics in Medicinal Chemistry*, *10*(8), 779–798.

Shim, J.Y., Bertalovitz, A. C., & Kendall, D. A. (2012). Probing the Interaction of SR141716A with the CB1 Receptor. *Journal of Biological Chemistry*, *287*(46), 38741–38754.

https://doi.org/10.1074/jbc.M112.390955

Shim, J.Y., & Howlett, A. C. (2006). WIN55212-2 Docking to the CB_1 Cannabinoid Receptor and Multiple Pathways for Conformational Induction. *Journal of Chemical Information and Modeling*, *46*(3), 1286–1300. https://doi.org/10.1021/ci0504824

Showalter, V. M., Compton, D. R., Martin, B. R., & Abood, M. E. (1996). Evaluation of binding in a transfected cell line expressing a peripheral cannabinoid receptor (CB2): identification of cannabinoid receptor subtype selective ligands. *The Journal of Pharmacology and Experimental Therapeutics*, *278*(3), 989–999.

Siavoush, D. (2016). *Methods and Algorithms for Molecular Docking-Based Drug Design and Discovery*. IGI Global.

Simmler, L., Buser, T., Donzelli, M., Schramm, Y., Dieu, L.-H., Huwyler, J., … Liechti, M. (2013). Pharmacological characterization of designer cathinones *in vitro*: Pharmacology of cathinones. *British Journal of Pharmacology*, *168*(2), 458–470. https://doi.org/10.1111/j.1476-5381.2012.02145.x

Simmler, L. D., Rickli, A., Schramm, Y., Hoener, M. C., & Liechti, M. E. (2014). Pharmacological profiles of aminoindanes, piperazines, and pipradrol derivatives. *Biochemical Pharmacology*, *88*(2), 237–244. https://doi.org/10.1016/j.bcp.2014.01.024

Sliwoski, G., Kothiwale, S., Meiler, J., & Lowe, E. W. (2013). Computational Methods in Drug Discovery. *Pharmacological Reviews*, *66*(1), 334–395. https://doi.org/10.1124/pr.112.007336

Somministration ways - ppt. Retrieved 6 October 2017, from http://slideplayer.it/slide/4250028/

Smith, A. J. T., Zhang, X., Leach, A. G., & Houk, K. N. (2009). Beyond picomolar affinities: quantitative aspects of noncovalent and covalent binding of drugs to proteins. *Journal of Medicinal Chemistry*, *52*(2), 225–233. https://doi.org/10.1021/jm800498e

Song, Z. H., & Bonner, T. I. (1996). A lysine residue of the cannabinoid receptor is critical for

receptor recognition by several agonists but not WIN55212-2. *Molecular Pharmacology*, *49*(5), 891–896.

Soudijn, W., Wijngaarden, I. van, & Ijzerman, A. P. (2005). Structure-activity relationships of inverse agonists for G-protein-coupled receptors. *Medicinal Research Reviews*, *25*(4), 398–426. https://doi.org/10.1002/med.20031

Sousa, S. F., Fernandes, P. A., & Ramos, M. J. (2006). Protein-ligand docking: Current status and future challenges. *Proteins: Structure, Function, and Bioinformatics*, *65*(1), 15–26. https://doi.org/10.1002/prot.21082

Soussan, C., & Kjellgren, A. (2016). The users of Novel Psychoactive Substances: Online survey about their characteristics, attitudes and motivations. *International Journal of Drug Policy*, *32*, 77–84. https://doi.org/10.1016/j.drugpo.2016.03.007

Spencer, H. C., & Rowe, V. K. (1948). Toxicological studies on laboratory animals of certain alkyldinitrophenols used in agriculture. *The Journal of Industrial Hygiene and Toxicology*, *30*(1), 10–25.

Stamford, J. A., Palij, P., Davidson, C., Jorm, C. M., & Phillips, P. E. (1995). Fast cyclic voltammetry in brain slices. *Voltammetric Methods in Brain Systems*, 81–116.

Stereotaxic Instrument. Retrieved 6 November 2017, from http://play.psych.mun.ca/~smilway/stereotax.html

Strazielle, C., Lalonde, R., Amdiss, F., Botez, M. I., Hébert, C., & Reader, T. A. (1998). Distribution of dopamine transporters in basal ganglia of cerebellar ataxic mice by [^{125}I]RTI-121 quantitative autoradiography. *Neurochemistry International*, *32*(1), 61–68.

Su, T.-P., Hayashi, T., & Vaupel, D. B. (2009). When the Endogenous Hallucinogenic Trace Amine N,N-Dimethyltryptamine Meets the Sigma-1 Receptor. *Science Signaling*, *2*(61), pe12–pe12. https://doi.org/10.1126/scisignal.261pe12

Südhof, T. C., & Starke, K. (2007). *Pharmacology of Neurotransmitter Release*. Springer Science &

Business Media.

Support, Spice Addiction (2017). 700 Street Names for Synthetic Marijuana (Spice, K2, etc.). Retrieved 10 September 2017, from https://spiceaddictionsupport.org/street-names-for-synthetic-marijuana/

Suyama, J. A., Sakloth, F., Kolanos, R., Glennon, R. A., Lazenka, M. F., Negus, S. S., & Banks, M. L. (2016). Abuse-Related Neurochemical Effects of Para-Substituted Methcathinone Analogs in Rats: Microdialysis Studies of Nucleus Accumbens Dopamine and Serotonin. *The Journal of Pharmacology and Experimental Therapeutics*, *356*(1), 182–190. https://doi.org/10.1124/jpet.115.229559

SWISS-MODEL. Documentation. Retrieved 23 March 2016, from https://swissmodel.expasy.org/docs/help

Szabo, B., Siemes, S., & Wallmichrath, I. (2002). Inhibition of GABAergic neurotransmission in the ventral tegmental area by cannabinoids. *The European Journal of Neuroscience*, *15*(12), 2057–2061.

Tai, S., & Fantegrossi, W. E. (2014). Synthetic Cannabinoids: Pharmacology, Behavioral Effects, and Abuse Potential. *Current Addiction Reports*, *1*(2), 129–136. https://doi.org/10.1007/s40429-014-0014-y

Tainter, M. L. (1938). Growth, life-span and food intake of white rats fed dinitrophenol throughout life. *Journal of Pharmacology and Experimental Therapeutics*, *63*(1), 51–57.

Tainter, M. L., Cutting, W. C., & Stockton, A. B. (1934). Use of Dinitrophenol in Nutritional Disorders: A Critical Survey of Clinical Results. *American Journal of Public Health and the Nation's Health*, *24*(10), 1045–1053.

Tainter, M. L., Stockton, A. B., & Cutting, W. C. (1933). Use of dinitrophenol in obesity and related conditions: a progress report. *Journal of the American Medical Association*, *101*(19), 1472. https://doi.org/10.1001/jama.1933.02740440032009

Tanda, G., Bassareo, V., & Di Chiara, G. (1996). Mianserin markedly and selectively increases extracellular dopamine in the prefrontal cortex as compared to the nucleus accumbens of the rat. *Psychopharmacology*, *123*(2), 127–130.

Tanda, G., Pontieri, F. E., & Di Chiara, G. (1997). Cannabinoid and heroin activation of mesolimbic dopamine transmission by a common μ1 opioid receptor mechanism. *Science*, *276*(5321), 2048–2050.

Tewari, A., Ali, A., O'Donnell, A., & Butt, M. S. (2009). Weight loss and 2,4-dinitrophenol poisoning. *British Journal of Anaesthesia*, *102*(4), 566–567. https://doi.org/10.1093/bja/aep033

Tittarelli, R., Mannocchi, G., Pantano, F., & Romolo, F. (2015). Recreational Use, Analysis and Toxicity of Tryptamines. *Current Neuropharmacology*, *13*(1), 26–46. https://doi.org/10.2174/1570159X13666141210222409

Tripod, J., Sury, E., & Hoffmann, K. (1954). Zentralerregende Wirkung eines neuen Piperidinderivates. *Experientia*, *10*(6), 261–262. https://doi.org/10.1007/BF02157398

Trott, O., & Olson, A. J. (2009). AutoDock Vina: Improving the speed and accuracy of docking with a new scoring function, efficient optimization, and multithreading. *Journal of Computational Chemistry*, NA–NA. https://doi.org/10.1002/jcc.21334

Turner, P. V., Pekow, C., Vasbinder, M. A., & Brabb, T. (2011). Administration of substances to laboratory animals: equipment considerations, vehicle selection, and solute preparation. *Journal of the American Association for Laboratory Animal Science*, *50*(5), 614–627.

Turu, G., & Hunyady, L. (2010). Signal transduction of the CB1 cannabinoid receptor. *Journal of Molecular Endocrinology*, *44*(2), 75–85. https://doi.org/10.1677/JME-08-0190

Uchiyama, N., Matsuda, S., Kawamura, M., Kikura-Hanajiri, R., & Goda, Y. (2013). Two new-type cannabimimetic quinolinyl carboxylates, QUPIC and QUCHIC, two new cannabimimetic carboxamide derivatives, ADB-FUBINACA and ADBICA, and five synthetic cannabinoids

detected with a thiophene derivative α-PVT and an opioid receptor agonist AH-7921 identified in illegal products. *Forensic Toxicology*, *31*(2), 223–240. https://doi.org/10.1007/s11419-013-0182-9

UNODC (2016). Commission on Narcotic Drugs decision on international control of PMMA, α-PVP, 4,4'-DMAR, MXE and Phenazepam enters into force. Retrieved 10 February 2017, from https://www.unodc.org/LSS/Announcement/Details/6dd8eae4-7b30-4ae1-889e-f8a03d62df18

UNODC-EWA: NPS emergence spreads to more than 100 countries. (2017). Retrieved 19 March 2017, from https://www.unodc.org/LSS/Announcement/Details/0f290c90-0d69-4b27-bd18-7df7cac432b5

Vandrey, R., Dunn, K. E., Fry, J. A., & Girling, E. R. (2012). A survey study to characterize use of Spice products (synthetic cannabinoids). *Drug and Alcohol Dependence*, *120*(1-3), 238–241. https://doi.org/10.1016/j.drugalcdep.2011.07.011

Ware, M. A., Daeninck, P., & Maida, V. (2008). A review of nabilone in the treatment of chemotherapy-induced nausea and vomiting. *Therapeutics and Clinical Risk Management*, *4*(1), 99–107.

Wilson, R. I. (2002). Endocannabinoid Signalling in the Brain. *Science*, *296*(5568), 678–682. https://doi.org/10.1126/science.1063545

Winstock, A. R., & Barratt, M. J. (2013). The 12-month prevalence and nature of adverse experiences resulting in emergency medical presentations associated with the use of synthetic cannabinoid products: adverse experiences with synthetic cannabinoids. *Human Psychopharmacology: Clinical and Experimental*, *28*(4), 390–393. https://doi.org/10.1002/hup.2292

Winstock, A., Lynskey, M., Borschmann, R., & Waldron, J. (2015). Risk of emergency medical treatment following consumption of cannabis or synthetic cannabinoids in a large global

sample. *Journal of Psychopharmacology*, *29*(6), 698–703. https://doi.org/10.1177/0269881115574493

Wood, D. M., Button, J., Lidder, S., Ovaska, H., Ramsey, J., Holt, D. W., & Dargan, P. (2008). Detection of the novel recreational drug diphenyl-2-pyrrolidinemethanol (D2PM) sold 'legally' in combination with glaucine. *Clinical Toxicology* Vol. 46:393–393.

Wood, D. M., Puchnarewicz, M., Johnston, A., & Dargan, P. I. (2012). A case series of individuals with analytically confirmed acute diphenyl-2-pyrrolidinemethanol (D2PM) toxicity. *European Journal of Clinical Pharmacology*, *68*(4), 349–353. https://doi.org/10.1007/s00228-011-1142-0

World Health Organization (2016). Critical review report. 5-F-APINACA. 38th ECDD (2016). Agenda item 4.10. Retrieved 20 September 2016, from http://www.who.int/medicines/access/controlled-substances/4.10_5F-APINACA_CritReview.pdf?ua=1

Young, D. C. (2009). *Computational Drug Design: A Guide for Computational and Medicinal Chemists*. John Wiley & Sons.

Zapata, A., Chefer, V. I., & Shippenberg, T. S. (2009). Microdialysis in Rodents. In J. N. Crawley, C. R. Gerfen, M. A. Rogawski, D. R. Sibley, P. Skolnick, & S. Wray (Eds.), *Current Protocols in Neuroscience*. Hoboken, NJ, USA: John Wiley & Sons, Inc. Retrieved 12th February 2017 from http://doi.wiley.com/10.1002/0471142301.ns0702s47

Zuba, D., Byrska, B., & Maciow, M. (2011). Comparison of 'herbal highs' composition. *Analytical and Bioanalytical Chemistry*, *400*(1), 119–126. https://doi.org/10.1007/s00216-011-4743-7

Published work included in this thesis

De Luca, M. A., Castelli, M. P., **Loi, B.,** Porcu, A., Martorelli, M., Miliano, C., … Di Chiara, G. (2016). Native CB1 receptor affinity, intrinsic activity and accumbens shell dopamine stimulant properties of third generation SPICE/K2 cannabinoids: BB-22, 5F-PB-22, 5F-AKB-48 and STS-135. *Neuropharmacology*, *105*, 630–638. https://doi.org/10.1016/j.neuropharm.2015.11.017

Loi, B., Zloh, M., De Luca, M. A., Pintori, N., Corkery, J., & Schifano, F. (2017). 4,4′-Dimethylaminorex (‘4,4′-DMAR’; ‘Serotoni’) misuse: A Web-based study. *Human Psychopharmacology: Clinical and Experimental*, *32*(3), e2575. https://doi.org/10.1002/hup.2575

Pintori, N., **Loi, B.,** & Mereu, M. (2017). Synthetic cannabinoids: the hidden side of Spice drugs. *Behavioural Pharmacology*, *28*(6), 409–419. https://doi.org/10.1097/FBP.0000000000000323

Poster presentations

Barrese V., Dutta N., Miliano C., **Loi B.,** Cadoni C., Ambrosio E., Opacka-Juffry J., Schifano F., Di Chiara G., Davidson C. Potential Psychoactive Effects of the weight loss drug 2,4-Dinitrophenol (DNP). British Pharmacology Society. London (UK), December 2014.

Loi B., De Luca M.A., Miliano C., Corkery J., Zloh M., Schifano F., Di Chiara G. Microdialysis study of dopamine transmission in nucleus accumbens (NAc) shell and Caudate-Putamen (CPu) after 2,4-DNP administration in adult rats. LMS research conference. University of Hertfordshire, Hatfield, (UK), April 2015.

Miliano C., Ossato A., Marti M., **Loi B.,** Mulas G., Carta A., Di Chiara G., De Luca M.A. Effects of 25I-NBOMe, a new potent $5HT_{2A}$ agonist, on the central nervous system of rodents. Mediterranean Neuroscience Society - 5^{th} Meeting 2015. Santa Margherita di Pula, Sardinia, Italy, October 2015.

Loi B., De Luca M.A., Miliano C., Porcu A., Martorelli M., Davidson C., Castelli M.P., Schifano F. & Di Chiara G. Native CB_1 receptor affinity, intrinsic activity and nucleus accumbens shell dopamine stimulant properties of third generation spice/K2: BB-22, 5F-PB-22, 5F-AKB-48 AND STS-135. XVI Congress of the Italian Society of Neuroscience. Cagliari-Sardinia-Italy, October 2015.

Loi, B., De Luca, M.A., Miliano, C., Davidson, C., Castelli, M.P., Schifano, F.; Di Chiara, G. Effect of BB-22 on dopamine release: comparison between *in vivo* microdialysis studies and *in vitro* Fast Scan Cyclic Voltammetry studies. LMS research conference, University of Hertfordshire, Hatfield, (UK), April 2016.

Opacka-Juffry, J., Sahai, M., **Loi, B.,** Dutta, N., Barrese V., Davidson C. *In vitro* and *in silico* assessment of stimulant properties of novel psychoactive substances (NPS). SSA Conference, York, November, 2016 and British Pharmacological Soc. London, December 2016.

Loi, B., Zloh, M., De Luca, M.A., Pintori N., Corkery J.M., Schifano, F. 4,4'-dimethylaminorex ('4,4'-DMAR'; 'Serotoni') misuse; a web-based study. LMS research conference, University of Hertfordshire, Hatfield, (UK), April 2017.

Loi, B.; De Luca, M.A.; Margiani, G.; Pintori, N.; Miliano, C.; Di Chiara, G.; Schifano F. Neurochemical characterisation of the synthetic stimulants 2-DPMP and D2PM. Novel

Psychoactive Substances: new frontiers in addiction? Sardegna Ricerche, Pula, Sardinia, Italy, October 2017. **Poster prize award.**

Loi, B., Zloh, M., De Luca, M.A., Pintori N., Corkery J.M., Schifano, F. 4,4'-dimethylaminorex ('4,4'-DMAR'; 'Serotoni') misuse; a web-based study. Novel Psychoactive Substances: new frontiers in addiction? Sardegna Ricerche, Pula, Sardinia, Italy, October 2017.